Monofunctional Hyperbranched Ethylene Oligomers via Ni(II) Catalysis Controlled by Remote Substituents

Dissertation

zur Erlangung des akademischen Grades eines
Doktors der Naturwissenschaften (Dr. rer. nat.)

vorgelegt von

Thomas Wiedemann

an der Universität Konstanz
Mathematisch-Naturwissenschaftliche Sektion
Fachbereich Chemie

Konstanz 2016

Abgabedatum: 07.11.2016

Tag der mündlichen Prüfung: 02.06.2017

Prüfungsvorsitz:	Herr Prof. Dr. Valentin Wittmann
1. Referent:	Herr Prof. Dr. Stefan Mecking
2. Referent:	Herr Prof. Dr. Rainer Winter
3. Referent:	Herr Prof. Dr. Alexander Wittemann

Die vorliegende Dissertation entstand in der Zeit von März 2012 bis Juli 2015 unter der Leitung von Herrn Prof. Dr. Stefan Mecking am Fachbereich Chemie der Universität Konstanz.

Acknowledgment / Danksagung

Mein herzlichster Dank geht an Prof. Dr. Stefan Mecking für die ausgezeichnete Betreuung meiner Arbeit und sein fortwährendes Interesse an meiner Forschung. Ich danke Ihm außerdem für die zahlreichen Diskussionen und Anregungen und für die Möglichkeit ein so interessantes Thema zu erforschen.

Bei Prof. Dr. Rainer Winter bedanke ich mich herzlich für die Übernahme des Zweitgutachtens und bei Prof. Dr. Valentin Wittmann für den Vorsitz der Prüfungskommission.

Weiter möchte ich mich bei Byk Additives & Instruments für die Finanzierung dieser Doktorarbeit im Rahmen einer Kooperation bedanken. Besonderer Dank gebührt Dr. Jürgen Omeis, Dr. Michael Bessel, Dr. Dominika Bernert und Dr. Verena Wintermeyer für ergiebige Diskussionen, neue Anregungen und für die anwendungstechnischen Untersuchungen meiner Oligomere.

Besonderer Dank geht auch an Dr. Inigo Göttker-Schnetmann. Ich habe viel von Ihm gelernt und seine große Hilfsbereitschaft, zahlreichen Diskussionen und Hilfestellungen zur Nickel-Chemie und die Zusammenarbeit bei der Epoxidierung der Oligomere haben zum Gelingen der Arbeit beigetragen. Außerdem danke ich ihm für die Synthese von Nickel-Vorstufen, **^{pF}2-pyr** und **^{pMe}3-pyr**, für das Messen von Röntgenkristallstrukturen und DOSY NMR Spektren und für die kritische Durchsicht der schriftlichen Arbeit.

Philipp Roesle und Florian Stempfle danke ich für die Synthese und Bereitstellung von $[Pd(dba)_2]$ und $[(dtbpx)Pd(OTf)_2]$. Alexandra Tchernook danke ich für die anfängliche Hilfestellung bei der Bedienung der Polymerisationsreaktoren und für das Überlassen von **^{CF3}1-N^OH**.

Meinen Laborpartnern und Mitstreitern aus dem „Nickel-Team“ Anna Osichow, Philip Kenyon und Franz Ölscher möchte ich für die hilfreichen Diskussionen und den angenehmen Laboralltag danken. Ich möchte mich auch herzlich bei allen meinen Bachelor-Studenten (Gregor Voit, Andreas Wieser, Sarah Vogl), Mitarbeiterpraktikanten (David Siebert, Daniel Fink) und Hiwis (Verena Goldbach, Adrian Donner, Florian Wimmer) für Ihre Mühe und Ihren Beitrag zu dieser Arbeit danken.

Robin Kirsten und Werner Röll gebührt Dank für technische Hilfestellungen im Labor und für die Versorgung mit allem, was man so zum Forschen braucht. Lars Bolk danke ich für zahlreiche DSC und GPC Messungen und für das Lösen aller Computerprobleme. Ulrich Haunz und Anke Friemel aus der NMR-Core-Facility sei gedankt für ihre stetige Hilfsbereitschaft und das Messen unzähliger NMR Spektren. Der AG Winter, insbesondere Steffen Oßwald und Stefan Scheerer sei für die Hilfe bei den Cyclovoltammetrie-Messungen gedankt.

Mein herzlicher Dank geht auch an Prof. Dr. Lucia Caporaso (Universität Salerno in Italien) und Dr. Laura Falivene (King Abdullah University of Science & Technology in Saudi Arabien) für das Beisteuern der DFT Rechnungen zu dieser Arbeit.

Der ganzen Arbeitsgruppe inklusive aller ehemaligen Mitarbeiter der letzten Jahre danke ich für die super angenehme Arbeitsatmosphäre auf L7. Es hat Spaß gemacht mit Euch!

Bei meiner Familie, meinen Freunden und meiner Freundin bedanke ich mich von Herzen für die fortwährende Unterstützung, den Rückhalt während des gesamten Studiums und die schönen Jahre in Konstanz. Ganz besonders dankbar bin ich meinen Eltern, die mir das Chemiestudium erst ermöglicht haben.

Publications

Parts of this thesis have been published

Journal Publication:

- Wiedemann, T.; Voit, G.; Tchernook, A.; Roesle, P.; Göttker-Schnetmann, I.; Mecking, S. *J. Am. Chem. Soc.* **2014**, *136*, 2078-2085. „*Monofunctional Hyperbranched Ethylene Oligomers*“

European Patent Application:

- Bessel, M.; Mecking, S.; Wiedemann, T.; Frank, A.; Omeis, J.; Tchernook, A.; Göttker-Schnetmann, I. (Byk Chemie GmbH) EP2891511 (A1), 2015. "*Ethylene-based polymer as defoamer additive*"

Poster Presentations:

- Wiedemann, T.; Osichow, A.; Voit G.; Tchernook, A.; Roesle, P.; Göttker-Schnetmann, I.; Mecking, S. at the **19th *International Symposium on Homogeneous Catalysis***, Ottawa/Canada 2014 „*Monofunctional Hyperbranched Ethylene Oligomers*“
- Wiedemann, T.; Osichow, A.; Göttker-Schnetmann, I.; Mecking, S. at the **48. *Jahrestreffen deutscher Katalytiker***, Weimar/Germany 2015 „*Monofunctional Hyperbranched Ethylene Oligomers*“

Abstract / Zusammenfassung

Polyethylen stellt in seinen zahlreichen Varianten von HDPE bis LDPE eines der wichtigsten Materialen und Werkstoffe unserer Zeit dar. Jedoch sind auch kurzkettige (funktionalisierte) Oligomere, mit Molmassen von wenigen 1,000 g mol^{-1} technisch interessante Verbindungen. Während lineare, monofunktionalisierte Ethylenoligomere aus dem Ziegler-Alfol-Prozess seit langem bekannt sind und breite Anwendung finden, ist bisher keine Möglichkeit zur Synthese entsprechender hochverzweigter Verbindungen bekannt. Diese sind beispielsweise als Verträglichkeitsvermittler für Formulierungen mit lipophilen Anteil von Interesse. Dabei ist es wünschenswert, dass die Oligomere genau eine funktionelle Gruppe aufweisen und die Neigung zur Kristallisation durch hohe Verzweigungsgrade möglichst vollständig unterdrückt wird.

Für die Synthese solcher hochverzweigter Oligomere erscheinen Ni(II) Salicylaldiminato Komplexe mit *N*-Terphenylgruppen vielversprechend. Die resultierenden Mikrostrukturen lassen sich durch weit entfernte Substituenten am Liganden kontrollieren. Komplexe mit elektronenziehenden Gruppen liefern lineares, hochmolekulares Polyethylen, während mit elektronenschiebend substituierten Komplexen hochverzweigte Oligomere erhalten werden.

In der vorliegenden Arbeit wurden zum ersten Mal hochverzweigte Ethylenoligomere systematisch synthetisiert und charakterisiert. Besonderes Augenmerk lag dabei auf der detaillierten Analyse der mikroskopischen Verzweigungsstruktur der mit Ni(II) Salicylaldiminato Komplexen erhaltenen Oligomere. Alle Oligomere, die mit elektronenreich substituierten Komplexen erhalten werden, weisen neben Methyl- auch Ethyl-, Propyl- und langkettige Alkylverzweigungen (C_{4+}) auf. Erstaunlicherweise besitzen die Oligomere eine hyperverzweigte Mikrostruktur, worauf die Anwesenheit von Verzweigungen auf Verzweigungen (sekundäre Butylverzweigungen) schließen lässt. Eine solche hyperverzweigte Struktur war für niedermolekulare Ethylenoligomere bisher nicht bekannt.

Im Rahmen der Arbeit wurden auch erstmals detaillierte Oligomerisierungsstudien mit unterschiedlichen Ni(II) Salicylaldiminato Komplexen bei verschiedenen Bedingungen durchgeführt. Es wurde gezeigt, dass sowohl die Molekulargewichte der Oligomere als auch deren Verzweigungsgrade und die Verteilung verschiedener Verzweigungslängen stark von den

Reaktionsbedingungen abhängen. So werden bei niedrigen Ethylendrücken und hohen Temperaturen kurzkettigere Oligomere mit mehr Verzweigungen erhalten. Außerdem werden bei den gleichen Bedingungen mehr langkettige Verzweigungen und hyperverzweigte Strukturen erhalten.

Durch β-Hydrideliminierung als zugrundeliegende Reaktion für den Kettentransfer weist jede Oligomerkette eine ungesättigte Endgruppe auf. Die in der vorliegenden Arbeit untersuchte selektive Funktionalisierung dieser Doppelbindung beschreibt erstmals die Synthese von monofunktionalisierten, hyperverzweigten Ethylenoligomeren. Die Funktionalisierung mit terminalen Estergruppen konnte wahlweise mit einer isomerisierenden Alkoxycarbonylierung oder einer Kreuzmetathese mit Ethylacrylat gefolgt von einer Hydrierung erreicht werden. Letztere Methode erlaubte die quantitative Umsetzung der Doppelbindungen. Durch Reduktion können ebenfalls alkoholfunktionalisierte Oligomere erhalten werden. Die Epoxidierung der Doppelbindung erfolgt selektiv und unter milden Reaktionsbedingungen. Die anschließende Ringöffnung mit Acrylsäure erlaubt außerdem die Synthese von acrylatfunktionalisierten Makromonomeren, die in einer radikalischen Copolymerisation mit Butylacrylat Anwendung fanden.

Weiterhin wurden im Rahmen dieser Arbeit eine Reihe neuer Ni(II) Salicylaldiminato-Komplexe mit stark vereinfachter Ligandstruktur synthetisiert. Diese erlauben eine deutlich vereinfachte und preiswertere Katalysatorsynthese und sind prinzipiell in der Lage ähnliche Produkte bezüglich des Molekulargewichts und der Verzweigungsstruktur zu liefern.

Des Weiteren wurde der bemerkenswerte Einfluss der weit entfernten Substituenten auf die katalytischen Eigenschaften des Metallzentrums bei Ni(II) Salicylaldiminato-Komplexen genauer untersucht. Die Hypothese einer potentiellen, schwachen π-Wechselwirkung zwischen den entfernten Arylgruppen und dem Nickelzentrum konnte durch die Synthese asymmetrischer Komplexe mit gemischt elektronenziehend und –schiebend substituierten Liganden nicht untermauert werden. Komplexe mit potentiell schwach koordinierenden Gruppen im Ligandrückgrat zeigten hingegen ein außergewöhnliches katalytisches Verhalten und lieferten Oligomere mit beispiellos hohen Verzweigungsgraden und ungewöhnlichen Verzweigungsstrukturen (fast ausschließlich Methylverzweigungen). Die Untersuchung der Katalysatorvorstufen mittels Cyclovoltammetrie ergab, dass die elektronische Situation am Metall durch die Natur der weit entfernten Aryl-Substituenten des Liganden beeinflusst wird. DFT-Studien zeigen schließlich auf, dass eine π-Wechselwirkung, welche nur für die elektronenreich substituierten aromatischen Reste auftritt, für die hohen Verzweigungsgrade und die Kettenübertragung dieser Katalysatoren relevant ist.

Table of Contents

I Annotations

Abbreviations

Abbreviations of the 'International System of Units' (SI-Units), chemical formulas, and abbreviations of chemical groups (Me, Et, etc.) according to the IUPAC (International Union of Pure and Applied Chemistry) nomenclature are not listed.

acac	Acetylacetone
ADMET	Acyclic diene metathesis
ATRP	Atom transfer radical polymerization
CCG	Catalytic chain growth
COE	Cyclooctene
COSY	Correlation spectroscopy
Cp	Cyclopentadiene
CTA	Chain transfer agent
dba	Dibenzylideneacetone
DCM	Dichloromethane
DFT	Density functional theory
dmso	Dimethyl sulfoxide
DOSY	Diffusion-ordered spectroscopy
DSC	Differential scanning calorimetry
dtbpy	4,4′-Di-tert-butyl-2,2′-dipyridyl
ESI-MS	Electronspray-ionization mass spectrometry
equiv	Equivalent
GPC	Gel permeation chromatography
HDPE	High density polyethylene
HG II	Hoveyda-Grubbs 2nd generation catalyst
HMBC	Heteronuclear multiple bond correlation
HSQC	Heteronuclear single quantum coherence
LDPE	Low density polyethylene
LLDPE	Linear low density polyethylene
*m*CPBA	*meta*-Chloroperoxybenzoic acid

MM	Macromonomer
M_n	Number average molecular weight
M_w	Weight average molecular weight
M_w/M_n	Molecular weight distribution
nBuA	*n*-Butyl acrylate
NMR	Nuclear magnetic resonance
PE	Polyethylene
PMDETA	*N,N,N′,N″,N″*-Pentamethyldiethylenetriamine
ppm	Parts per million
pTsOH	*para*-Toluenesulfonic acid
pyr	Pyridine
ROMP	Ring opening metathesis polymerization
THF	Tetrahydrofuran
T_m	Melting temperature
tmeda	*N,N,N',N'*-Tetramethylethylene-1,2-diamine
TOF	Turnover frequency
TON	Turnover number
UHMWPE	Ultra high molecular weight polyethylene
vs.	versus
δ	Chemical shift in ppm

II Index of Complexes and Nomenclature

All ligands and amines/anilines used for complex synthesis are named according to their corresponding complexes with for example ^{Me}**1-N^OH** and ^{Me}**1-NH$_2$** for the ligand and terphenyl amine of ^{Me}**1-pyr**, respectively.

The L in ^{x}**1-L** designates the labile ligand on the nickel center and is either pyridine (L = pyr), dmso (L = dmso), or tmeda (L = tmeda).

Standard Catalyst Precursors with Different Substituents on the Terphenyl amine

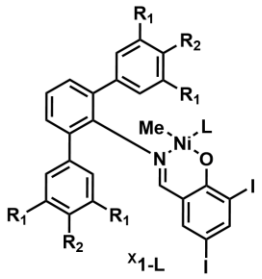

^{x}1-L

X = Me: R_1 = CH_3, R_2 = H
X = Et: R_1 = Et, R_2 = H
X = iPr: R_1 = *i*Pr, R_2 = H
X = CF3: R_1 = CF_3, R_2 = H
X = Me;OMe: R_1 = Me, R_2 = OMe

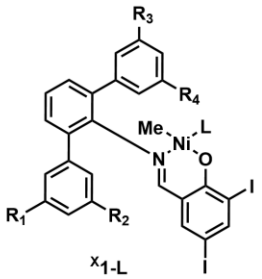

^{x}1-L

X = Me/CF3: R_1 = R_2 = Me, R_3 = R_4 = CF_3
X = (MeCF3): R_1 = R_3 = Me, R_2 = R_4 = CF_3

Complexes from Para Substituted Anilines

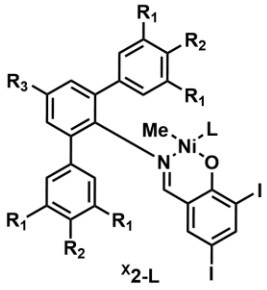

^{x}2-L

X = pMe: R_1 = CH_3, R_2 = H, R_3 = Me
X = pF: R_1 = CH_3, R_2 = H, R_3 = F
X = pOMe: R_1 = CH_3, R_2 = H, R_3 = OMe
X = pNMe$_2$: R_1 = CH_3, R_2 = H, R_3 = NMe_2
X = p(Ar-OMe): R_1 = CH_3, R_2 = OMe,
R_3 = (3,5-Me_2-4-OMe-C_6H_2)
X = p(Ar-Me): R_1 = CH_3, R_2 = Me, R_3 = (3,5-Me_2-C_6H_3)

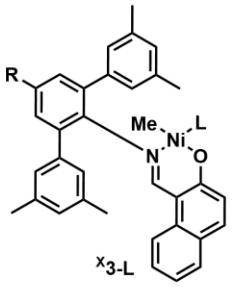

^{x}3-L

X = pF: R = F
X = pMe: R = Me

Complexes with Simplified Ligands

R = H, F, Me

R = H, F, Me

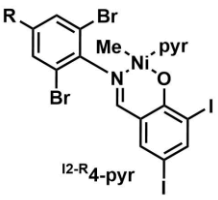

R = H, F, Me

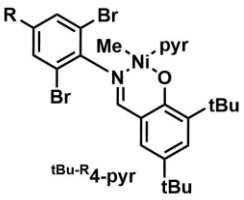

R = H, F, Me

Complexes with Additional Motifs on the Salicylaldiminato Ligand

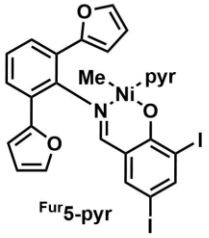

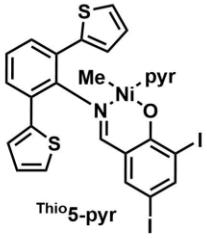

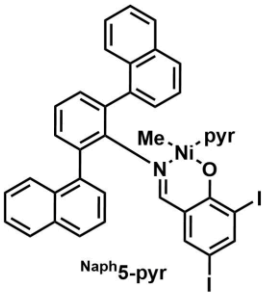

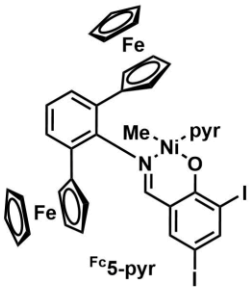

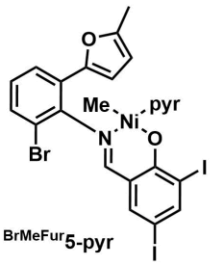

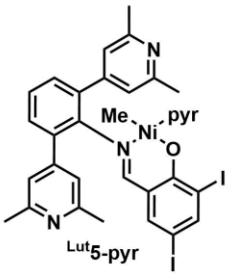

1 General Introduction

Polyolefins with their wide range of different applications are amongst the most important and versatile materials of our time. An annual estimated demand of over 100 million tons underlines their importance for modern life.[1,2] Especially polyethylene which accounts for one third of the overall polymer production stands out due to its versatile material properties ranging from soft plastic bags made from LDPE (low density polyethylene) over robust water pipes made from HDPE (high density polyethylene) to artificial joint replacements made from UHMWPE (ultra high molecular weight polyethylene). This variability in properties results from a different microscopic chain architecture of these materials (**Scheme 1.1**).

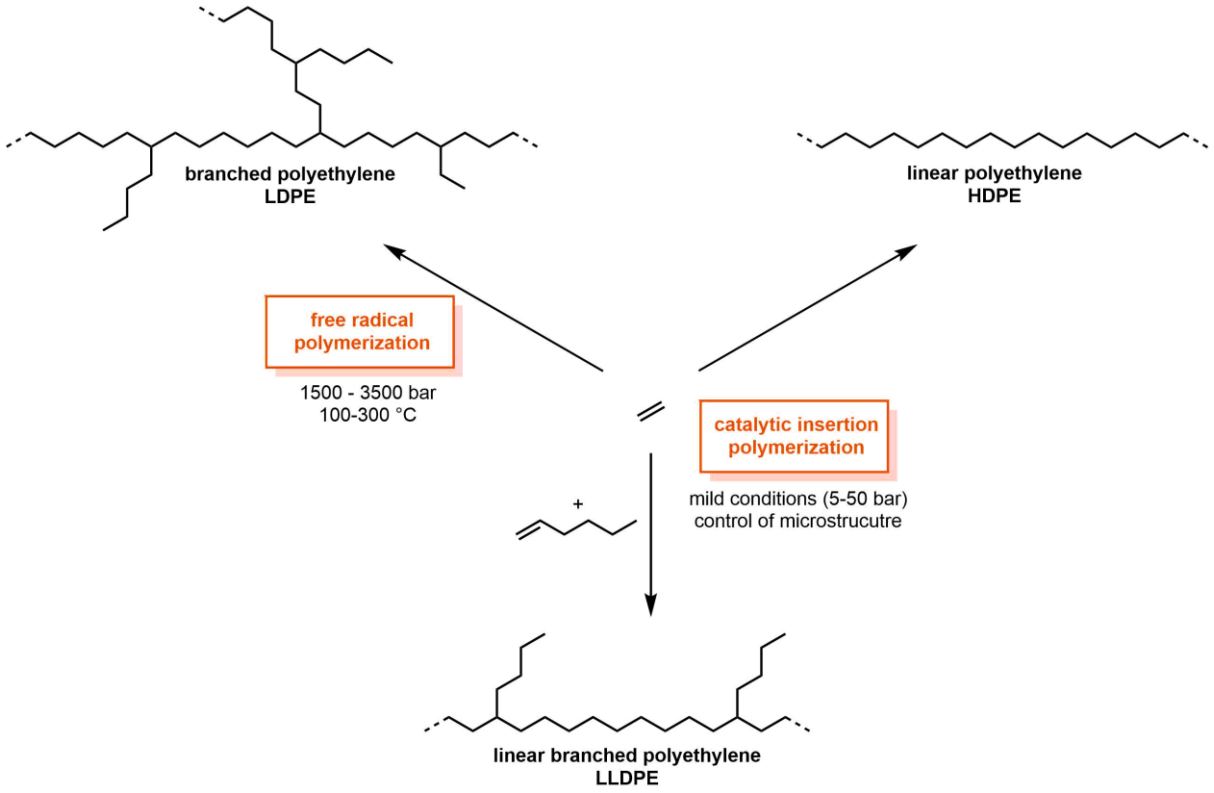

Scheme 1.1: Schematic microstructure of different types of polyethylene.

LDPE is produced since 1940 by a free radical polymerization of ethylene at high temperatures (> 100 °C) and high pressures (> 1,000 bar). These harsh conditions result in a

chain structure with short chain branches (mainly butyl) as well as long chain branches (> 100 carbons) and branch on branch motifs.[3] Due to the presence of about 20 - 40 branches per 1,000 carbon atoms, LDPE is soft and therefore lends itself for the fabrication of thin films. Major breakthroughs were reported by Ziegler and Natta in the 1950s. The catalytic insertion polymerization of ethylene for the first time allowed for the synthesis of linear polyethylene (HDPE) under mild reaction conditions.[4-6] In contrast to LDPE, this material is hard and has a higher crystallinity ($\chi \approx 65$ %), and is therefore suitable for more demanding applications. LLDPE (linear low density polyethylene) contains only branches of uniform length on the linear polymer backbone and is obtained by a random copolymerization of ethylene and 1-olefins like 1-hexene or 1-octene. Nowadays HDPE and LLDPE are produced by catalytic insertion polymerization with early transition metal complexes (Zr, Ti, Cr, V) based on the Ziegler-Natta and Phillips catalysts.[7] Therefore, catalytic insertion polymerization of apolar olefins became one of the most well-studied reactions in chemistry. In strong contrast to the little controlled free radical polymerization, catalytic chain growth via insertion in a polymeryl(R)-olefin complex [L_nMR(olefin)] can provide control over the regio and stereoselectivity of the chain growth via the metal fragment L_nM. Hence, catalytic insertion polymerization offers the opportunity to control the microstructure of the resulting polymer and therefore its material properties by elaborate catalyst design.[8] However, the early transition metal catalysts applied for industrial scale polyolefin production only afford linear products or short chain branched (co-)polymers. The synthesis of highly branched or hyperbranched polyethylene is not feasible with these catalysts. Furthermore, the early transition metals exhibit a very high oxophilicity. Thus, they are very sensitive towards any kind of monomer containing heteroatoms like oxygen or nitrogen. Therefore, much effort was devoted to the development of new types of polymerization catalyst systems based on late transition metals like palladium and nickel.[2,9,10]

1.1 Oligomerization and Polymerization with Cationic Ni(II)-α-Diimine Complexes

Until the 1990s late transition metal polymerization catalysts have been little investigated and few reports about catalysts for olefin polymerization have been published. This can be attributed to the generally lower activity of these metals for olefin polymerization compared to early transition metals. In addition, chain growth always competes with β-hydride elimination resulting in the formation of short chain oligomers, which is the basis of the Shell Higher Olefin Process (SHOP).[9,11-13] This general observation changed with the seminal discovery of Brookhart

and coworkers. In 1995 they reported a series of cationic Pd(II) and Ni(II) α-diimine complexes exhibiting high activities for the homopolymerization of ethylene (**Figure 1.1**).[14]

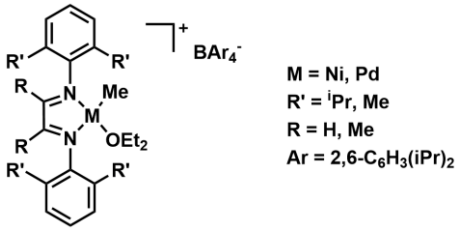

Figure 1.1: Cationic Pd(II)- and Ni(II)-α-diimine complexes.

For a high activity, these catalysts comprise three key features, namely (1) highly electrophilic cationic metal centers; (2) sterically bulky α-diimine ligands; and (3) non-coordinating counter-ions.[9] Depending on the reaction conditions (temperature, ethylene pressure) and the ligand structure, the polyethylene microstructure can vary from strictly linear and highly crystalline to highly branched and completely amorphous.[15] Branches are introduced by extensive chain walking, a series of β-hydride elimination, olefin rotation and 2,1-reinsertion. Thus, the Ni(II) and Pd(II) α-diimine catalysts for the first time gave access to highly branched, amorphous polyethylene via a controlled catalytic insertion polymerization of ethylene without the need for an ethylene α-olefin copolymerization. Generally, for the α-diimine systems, nickel based catalysts provide polymers with lower degrees of branching than their palladium analogues.[14,16,17] Additionally, due to their lower oxophilicity and higher functional group tolerance, these late transition metal catalysts for the first time allowed for the copolymerization of apolar olefins with polar vinyl monomers.[14,18-21]

1.1.1 Mechanistic Investigations

A detailed mechanistic picture of the polymerization with cationic Ni(II)-α-diimine catalysts was gained by following the chain growth by low-temperature NMR spectroscopy. The general mechanism for the polymerization including chain propagation, chain transfer, and the branch formation is depicted in **Scheme 1.2**.[22] Under the conditions studied by Svejda and coworkers, the olefin alkyl complex was found to be the catalyst resting state which is in strong contrast to early transition metal catalysts. Thus, the rate limiting step of the polymerization is the insertion of ethylene in the nickel alkyl bond and the migratory insertion is zero order in ethylene. The barrier for insertion of ethylene is dependent on the steric bulk of the ligand and the lowest barriers are found for the ligands with the highest steric demand. Additionally, the barriers for the insertion in the nickel complexes are significantly lower than those for the palladium analogues and account for their much higher activities in polymerization. Increasing

the steric bulk of the ligand was found to increase the ground state energy of the resting state relative to the migratory insertion transition state resulting in a lower overall barrier for insertion.[23,24] Following the migratory insertion step, a 14-electron cationic alkyl complex with a β-agostic interaction is formed. Addition of ethylene followed by insertion results in chain propagation without the formation of branches. Alternatively, the β-agostic complex can also undergo β-hydride elimination prior to the addition of ethylene resulting in the formation of the hydride olefin complex. After rotation of the olefin and reinsertion in a 2,1-fashion, subsequent insertion of ethylene introduces a methyl branch. A series of β-hydride elimination, rotation, and reinsertion results in a 'walking' of the metal center along the polymer chain and introduces longer alkyl branches. The formation of branch-on-branch motifs indicates that the catalyst can also migrate past tertiary carbon atoms. Note, that a similar mechanism had also been found previously by Fink in the 2,ω-polymerization of 1-olefins by certain Ni(II) catalysts.[25]

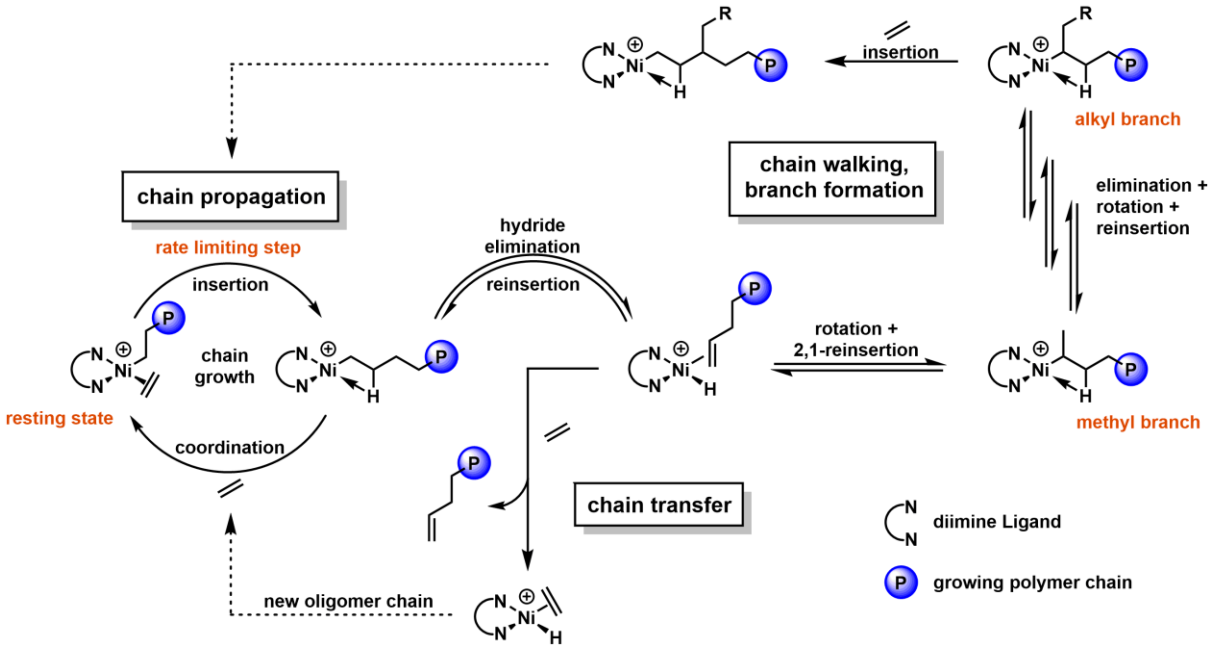

Scheme 1.2: Mechanism for ethylene polymerization and formation of hyperbranched polyethylene via chain walking.

In contrast to most late transition metal complexes, chain transfer is relatively slow in the α-diimine system which results in the production of high molecular weight polymers. Chain transfer can occur either from the hydride olefin intermediate after β-hydride elimination via an associative displacement (**Scheme 1.3** A) or from the alkyl olefin resting state by direct β-hydride transfer to the monomer (**Scheme 1.3** B). Both mechanisms involve a five-coordinate transition state. Although theoretical calculations indicate that chain transfer likely proceeds via direct β-hydride transfer to the monomer in the nickel systems,[23,26,27] experimental data rather suggest the associative displacement mechanism from the hydride olefin complex to be operative.

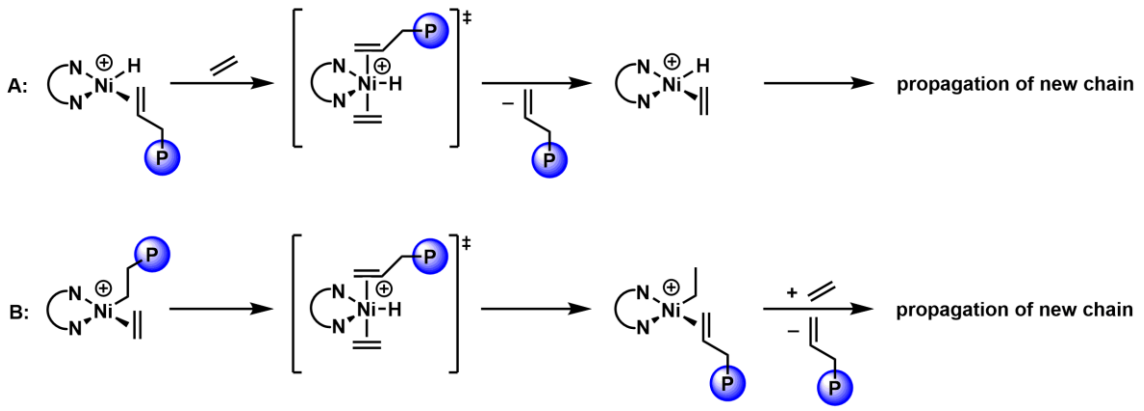

Scheme 1.3: Possible modes of chain transfer via associative displacement from the olefin hydride intermediate (A) or direct β-hydride transfer to monomer from the alkyl olefin resting state (B).[9]

From the two presented chain transfer modes the importance of steric bulk of the ligand becomes evident. The aryl rings of the diimine are oriented perpendicular to the square plane of the metal center and the *ortho*-substituents are then directed to the axial positions of the metal. Thus, bulky substituents block the axial sites more efficiently and significantly slow down the rate for chain transfer because the five-coordinate transition state is destabilized relative to the ethylene alkyl resting state.[28] A bulky and rigid ligand backbone amplifies the effect of the bulky *ortho*-substituents by locking them in place below and above the nickel plane.

1.1.2 Polymer Microstructure

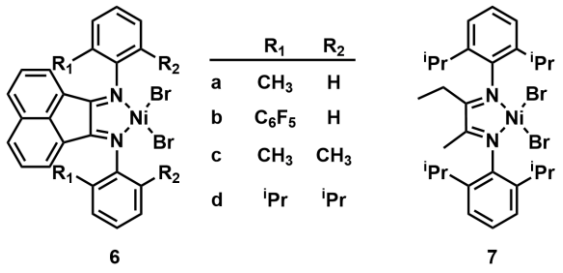

Figure 1.2: Ni(II)-α-diimine complexes with different steric bulk of the *ortho*-substituents.

The influence of ligand structure, polymerization temperature, and ethylene pressure on the molecular weight, degree of branching, and branch distributions of polymers obtained with Ni(II)-α-diimine catalysts was extensively studied.[14-16,29-32] As expected from the mechanistic investigations, a very distinct effect of ligand steric bulk on the polymer microstructure is observed. Decreasing the steric bulk of the *ortho*-substituents on the α-diimine ligand result in a significant drop of molecular weight of the PE. This is explained by the higher barrier for insertion which slows down chain propagation. Additionally, the reduced steric bulk results in a less effective shielding of the axial sites of the metal center and the propensity for chain transfer

increases relative to chain propagation. Thus oligomers rather than high molecular weight polymer are formed. Furthermore, these oligomers exhibit significantly lower degrees of branching and are even linear in some cases. This is also a result of the lack of steric bulk in the axial positions favoring chain transfer after β-hydride elimination over chain walking. Catalysts **6a** and **6b**, bearing only one *ortho*-substituent, therefore yield oligomers with molecular weights of 1,300 and 970 g mol^{-1} and degrees of branching of 2 and 5 branches per 1,000 carbon atoms (at 35 °C, 15 atm of C_2H_4), respectively, whereas polyethylene with 337,000 and 844,000 g mol^{-1} containing 24 and 39 branches per 1,000 carbons, respectively, is obtained with the bulky *iso*-propyl groups of catalysts **6d** and **7**.[15] With the presence of a second methyl group in the remaining *ortho*-position (**6c**), the polymer molecular weight increases significantly (M_n = 59,200 vs. 1,300 g mol^{-1}). Also, the turnover frequencies are an order of magnitude higher for the bulkier catalysts. Catalysts bearing alkyl substituents on the ligand backbone tend to yield higher molecular weight polymers compared to those bearing the planar aromatic acenaphthyl backbone while their activities are comparable. The polymer microstructure is also strongly dependent on the polymerization conditions. Increasing the ethylene pressure leads to a dramatic reduction of the degrees of branching (5 vs 29 branches at 15 and 1 atm, respectively with **6b**) due to an increased rate of trapping the β-agostic complex by ethylene coordination and migratory insertion compared to isomerization. In contrast, high temperatures favor β-hydride elimination and chain walking and therefore give rise to a higher extent of branching and lower molecular weights.

In summary, for this type of catalysts the synthesis of highly branched material is limited to high molecular weight polymers and the oligomerization of ethylene with catalysts lacking bulky *ortho*-aryl substituents always results in the formation of linear α-olefins. Hence, these catalysts generally do not allow for the synthesis of highly branched ethylene oligomers.

1.2 Oligomerization and Polymerization with Neutral Ni(II) Catalysts

1.2.1 Shell Higher Olefin Process

The Shell Higher Olefin Process (SHOP) is the earliest example of a chain growth reaction based solely on a late transition metal catalyst. In this process, neutral Ni(II) complexes with chelating κ^2-*P,O*-ligands are applied for the selective oligomerization of ethylene to linear α-olefins (C_6 – C_{20}).[11,13,33]

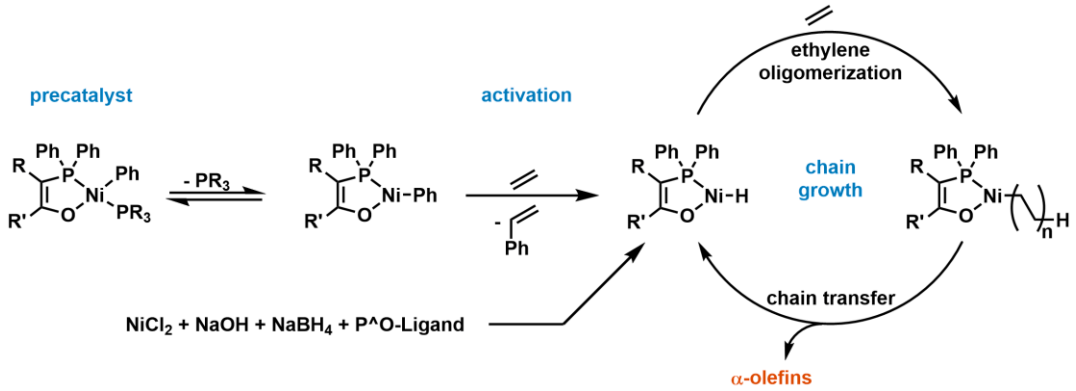

Scheme 1.4: Shell Higher Olefin Process for the synthesis of linear α-olefins.

A phosphine phenyl precatalyst for the SHOP can be obtained by oxidative addition of a P-Ph bond of a keto phosphorus-ylide ligand (Ph_3P=CH-C(O)Ph) to a Ni^0 source like $[Ni(COD)_2]$.[34] The coordinatively unsaturated 14-electron complex is stabilized by the coordination of a neutral σ-donor ligand (e.g. PPh_3). After dissociation of the labile ligand, the resulting phenyl complex is transformed into the catalytically active hydride complex by ethylene insertion and subsequent elimination of styrene. Alternatively, the nickel hydride complex can be prepared *in situ* by reaction of a Ni(II) salt, base, a boron hydride, and the corresponding bidentate P^O-ligand, (*o*-diphenylphosphino)phenol.[35] Ethylene oligomerization is typically carried out in a polar reaction medium like 1,4-butanediol containing small amounts of water (4 wt-%). This allows for separation of the oligomer products from the catalyst by extraction with an apolar solvent. The product phase contains linear α-olefins of different lengths with a Schulz-Flory distribution.[36] The shorter chain fraction can be used as comonomers for LLDPE synthesis and the C_{12}-C_{14} fraction for the synthesis of detergents. In order to use the whole range of products, the longer chain olefin fraction can be converted to the desired chain length by subsequent isomerization and metathesis steps.

Some SHOP catalysts can also be used for the synthesis of linear to moderately branched polyethylene in aliphatic hydrocarbon solvents or in the presence of phosphine scavengers like $[Ni(COD)_2]$ or $[Rh(acac)(C_2H_4)_2]$.[37-39] Higher molecular weight polyethylene is also produced by complexes with weak σ-donors as for example pyridine or phosphine oxides.[39,40] In some cases, high weight average molecular weights (M_w) are achieved, but as far as reported, M_n is always 10^3 – 10^4 g mol^{-1}. Branched, low molecular weight oligoethylenes however, are also not accessible with these catalysts.

1.2.2 Neutral κ^2–[*N,O*] Chelated Nickel (II) Complexes

In the late 1990s, Johnson *et al*. (DuPont) and Grubbs and coworkers independently reported a series of neutral nickel complexes based on the SHOP catalysts where the phosphorus atom of the chelating *P,O*-ligand was replaced by nitrogen as a harder σ-donor (**Figure 1.3**).[41-43] The resulting neutral Ni(II) salicylaldiminato complexes with anionic *N,O*-ligands were shown to be very active catalysts for the polymerization of ethylene.

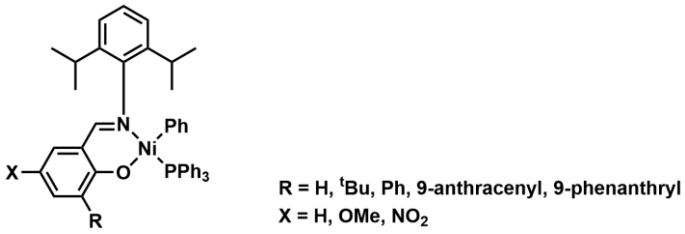

Figure 1.3: Neutral Ni(II) salicylaldiminato precatalysts with anionic *N,O*-ligands.

In the initial reports, the salicylaldiminato ligands were derived from condensation of a range of different salicylaldehydes with a variety of substituents in the 3,5-positions with 2,6-di-*iso*-propylaniline. Complex synthesis was then carried out by reaction of the deprotonated ligands (N,O)Na with nickel precursors like $[NiPh(Cl)(PPh_3)_2]$ or $[\{(allyl)Ni(\mu^2\text{-}Cl)\}_2]$. The diamagnetic complexes adopt a square planar geometry with the phosphine bound *trans* to the imine-nitrogen.

Upon sequestration of the σ-donor phosphine ligand with $[Ni(COD)_2]$ or $B(C_6F_5)_3$ in the presence of ethylene, the nickel catalysts produce polyethylene with molecular weights of M_w = 11,400 to 54,000 g mol^{-1} and moderate degrees of branching (about 30 branches per 1,000 carbon atoms) depending on the substituents on the aldehyde. A key feature of the catalyst is the introduction of bulky *iso*-propyl groups in the *ortho*-positions of the aniline. Sufficient bulk is assumed to aid phosphine dissociation and prevent deactivation via formation of the bischelated nickel complex. Additionally, theoretical work suggests that they shield the axial positions in a similar manner as observed for the Ni(II)-α-diimine catalysts, suppressing chain transfer reactions.[44,45] As indicated by a long induction period, the dissociation of the phosphine ligand appears to be the rate limiting step for these catalysts. This limitation was overcome by substitution of the phosphine by acetonitrile as the labile ligand.[43] These catalysts are not only significantly more active but also produce polymers with M_w > 200,000 g mol^{-1} and 5 to 20 branches per 1,000 carbon atoms. An alternative route to highly active catalysts uses the neutral ligand (N,O)H in an acid-base reaction with $[(tmeda)NiMe_2]$ where the corresponding Ni-methyl tmeda complex is formed by protonation of a methyl group with evolution the of methane.

A detailed and systematic investigation of substituent effects of neutral nickel salicylaldiminato complexes was carried out by Mecking and coworkers.[46–52] The activity could be increased significantly by the introduction of sterically demanding, substituted terphenyl groups on the imine instead of 2,6-di-*iso*-propylphenyl (**Figure 1.4**).[53]

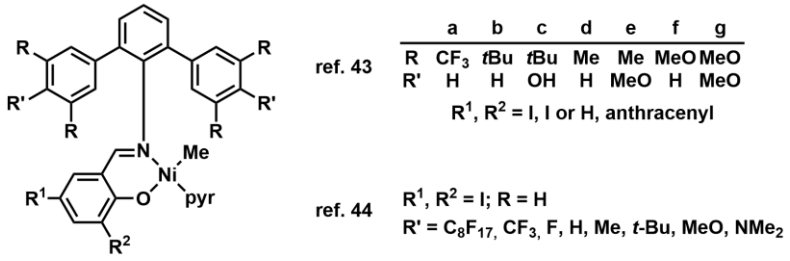

Figure 1.4: Neutral Ni(II) salicylaldiminato complexes with sterically demanding terphenyl amines.

Furthermore, the substitution of the phosphine ligand by weakly coordinating pyridine allows for the use of these complexes as single-component catalysts eliminating the need for an additional co-catalyst. It was shown that despite their remoteness to the active nickel center, the 3,4,5-substituents of the terphenyl amine (R and R') exert a remarkable influence on the polymer microstructure and the molecular weight. The polymer properties are thus controlled by the electronic nature of the substituents and range from linear and semicrystalline high molecular weight polyethylene for electron withdrawing ones (**Figure 1.4 a**: R = CF_3 or NO_2; R' = H) to highly branched and amorphous oligoethylene for electron rich substituents (**Figure 1.4 d** and **f**: R = Me, OMe; R' = H).[50,52,53] More electron donating substituents favor branch formation and chain transfer, which both occur through β-hydride elimination as the underlying step. The observed effect can be related to very similar barriers of β-hydride elimination ($\Delta G^{\ddagger}_{\beta\text{-elim}}$) and ethylene insertion chain growth ($\Delta G^{\ddagger}_{ins}$) as reported by Jenkins and Brookhart for the related neutral Ni(II) anilinotropone system.[54] Small relative changes in $\Delta G^{\ddagger}_{\beta\text{-elim}}$ and $\Delta G^{\ddagger}_{ins}$ exerted by the electronics of R can then alter the ratio $\Delta G^{\ddagger}_{\beta\text{-elim}}/\Delta G^{\ddagger}_{ins}$ to a noticeable extent, resulting in the entirely different materials obtained. Beside the electronics governing the polymerization, sterics were found to have an additional, smaller influence which leads to the formation of more linear, higher molecular weight oligomers with R = ^{t}Bu. However, via changing the substitution of the 4-position (R' = CF_3, F, H, Me, ^{t}Bu, OMe, NMe_2) with R = H, it was shown that the polymer microstructure and material properties can be controlled by electronics exclusively.[51]

Following the catalysts' activity over time by monitoring the ethylene uptake reveals a greater stability of the catalysts bearing electron withdrawing substituents (R = CF_3) which show more or less constant activity over a period of 2 hours (at 50 °C, 40 bar). In contrast, electron donating substituents result in significant catalyst deactivation within 1 hour under identical conditions.[50] The stability of a given catalyst appears to correlate with its propensity for

β-hydride elimination. This suggests that the intermediate olefin hydride complex which is formed after β-hydride elimination plays a key role in the deactivation of the catalyst. A detailed investigation of the deactivation pathways of neutral Ni(II) salicylaldiminato polymerization catalysts was carried out by Andreas Berkefeld in our group.[55,56] The deactivation of Ni(II)-alkyl complexes was found to occur in a bimolecular reaction with a hydride complex (**Scheme 1.5**). This was proposed to proceed via an alkyl bridged dimer with subsequent elimination of for example ethane (for R = Me; R' = Me) which was observed in NMR spectroscopic studies at elevated temperatures.

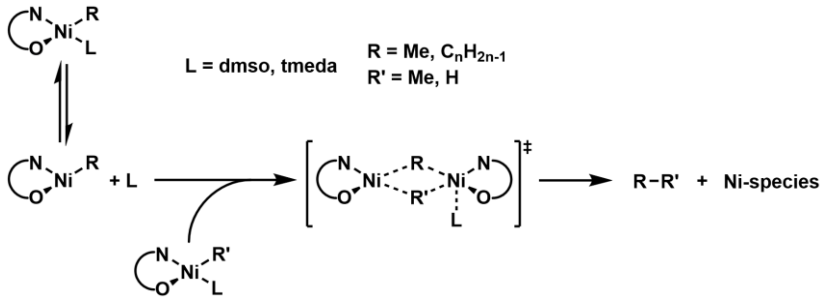

Scheme 1.5: Proposed mechanism for the bimolecular deactivation via an alkyl bridged dimer.[57]

Additionally, the identification of the bis-ligated Ni(II) complex [(N^O)$_2$Ni] as the final deactivation product of such nickel alkyl complexes supports the hypothesis of a bimolecular deactivation pathway.[43,58] The study of decomposition pathways for the related anilinotropone system by Jenkins and Brookhart also found the bis-ligated nickel complex as an ultimate product upon heating the corresponding nickel alkyl complex [(N^O)Ni(alkyl)(PPh_3)], which is an important intermediate in the chain growth polymerization.[54] They found a mechanism involving the acid-base reaction of free anilinotropone ligand (N^O)H with the corresponding nickel alkyl complex. The free (*N^O*)-ligand is formed by reductive elimination from the intermediately produced nickel hydride complex (**Scheme 1.6**).

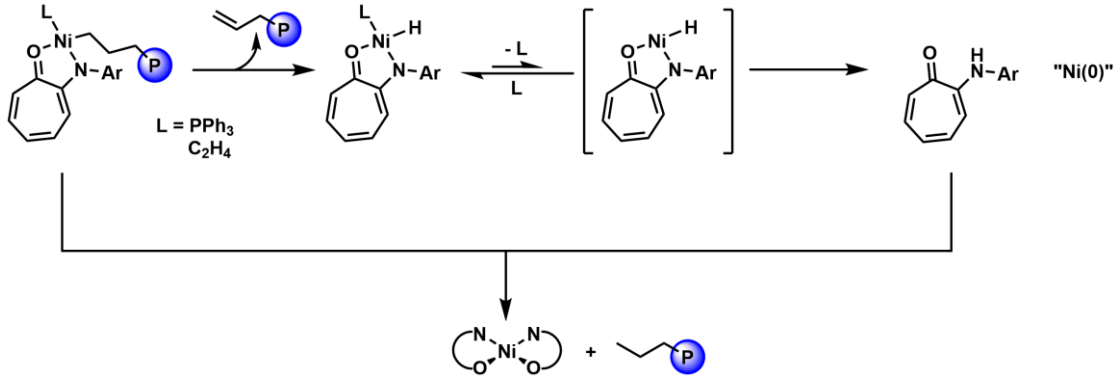

Scheme 1.6: Possible decomposition pathway of anilinotropone Ni(II)-alkyl complexes.[54]

The formation of the bischelated nickel complex also suggests that the steric bulk of the substituents on the ligand plays a key role in suppressing catalyst deactivation.[53] Following this concept, Brookhart and coworkers recently reported the synthesis of "half-sandwich" nickel salicylaldiminato complexes which show very high activities for the polymerization of ethylene to branched ultrahigh-molecular-weight polyethylene in a "quasi-living" fashion (**Figure 1.5**).[59]

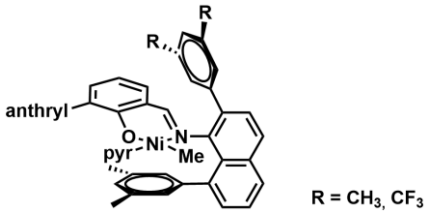

Figure 1.5: "Half-sandwich" salicylaldiminato nickel catalysts.[59]

Investigation of the displacement of pyridine by 4-picoline under pseudo-first order conditions implies that it is clearly associative even in this highly hindered system and it was assumed that the exchange of pyridine by ethylene follows an analogous associative mechanism. This is supported by the finding, that dissociation of pyridine appears to be the rate limiting step of the polymerization and the rate of ethylene insertion in the methyl pyridine precatalyst is much slower than subsequent insertions.

In strong contrast to the trends observed with Brookharts α-diimine system, with Ni(II) salicylaldiminato complexes low molecular weights and high degrees of branching always go along with one another. β-Hydride elimination is the underlying step for both chain transfer and chain walking for these catalyst. However, neither one of those reactions seems to be favored over the other. This makes this class of complexes a unique example of polymerization catalysts in terms of their ability to produce high degrees of branching in a low molecular weight regime. However, these low molecular weight products have found little attention and their exact microstructure including the distribution of different branch lengths has not been investigated in detail.

1.3 Functional Oligomers via Chain Growth on Main Group Metals

In the early 1950s, Ziegler reported the 'Aufbau Reaktion' which is the basis for the synthesis of linear α-olefins.[60] At high temperatures and ethylene pressures chain growth proceeds via repeated insertion of ethylene into the Al-C bond of eg. $AlEt_3$ to produce long-chain aluminum trialkyls. In the Ziegler Process, these linear α-olefins are formed by a subsequent displacement reaction with ethylene (**Scheme 1.7**). Oxidation of the aluminum trialkyls formed in the Ziegler

Process by atmospheric oxygen allows for the synthesis of aluminum trialkoxides to afford linear long-chain alcohols after hydrolysis. This Ziegler alcohol synthesis which is stoichiometric in aluminum was commercialized as the Alfol Process by Conoco in 1962.[61]

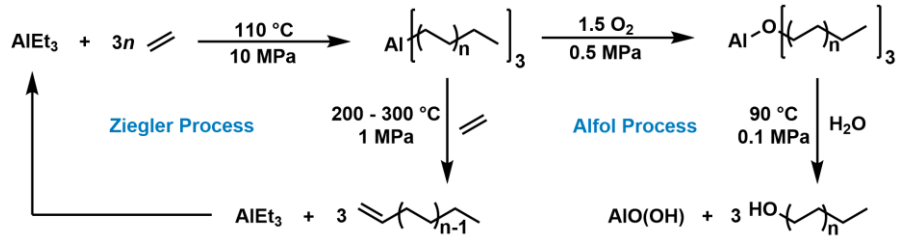

Scheme 1.7: Synthesis of linear α-olefins and alcohols in the Ziegler Process (left) and the Alfol Process (right).[62]

As an alternative to synthesize precisely chain-end functionalized linear oligoethylenes via chain growth on main group metals, the more recent 'chain-shuttling' processes appear attractive.[63-68] Here, the reaction is carried out under mild reaction conditions where the chain growth on the main group metal does not take place and they only serve as chain transfer agents (CTA). A fast and more importantly reversible exchange of alkyl chains between the main group metal and a polymerization active transition metal catalyst allows for a polymerization where the growing chains are almost exclusively rendered dormant on the main group metal (**Scheme 1.8**).

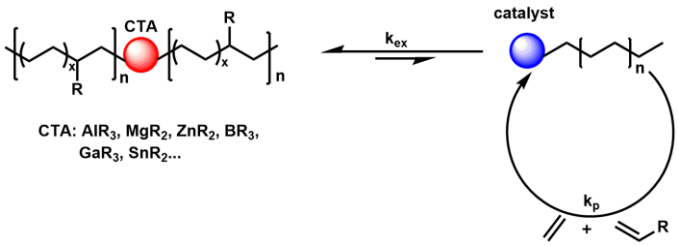

Scheme 1.8: Principle of an ideal catalytic chain growth polymerization with a fast and reversible chain transfer between the CTA and the active catalyst.

If chain exchange is much faster than chain growth ($k_{ex}>>k_p$) for the CCG (catalytiv chain growth), chain termination reactions like β-hydride elimination are completely suppressed, and the polymerization proceeds in a living fashion resulting in a Poisson distribution of the products.[69,70] Since all polymer chains are resting on the chain transfer agent a selective functionalization following the polymerization becomes possible without making the reaction stoichiometric in expensive transition metal catalyst. Depending on the work-up procedure, a range of different functional end groups like alcohols, amines, and even porphyrines are accessible.[68] The molecular weight of polymers produced by such a living polymerization can be

controlled by the polymerization time and is often limited to ~5,000 g mol^{-1} due to precipitation of the main group metal alkyls which prohibits further exchange to the transition metal catalyst. In principle, with this technique, also branched oligomers can be obtained by application of a catalyst that allows for the copolymerization of α-olefins.[66]

2 Scope of the Thesis

Beyond the extensively studied high molecular weight polyethylenes such as HDPE and LDPE, lower molecular weight oligomers are also of practical importance. This is illustrated by the well-established 1-olefins from the Shell higher olefin process, or alcohols from the Ziegler Alfol process. These procedures afford linear, wax-like oligoethylenes. In addition to these linear oligomers, highly branched oligoethylenes, in particular functionalized analogues, are also of interest as functional additives, for example in lubricants or surface modifiers. However, there are very few examples for the synthesis of ethylene oligomers (< 5,000 g mol^{-1}) with high degrees of branching, and such materials have been little characterized and studied. Functionalized and especially precisely monofunctionalized materials have not yet been reported.

Considering possible approaches for the synthesis of hyperbranched oligoethylenes, the known capability of late-transition-metal catalysts to produce highly branched polyethylene appears attractive. Especially neutral Ni(II) κ^2-*N,O*-salicylaldiminato complexes are promising candidates. Depending on the electronic nature of the remote substituents on the bidentate ligand, high-molecular-weight linear polyethylene or low-molecular-weight hyperbranched oligomers are formed. Yet, the exact microstructure of these unique materials has not been studied and the origin of the electronic effect exerted by the remote substituents on the material properties remained elusive.

A special focus of interest of this thesis is dedicated to the detailed investigation of the microstructure of hyperbranched oligomers produced by electron rich Ni(II) κ^2-*N,O*-salicylaldiminato complexes. Exhaustive analysis of the microscopic chain architecture with the distribution of different branch lengths was carried out and its dependence on the oligomerization conditions as well as the catalyst design was studied.

The single unsaturated end group present in every oligomer chain, originating from chain termination via β-hydride elimination, exhibits potential for further functionalization and for the synthesis of monofunctional oligomers. Different reactions for the conversion of these double bonds were investigated regarding their potential for a selective post polymerization functionalization.

For a prospective industrial scale application of these highly branched materials low-cost catalysts would be required. Therefore, a range of catalysts with simplified ligand structures, accessible from inexpensive, commercial compounds was screened regarding their capability to produce similar highly branched products.

In order to investigate the remarkable electronic effect of the remote substituents, systematic modifications on the ligand were carried out. With a series of catalysts bearing coordinating motifs on the ligand, a potential weak interaction of the salicylaldiminato ligand with the nickel center via a hemilabile coordination was studied.

3 Salicylaldiminato Ni(II) Complexes for Ethylene Oligomerization

3.1 Introduction

Beyond the extensively studied high molecular weight polyethylenes, lower molecular weight oligomers are also of practical importance. Remarkably, in strong contrast to their linear analogues, branched ethylene oligomers have found little attention although such materials would be of fundamental as well as practical interest, for example as functional additives in lubricants or surface modifiers.[71-73] This is due to a lack of synthetic accessibility. Well-established processes for the synthesis of oligoethylenes like the Shell Higher Olefin Process or the Ziegler Process only afford linear wax-like products.[62,74]

Considering possible approaches for the synthesis of highly branched analogues, the known capability of late transition metal catalysts to produce highly branched high molecular weight polyethylenes appears attractive. Cationic Pd and Ni α-diimine catalysts can undergo extensive chain walking during polymerization.[14,75] Thus, particularly with the Pd-catalysts, ethylene is polymerized to highly branched, high molecular weight, entirely amorphous rubbery materials. These even possess a hyperbranched structure as indicated by the presence of branch on branch motifs.[14,76,77] For the α-diimine catalysts, bulky substituents on the diimine ligand are responsible for the formation of high molecular weight polymer.[15] Shielding of the apical positions of the square-planar metal centers suppresses chain transfer reactions. At the same time, these bulky substituents also enhance chain growth rates. This has been ascribed to a destabilization of the ground state of the polymeryl ethylene coordinated catalyst resting state.[14,23] Consequently, less bulky substituted Pd diimine catalysts produce lower molecular weight branched oligomers with low activities.[78]

In addition to the low activity being a limitation of these Pd(II) oligomerization catalysts, catalysts based on nickel are often more favorable in terms of abundant availability of the metal and large scale applicability. This is illustrated by the Shell higher olefin process. Here, neutral

Ni(II) catalysts convert ethylene to strictly linear longer α-olefins.[12,36,79] Cationic Ni(II) diimine catalysts lacking bulky *o*-aryl substituents also oligomerize ethylene to the linear α-olefins.[16,29] Thus, for this type of catalyst the synthesis of highly branched material is usually limited to high molecular weights. For the generation of branched oligoethylenes with neutral Ni(II) catalysts, κ^2-(*N,O*)-salicylaldiminato complexes are promising candidates. Complexes with the 2,6-diisopropyl *N*-phenyl motif inspired by the aforementioned diimines polymerize ethylene to moderately branched, high molecular weight material.[41-43,80]

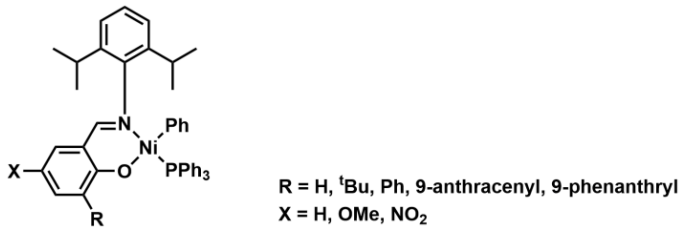

Figure 3.1: Neutral Ni(II) salicylaldiminato complexes with the 2,6-diisopropyl *N*-phenyl motif.

In these complexes, the substituents R and X on the salicylaldiminato ring were found to hardly affect the molecular weight and polymer microstructure but influence the activity of the catalyst (**Figure 3.1**).[42] Bulky groups R in the 3-position enhance the activity of the catalyst and lower the amount of branches in the polymer. Complexes with electron withdrawing substituents in the 5-position (e.g. X = NO_2) also exhibit higher activities.

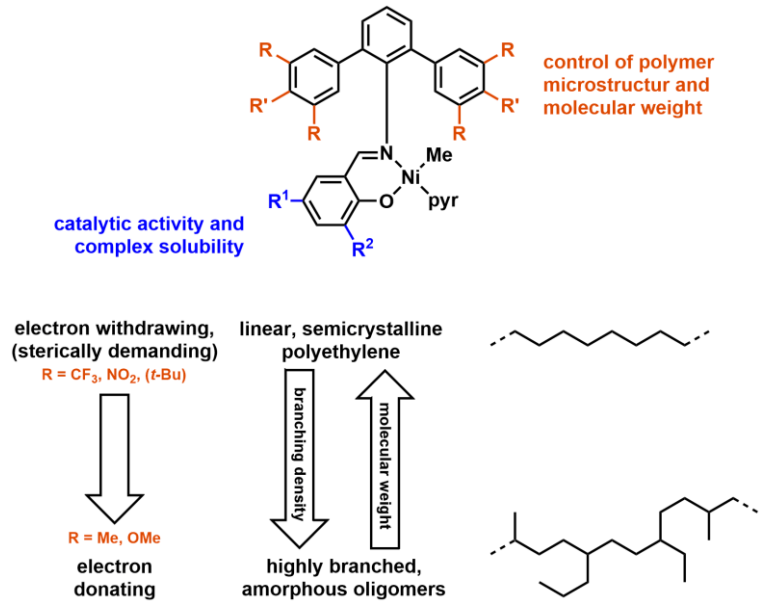

Figure 3.2: Influence of different substituents on the polymerization behavior of neutral Ni(II) salicylaldiminato complexes with *N*-terphenyl motif.

In *N*-terphenyl substituted catalysts, substituents on the peripheral aromatic rings have a remarkable effect on the catalytic properties, despite their remoteness from the active sites

(**Figure 3.2**).[53] Depending on the substituents, high molecular weight linear polyethylene (for R = CF_3, NO_2) or low molecular weight, amorphous, highly branched oligomers (for R = CH_3, OCH_3) are formed. More electron donating substituents favor branch formation and chain transfer, which both occur through ß-hydride elimination as the underlying step.[50-52,81-83]

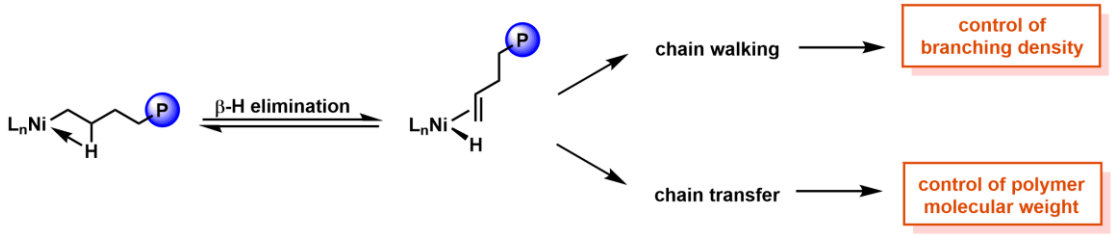

Scheme 3.1: Control of molecular weight and degree of branching after β-hydride elimination by chain walking and chain transfer, respectively.

It is important to note that β-hydride elimination alone must not be confused with chain transfer. From the resulting olefin hydride complex, two separate pathways are accessible: chain walking, which controls the degree of branching, and chain transfer by release of the olefin which controls the polymer molecular weight (**Scheme 3.1**). For example, Ni(II) α-diimine complexes exhibit a high propensity for β-hydride elimination – as evidenced by the high degree of branching of the products – but still afford high molecular weight polymers, since chain transfer is suppressed by the bulky substituents.

The observed influence of the substituents in Ni(II) salicylaldiminato complexes can be related to very similar barriers of ß-hydride elimination ($\Delta G^{\ddagger}_{\beta\text{-elim}}$) and ethylene insertion chain growth ($\Delta G^{\ddagger}_{ins}$).[54] Small relative changes in $\Delta G^{\ddagger}_{\beta\text{-elim}}$ and $\Delta G^{\ddagger}_{ins}$ exerted by the electronics of R can then alter the ratio $\Delta G^{\ddagger}_{ins}/\Delta G^{\ddagger}_{\beta\text{-elim}}$ to a noticeable extent, resulting in the entirely different materials obtained. Aside from the electronic nature of the substituents governing the polymerization behavior, sterics were found to have an additional, smaller influence. This accounts for the semicrystalline polyethylene with an only moderate degree of branching obtained with electron donating R = *t*-Bu substituents.

Hence, Ni(II) salicylaldiminato complexes with electron donating substituents on the *N*-terphenyl moiety present a unique possibility to synthesize high degrees of branching in a low molecular weight regime. Their great versatility allows for the synthesis of a wide range of different materials which lends itself as a basis for the subsequent synthesis of monofunctional hyperbranched oligoethylenes.

3.2 Results and Discussion

Terphenyl amine based Ni(II) salicylaldiminato complexes with electron rich substituents are known to produce highly branched ethylene oligomers. For a detailed investigation of the scope and limitations of these complexes regarding their capability to afford such products, a range of different complexes with electron donating substituents was synthesized and subjected to ethylene oligomerization. Both **^{Me}1-pyr** and **^{OMe}1-pyr** with methyl and methoxy substituents, respectively, have been reported previously.[50] Though **^{OMe}1-pyr** was reported to produce oligomers with slightly higher degrees of branching, **^{Me}1-pyr** was selected as a benchmark complex because of its easier synthetic accessibility. Furthermore, for all investigations nickel methyl pyridine complexes are applied. They are easy to synthesize and pyridine as the labile ligands eliminates the need for a co-catalyst and allows for their application as single-component catalysts.

For all oligomers obtained, a detailed investigation of the microscopic chain architecture is the focus of interest. Furthermore, the dependence of material properties like molecular weight and degree of branching on the reaction conditions is of great interest and can be investigated with temperature and pressure dependent oligomerization studies. New complexes with new electron rich substituents present a straightforward possibility to even further increase the versatility of this catalyst system regarding the range of highly branched, low molecular weight materials accessible. Substituent effects in other positions of the ligand, e.g. *para* to the *N* of the terphenyl amine and different aldehyde building blocks for the ligand synthesis, are also of interest and can give more insight in the catalytic behavior and properties of Ni(II) salicylaldiminato complexes.

3.2.1 Alkyl Substituted Salicylaldiminato Ni(II) Complexes

In previous reports, different complexes with 3,5-dialkyl substituted terphenyl amines (**^{Me}1-pyr** and **^{tBu}1-pyr**, with methyl and *tert*-butyl substituents, respectively) were synthesized and studied as single-component catalysts for the oligomerization of ethylene. Though the *tert*-butyl substituents of **^{tBu}1-pyr** are clearly electron donating, this complex affords semicrystalline polyethylene (11,000 g mol^{-1}) with moderate degrees of branching (38 branches/1,000 C) compared to the highly branched oligoethylene (1,000 g mol^{-1}, 76 branches/1,000 C) obtained with **^{Me}1-pyr** under identical conditions. This was attributed to the steric demand of the *tert*-butyl substituents which has an additional but smaller influence. For more insight on the influence of steric bulk on the oligomerization reaction, the two

complexes ^{Et}**1-pyr** and ^{iPr}**1-pyr** are of special interest. Both bear alkyl substituents that are more electron donating than the methyl substituents in ^{Me}**1-pyr** but introduce much less steric bulk than the *tert*-butyl groups of ^{tBu}**1-pyr**. Therefore they offer potential for the synthesis of oligoethylene with even higher degrees of branching than ^{Me}**1-pyr**.

Synthesis of Alkyl Substituted Salicylaldiminato Ni(II) Complexes

Salicylaldiminato Ni(II) complexes with different alkyl substituents on the terphenyl amine were prepared similar to the procedure reported by us (**Scheme 3.2**).[50] Starting from the different 3,5-dialkyl substituted phenylbromides, the corresponding phenylboronic acids were obtained by lithiation at -78 °C and subsequent addition of $B(OMe)_3$ followed by an acidic work-up. While the methyl and ethyl substituted phenylbromides are commercially available, the *iso*-propyl analog had to be prepared by bromination of 2,6-di-*iso*-propylaniline and a following Sandmeyer type reaction.[84] Terphenyl amines (^{x}**1-NH$_2$**) were prepared by Suzuki coupling of the phenylboronic acids with dibromoaniline. Condensation with 3,5-diiodosalicylaldehyde afforded the salicylaldimine ligands ^{X}**1-N^OH**. Reaction with 1.2 equiv of [(tmeda)NiMe$_2$] and excess pyridine in benzene at ambient temperature yielded the complexes ^{Me}**1-pyr**, ^{Et}**1-pyr** and ^{iPr}**1-pyr**.

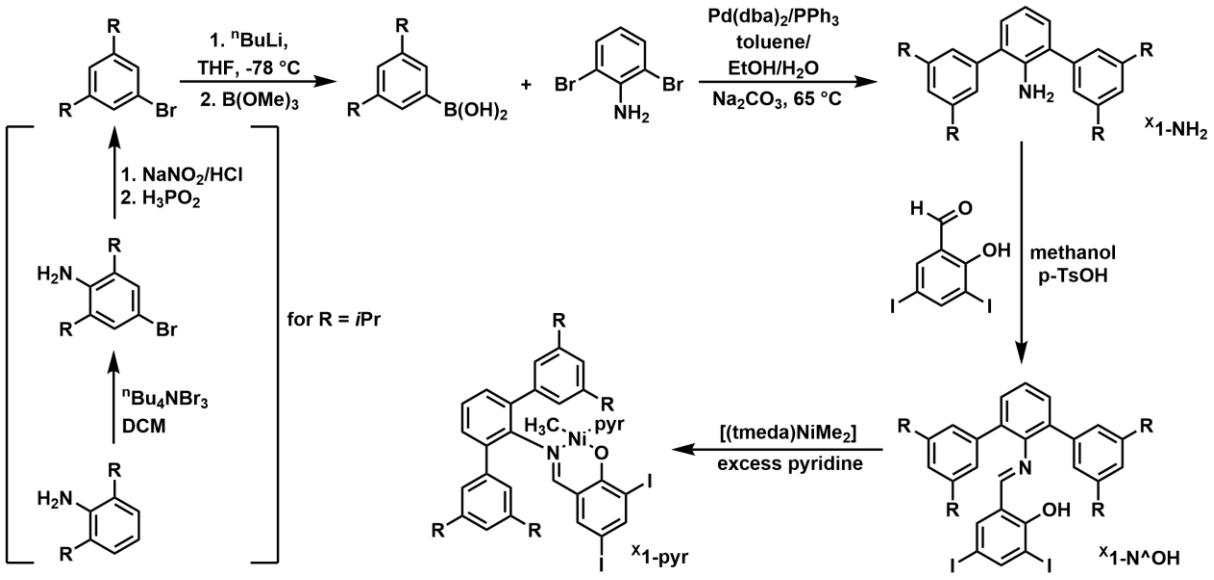

Scheme 3.2: Synthesis route of complexes ^{Me}**1-pyr**, ^{Et}**1-pyr** and ^{iPr}**1-pyr** with different remote alkyl substituents.

Indicative NMR resonances are found at -0.56, -0.54, and -0.54 ppm for the Ni-Me protons for the catalyst precursors ^{Me}**1-pyr**, ^{Et}**1-pyr** and ^{iPr}**1-pyr**, respectively. The presence of only one signal for these groups proves the formation of a single isomer with the imine-N in *trans*-position to the pyridine and the phenolate-O *trans* to the methyl group. A single set of

resonances is observed for all remote substituents R in ^{Me}**1-pyr**, ^{Et}**1-pyr** and ^{iPr}**1-pyr**, giving no evidence of hindered rotation in the terphenyl moiety in solution on the NMR time scale. Complete NMR spectroscopic characterization with complete ^{1}H and ^{13}C assignment of all complexes is provided in Chapter 3.4 Experimental Section. Single crystals of ^{Me}**1-pyr** suitable for X-ray diffraction analysis were obtained within 1 day at -60 °C after layering a solution of the complex (9 mg) in toluene (2 mL) with pentane. The *trans* coordination geometry of the methyl group and the oxygen donor in **Figure 3.3** agrees with the structures of other salicylaldiminato complexes reported.[43,52,53] The deviation of the nickel atom from the root-mean-square plane defined by O1, N1, C35, and N2 amounts to 0.0117(15) Å, which indicates an only minuscule deviation of the coordination geometry of nickel from planarity.

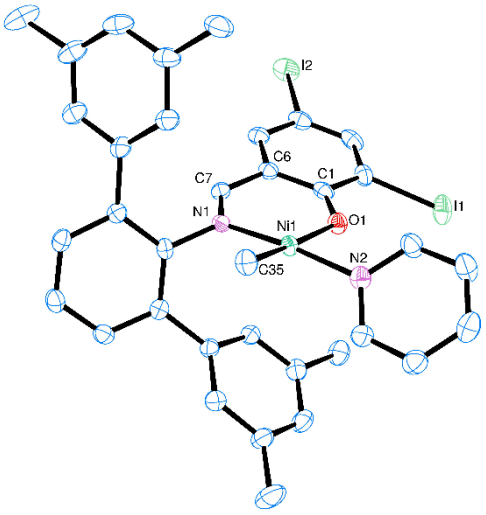

Figure 3.3: ORTEP of complex ^{Me}**1-pyr** with 50 % probability ellipsoids. Hydrogen atoms are omitted for clarity. Figure taken from ref. 85.

Catalytic Oligomerization with ^{Me}1–pyr

Precatalyst ^{Me}**1-pyr** is known to produce low molecular weight oligoethylenes with high degrees of branching (1,100 g mol^{-1}, 76 branches per 1000 carbons at 50 °C and 40 bar of ethylene).[50,53] **Figure 3.4** depicts a typical proton NMR spectrum of a highly branched oligoethylene obtained using ^{Me}**1-pyr**.

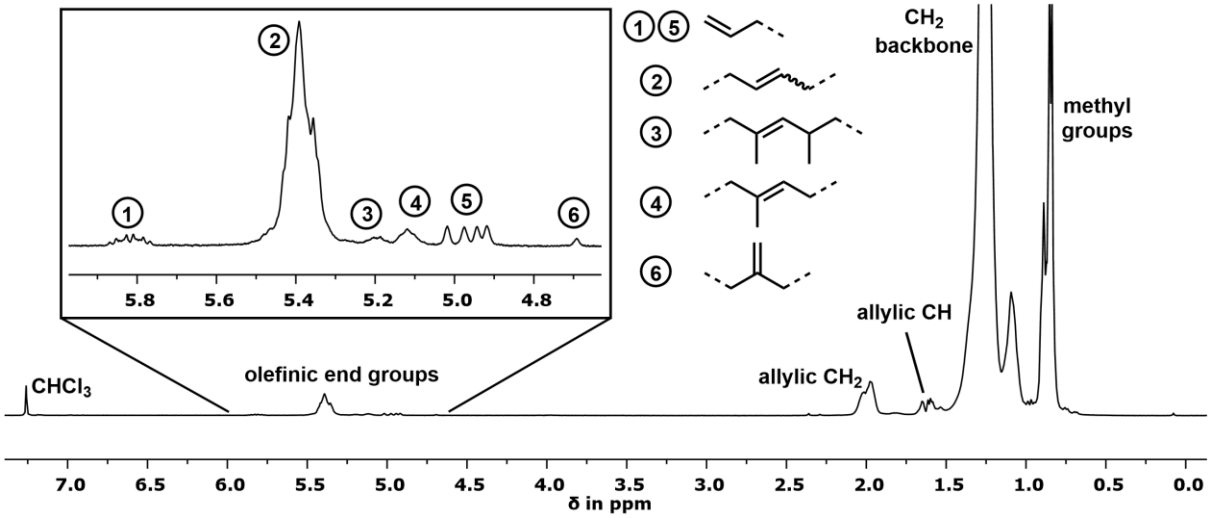

Figure 3.4: Typical ^{1}H NMR spectrum of a highly branched ethylene oligomer.

Considering that every oligomer chain comprises exactly one olefinic end group from chain transfer by β-hydride elimination, the number average molecular weight M_n can be calculated from the relative intensity ratio of the overall integral (I_{tot}) to the integral of the olefinic signals ($I_{2\text{-}6}$) in the proton spectrum with **Equation (3-1)**.[86] A possible route of catalyst deactivation involves reductive coupling of a growing Ni-alkyl species with and Ni-H or another Ni-alkyl. This would result in chains with two saturated end groups. Given that in the oligomerizations studied here several 100 oligomer chains are formed per Ni(II) center, any such deactivation reaction would be negligible in terms of oligomer microstructure and analysis.

$$M_n = \frac{\left(\frac{I_{tot}}{4}\right)}{\left(\frac{I_2 + 2I_3 + 2I_4 + I_5 + I_6}{2}\right)} \cdot 28\,\frac{g}{mol} \qquad \textbf{(3-1)}$$

Additionally, the degree of branching can be calculated from the number of methyl groups per 1,000 carbon atoms which is given by the intensity ratio of the integral of the methyl groups (I_{Me}) to the overall integral (I_{tot}). Note that for such low molecular weight oligoethylenes the amount of methyl groups ($N_{Me\ groups/1000C}$) has to be corrected for methyl groups which do not originate from a branch but from a saturated chain end. Considering the high amount of internal

double bonds in these oligomers (> 80 %), $N_{Me\ groups/1000C}$ was corrected for two methyl end groups for each chain.

$$N_{Me\ groups/1000\ C} = \frac{2 \cdot I_{Me}}{3 \cdot I_{tot}} \cdot 1000 \qquad \textbf{(3-2)}$$

$$N_{branches/1000\ C} = \left[\frac{N_{Me\ groups/1000C}}{1000} \cdot \frac{M_n}{14\ g\ mol^{-1}} - 2\right] \cdot \frac{1000}{M_n} \cdot 14\ g\ mol^{-1} \qquad (3\text{-}3)$$

To study the influence of the reaction conditions on the oligomerization with **^{Me}1-pyr**, the catalyst was subjected to different ethylene pressures from 5 to 30 bar and reaction temperatures between 20 and 70 °C. All polymerization reactions were carried out in a homogeneous toluene solution. The results of all oligomerization runs are listed in **Table 3.1**, and are also depicted in **Figure 3.5**.

Table 3.1: Oligomerization results with complex **^{Me}1-pyr** at different reaction conditions.

entry	p [bar]	T [°C]	yield [g]	TON[a]	M_n (NMR) [g mol^{-1}][b]	M_n (GPC) [g mol^{-1}][c]	M_w/M_n (GPC)[c]	branches /1000 C[d]
1	30	50	54.2	48,400	1,300	2,900	1.7	75
2	25	50	56.6	50,500	1,300	2,600	1.8	75
3	20	50	51.3	45,800	1,300	2,600	1.7	77
4	15	50	45.5	40,600	1,200	2,500	1.7	78
5	10	50	35.0	31,300	1,100	2,500	1.7	78
6	5	50	22.6	20,200	1,000	2,200	1.6	81
7	20	70	12.8	11,400	850	1,800	1.5	80
8	20	60	29.6	26,400	1,000	2,300	1.6	77
9	20	50	51.3	45,800	1,300	2,600	1.7	77
10	20	40	55.0	49,100	1,600	3,500	1.7	77
11	20	30	33.1	29,600	2,100	4,300	1.8	76
12	20	20	13.2	11,800	2,600	5,900	1.7	74

reaction conditions: 40 µmol **^{Me}1-pyr** in 200 mL of toluene for 5 h. [a] TON x mol [C_2H_4] x mol^{-1} [Ni]. [b] molecular weights calculated from ^{1}H NMR intensity ratio of unsaturated end groups vs. overall integral. [c] in THF vs. polystyrene standards. [d] degree of branching calculated from ^{1}H NMR intensity ratio of methyl groups (corrected for saturated end groups) vs. overall integral.

It becomes evident that **^{Me}1-pyr** produces highly branched oligoethylenes independent of the reaction conditions applied. Notwithstanding, the degree of branching of the oligoethylenes decreases with increasing pressure from 81 branches/1,000 C (at 5 bar) to 75 (at 30 bar). This is consistent with the assumption that higher ethylene pressures favor the insertion of a monomer unit, thus suppressing chain walking. This also becomes apparent from the increasing molecular weight at higher pressures. However, this effect is not very pronounced which is why molecular

weights are all in the region of 1,200 g mol^{-1} for a pressure range of 5 to 30 bar. Some mechanistic aspects of the insertion polymerization are discussed in more detail below.

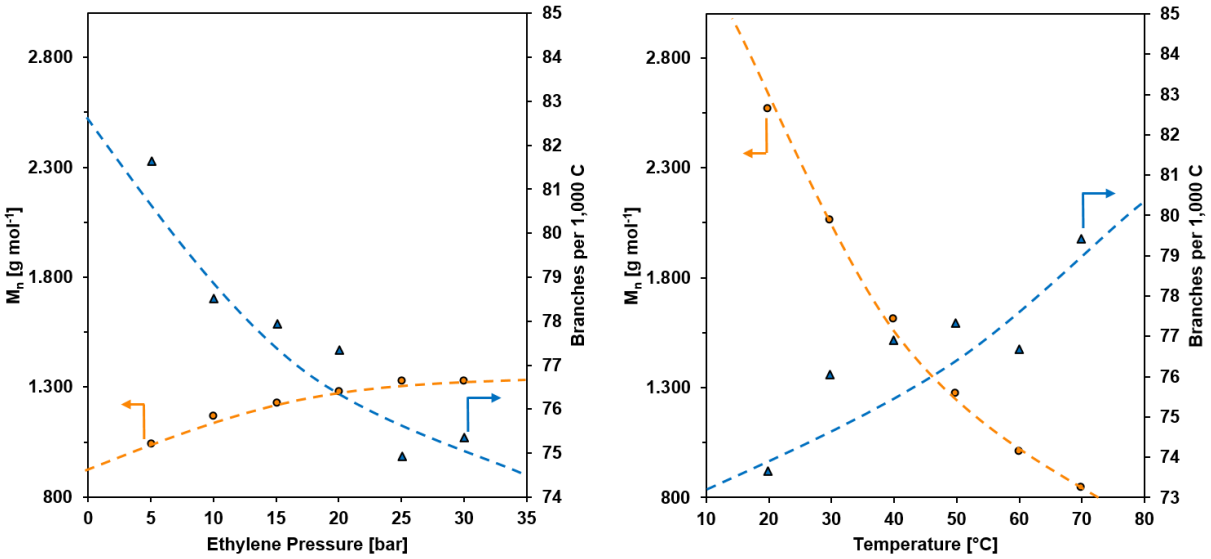

Figure 3.5: Pressure and temperature dependence of the product molecular weights and degrees of branching. Dashed lines are merely a guide to the eye.

The results reveal, that the polymerization temperature has a much more pronounced influence on the molecular weights than the ethylene pressure. At low temperatures, β-hydride elimination is suppressed significantly and therefore a much higher molecular weight of 2,600 g mol^{-1} was obtained at 20 °C. In contrast, at high temperatures, the entropically unfavorable chain growth is reduced, therefore resulting in lower molecular weight oligomers (850 g mol^{-1}). The reaction temperature also influences the degree of branching. Higher degrees of branching are obtained at higher temperatures due to an increase of β-hydride elimination. Overall however, the reaction conditions have a more pronounced effect on the molecular weight of the resulting oligoethylenes than on their degree of branching. In the pressure and temperature range studied, degrees of branching vary only to a small extent from 74 to 81 branches per 1,000 C atoms. All these low molecular weight oligomers are viscous liquids and do not show a melt or crystallization transition during DSC measurements. Furthermore, molecular weight distributions of $M_w/M_n \approx 2$ (Schulz-Flory-Distribution) indicate a well-behaved single-site insertion polymerization behavior. Note that GPC analyses are against polystyrene standards; thus, they only yield apparent molecular weights. As expected, they exceed the true M_n value from NMR spectroscopy, with a ca. 2-fold deviation.

In summary, the degree of branching and the molecular weight of the oligoethylene depend on the reaction temperature as well as on the ethylene pressure (**Figure 3.5**). Generally, at elevated temperatures, lower molecular weight oligomers with higher degrees of branching are

obtained. At the same time, increasing ethylene pressures favor the formation of longer chain products with a more linear structure. This presents an easy to use and straightforward method for fine tuning of the oligomer microstructure by simply adjusting the reaction conditions of the oligomerization. Both low ethylene pressures and high temperatures increase the tendency for β-hydride elimination which is the underlying reaction for branch formation via chain walking as well as for chain termination which controls the molecular weight of the product. This is a major difference to the catalytic behavior observed for Ni(II) α-diimine complexes. For Ni(II) salicylaldiminato catalyst, increasing the tendency for β-hydride elimination always goes along with increased chain walking *and* chain transfer. In contrast, Ni(II) α-diimine complexes also exhibit a high propensity for β-hydride elimination but subsequent chain transfer is hindered by the bulky *ortho*-substituents and only the chain walking pathway is readily accessible. Thus, with the diimine complexes, the high amount of β-hydride elimination does not limit the molecular weight as observed for the salicylaldiminato complexes, but only results in high degrees of branching.

Table 3.1 discloses, that also the oligomer yields are strongly dependent on the reaction conditions. While the activity of the catalyst is generally high, the highest productivity was observed at intermediate pressures (20-25 bar) and slightly elevated temperatures (40-50 °C) with turnover numbers as high as 50,500 mol [C_2H_4]/mol [Ni] (entry 3.1-2, 25 bar at 50 °C). For the variation of ethylene pressure, a clear trend of the oligomer yield can be observed. Higher pressures result in higher catalyst productivities which is attributed to a longer catalyst lifetime due to the higher ethylene concentration in the toluene solution which prevents decomposition in helping to stabilize any three coordinate intermediates present in the catalytic cycle (cf. Mechanistic Considerations, p. 29). The productivity of the catalyst at 50 °C appears to level off at a pressure of 25 – 30 bar. A clear trend for the temperature dependence of the oligomer yield is not visible from the data since two opposing effects are observed. Ethylene mass flow traces reveal that although the activity increases for higher temperatures, significant catalyst degradation occurs, resulting in lower yields (**Figure 3.6**). For low temperatures the activity is significantly reduced, but no observable catalyst decomposition occurred over the 5 h period studied, while at 70 °C the polymerization came to an end after 3 h. Note that the very high initial ethylene uptake is mainly attributable to the saturation of the toluene solution.

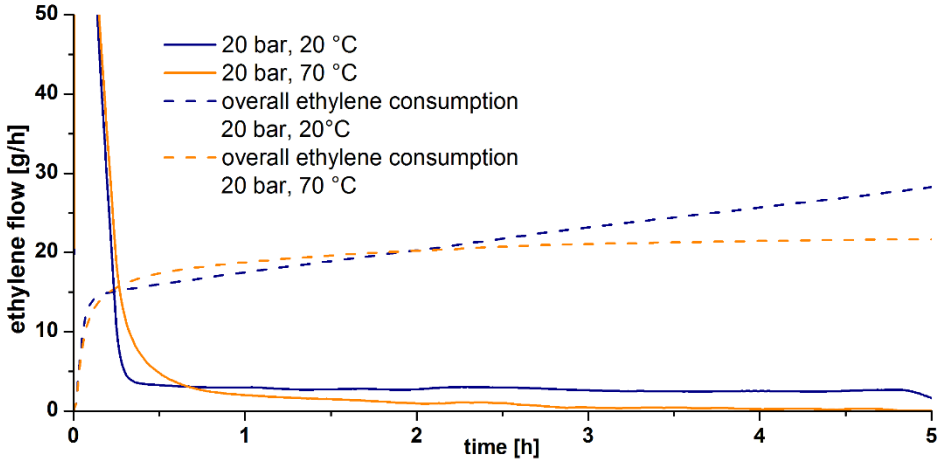

Figure 3.6: Ethylene uptake for selected runs at 20 bar, 20 °C and 20 bar, 70 °C with catalyst ^{Me}**1-pyr**.

Catalytic Oligomerization with ^{Et}1–pyr and ^{iPr}1–pyr

The effect of remote alkyl substituents on the catalyst and its potential utility for fine tuning of the oligomer microstructure was probed by oligomerizations with ^{Et}**1-pyr** and ^{iPr}**1-pyr** as catalyst precursors. For this purpose, similar pressure and temperature dependent oligomerization studies were carried out (**Table 3.2** and **Table 3.3**). In agreement with the findings that the electronic character of the remote substituents governs the polymerization behavior, highly branched oligomers are formed with all of these electron-donating substituents.[51] Both catalysts follow the same temperature and pressure dependent trends described above for precatalyst ^{Me}**1-pyr**. Lower molecular weight oligomers with higher degrees of branching are produced at high temperatures and low ethylene pressures whereas longer chain oligomers with a lower degree of branching are formed at lower temperatures and high pressures. Catalyst activity and stability also follow the same trends mentioned before. The highest productivity was also observed for high pressures (20-35 bar) and slightly elevated temperatures (40-50 °C) for the same reasons. The decrease of productivity when going from 35 to 40 bar is not understood but was also observed for other catalyst systems.[29] A possible explanation could be a decrease in solvent polarity at high ethylene concentrations or catalyst inhibition due to the formation of less active five-coordinate intermediates.[87]

Table 3.2: Oligomerization results with complex ^{Et}**1-pyr** at different reaction conditions.

entry	p [bar]	T [°C]	yield [g]	TOF[a]	M_n (NMR) [g mol^{-1}][b]	M_n (GPC) [g mol^{-1}][c]	M_w/M_n (GPC)[c]	branches /1000 C[d]	T_m [°C]
1	10	40	7.1	6.3	2,300	1,600	1.9	71	-
2	15	40	8.3	7.4	2,500	1,700	2.0	68	-
3	20	40	9.0	8.0	2,600	1,900	1.9	67	-
4	25	40	11.0	9.8	2,600	1,800	2.0	67	-
5	30	40	16.6	14.8	2,400	1,900	2.0	66	-
6	35	40	16.6	14.8	2,600	1,800	2.0	65	-
7	40	40	12.3	11.0	2,500	1,900	2.0	65	-
8	20	20	2.3	2.0	3,700	3,100	2.1	65	70
9	20	30	6.5	5.8	3,000	2,400	2.0	66	67
10	20	40	9.0	8.0	2,600	1,900	1.9	67	-
11	20	50	16.4	14.6	2,000	1,500	1.8	70	-
12	20	60	15.2	13.5	1,500	1,500	1.7	73	-

reaction conditions: 10 µmol ^{Et}**1-pyr** in 100 mL of toluene for 1 h. [a] TOF x 10^4 mol [C_2H_4] x mol^{-1} [Ni] h^{-1}. [b] molecular weights calculated from ^{1}H NMR intensity ratio of unsaturated end groups vs. overall integral. [c] in trichlorobenzene (160 °C) vs. polyethylene standards with linear calibration. [d] degree of branching calculated from ^{1}H NMR intensity ratio of methyl groups (corrected for saturated end groups) vs. overall integral.

Comparison of the two catalysts ^{Et}**1-pyr**, and ^{iPr}**1-pyr** with ^{Me}**1-pyr** shows that higher molecular weight products with lower degrees of branching are obtained under the same reaction conditions when going from methyl to ethyl and isopropyl substituents. Therefore, oligomers with molecular weights of up to 3,700 (65 branches) and 13,300 g mol^{-1} (44 branches) are obtained at 20 bar and 20 °C with precatalyst ^{Et}**1-pyr** and ^{iPr}**1-pyr**, respectively. The sterically demanding substituents probably block the axial positions of the square planar Ni complex since the terphenyl amine group is oriented perpendicular to the NiL_4 plane. This apparently affects chain termination as well as chain walking. Hence, higher molecular weights and lower degrees of branching are obtained. The known smaller influence of the sterics of the substituents is already very pronounced for the ethyl substituted complex. This is surprising considering the only minor increase of steric bulk introduced by the ethyl substituents compared to methyl groups.

Table 3.3: Oligomerization results with complex ^{iPr}**1-pyr** at different reaction conditions.

entry	p [bar]	T [°C]	yield [g]	TOF[a]	M_n (NMR) [g mol^{-1}][b]	M_n (GPC) [g mol^{-1}][c]	M_w/M_n (GPC)[c]	branches /1000 C[d]	T_m [°C]
1	10	40	4.6	4.1	5,600	3,200	1.9	52	77
2	15	40	9.1	8.1	7,200	3,500	1.9	51	79
3	20	40	12.5	11.1	6,300	3,500	2.0	50	80
4	25	40	10.8	9.6	6,100	3,000	2.0	51	79
5	30	40	19.0	17.0	7,600	3,600	2.1	49	81
6	35	40	15.3	13.6	7,400	3,700	2.1	48	82
7	40	40	21.0	18.7	7,300	3,700	2.1	48	82
8	20	20	0.8	0.7	13,300	6,000	2.5	44	88
9	20	30	2.0	1.8	10,100	4,700	2.1	47	84
10	20	40	12.5	11.1	6,300	3,500	2.0	50	80
11	20	50	9.3	8.3	5,100	2,500	2.0	53	77
12	20	60	14.2	12.6	3,300	2,000	1.8	57	71

reaction conditions: 10 µmol ^{iPr}**1-pyr** in 100 mL of toluene for 1 h. [a] TOF x 10^4 mol [C_2H_4] x mol^{-1} [Ni] h^{-1}. [b] molecular weights calculated from ^{1}H NMR intensity ratio of unsaturated end groups vs. overall integral. [c] in trichlorobenzene (160 °C) vs. polyethylene standards with linear calibration. [d] degree of branching calculated from ^{1}H NMR intensity ratio of methyl groups (corrected for saturated end groups) vs. overall integral.

Most of the oligomers obtained with the two sterically more demanding catalysts ^{Et}**1-pyr** and ^{iPr}**1-pyr** are not soluble in THF and chloroform at room temperature which is why high temperature GPC measurements in trichlorobenzene at 160 °C were performed for all oligoethylenes and NMR spectra were recorded in tetrachloroethane at 130 °C with the addition of $Cr(acac)_3$ to facilitate relaxation and ensure reliable integration. While all oligomers produced with ^{Me}**1-pyr** are completely amorphous, some of the oligomers obtained with ^{Et}**1-pyr** and all of those from oligomerizations with ^{iPr}**1-pyr** show distinct melt and crystallization transitions in DSC measurements. However, for all of the semicrystalline materials additional, very broad melting endotherms are observed between -20 and 70 °C. Due to this broad melting transition, determination of crystallinities χ was not possible. Melting transitions for the oligomers of ^{iPr}**1-pyr** are found between 71 and 88 °C. The melting temperature increases for higher molecular weight oligomers with lower degrees of branching (**Table 3.3**).

Mechanistic Considerations based on Experimental Results

The polymerization results also allow for discussion of some mechanistic aspects of the reaction. **Scheme 3.3** depicts the most important intermediates of the catalytic cycle involved in chain propagation, branch formation, and chain transfer reactions. After ethylene insertion, the three coordinate intermediate which is stabilized by a β-agostic interaction of the growing

polymer chain is trapped by the coordination of ethylene. This step is assumed to be associative and strongly dependent on the ethylene concentration. The ethylene polymeryl complex can undergo chain propagation by insertion of ethylene or chain termination by direct transfer to the monomer. Alternatively, from the β-agostic intermediate, β-hydride elimination can occur before trapping by ethylene, resulting in the formation of a hydride olefin complex. This is the key step both for branch formation by chain walking and for chain transfer via associative displacement. It is reasonable to assume that chain transfer is associative in this catalyst system since even for the sterically shielded 'half-sandwich' complex reported by Brookhart *et al.* displacement of pyridine by 4-picoline was shown to occur via an associative mechanism (cf. **Figure 1.5**).[59]

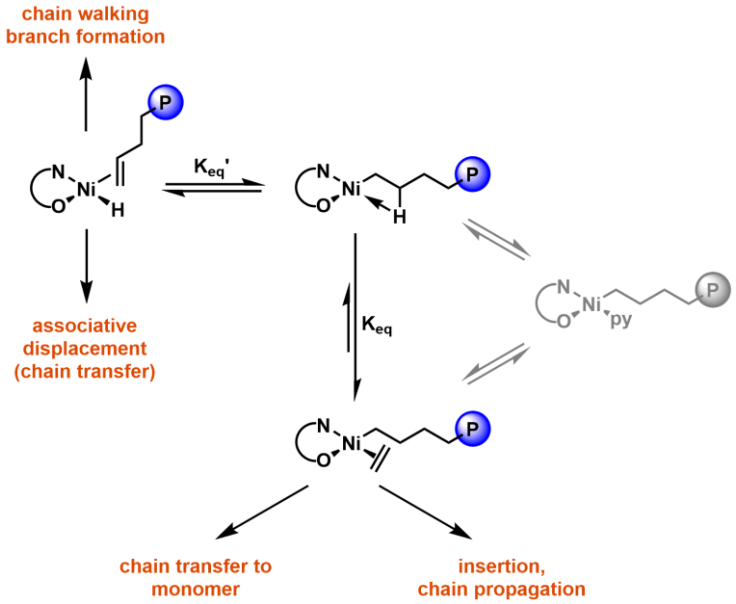

Scheme 3.3: Relevant intermediates during branching insertion polymerization of ethylene.

For nickel α-diimine catalysts, insertion occurs from the ethylene polymeryl resting state and therefore, it is zero-order in ethylene.[9,22] The results in **Table 3.1**, **Table 3.2**, and **Table 3.3** show that for the nickel salicylaldiminato complexes yields are strongly dependent on the ethylene pressure and the insertion is clearly not zero-order in ethylene. At higher pressures of 25 – 30 bar however, the productivity levels off. The high ethylene concentration shifts the equilibrium K_{eq} more to the side of the ethylene polymeryl complex and only at these high pressures saturation kinetics are reached. At lower pressures also the pyridine coordinated complex is a relevant intermediate and pyridine coordination always competes with ethylene coordination (cf. Chapter 3.2.3, p. 44). Molecular weights are controlled by the two possible chain termination reactions. Direct transfer to monomer is the major termination reaction observed in early transition metal catalysis. Although DFT calculations suggest this to be

operative for late transition metal α-diimine complexes, too,[23,26,27] according to experimental data associative displacement after β-hydride elimination appears to be favored.[9] For transfer to the monomer, the molecular weight of the products should be independent of the ethylene pressure since both chain growth and chain transfer occur from the same ethylene polymeryl intermediate. In contrast, for associative displacement after β-hydride elimination, the molecular weights increase at high ethylene pressures since the concentration of the hydride olefin intermediate is also indirectly controlled by the pre-equilibrium K_{eq}. Shifting K_{eq} to the side of the β-agostic complex also increases the concentration of the olefin hydride intermediate via the equilibrium K_{eq}'. The molecular weight of polymers produced by **^{Me}1-pyr**, **^{Et}1-pyr**, and **^{iPr}1-pyr** is very little dependent on the ethylene concentration. It increases only slightly at higher monomer pressures and also levels off once saturation kinetics are reached. The increasing molecular weight clearly suggests a chain termination mechanism involving associative displacement in addition to transfer to monomer. This is in agreement with mechanistic studies showing that for the related nickel anilinotropone system transfer to monomer is not the major chain transfer mechanism.[54] This was reasoned with the strong dependence of the polymer molecular weight on the ethylene concentration. Notwithstanding, the only minor changes in polymer molecular weight with increasing ethylene concentration observed for Ni(II) salicylaldiminato complexes, indicate that transfer to monomer might still play a decisive role.

In contrast, increasing temperatures result in a significant reduction of the molar mass of the oligomers. This can be explained by either one of the two mechanisms. On the one hand, trapping of the β-agostic complex with ethylene is entropically unfavorable and therefore, the pre-equilibrium is shifted to the side of the β-agostic intermediate. As a consequence, β-hydride elimination becomes more dominant and the higher concentration of hydride olefin complex gives rise to both chain transfer and chain walking resulting in the lower molecular weights and higher degree of branching observed. On the other hand, from the ethylene polymeryl complex, chain propagation via ethylene insertion is also entropically unfavorable in contrast to chain termination via transfer to monomer. Consequently, at high temperatures the ratio of reaction rates of the two steps changes in favor of chain transfer and shorter chains are formed.

The influence of sterically demanding substituents on the catalysis with Ni(II) salicylaldiminato complexes is very distinct. The higher molecular weight polymers obtained with **^{Et}1-pyr** and **^{iPr}1-pyr** as compared to **^{Me}1-pyr** can be explained with the suppression of chain transfer reactions since both mechanisms involve an associative displacement of the unsaturated polymer chain by ethylene via a five coordinate transition state (cf. **Scheme 1.3**, p. 5). The bulky substituents block the axial positions of the square planar nickel complex and therefore these coordination sites which are required for chain transfer are not as readily available. Suppression

of chain transfer via associative displacement after β-hydride elimination should favor chain walking and result in higher degrees of branching. However, the opposite is found using ^{Et}**1-pyr** and ^{iPr}**1-pyr** instead of ^{Me}**1-pyr**. Both higher molecular weights and lower degrees of branching could be explained by suppression of β-hydride elimination as the underlying step for chain transfer as well as chain walking. This would suggest that β-hydride elimination involves a sterically crowded transition state and might even occur from the ethylene polymeryl complex via a five coordinate intermediate. For the α-diimine system developed by Brookhart and coworkers, an increased ground state energy of the ethylene polymeryl complex was found to lower the overall barrier for ethylene insertion and is responsible for the high molecular weight polymers obtained with sterically demanding ligands. A faster insertion in sterically demanding complexes would also explain the higher molecular weights and lower degrees of branching for the nickel salicylaldiminato system, though there are no theoretical studies supporting this theory, yet.

In summary, the polymerization results do not allow for a final determination of either one of the two possible pathways for chain termination in nickel salicylaldiminato complexes. The data suggests that most likely both transfer to monomer from the ethylene polymeryl complex as well as associative displacement from the hydride olefin complex are viable routes for chain termination.

Oligomer Microstructure Analysis

Analysis of the unsaturated end groups arising from chain transfer reaction was carried out via ^{1}H NMR spectroscopy. As already shown in **Figure 3.4** (p. 23) the major amount of end groups found in the oligomers are internal double bonds. For all oligomerizations, regardless of the reaction conditions, about 80-90 % of the double bonds are internal RCH=CHR groups and terminal double bonds only amount to 5 %. As an additional end group about 5-10 % of double bonds are located at a branching point resulting in a RCH=C(R)R group. The low amount of terminal end groups is easily explained by the catalysts distinct propensity for chain walking (isomerization) which promotes the formation of the more stable internal olefins. Hence, the ratio of internal to terminal double bonds increases at elevated oligomerization temperatures and low ethylene pressures since these reaction conditions favor β-hydride elimination and therefore chain walking. From the proton NMR spectra it remains unclear whether the internal double bonds are equally distributed over the whole length of the oligomer chains or whether they are located in close proximity to a chain end. This issue will be further illuminated in Chapter 4. A detailed picture of the oligomer microstructure including the distribution of different branch lengths can be gained from the ^{13}C NMR spectra of the oligomers. A special

focus was laid on distinguishing between a highly branched and a hyperbranched microstructure of the oligomers (**Figure 3.7**).

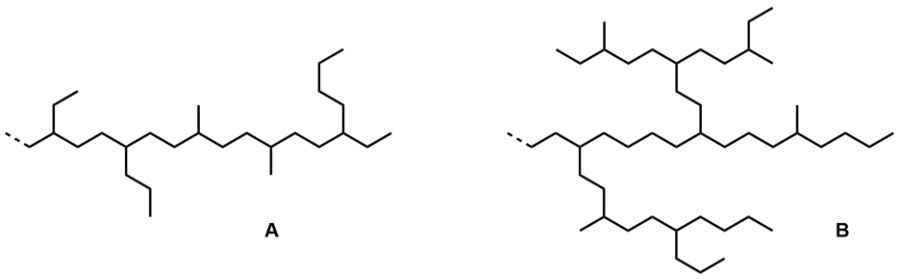

Figure 3.7: Comparison of a highly branched and a hyperbranched polyethylene microstructure.

All signals of the carbon NMR spectra can be assigned to the different carbon atoms belonging to different branches.[76,88-90] **Figure 3.8** depicts a typical ^{13}C NMR spectrum with an assignment of the most important signals using the nomenclature introduced by Randall.[88] All oligomers obtained from oligomerization runs with ^{Me}**1-pyr** not only contain short methyl branches but also ethyl, propyl and butyl branches (or longer).

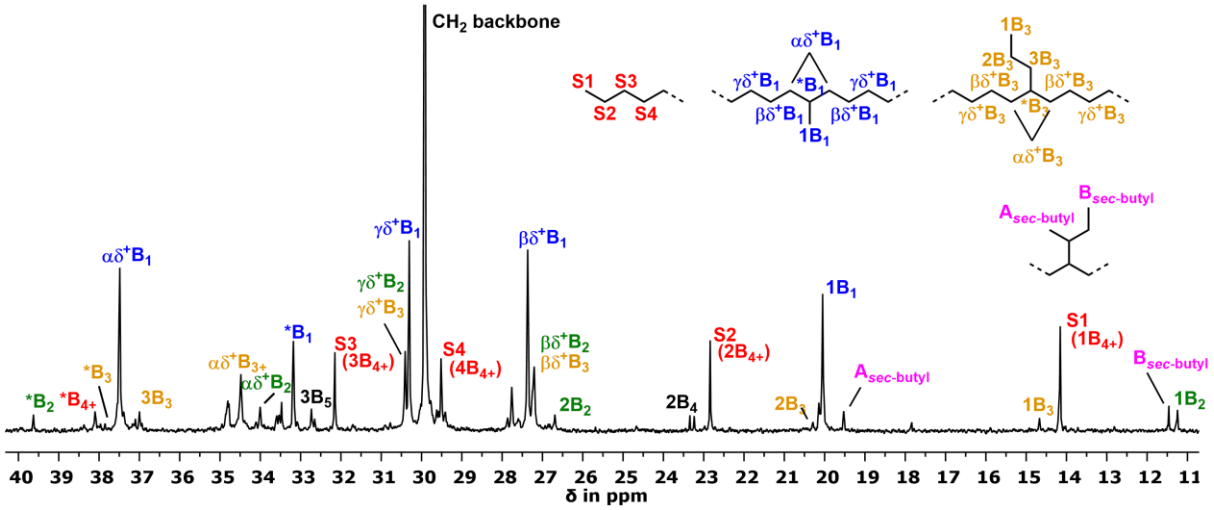

Figure 3.8: Typical ^{13}C NMR spectrum (inverse gated decoupled) of a hyperbranched ethylene oligomer (entry 3.1-8 **Table 3.1**, 1,000 g mol^{-1}, 77 branches/1,000 C). Chain ends are assigned with S_1-S_4. Branches are labeled as xB_y, where y is the branch length and x is the carbon corresponding to the signal, starting from the methyl end with 1. The methine groups for the different branches are labled with $*B_y$. A and B are the methyl groups of a *sec*-butyl branch. Figure taken from ref. 85.

Remarkably, all oligomers obtained with ^{Me}**1-pyr** contain hyperbranched structures. This is clearly evidenced by the presence of significant amounts of *sec*-butyl groups. These groups serve as an important indicator for a hyperbranched structure since they represent the smallest possible and only detectable branch-on-branch motif. Integration of the corresponding signals of the different branches ($1B_1$, $1B_2$, $1B_3$, $B_{sec\text{-}butyl}$, and $*B_{4+}$) gives the fractional amount of different

branch lengths. Branches of four carbon atoms (butyl) and longer cannot be distinguished from one another in the ^{13}C NMR spectra. Therefore, the overall amount of long chain branches (C_{4+}) was calculated. Since the signal $1B_{4+}$ is superimposed by the signal of saturated methyl end groups (S1), $*B_{4+}$ was chosen to calculate the amount of long chain branches.

The results of the detailed microstructure analysis of all oligomers obtained with **^{Me}1-pyr** are listed in **Table 3.4**. Although the oligomers have similar overall degrees of branching (vide supra), their microscopic chain architectures differ significantly. While oligomers obtained at low temperatures or high pressures comprise mainly methyl branches and only low amounts of longer chain branches or branch-on-branch structures, those obtained at higher temperatures and low pressures show significantly reduced amounts of these methyl branches in favor of hyperbranched structures which are found with up to 15 % of all branches. Such hyperbranched chain architectures are unprecedented in this low molecular weight regime and their synthesis presents a unique feature of such electron rich, neutral Ni(II) salicylaldiminato catalysts. Further analysis of the ^{13}C NMR spectra reveals that in all these oligomers the major amount of branches are isolated and have more than four carbon atoms spacing in between each other. Signals for directly adjacent branches are not present. Such branches would have a characteristic signal at 46 ppm in the carbon NMR spectrum.[88] However, these signals are not observed, but there is a minor amount of branches with a C_4-spacer to the next branching point present in the oligomers.

Table 3.4: Microstructure analysis of oligomers obtained with **^{Me}1-pyr** with fractional amount of different branch lengths.[a]

entry	p [bar]	T [°C]	branches /1000 C	methyl[a] [%]	ethyl[a] [%]	propyl[a] [%]	C_{4+}[a] [%]	*sec*-butyl[a] [%]
1	30	50	75	68	12	4	8	7
2	25	50	75	70	9	5	7	9
3	20	50	77	70	10	5	8	8
4	15	50	78	68	11	4	7	11
5	10	50	78	67	10	3	10	10
6	5	50	81	63	10	4	9	14
7	20	70	80	57	14	4	9	15
8	20	60	77	69	7	4	12	8
9	20	50	77	70	10	5	8	8
10	20	40	77	71	8	3	12	6
11	20	30	76	80	6	3	7	4
12	20	20	74	81	5	4	6	4

[a] percentage of different branch lengths can be calculated from relative intensity ratios of the corresponding signals ($1B_1$, $1B_2$, $1B_3$, $*B_{4+}$, B) of the respective branch in the ^{13}C NMR spectrum.

As already observed for the molecular weights, the oligomerization temperature also has a more pronounced influence on the chain architecture than ethylene pressure. Overall, reducing the tendency for chain walking at lower temperatures or high pressures not only decreases the overall degree of branching, but also the average branch length (**Figure 3.9**). These findings show that the molecular weight of an oligomer not only correlates with its overall degree of branching but also with the average branch length. As a result, higher molecular weight oligomers always come with lower branch densities and almost exclusively methyl branches. Beneficially, desirable features such as high degrees of branching and hyperbranched structures as well as low oligomer molecular weights (ca. 1,000 g mol^{-1}) go along with one another.

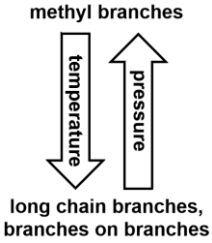

Figure 3.9: Temperature and ethylene pressure dependence of the oligomer microstructure.

Table 3.5: Microstructure analysis of an oligomer obtained with ^{Et}**1-pyr** with fractional amount of different branch lengths.[a]

entry	p [bar]	T [°C]	branches /1000 C	methyl[a] [%]	ethyl[a] [%]	propyl[a] [%]	C_{4+}[a] [%]	*sec*-butyl[a] [%]
1	10	40	71	83	6	3	6	2
2	15	40	68	83	5	3	7	2
3	20	40	67	88	5	3	3	1
4	25	40	67	86	6	3	5	2
5	30	40	66	90	6	2	2	-
6	35	40	65	87	5	3	4	2
7	40	40	65	85	5	3	5	2
8	20	20	65	93	4	1	2	-
9	20	30	66	91	4	2	2	1
10	20	40	67	88	5	3	3	1
11	20	50	70	83	6	3	5	2
12	20	60	73	82	8	3	2	4

[a] percentage of different branch lengths can be calculated from relative intensity ratios of the corresponding signals ($1B_1$, $1B_2$, $1B_3$, $^*B_{4+}$, B) of the respective branch in the ^{13}C NMR spectrum.

The results of the chain architecture analysis of the oligomers obtained with catalysts ^{Et}**1-pyr** and ^{iPr}**1-pyr** are listed in **Table 3.5** and **Table 3.6**, respectively. The chain architecture is also strongly influenced by the remote substituents on the terphenyl amine. Also catalysts ^{Et}**1-pyr**

and **^{iPr}1-pyr** are capable of producing hyperbranched structures as indicated by the presence of *sec*-butyl branches. Notwithstanding, they produce oligomers with distinctly higher percentages of methyl branches (> 80 %) and minor amounts of longer chain branches. *sec*-Butyl branches as indicators for a hyperbranched structure can only be obtained at high reaction temperatures using these two catalysts. This is in accordance with the lower propensity of catalysts with sterically more demanding ligands for β-hydride elimination and chain walking. These findings show that the correlation between the oligomer molecular weight, the degree of branching, and the average branch length is not limited to a given catalyst at different reaction conditions, but also holds true for different catalysts. This allows for precise fine tuning of the oligomer microstructure by choice of the right combination of catalyst and reaction conditions and gives access to a wide variety of different materials.

Table 3.6: Microstructure analysis of an oligomer obtained with **^{iPr}1-pyr** with fractional amount of different branch lengths.[a]

entry	p [bar]	T [°C]	branches /1000 C	methyl[a] [%]	ethyl[a] [%]	propyl[a] [%]	C_{4+}[a] [%]	*sec*-butyl[a] [%]
1	10	40	52	91	5	2	3	-
2	15	40	51	90	5	2	3	1
3	20	40	50	89	4	3	2	2
4	25	40	51	92	4	1	2	1
5	30	40	49	94	4	1	1	0.5
6	35	40	48	94	3	-	3	-
7	40	40	48	94	4	1	1	-
8	20	20	44	95	2	2	1	-
9	20	30	47	95	4	1	0.5	-
10	20	40	50	89	4	3	2	2
11	20	50	53	89	6	2	2	1
12	20	60	57	90	6	1	1	2

[a] percentage of different branch lengths can be calculated from relative intensity ratios of the corresponding signals ($1B_1$, $1B_2$, $1B_3$, $*B_{4+}$, B) of the respective branch in the ^{13}C NMR spectrum.

General Conclusion for Alkyl Substituted Salicylaldiminato Ni(II) Catalysts

Low molecular weight products with an unprecedented hyperbranched microstructure are accessible by oligomerization of ethylene with the Ni(II) salicylaldiminato catalysts presented over a wide range of different reaction temperatures and ethylene pressures. As expected, β-hydride elimination was found to be favored at higher temperatures and low pressures. As a consequence, chain transfer and chain walking are more dominant resulting in lower molecular weight oligomers with a higher degree of branching. In this context, the temperature

dependence of molecular weights and degrees of branching is much more pronounced than the pressure dependence. The dependence of molecular weights and microscopic chain architecture on the oligomerization conditions is a valuable tool for the precise control of these material properties. While catalyst **^{Me}1-pyr** shows a high activity in a broad temperature and pressure range, the highest productivity of up to 50,000 turnovers in 5 hours was found at an intermediate pressure of 25 bar and a slightly elevated temperature of 50 °C.

All catalysts precursors studied, regardless of the nature of remote alkyl substituent, are capable of producing hyperbranched structures, indicated by the presence of *sec*-butyl branches, which are unprecedented in this low molecular weight regime. At high ethylene pressures and low temperature the amount of long chain branches (butyl) and hyperbranched structures (*sec*-butyl) decreases in favor for a higher percentage of methyl branches. Additionally, a correlation between molecular weights, degrees of branching, and the average branch length was found. Desirable features such as high degrees of branching and hyperbranched structures as well as low oligomer molecular weight go along with one another.

In addition to the electronic nature of the remote substituents that mainly governs the polymerization behavior of these nickel catalyst, an additional, smaller influence of sterics was found. Therefore, higher molecular weight oligomers with lower degrees of branching are produced on going from **^{Me}1-pyr**, **^{Et}1-pyr**, to **^{iPr}1-pyr** with methyl, ethyl, and isopropyl substituents, respectively. This effect can already be observed for ethyl substituents which is somewhat surprising, since ethyl groups only present a minor increase in steric bulk compared to methyl groups.

3.2.2 Complexes from *para*-Substituted Anilines

The influence of substituents – electronically and sterically – in different positions of the ligand has been studied in detail for Ni(II) salicylaldiminato complexes. Though the introduction of an additional 3,5-bis(trifluoromethyl)phenyl group in the *para*-position of the terphenyl amine in **^{CF_3}1-pyr** yields a catalyst (**$^{(CF_3pCF_3}$1-tppts, Figure 3.10**) that affords ultrahigh molecular weight polyethylene which is virtually devoid of any branches in the form of ordered PE nanocrystals, the *para*-position of the aniline has been subjected to very little variation otherwise.[81,91]

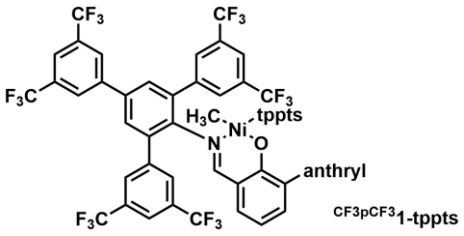

Figure 3.10: Para-substituted complex ^{CF_3pCF_3}**1-tppts** for the synthesis of ideal polyethylene nanocrystals.

To investigate the effect of additional aryl and non-aryl substituents in the *para*-position of the aniline for electron rich nickel salicylaldiminato complexes, a range of new single component catalysts with different *para*-substituents were synthesized and subjected to ethylene oligomerization.

Syntheses of *para*-Substituted Complexes

Both complexes $^{p(Ar\text{-}Me)}$**2-pyr** and $^{p(Ar\text{-}OMe)}$**2-pyr** with additional aryl substituents were obtained following the standard synthesis procedure for nickel salicylaldiminato complexes starting from the corresponding 3,4,5-substituted bromobenzenes (**Scheme 3.4**). Suzuki coupling of their respective boronic acids with 2,4,6-tribromoaniline yielded the *para*-substituted amines ^{pX}**2-NH$_2$**. The salicylaldimines obtained from imine condensation with 3,5-diiodosalicylaldehyde were reacted with [(tmeda)NiMe$_2$] in the presence of excess pyridine to yield the desired Ni(II) salicylaldiminato complexes $^{p(Ar\text{-}Me)}$**2-pyr** and $^{p(Ar\text{-}OMe)}$**2-pyr**.

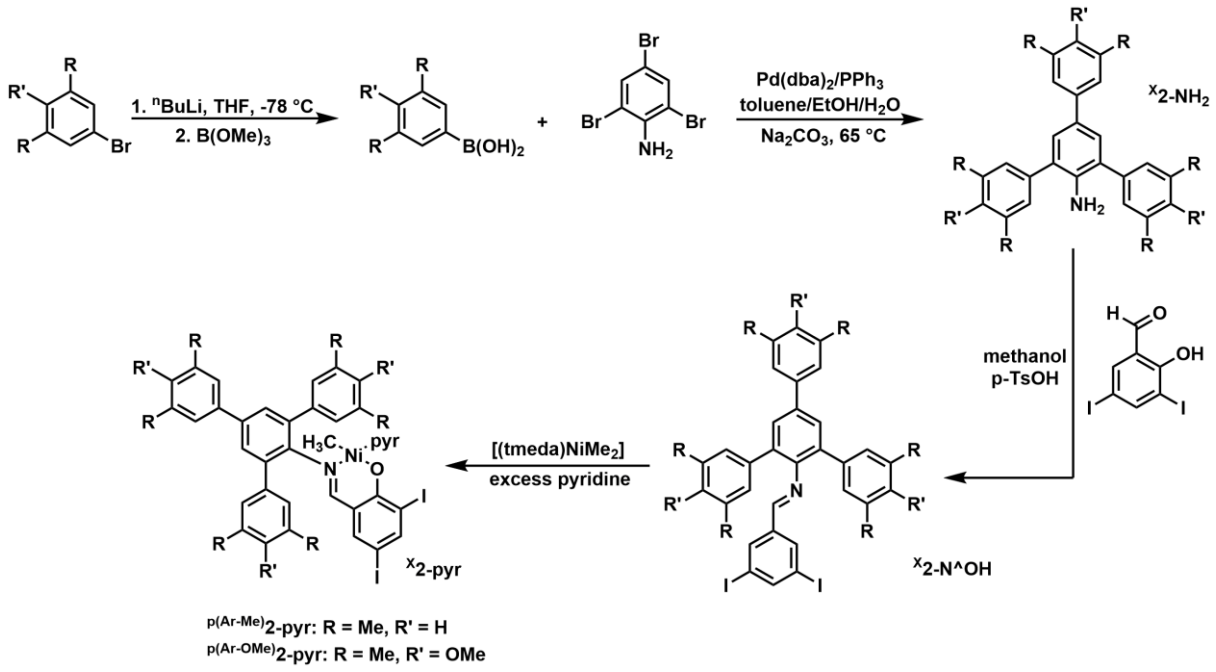

Scheme 3.4: Synthesis procedure for *para*-aryl substituted complexes $^{p(Ar\text{-}Me)}$**2-pyr** and $^{p(Ar\text{-}OMe)}$**2-pyr**.

Detailed synthetic procedures and complete NMR spectroscopic characterization of all products is provided in Chapter 3.4 Experimental Section. The known terphenyl amine based catalyst without *para*-aryl substituent ^{MeOMe}**1-pyr** was synthesized according to a reported procedure for comparison to the results obtained with its *para*-substituted analogue.[50]

Additionally, complexes with different non-aryl *para*-substituents (-OMe, -NMe_2, -Me, -F) were synthesized starting from 3,5-dimethylphenylboronic acid and the corresponding *para*-substituted 2,6-dibromoaniline.

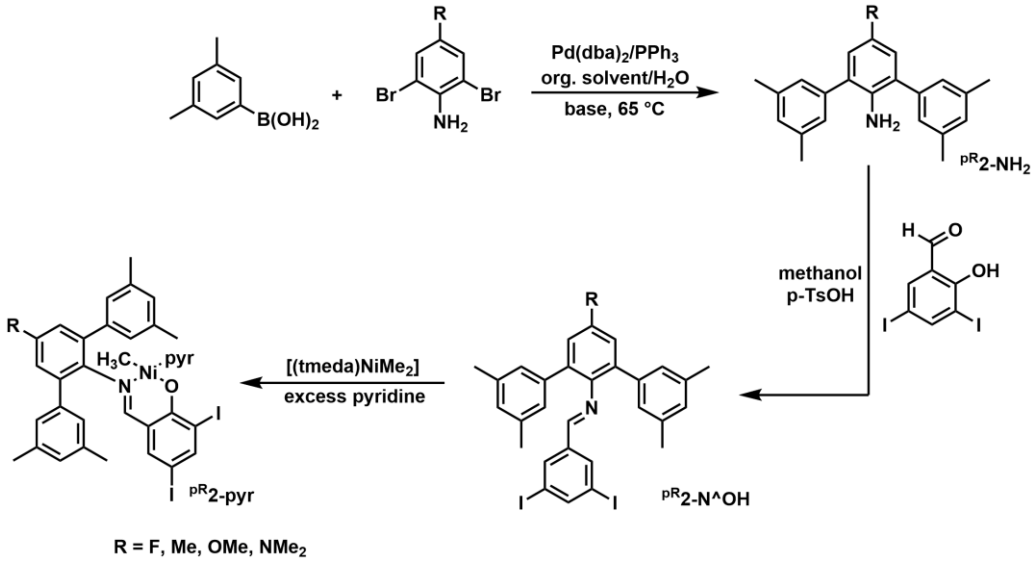

Scheme 3.5: Synthesis procedure for *para*-R substituted complexes ^{pR}**2-pyr**.

While 2,6-dibromo-4-methylaniline and 2,6-dibromo-4-fluoroaniline are commercially available, 2,6-dibromo-4-methoxyaniline and 2,6-dibromo-4-(dimethylamino)aniline were synthesized following literature procedures.[92,93] For R = OMe, Me, and F, the same reaction sequence of Suzuki coupling, imine condensation, and complexation described before yielded the desired Ni(II) salicylaldiminato complexes ^{pR}**2-pyr** in high purity. Detailed synthetic procedures and complete NMR spectroscopic characterization of all products are provided in the Experimental Section. ^{pF}**2-pyr** was provided by Inigo Göttker-Schnetmann and was synthesized following the same procedure. Clean complex ^{pNMe2}**2-pyr** could not be obtained by reaction of the ligand ^{pNMe2}**2-N^OH** and [(tmeda)$NiMe_2$] after several attempts. The presence of signals for the Ni-*Me* group at -0.43 ppm in the ^{1}H NMR spectra of the orange reaction product indicates that complex formation occurs in general but all signals are broadened significantly and multiple species are present. Therefore, ^{pNMe2}**2-pyr** was not subjected to ethylene oligomerization.

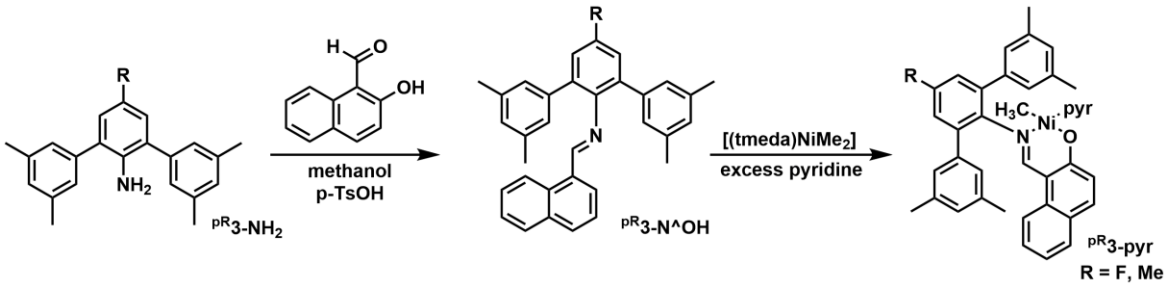

Scheme 3.6: Synthesis of 2-hydroxynaphthaldehyde based complexes.

Additionally, the influence of the aldehyde moiety on the oligomerization behavior of Ni(II) salicylaldiminato complexes was investigated with two complexes based on 2-hydroxynaphthaldehyde (**Scheme 3.6**). This aldehyde building block was chosen to substitute 3,5-diiodosalicylaldehyde due to its cheap and abundant availability (also cf. Chapter 5).

The imine condensation of the same terphenyl amines with 2-hydroxynaphthaldehyde yielded the two salicylaldimines **^{pF}3-N^OH** and **^{pMe}3-N^OH** in excellent yields (> 90 %). Subsequent reaction with [(tmeda)NiMe$_2$] in the presence of excess pyridine resulted in the clean formation of the desired Ni(II) methyl pyridine complexes **^{pF}3-pyr** and **^{pMe}3-pyr** (yield > 90 %).

Ethylene Oligomerization with *para*–Substituted Aniline Based Complexes

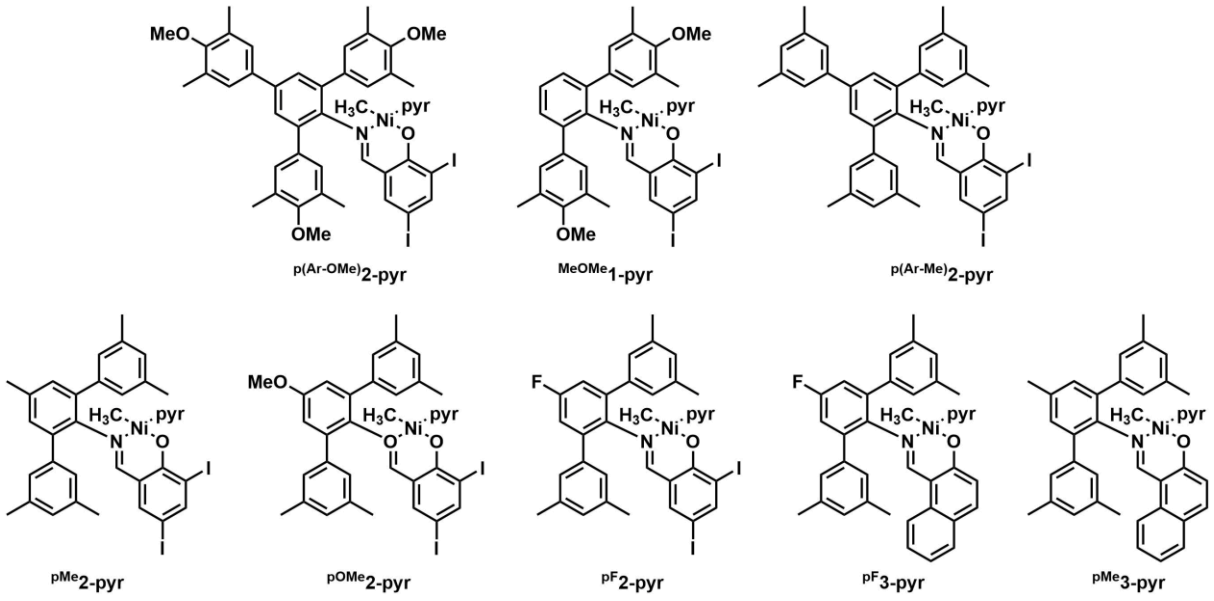

Figure 3.11: New *para*-substituted Ni(II) salicylaldiminato complexes used in ethylene oligomerization studies.

An overview of the complexes studied for the investigation of substituent effects in the *para*-position of the aniline is given in **Figure 3.11**. Catalyst precursors **^{MeOMe}1-pyr** with electron

donating methyl and methoxy substituents had already been reported and is known to produce highly branched low molecular weight ethylene oligomers.[50] For comparison with $^{p(Ar\text{-}OMe)}$**2-pyr** and quantification of the influence of the *para*-aryl substituent of the latter, ^{MeOMe}**2-pyr** was also subjected to ethylene oligomerization at different temperatures and ethylene pressures. For the top three complexes in **Figure 3.11** (^{MeOMe}**1-pyr**, $^{p(Ar\text{-}OMe)}$**2-pyr**, and $^{p(Ar\text{-}Me)}$**2-pyr**), complete pressure and temperature dependent investigation of the oligomerization behavior was carried out. All detailed polymerization results including microstructure analyses are listed in Chapter 3.4.5 Additional Spectra and Data. Oligomer yields, molecular weights, degrees of branching and average branch lengths of polymers obtained with a given catalyst follow the same trends for the pressure and temperature dependence which were disclosed earlier. Here, only the general effects of *para*-substituents and differences between the eight complexes are discussed. Exemplary results of oligomerization runs carried out with the different catalysts at an ethylene pressure of 20 bar at 60 °C are listed in **Table 3.7**.

Comparison of entry 3.7-1 vs. 3.7-2 and 3.7-3 vs. 3.7-4 shows that all four complexes ^{Me}**1-pyr**, $^{p(Ar\text{-}Me)}$**2-pyr**, ^{MeOMe}**1-pyr**, and $^{p(Ar\text{-}OMe)}$**2-pyr** yield similar products in terms of their molecular weights (900 – 1,000 g mol^{-1}) and overall degrees of branching (77 – 81 branches per 1,000 C). At 60 °C and 20 bar ethylene pressure, the *para*-aryl substituted complex $^{p(Ar\text{-}Me)}$**2-pyr** produces a slightly more branched oligomer compared to the benchmark catalyst ^{Me}**1-pyr**. The detailed oligomerization results in the Experimental Section confirm this observation. Though the molecular weights and degrees of branching of the products are in the same range as those of oligomers obtained with ^{Me}**1-pyr**, complex $^{p(Ar\text{-}Me)}$**2-pyr** allows for the synthesis of oligoethylenes with higher branch content at the same molecular weight (cf. **Table 3.15**, p. 74). For example, oligomers with 1,200 g mol^{-1} containing 77 and 81 branches per 1,000 carbon atoms are obtained with ^{Me}**1-pyr** and $^{p(Ar\text{-}Me)}$**2-pyr**, respectively. However, the influence of the additional aryl moiety on the ligand is very subtle. Comparison of complexes ^{MeOMe}**1-pyr** and $^{p(Ar\text{-}OMe)}$**2-pyr** (entries 3.7-3 and 3.7-4) even shows an almost negligible effect of the *para*-aryl substituent not only on the molecular weight and overall branch content but also on the microscopic chain architecture of the oligomer. Under these conditions, both complexes produce virtually the same product.

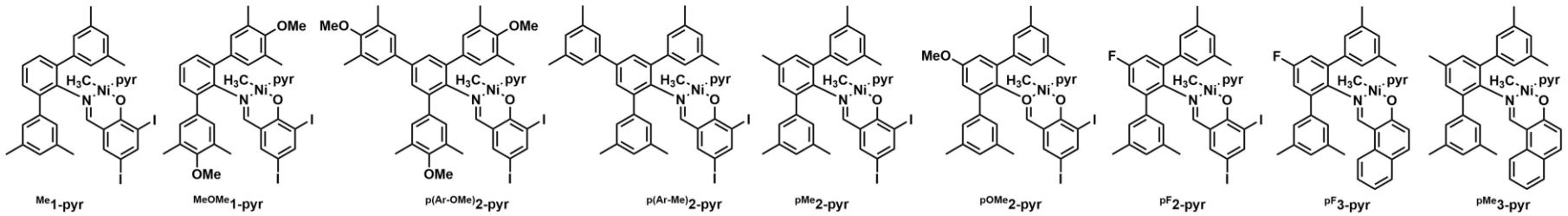

Table 3.7: Oligomerization results for complexes with different substituents in *para*-position of the aniline.

entry	catalyst	reaction conditions	yield [g]	TON[a]	M_n (NMR) [g mol^{-1}][b]	M_n (GPC) [g mol^{-1}][c]	M_w/M_n (GPC)[c]	branches /1000 C[d]	methyl[e] [%]	ethyl[e] [%]	propyl[e] [%]	C_{4+}[e] [%]	*sec*-butyl[e] [%]
1	^{Me}**1-pyr**	**1**	82.2	24,400	**1,000**	2,300	**1.6**	77	69	7	4	12	8
2	$^{p(Ar\text{-}Me)}$**2-pyr**	**2**	4.9	17,500	**900**	2,100	**1.6**	81	64	11	3	13	9
3	^{MeOMe}**1-pyr**	**2**	3.0	10,700	**900**	2,100	**1.5**	81	65	11	3	10	11
4	$^{p(Ar\text{-}OMe)}$**2-pyr**	**2**	5.0	17,900	**900**	1,900	**1.5**	81	66	11	3	8	13
5	^{pMe}**2-pyr**	**2**	6.1	21,800	**900**	1,700	**1.8**	79	72	11	3	6	8
6	^{pOMe}**2-pyr**	**2**	1.1	2,000	**1,000**	1,600	**1.9**	82	69	9	4	8	9
7	^{pF}**2-pyr**	**1**	90.0	26,800	**1,000**	-	-	74	68	11	4	7	10
8	^{pMe}**3-pyr**	**1**	35.1	10,400	**2,200**	-	-	88	59	12	5	15	8
9	^{pF}**3-pyr**	**1**	65.3	19,300	**2,500**	4,400	**2.1**	88	57	14	8	14	7

reaction conditions: **1:** 120 µmol of Ni complex in 600 mL of toluene, 20 bar ethylene, 60 °C for 3 h; **2:** 10 µmol of Ni complex in 100 mL of toluene, 20 bar ethylene, 60 °C for 1 h; [a] TON x mol [C_2H_4] x mol^{-1} [Ni]. [b] molecular weights calculated from ^{1}H NMR intensity ratio of unsaturated end groups vs. overall integral. [c] in THF vs. polystyrene standards. [d] degree of branching calculated from ^{1}H NMR intensity ratio of methyl groups (corrected for saturated end groups) vs. overall integral. [e] percentage of different branch lengths can be calculated from relative intensity ratios of the corresponding signals ($1B_1$, $1B_2$, $1B_3$, $*B_{4+}$, B) of the respective branch in the ^{13}C NMR spectrum.

Also the methyl and methoxy substituent in **^{pMe}2-pyr** and **^{pOMe}2-pyr** (entries 3.7-5 and 3.7-6), respectively, have little influence on the resulting polymer properties. The molecular weights are the same compared to the benchmark catalyst und both oligomers have only slightly higher degrees of branching and the distribution of different branch lengths is also unaltered. Surprisingly, **^{pOMe}2-pyr** is significantly less active (an order of magnitude) than all other complexes tested in this study.

The only significant effect of a *para*-substituent was found for the *para*-fluorine substituted complex **^{pF}2-pyr**. While fluorine also does not affect any properties of the resulting oligomer the fluorine substituent appears to increase the activity of the catalyst. Under exactly identical reaction conditions, **^{pF}2-pyr** yields 10 % more oligomer material than **^{Me}1-pyr**. Thus, this is the most active Ni(II) salicylaldiminato complex tested in this thesis capable of producing highly branched and low molecular weight ethylene oligomers.

Substitution of 3,5-diiodosalicylaldehyde by 2-hydroxynaphthaldehyde in **^{pMe}3-pyr** results in the formation of significantly higher molecular weight oligomers (entry 3.7-8: 2,200 g mol^{-1} vs. 900 g mol^{-1} with **^{pMe}3-pyr**). At the same time, the oligomer exhibits a significantly higher amount of branches (88 per 1,000 C) and a different microstructure. The catalyst based on naphthaldehyde appears to have a higher propensity for chain walking which is not only displayed by the higher overall degree of branching but also by the reduced amount of methyl branches in favor of longer chain alkyl branches. The amount of C_{4+} branches is doubled and they represent up to 15 % of all branches present in the oligomer. This microstructure with a much longer average branch length is a unique feature of nickel naphthaldiminato complexes. However, a major drawback of **^{pMe}3-pyr** is its much lower productivity compared to its 3,5-diiodosalicylaldehyde based analogue **^{pMe}2-pyr** (10,400 vs. 21,800 turnovers). This can be compensated for with a *para*-fluorine substituent on the aniline which was found to enhance the activity. Indeed, complex **^{pF}3-pyr** (entry 3.7-9) produces twice as much oligomer material compared to **^{pMe}3-pyr**. As expected from the earlier findings, the microstructure (molecular weight, degree of branching, and average branch length) is not affected significantly by this replacement of the *para*-substituent. Additional 2-hydroxynaphthaldehyde based complexes were investigated in Chapter 5. Oligomerization studies confirm that all these complexes are prone to chain walking and favor the formation of long chain branches.

In summary, apart from the higher activity of **^{pF}2-pyr** and **^{pF}3-pyr**, substitution of the *para*-position has very little influence on the catalytic behavior of nickel salicylaldiminato complexes. While it basically does not affect the molecular weight and the microscopic chain architecture of the resulting oligomer at all, only minor increases of the overall degree of branching were observed with all *para*-substituted complexes.

3.2.3 Optimization of the Oligomerization Procedure

From the evaluation of the mass flow data collected for all the oligomerization reactions presented above, it becomes obvious that the performance of all catalysts studied follows a general trend. The catalysts generally exhibit a very high activity at the beginning of the oligomerization. This is followed by a rapid decrease of ethylene uptake due to catalyst decomposition. The fast deactivation at the beginning of the reaction can be attributed to different reasons. First, it was shown that one major reaction for catalyst decomposition follows a bimolecular pathway involving the reaction of a nickel hydride complex with a nickel alkyl species (**Scheme 1.5**, p. 10).[55] At the high initial catalyst loadings, such bimolecular deactivation reactions would be favored. A second reason for catalyst decomposition could be a limitation arising from the applied polymerization procedure during which the catalyst is added to the reactor followed by pressurization with ethylene. Throughout saturation of the toluene solution with ethylene at the beginning, the ethylene pressure and concentration is very low and due to the high solubility of ethylene, it takes up to 15 minutes to reach the desired ethylene concentration in solution. As shown above, the catalyst exhibits a much lower stability at such low pressures. Furthermore, the saturation of toluene with ethylene is an exothermic process and results in a significant increase of temperature of up to 20 K. Especially the combination of low pressures and high temperatures present during pressurization leads to a low catalyst stability. As discussed before, both favor β-hydride elimination and therefore result in more chain walking and chain transfer. Thus, the concentration of the hydride nickel complex is possibly increased which is prone to deactivation and an important intermediate for the bimolecular deactivation pathway.

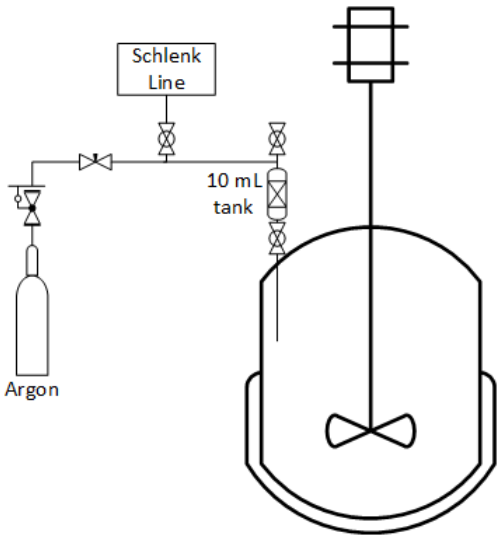

Figure 3.12: Flow chart of the pressure burette used. All other fittings of the reactor are omitted for clarity.

Consequently, saturation of the toluene solution with ethylene prior to the catalyst addition would be beneficial to suppress catalyst deactivation at this early stage since it prevents the initial temperature increase as well as the low ethylene concentrations. Such ethylene saturation of the reaction mixture prior to polymerization was achieved by use of a custom made pressure burette (**Figure 3.12**). The burette allows for addition of catalyst under an inert atmosphere against internal pressures of the reactor of up to 60 bar. Moreover, with the pressure burette, additional catalyst can be added during the polymerization and the actual ethylene uptake can be monitored over the whole period of time without corruption due to saturation of toluene. The results of oligomerization runs conducted with addition of catalyst **^{Me}1-pyr** via the pressure burette are listed in **Table 3.8** (entries 3.8-2 to 3.8-4).

Table 3.8: Oligomerization results with catalyst addition via the pressure burette.

entry	t [h]	^{Me}1-pyr [µmol]	yield [g]	TON[b]	TOF[c]	M_n (NMR) [g mol^{-1}][d]	branches/ 1,000 C[e]
1[a]	5	120	75	22,300	4,460	1,000	75
2	5	120	71	21,100	4,200	1,000	77
3	5	5 x 24	54	16,100	5,300	1,000	76
4	8.3	5 x 24	100	29,800	5,960	1,000	77

reaction conditions: 600 mL toluene, 20 bar ethylene, 60 °C. [a] conventional addition of catalyst and subsequent saturation with ethylene [b] TON x mol [C_2H_4] x mol^{-1} [Ni]. [c] TOF x mol [C_2H_4] x mol^{-1} [Ni] h^{-1}. [d] molecular weights calculated from ^{1}H NMR intensity ratio of unsaturated end groups vs. overall integral. [e] degree of branching calculated from ^{1}H NMR intensity ratio of methyl groups (corrected for saturated end groups) vs. overall integral.

The data of entry 3.8-1 is listed as comparison and was collected from an oligomerization carried out by conventional addition of catalyst without pressure burette followed by pressurizing the reactor with toluene. Adding the catalyst via the pressure burette after pressurizing the reactor with 20 bar of ethylene surprisingly resulted in a slightly lower oligomer yield of 71 g (entry 3.8-2) instead of 75 g while the material properties like molecular weight and degree of branching remain unaffected. The decrease in productivity is probably due to the construction of the burette. Although it was rinsed with additional toluene, quantitative addition of all the catalyst solution could not be accomplished. The time resolved ethylene uptake of entry 3.8-2 is depicted in **Figure 3.13**.

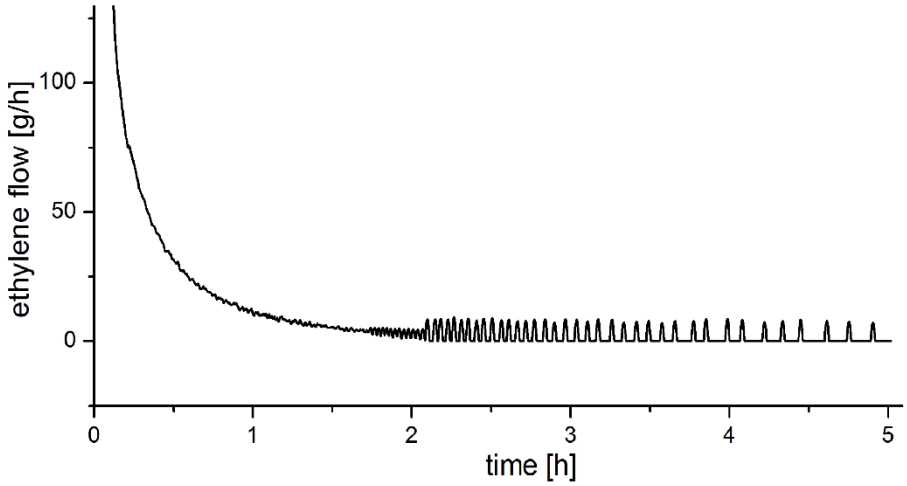

Figure 3.13: Ethylene uptake during a polymerization with ^{Me}**1-pyr** (20 bar, 60 °C) with addition of catalyst (120 µmol) via pressure burette after saturation with ethylene.

The catalyst exhibits a very high activity at the beginning of the reaction which indicates a relatively rapid activation under the conditions studied. Despite the saturation with ethylene prior to catalyst addition, this is followed by a rapid decrease during the first 30 minutes due to irreversible catalyst deactivation. Therefore, the saturation with ethylene prior to catalyst addition is not able to increase the productivity by suppressing catalyst deactivation. Still, the catalyst decomposition is very fast at the beginning. This might be explained by the high initial catalyst loading which favors bimolecular deactivation pathways. In additional experiments the average catalyst loading was reduced by addition of the same overall amount of ^{Me}**1-pyr** (120 µmol) in smaller portions over time (entry 3.8-3). The oligomerization was started with the addition of 24 µmol of catalyst and additional 24 µmol were added every 60 minutes over a period of 5 hours total. The resulting ethylene uptake of the reaction is depicted in **Figure 3.14**.

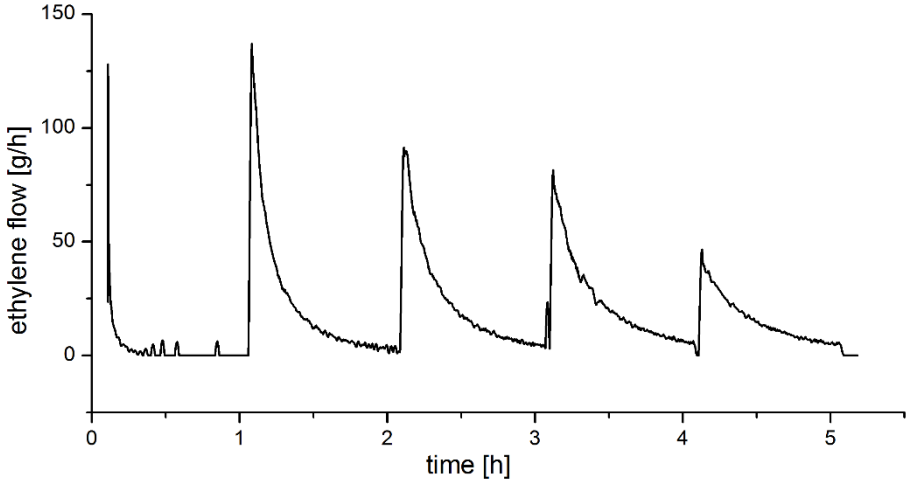

Figure 3.14: Ethylene uptake with subsequent addition of ^{Me}**1-pyr** in 5 portions of 24 µmol over a period of 5 hours (20 bar, 60 °C).

In this experiment 54 g of oligomer material was obtained which corresponds to a productivity of TON = 16,100 mol [C_2H_4]/mol [Ni] and an activity of TOF = 5,300 mol [C_2H_4]/mol [Ni]. Note that despite the lower productivity, the activity is 25 % higher with the stepwise addition due to a shorter average residence time of the catalyst in the reactor (3 hours). Addition of catalyst every 100 minutes over a period of 8.3 hours, which resembles an average residence time of 5 hours, resulted in a 43 % increase in productivity as well as activity with the same amount of catalyst (entry 3.8-2). These findings show that catalyst deactivation can be effectively reduced by reducing the amount of catalyst via a stepwise addition over the course of the reaction.

For both experiments with a stepwise addition of ^{Me}**1-pyr**, the deactivation of the first 24 µmol of catalyst is much faster than for the following portions. This is attributed to impurities in the toluene which scavenge the greater part of the first catalyst portion. Using distilled toluene however, could not prevent the fast deactivation. Thus, the true activity of the salicylaldiminato Ni(II) active species studied in this work must be even higher than calculated from the oligomer yields. Integration of the mass flow data revealed a similar productivity of the following three additions.

Since the deactivation of the catalyst, which can directly be monitored from the decreasing ethylene uptake during the polymerization, is assumed to be a bimolecular reaction, the mass flow data was fitted with a second order kinetic (**3-4**).[55]

$$[A]_t = \frac{1}{2k \cdot t + \frac{1}{[A]_0}} \qquad (3\text{-}4)$$

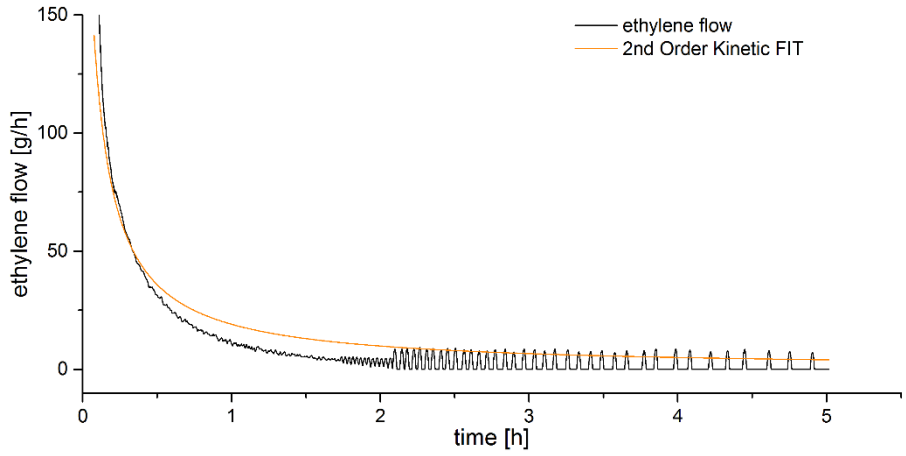

Figure 3.15: Ethylene uptake during a polymerization with ^{Me}**1-pyr**, (20 bar, 60 °C) with addition of catalyst (120 µmol) via pressure burette after saturation with ethylene fitted with a 2nd order kinetic (orange) from equation (**3-4**).

This fit however, does not satisfactorily represent the data (**Figure 3.15**). The actual deactivation is significantly faster than expected for a bimolecular deactivation. This suggests that additional pathways for catalyst deactivation play a role under reactor conditions. Since at higher temperatures catalyst deactivation is even more pronounced, the stepwise addition of catalyst should be even more effective under such conditions. In **Table 3.9** results of oligomerization runs at different temperatures are listed. As expected the productivity decreases while going from 60 to 70 and 80 °C (for mass flow traces of all the oligomerization runs cf. **Figure 3.20**, in 3.4.5 Additional Spectra and Data). But the decrease is much lower than expected from the results obtained with **^{Me}1-pyr** under the same reaction conditions without the pressure burette (**Table 3.9** vs. **Table 3.1**, p. 24). Entries 3.1-7 and 3.1-6 show that the productivity of **^{Me}1-pyr** decreases by 57 % when going from 60 °C to 70 °C. In contrast, addition of smaller amounts of catalyst over time only resulted in a 39 % lower yield. Thus, the stepwise addition of catalyst is, especially at high temperatures, an effective tool to suppress deactivation reactions which are favored under these conditions.

Table 3.9: Oligomerization results with catalyst addition via the pressure burette.

entry	T [°C]	^{Me}1-pyr [µmol]	yield [g]	TON[a]	TOF[b]	M_n (NMR) [g mol^{-1}][c]	branches/ 1,000 C[d]
1	60	5 x 24	100	29,800	5,960	1,000	77
2	70	5 x 24	61	18,200	3,640	900	76
3	80	5 x 24	36	10,800	2,160	750	77

reaction conditions: 600 mL toluene, 20 bar ethylene, 60 °C, 8.3 hours. [a] TON x mol [C_2H_4] x mol^{-1} [Ni]. [b] TOF x mol [C_2H_4] x mol^{-1} [Ni] h^{-1}. [c] molecular weights calculated from ^{1}H NMR intensity ratio of unsaturated end groups vs. overall integral. [d] degree of branching calculated from ^{1}H NMR intensity ratio of methyl groups (corrected for saturated end groups) vs. overall integral.

A different strategy to increase the stability of the catalyst was studied with the addition of weakly coordinating monodentate ligands to the polymerization. The labile ligand competes with ethylene for coordination to the active site of the catalyst. This results in an equilibrium between the ligand coordinated complex as a resting state and ethylene coordinated active species (**Scheme 3.7**). Thus, the amount of active species is reduced which suppresses deactivation but also limits the activity of the catalyst.

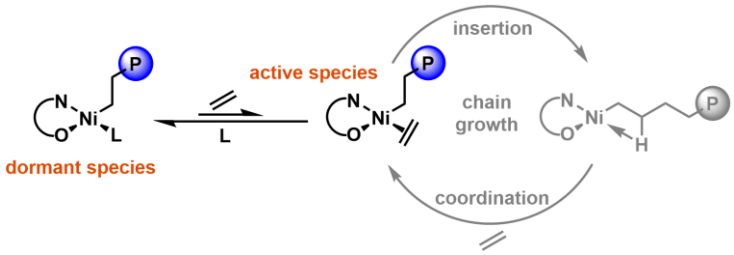

Scheme 3.7: Equilibrium between coordination of a labile ligand L and ethylene.

Since pyridine coordinated catalyst precursor ^{Me}**1-pyr** was used for the polymerization, the effect of excess pyridine was studied. The results of polymerizations with addition of 1, 2, and 5 equiv of pyridine are listed in **Table 3.10**.

Table 3.10: Polymerization results with addition of excess pyridine.

entry	pyridine [equiv]	t [h]	yield [g]	TON[a]	M_n (NMR) [g mol^{-1}][b]	branches/ 1,000 C[c]
1	0	5	71	21,100	1,000	77
2	1	5	75	22,400	1,000	75
3	2	5	72	21,500	950	75
4	5	7	70	20,800	1,000	74

reaction conditions: 120 µmol ^{Me}**1-pyr**, 600 mL toluene, 20 bar ethylene, 60 °C. [a] TON x mol [C_2H_4] x mol^{-1} [Ni]. [b] molecular weights calculated from ^{1}H NMR intensity ratio of unsaturated end groups vs. overall integral. [c] degree of branching calculated from ^{1}H NMR intensity ratio of methyl groups (corrected for saturated end groups) vs. overall integral.

All polymerizations were carried out until complete deactivation of the catalyst and no further ethylene uptake was observed. The results reveal a more or less constant productivity of the catalyst independent of the amount of pyridine present in the reactor. Mass flow data however, indicate a significant difference in catalyst activity (**Figure 3.16**). On the one hand, the addition of pyridine resulted in the expected stabilization of the catalyst. With 5 equiv of pyridine, the activity of the catalyst decreases much more slowly than without. Furthermore, the catalyst remains active for up to 7 hours while for entries 3.10-1 to 3.10-3 (0, 1, and 2 equiv of pyridine) the polymerization has come to an end after 5 hours at the latest. On the other hand, excess pyridine significantly decreases the activity of the catalyst especially at the beginning of the polymerization. It appears that these two effects level each other and therefore the same overall productivity is observed.

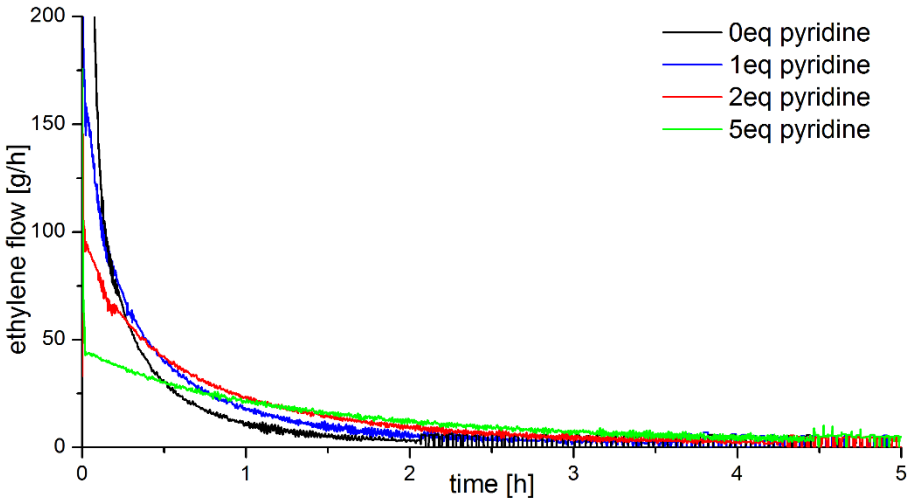

Figure 3.16: Ethylene uptake during polymerizations with addition of different amounts of pyridine.

3.3 Summary and Conclusion

Beyond the extensively studied high molecular weight polyethylenes, lower molecular weight oligomers are also of practical importance. This is illustrated by the well-established 1-olefins from the Shell higher olefin process, or alcohols from the Ziegler Alfol process. Remarkably, by strong contrast to these linear products, highly branched oligomers have found little attention although such materials would be of fundamental as well as practical interest, for example as functional additives in lubricants or surface modifiers. This is due to a lack of synthetic accessibility. Considering possible approaches for their synthesis, neutral κ^2-(*N,O*)-salicylaldiminato Ni(II) complexes are promising candidates. Though several complexes with electron donating substituents capable of producing highly branched oligomers are known, they have not been studied in detail.

In this chapter, the catalytic behavior of these complexes and the microstructure of the resulting oligomers were studied in full detail for the first time. It was shown, that the catalytic behavior of Ni(II) salicylaldiminato complexes strongly depends on the oligomerization conditions. High temperatures and low ethylene pressures favor β-hydride elimination. As a consequence, the resulting nickel hydride olefin complex gives access to chain termination reactions and chain walking which results in the formation of shorter chains with higher degrees of branching. Increasing temperatures mainly promote chain transfer as indicated by a strong decrease of polymer molecular weights and only minor changes of the overall degree of branching and the length of the branches. A detailed investigation of the microscopic chain architecture of the highly branched oligomers was carried out by ^{13}C NMR spectroscopy. Methyl branches represent the major amount of all branches (> 60 %) present in all oligomers

synthesized. Additionally, smaller amounts of ethyl, propyl and longer chain alkyl branches (C_{4+}) are found. Remarkably, all complexes studied are capable of producing hyperbranched oligoethylenes as indicated by the presence of significant amounts of *sec*-butyl branches (up to 15 %). As the smallest possible branch on branch motif and the only one detectable by NMR spectroscopy, they are an important evidence for a hyperbranched microstructure. Such hyperbranched structures are unprecedented in this low molecular weight regime and their synthesis is a unique feature of Ni(II) salicylaldiminato complexes with electron donating substituents. The distribution of different branch lengths also depends on the oligomerization conditions. At higher temperatures and low ethylene pressures the amount of methyl branches decreases in favor of longer chain branches and branch on branch motifs. It was also shown that molecular weights correlate with the overall branch density as well as the average branch length. As a result, higher molecular weight oligomers always come with lower branch densities and almost exclusively comprise methyl branches. Beneficially, desirable features such as high degrees of branching and hyperbranched structures as well as low oligomer molecular weight (ca. 1,000) go along with one another.

Increasing the steric bulk on the salicylaldiminato ligand with the three complexes **^{Me}1-pyr**, **^{Et}1-pyr**, and **^{iPr}1-pyr** confirmed that though the resulting material properties are mainly governed by the electronic nature of the substituents, sterics play an additional smaller role. With the bulky *iso*-propyl substituted complexes **^{iPr}1-pyr** higher molecular weight products (3,000 – 13,000 g mol^{-1}) with significantly less branches (ca. 50 per 1,000 C) are obtained compared to **^{Me}1-pyr** (ca. 1,000 g mol^{-1}, 77 branches per 1,000 C).

Furthermore, the influence of substituents on the *para*-position of the aniline on the resulting microstructures was investigated. Compared to **^{Me}1-pyr,** additional aryl substituents in the complexes **$^{p(Ar\text{-}Me)}$2-pyr** and **$^{p(Ar\text{-}OMe)}$2-pyr** allow for the synthesis of oligomers with higher degrees of branching at a given molecular weight though there are only minor differences. Also methyl, methoxy or fluorine substituents do not affect the material properties to a noticeable extent. Surprisingly though, the *para*-fluorine substituted complex **^{pF}2-pyr** exhibits a 10 % higher productivity than **^{Me}1-pyr** and is the most active catalyst capable of producing hyperbranched oligomers studied in this thesis.

Substitution of the 3,5-diiodosalicylaldehyde building block with 2-hydroxynaphthaldehyde in the complexes **^{Me}3-pyr** and **^{pF}3-pyr** showed that naphthaldehyde based catalysts appear to have a higher propensity for chain walking. They not only produce oligomers with higher degrees of branching but also incorporate less methyl branches and favor the formation of the desired long chain alkyl branches and hyperbranched structures (*sec*-butyl groups).

Catalyst deactivation for Ni(II) salicylaldiminato complexes is assumed to proceed via a bimolecular reaction pathway. Ethylene mass flow traces collected throughout the oligomerization indicate a fast catalyst decomposition during the first 30 min of the reaction. This is consistent with a bimolecular deactivation pathway that is favored at the high initial catalyst loading. Repeated additions of smaller amounts of catalyst over the course of the reaction allowed for a significantly improved oligomerization procedure and increased the productivity of the catalyst up to 43 %. Additionally, the catalyst life-time can be increased from 3 to 7 h with the addition of pyridine to the reaction. At the same time however, a reduced activity results in a constant oligomer yield independent of the amount of pyridine added.

3.4 Experimental Section

3.4.1 Materials and General Considerations

All complex syntheses were carried out under an argon or nitrogen atmosphere using standard Schlenk or glovebox techniques. Solvents were dried and degassed using standard laboratory techniques.[94] Benzene and toluene were distilled from sodium, methylene chloride was distilled from CaH_2, pyridine from KOH and THF and Et_2O were distilled from blue sodium/benzophenone ketyl. Pentane, Et_2O and toluene used for complex syntheses and ethylene polymerization were dried by passing through columns equipped with aluminum oxide/molecular sieve 3 Å. Ethylene for polymerization (3.5 grade) was supplied by AirLiquide and used as received. [(tmeda)$NiMe_2$] was purchased from MCAT. **^{Me}1-pyr**,[50] **^{MeOMe}1-pyr**,[50] 2,6-dibromo-4-methoxyaniline,[92] and 2,6-dibromo-4-(dimethylamino)aniline[93] were prepared according to known procedures. **^{pF}2-pyr** and **^{pMe}3-pyr** were kindly provided by Inigo Göttker-Schnetmann. All commercially available compounds and starting materials were purchased from Aldrich, Acros, TCI, ABCR, or ApolloScientific. All deuterated solvents were supplied by Eurisotop.

NMR-Spectroscopy

NMR spectra were recorded on a Varian Unity Inova 400 (^{1}H: 400 MHz, ^{13}C: 101 MHz, ^{19}F: 376 MHz), a Bruker Avance III 400 (^{1}H: 400 MHz, ^{13}C: 101 MHz, ^{19}F: 376 MHz), or a Bruker Avance III 600 spectrometer (^{1}H: 600 MHz, ^{13}C: 151 MHz, ^{19}F: 564 MHz). ^{1}H chemical shifts were referenced to the residual proton signal of the deuterated solvent. ^{13}C chemical shifts were referenced to the carbon signal of the deuterated solvent. Multiplicities are given as follows: s: singlet, d: doublet, t: triplet, q: quartet, quint: quintet, v: virtual multiplet, m: multiplet, br: broad

signal or combination thereof. NMR spectra of polyethylenes not soluble in chloroform at room temperature were recorded at 130 °C with addition of 5 mg mL^{-1} of $Cr(acac)_3$ and CD_2Cl_4 as the solvent. For reliable integration all spectra were recorded inverse gated without NOE using a relaxation delay of 2s.

Differential Scanning Calorimetry

Differential scanning calorimetry (DSC) was carried out on a Netzsch DSC 204 F1 instrument in closed 40 µL Pan alumina crucible under a nitrogen atmosphere. The samples were heated with a bicyclic temperature program from -50 °C to 160 °C with heating and cooling rates of 10 K/min. For determination of melting temperatures and degrees of crystallization, the second heating curve was used. For determination of the degree of crystallization, the enthalpy of fusion of the measured polymer was compared to 100 % crystalline PE (293 J/g).[95]

Gel Permeation Chromatography

High temperature gel permeation chromatography for PE molecular weight determination was carried out by Lars Bolk at the University of Konstanz in 1,2,4-trichlorobenzene at 160 °C at a flow rate of 1 mL min^{-1} on a 'Polymer Laboratories GPC 220' instrument equipped with 'PLgel Olexis' columns with differential refractive index-, viscostity- and light scattering- (15° and 90°) detectors. Data reported were determined with RI-detection against calibration with linear polyethylene standards.

For oligomers soluble in THF at 50 °C, molecular weight determination was carried out on a Polymer Laboratories PL-GPC 50 instrument with two PLGel 5 µm MIXED-C columns and an RI-detector in THF against polystyrene standards.

Mass Spectroscopy

Electron spray ionization (ESI) mass spectra were recorded on a 'Bruker Esquire 3000+' instrument at the University of Konstanz.

Elemental Analyses

Elemental analyses were obtained by the Analytical Services at the Department of Chemistry, University of Konstanz. Elemental analyses were performed on an 'Elementar Vario MICRO cube' instrument.

Ethylene Oligomerization

All ethylene oligomerization reactions were conducted either in a *Büchi ecoclave* equipped with a 600 mL or 1,100 mL steel vessel or in a *Büchi miniclave* with a 200 mL steel vessel respectively. All reactors are equipped with a cooling and heating jacket, supplied by a thermostat controlled by a thermocouple dipping into the polymerization mixture. Ethylene uptake of the reactor was monitored via Bronkhorst mass-flow meters. Flow charts of the reactors used are provided in 3.4.5 Additional Spectra and Data (p. 70).

The reactor was evacuated and refilled with argon repeatedly and toluene was added via cannula transfer. After heating to the desired temperature under stirring with 1,000 rpm, a catalyst solution in toluene was added and the reactor was pressurized to the desired pressure. Oligomerization was conducted at constant pressure for the given time. The reactor was vented and the obtained reaction mixture was washed several times with 3 M HCl. The organic layer was dried over $MgSO_4$ and the solvent was removed under vacuum.

3.4.2 Synthesis and Characterization of Alkyl Substituted Salicylaldiminato Ni(II) Complexes

4-Bromo-2,6-diisopropylaniline

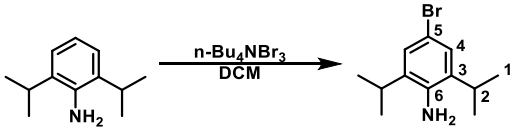

4-Bromo-2,6-diisopropylaniline was synthesized according to a literature procedure.[84] To a solution of 12.8 g (26.5 mmol, 1.0 eq) of *n*-Bu_4NBr_3 in 250 mL of dichloromethane 5 mL (26.5 mmol, 1.0 eq) of 2,6-diisopropylaniline were added and the reaction was stirred for 30 minutes at room temperature. After evaporation of the solvent, 250 mL of Et_2O was added and the biphasic mixture was extracted with 0.5 M NaOH and water. The organic layer was dried over $MgSO_4$ and the solvent was removed under vacuum to yield the product as a yellow liquid (6.6 g, 25.7 mmol, 97 %).

^{1}H NMR (400 MHz, $CDCl_3$): δ (ppm) = 7.12 (s, 2H, *H-4*), 3.80 (s, br, 2H, *NH*$_2$), 2.89 (sept., $^3J_{HH}$=6.8 Hz, 2H, *H-2*), 1.26 (d,$^3J_{HH}$=6.8 Hz, 12H, *H-1*).

^{13}C-NMR (101 MHz, $CDCl_3$): δ (ppm) = 139.3 (C-6), 134.8 (C-3), 125.9 (C-4), 111.4 (C-5), 28.2 (C-2), 22.4 (C-1).

Bromo-3,5-diisopropylbenzene

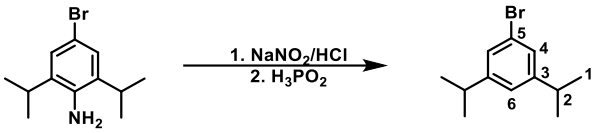

Bromo-3,5-diethylbenzene was synthesized according to a literature procedure.[84] In a round bottom flask, 6-Bromo-3,5-diethylaniline (6.6 g, 25.7 mmol, 1.0 eq) was dispersed in 70 mL of 2 M HCl and cooled to -5 °C. $NaNO_2$ (4.4 g, 64.3 mmol, 2.5 eq) was added in small portions. After stirring for 10 minutes at this temperature, 50 % H_3PO_2 (30 mL, 257 mmol, 10 eq) was added. The reaction was then stirred for one day at 4 °C and one day at room temperature. The biphasic mixture was extracted three times with ether and the organic layer was dried over $MgSO_4$. Removing the solvent under vacuum yielded the product as yellow oil (5.1 g, 21.1 mmol, 82 %).

^{1}H-NMR (400 MHz, $CDCl_3$): δ (ppm) = 7.19 (s, 2H, *H-4*), 7.00 (s, 1H, *H-6*), 2.86 (sept., $^3J_{HH}$=6.9 Hz, 2H, *H-2*), 1.25 (d, $^3J_{HH}$=6.9 Hz, 12H, *H-1*).

^{13}C-NMR (101 MHz, $CDCl_3$): δ (ppm) = 151.2 (C-3), 127.0 (C-4), 123.8 (C-6), 122.5 (C-5), 34.24 (C-2), 24.0 (C-1).

3,5-Diethylphenylboronicacid

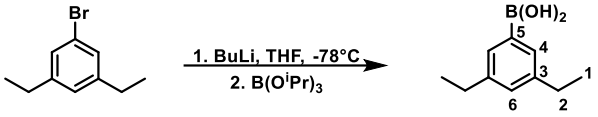

To a solution of bromo-3,5-diethylbenzene (2.0 g, 9.4 mmol, 1.0 eq) in 25 mL of THF 2.5 M butyl lithium solution in hexane (6.4 mL, 20 mmol, 1.7 eq) was added at -78 °C. After stirring for 30 minutes at this temperature a solution of $B(O^iPr)_3$ (4.3 mL, 2.0 mmol, 2.0 eq) in 15 mL of THF (cooled to -78 °C) was added. After stirring for 2 hours, the mixture was allowed to warm to room temperature. 50 mL of water was added and the reaction was acidified with 1 M H_2SO_4 to pH 2. After phase separation, the water phase was extracted three times with ethyl acetate and the combined organic layers were dried over $MgSO_4$. After removal of the solvent under vacuum, the off white solid was recrystallized from water to give the product as a white solid (1.2 g, 6.5 mmol, 70 %).

^{1}H-NMR (400 MHz, dmso-*d*6): δ (ppm) = 7.41 (d, $^4J_{HH}$=1.7 Hz, 2H, *H-4*), 7.06 (t, $^4J_{HH}$=1.7 Hz, 1H, *H-6*), 2.55 (q, $^3J_{HH}$=7.6 Hz, 4H, *H-2*), 1.16 (t, $^3J_{HH}$=7.6 Hz, 6H, *H-1*).

^{13}C-NMR (101 MHz, dmso-*d*6): δ (ppm) = 142.8 (C-3), 131.2 (C-4), 129.4 (C-6), 28.5 (C-2), 16.0 (C-1). *Note: C-5 adjacent to the boron was not detected in the ^{13}C NMR spectrum.*

3,5-Diisopropylphenylboronic acid

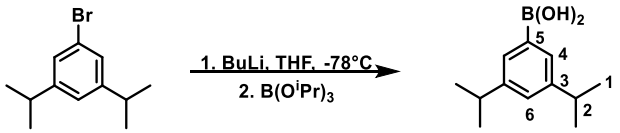

To a solution of Bromo-3,5-diisopropylbenzene (5.0 g, 20.7 mmol, 1.0 eq) in 30 mL of THF 2.5 M butyl lithium solution in hexane (14.1 mL, 35.2 mmol, 1.7 eq) was added at -78 °C. After stirring for 30 minutes at this temperature a solution of $B(O^iPr)_3$ (9.5 mL, 41.4 mmol, 2.0 eq) in 30 mL of THF (cooled to -78 °C) was added. After stirring for 2 hours, the mixture was allowed to warm to room temperature. 75 mL of water was added and the reaction was acidified with 1 M H_2SO_4 to pH 2. After phase separation, the water phase was extracted three times with ethyl acetate and the combined organic layers were dried over $MgSO_4$. After removal of the solvent under vacuum, the off white solid was recrystallized from water to give the product as a white solid (2.7 g, 13.3 mmol, 50 %).

^{1}H-NMR (400 MHz, dmso-*d*6): δ (ppm) = 7.46 (d, $^4J_{HH}$=1.8 Hz, 2H, *H-4*), 7.10 (t, $^4J_{HH}$=1.8 Hz, 1H, *H-6*), 2.82 (sept., $^3J_{HH}$=6.9 Hz, 2H, *H-2*), 1.18 (d, $^3J_{HH}$=6.9 Hz, 12H, *H-1*).
^{13}C-NMR (101 MHz, dmso-*d*6): δ (ppm) = 147.4 (C-3), 129.7 (C-4), 126.7 (C-6), 33.81 (C-2), 24.3 (C-1). *Note: C-5 adjacent to the boron was not detected in the ^{13}C NMR spectrum.*

2,6-Bis[3,5-diethylphenyl]aniline (^{Et}1-NH$_2$)

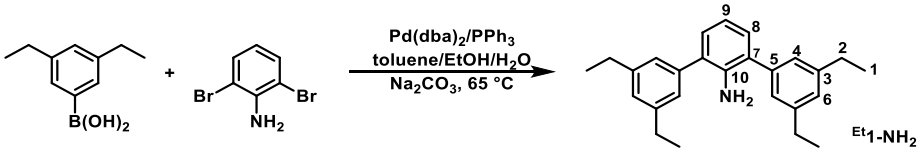

To a suspension of 3,5-diethylphenylboronicacid (1.0 g, 5.6 mmol, 2.3 eq), 2,6-dibromoaniline (612 mg, 2.4 mmol, 1.0 eq) and PPh_3 (14 mg, 51 µmol, 2.1 mol%) in 10 mL of toluene a solution of $Pd(dba)_2$ (14 mg, 24 µmol, 1 mol%) in 5 mL of toluene was added. The purple suspension was stirred for 10 minutes at room temperature to become orange. 1.5 mL of ethanol, 1.5 mL of water and Na_2CO_3 (1.0 g, 9.8 mmol, 4.0 eq) was added and the solution was heated for 21 hours to 95 °C. After cooling to room temperature the reaction was stirred for one hour under air and then extracted with 75 mL of water and 75 mL of ether. The water phase was extracted three times with ether and the combined organic layers were dried over $MgSO_4$. After removal of the solvent the product was purified via column chromatography on silica using pentane/toluene (5:1) as the eluent (R_f=0.7). **^{Et}1-NH$_2$** was obtained as a white solid (765 mg, 2.1 mmol, 87 %).

^{1}H-NMR (400 MHz, CD_2Cl_2): δ (ppm) = 7.14 (d, $^4J_{HH}$=1 Hz, 4H, *H-4*), 7.07 (d, $^3J_{HH}$=7.5 Hz, 2H, *H-8*), 7.05 (t, $^4J_{HH}$=1 Hz, 2H, *H-6*), 6.82 (t, $^3J_{HH}$=7.5 Hz, 1H, *H-9*), 3.93 (s, 2H, *NH*$_2$), 2.68 (q, $^3J_{HH}$=7.6 Hz, 8H, *H-2*), 1.26 (t, $^3J_{HH}$=7.6 Hz, 12H, *H-1*).

^{13}C-NMR (101 MHz, CD_2Cl_2): δ (ppm) = 145.5 (C-3), 141.5 (C-5), 140.4 (C-10), 130.0 (C-8), 128.7 (C-7), 127.0 (C-6), 126.5 (C-4), 118.3 (C-9), 29.4 (C-2), 16.1 (C-1).

Elemental Analysis (%) for $C_{26}H_{31}N$: Found (Calculated): C 87.28 (87.34); H 8.74 (8.74); N 3.92 (3.92).

2,6-Bis[3,5-diisopropylphenyl]aniline (^{iPr}1-NH$_2$)

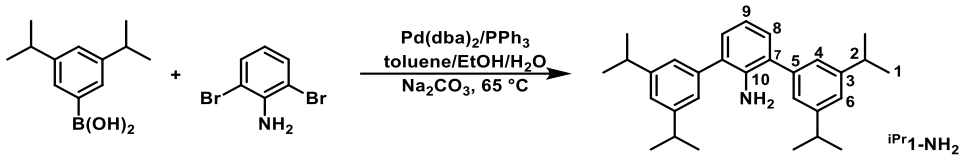

To a suspension of 3,5-diisopropylphenylboronic acid (1.5 g, 7.3 mmol, 2.3 eq), 2,6-dibromoaniline (790 mg, 3.2 mmol, 1.0 eq) and PPh_3 (17 mg, 67 µmol, 2.1 mol%) in 11 mL of toluene a solution of $Pd(dba)_2$ (18 mg, 32 µmol, 1 mol%) in 5 mL of toluene was added. The purple suspension was stirred for 10 minutes at room temperature to become orange. 2 mL of ethanol, 2 mL of water and Na_2CO_3 (3.0 g, 12.6 mmol, 4.0 eq) was added and the solution was heated for 21 hours to 95 °C. After cooling to room temperature the reaction was stirred for one hour under air and then extracted with 75 mL of water and 75 mL of ether. The water phase was extracted three times with ether and the combined organic layers were dried over $MgSO_4$. After removal of the solvent, the product was purified via column chromatography on silica using pentane/toluene (5:1) as the eluent (R_f=0.7). **^{iPr}1-NH$_2$** was obtained as a white solid (1.2 g, 2.9 mmol, 91 %).

^{1}H-NMR (400 MHz, CD_2Cl_2): δ (ppm) = 7.17 (d, $^4J_{HH}$=1.7 Hz, 4H, *H-4*), 7.08-7.10 (m, 4H, *H-6*/*H-8*), 6.83 (t, $^3J_{HH}$=7.5 Hz, 4H, *H-9*), 3.95 (s, 2H, *NH*$_2$), 2.95 (sept., $^3J_{HH}$=7.0 Hz, 4H, *H-2*), 1.28 (d, $^3J_{HH}$=7.0 Hz, 24H, *H-1*).

^{13}C-NMR (101 MHz, CD_2Cl_2): δ (ppm) = 150.1 (C-3), 141.5 (C-5), 140.4 (C-10), 130.0 (C8), 128.9 (C-7), 125.2 (C-4), 124.3 (C-6), 118.2 (C-9), 34.9 (C-2), 24.5 (C-1).

Elemental Analysis (%) for $C_{30}H_{39}N$: Found (Calculated): C 86.40 (87.11); H 9.50 (9.50); N 3.55 (3.39).

N-[2,6-bis(3,5-diethylphenyl)phenyl]-4,6-diiodosalicylaldimine (^{Et}1-N^OH)

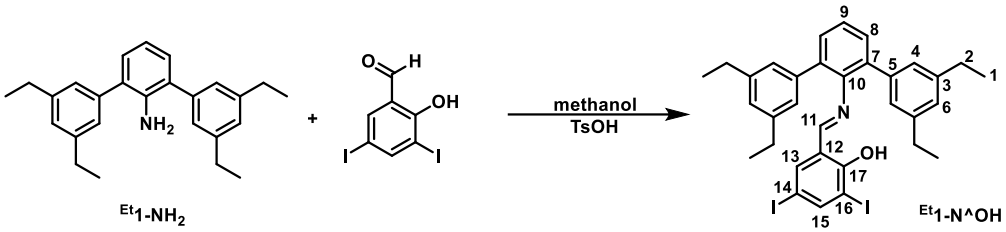

Under air, ^{Et}**1-NH$_2$** (603 mg, 1.7 mmol, 1.0 eq), 3,5-diiodosalicylaldehyde (631 mg, 1.7 mmol, 1.0 eq) and *p*-toluenesulfonic acid (7 mg, 41 µmol, 24 mol %) were suspended in 25 mL of methanol and heated to 65 °C for 30 minutes while all starting materials dissolved. The reaction was stirred for 15 hours at room temperature. After cooling the reaction mixture to 0 °C, the orange product was filtered off and washed with small portions of cold methanol. The product was dissolved in pentane to filter off residual aldehyde and then dried under vacuum. ^{Et}**1-N^OH** was obtained as an orange solid (1.0 g, 1.4 mmol, 84 %).

^{1}H-NMR (400 MHz, CD_2Cl_2): δ (ppm) = 13.92 (s, 1H, *OH*), 7.98 (d, $^4J_{HH}$=2.0 Hz, 1H, *H-15*), 7.76 (s, 1H, *H-11*), 7.42 (m, 2H, *H-8*), 7.37 (m, 1H, *H-9*), 7.08 (d, $^4J_{HH}$=2.0 Hz, 1H, *H-13*), 7.02 (d, $^4J_{HH}$=1.0 Hz, 4H, *H-4*), 6.96 (t, $^4J_{HH}$=1 Hz, 2H, *H-6*), 2.59 (q, $^3J_{HH}$=7.6 Hz, 8H, *H-2*), 1.13 (t, $^3J_{HH}$=7.6 Hz, 12H, *H-1*).
^{13}C-NMR (101 MHz, CD_2Cl_2): δ (ppm) = 166.8 (C-11), 160.6 (C-17), 149.7 (C-15), 145.1 (C-3), 144.3 (C-10), 140.7 (C-13), 139.6 (C-5), 136.6 (C-7), 130.5 (C-8), 127.3 (C-4), 127.0 (C-6), 126.9 (C-9), 120.9 (C-12), 87.1 (C-16), 79.7 (C-14), 29.4 (C-2), 16.0 (C-1).
Elemental Analysis (%) for $C_{33}H_{33}I_2NO$: Found (Calculated): C 55.93 (55.56), H 5.14 (4.66), N 2.11 (1.96).

N-[2,6-bis(3,5-diisopropylphenyl)phenyl]-4,6-diiodosalicylaldimine (^{iPr}1-N^OH)

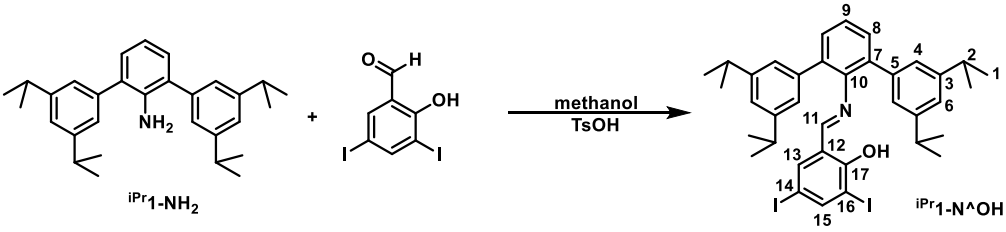

Under air, ^{iPr}**1-NH$_2$** (1.0 g, 2.4 mmol, 1.0 eq), 3,5-diiodosalicylaldehyde (904 mg, 2.4 mmol, 1.0 eq) and *p*-toluenesulfonic acid (12 mg, 70 µmol, 29 mol %) were suspended in 60 mL of methanol and heated to 65 °C for 30 minutes while all starting materials dissolved. The reaction was stirred for 15 hours at room temperature. After cooling the reaction mixture to 0 °C, the orange product was filtered off and washed with small portions of cold methanol. The product was dissolved in pentane to filter off residual aldehyde and then dried under vacuum. ^{iPr}**1-N^OH** was obtained as an orange solid (1.1 g, 1.4 mmol, 59 %).

^{1}H-NMR (400 MHz, CD_2Cl_2): δ (ppm) = 13.91 (s, 1H, *OH*), 7.96 (d, $^4J_{HH}$=2.1 Hz, 1H, *H-15*), 7.73 (s, 1H, *H-11*), 7.45 (d, $^3J_{HH}$=7.5 Hz, 2H, *H-8*), 7.37 (t, $^3J_{HH}$=7.5 Hz 1H, *H-9*), 7.05 (d, $^4J_{HH}$=1.7 Hz, 4H, *H-4*),7.03 (d, $^4J_{HH}$=2.1 Hz, 1H, *H-13*), 6.99 (t, $^4J_{HH}$=1 Hz, 2H, *H-6*), 2.85 (sept., $^3J_{HH}$=6.9 Hz, 4H, *H-2*), 1.16 (d, $^3J_{HH}$=6.9 Hz, 24H, *H-1*).

^{13}C-NMR (101 MHz, CD_2Cl_2): δ (ppm) = 167.0 (C-11), 160.6 (C-17), 149.7 (C-3), 149.4 (C-15), 144.4 (C-10), 140.6 (C-13), 139.5 (C-5), 136.1 (C-7), 130.5 (C-8), 126.9 (C-9), 126.0 (C-4), 124.5 (C-6), 121.0 (C-12), 87.1 (C-16), 79.6 (C-14), 34.8 (C-2), 24.3 (C-1).

Elemental Analysis (%) for $C_{37}H_{41}I_2NO$: Found (Calculated): C 60.30 (57.75), H 5.91 (5.37), N 2.00 (1.82).

{3,5-Diiodo-*N*-[2,6-bis(3,5-diethylphenyl)phenyl]salicylaldiminato-κ^2-*N,O*}-methylpyridinenickel(II) (^{Et}1-pyr)

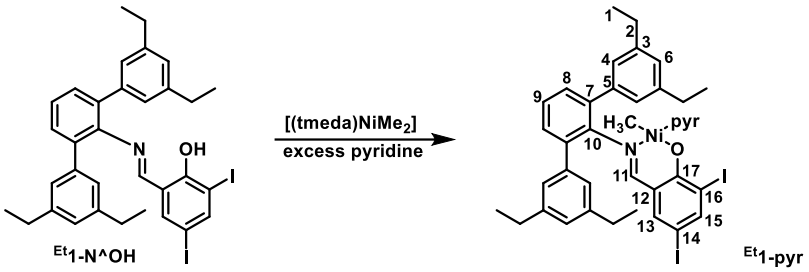

^{Et}1-N^OH ^{Et}1-pyr

In a Schlenk flask a mixture of **^{Et}1-N^OH** (71 mg, 100 µmol, 1.0 eq), [(tmeda)Ni(CH_3)$_2$] (25 mg, 120 µmol, 1.2 eq) and 20 eq of pyridine was dissolved in 10 mL of benzene and the solution was stirred for 1 hour at room temperature. The dark red solution was filtered via a syringe filter to remove Ni^0 and benzene was sublimated under vacuum. The orange solid was washed with methanol and pentane at -80 °C and dried under vacuum to give **^{Et}1-pyr** as an orange powder (188 mg, 217 µmol, 78 %).

^{1}H-NMR (400 MHz, C_6D_6): δ (ppm) = 8.24 (d, $^3J_{HH}$=5.2 Hz, 2H, *o*-H *pyr*), 7.96 (d, $^4J_{HH}$=2.2 Hz, 1H, *H-15*), 7.45 (s, 4H, *H-4*), 7.42 (d, $^3J_{HH}$=7.6 Hz, 2H, *H-8*), 7.16 (m, 1H, *H-9*), 7.09 (s, 1H, *H-11*),6.96 (s, 2H, *H-6*), 6.84 (d, $^4J_{HH}$=2.1 Hz, 1H, *H-13*), 6.64 (t, $^3J_{HH}$=7.6 Hz, 1H, *p*-H *pyr*), 6.34 (t, $^3J_{HH}$=6.8 Hz, 2H, *m*-H *pyr*), 2.59 (q, $^3J_{HH}$=7.7 Hz, 8H, *H-2*), 1.20 (t, $^3J_{HH}$=7.7 Hz, 12H, *H-1*), -0.54 (s, 3H, Ni–*CH$_3$*).

^{13}C-NMR (101 MHz, C_6D_6): δ (ppm) = 167.9 (C-11), 163.5 (C-17), 151.9 (*o*-C pyr), 150.2 (C-10), 148. 9 (C-15), 144.5 (C-3), 142.1 (C-13), 140.4 (C-5), 136.7 (C-7), 135.8 (*p*-C pyr), 130.1 (C-8), 128.4 (C-9), 128.0 (C-4), 127.0 (C-6), 122.7 (*m*-C pyr), 121.2 (C-12), 97.2 (C-16), 71.7 (C-14), 29.5 (C-2), 16.2 (C-1), -7.6 (Ni–CH_3).

Elemental Analysis (%) for $C_{39}H_{40}I_2N_2NiO$: Found (Calculated): C 53.66 (54.14), H 4.85 (4.66), N 3.49 (3.24).

{3,5-Diiodo-*N*-[2,6-bis(3,5-diisopropylphenyl)phenyl]salicylaldiminato-κ^2-*N,O*}-methylpyridinenickel(II) (^{iPr}1-pyr)

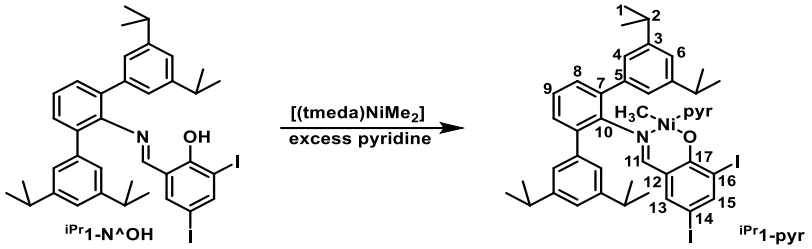

In a Schlenk flask a mixture of **^{iPr}1-N^OH** (77 mg, 100 µmol, 1.0 eq), [(tmeda)Ni(CH_3)$_2$] (20 mg, 120 µmol, 1.2 eq) and 20 eq of pyridine was dissolved in 10 mL of benzene and the solution was stirred for 1 hour at room temperature. The dark red solution was filtered via a syringe filter to remove Ni^0 and benzene was sublimated under vacuum. The orange solid was washed with methanol and pentane at -80 °C and dried under vacuum to give **^{iPr}1-pyr** as an orange powder (182 mg, 198 µmol, 76 %).

^{1}H-NMR (400 MHz, C_6D_6): δ (ppm) = 8.30 (d, $^3J_{HH}$=4.9 Hz, 2H, *o*-H *pyr*), 7.97 (d, $^4J_{HH}$=1.2 Hz, 1H, *H-15*), 7.51 (s, 4H, *H-4*), 7.45 (d, $^3J_{HH}$=7.7 Hz, 2H, *H-8*), 7.16 (m, 1H, *H-9*), 7.11 (s, 1H, *H11*),6.95 (s, 2H, *H-6*), 6.77 (d, $^4J_{HH}$=1.2 Hz, 1H, *H-13*), 6.66 (t, $^3J_{HH}$=7.2 Hz, 1H, *p*-H *pyr*), 6.38 (t, $^3J_{HH}$=6.4 Hz, 2H, *m*-H *pyr*), 2.88 (sept., $^3J_{HH}$=6.9 Hz, 4H, *H-2*), 1.31 (d, $^3J_{HH}$=6.9 Hz, 12H, *H-1*), 1.27 (d, $^3J_{HH}$=6.9 Hz, 12H, *H-1*), -0.54 (s, 3H, Ni–CH_3).
^{13}C-NMR (101 MHz, C_6D_6): δ (ppm) = 168.1 (C-11), 163.4 (C-17), 151.9 (*o*-C pyr), 149.2 (C-10), 148.8 (C-3), 146.1 (C-15), 142.1 (C-6), 140.4 (C-5), 136.9 (C-7), 135.9 (*p*-C pyr), 130.0 (C-8), 127.8 (C-9), 126.6 (C-12) 126.4 (C-4), 122.8 (*m*-C pyr), 121.3 (C-6), 97.0 (C-16), 71.6 (C-14), 34.9 (C-2), 24.5 (C-1), 24.2 (C-1), -7.5 (Ni–CH_3).
Elemental Analysis (%) for $C_{43}H_{48}I_2N_2NiO$: Found (Calculated): C 55.07 (56.05), H 5.35 (5.25), N 3.33 (3.04).

3.4.3 Synthesis and Characterization of *para*-Substituted Complexes

2,6-Bis(3,5-dimethylphenyl)-4-methylaniline (^{pMe}2-NH_2)

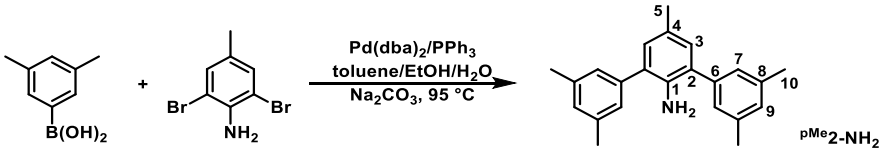

To a suspension of 3,5-dimethylpheynlboronic acid (3.45 g, 23 mmol, 2.3 eq), 2,6-dibromo-4-methylaniline (2.65 g, 10 mmol, 1.0 eq), PPh_3 (55 mg, 210 µmol, 2.1 mol %), and Na_2CO_3 (4.24 g, 40 mmol, 4.0 eq) in 25 mL of toluene a solution of Pd(dba)$_2$ (58 mg, 100 µmol, 1 mol%) in 5 mL of toluene was added. The purple suspension was stirred for 10 minutes at room temperature to become orange. 11.5 mL of ethanol and 11.5 mL of water were added and the solution was heated

for 21 hours to 95 °C. After cooling to room temperature the reaction was stirred for one hour under air and then extracted with 75 mL of water and 75 mL of ether. The water phase was extracted three times with ether and the combined organic layers were dried over $MgSO_4$. After removal of the solvent the product was purified via column chromatography on silica using pentane/toluene (5:1) as the eluent (R_f=0.6). **^{pMe}2-NH$_2$** was obtained as a white solid (3.16 g, 10 mmol, 100 %).

^{1}H-NMR (400 MHz, CD_2Cl_2): δ (ppm) = 7.07 (s, 4H, *H-7*), 6.99 (s, 2H, *H-9*), 6.87 (s, 2H, *H-3*), 3.75 (s, 2H, *NH$_2$*), 2.35 (s, 12H, *H-10*), 2.27 (s, 3H, *H-5*).

^{13}C-NMR (101 MHz, CD_2Cl_2): δ (ppm) = 140.5 (C-6), 138.9 (C-8), 138.9 (C-1), 130.5 (C-3), 129.2 (C-9), 128.7 (C-2), 127.5 (C-7), 127.4 (C-4), 21.6 (C-10), 20.6 (C-5).

2,6-Bis(3,5-dimethylphenyl)-4-fluoroaniline (^{pF}2-NH$_2$)

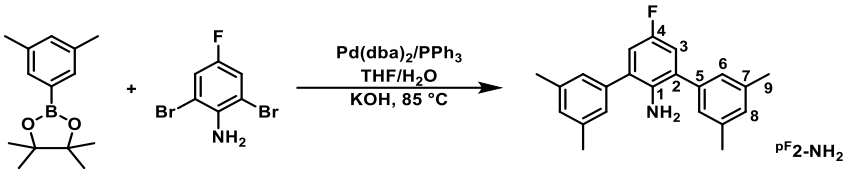

To a suspension of the 3,5-dimethylphenylboronic acid pinacol ester (24.15 g, 104 mmol, 2.1 eq), 2,6-dibromo-4-fluoroaniline (13.41 g, 50 mmol, 1.0 eq), and KOH (14.84 g, 265mmol, 5.0 eq) in 40 mL of THF and 50 mL of water a solution of $Pd(dba)_2$ (286 mg, 500 µmol, 1 mol%) and PPh_3 (382 mg, 1.5 mmol, 3.0 mol%) in 10 mL of THF was added. The solution was heated to 85 °C and stirred for 20 h. After cooling to room temperature the reaction was stirred for one hour under air. After addition of additional 50 mL of THF the organic phase was extracted with 5 M KOH solution repeatedly. The organic layer was dried over $MgSO_4$ and concentrated under reduced pressure. The brownish solid was recrystallized from pentane to yield **^{pF}2-NH$_2$** as a white solid after drying under vacuum (8.19 g, 26 mmol, 51 %).

^{1}H-NMR (400 MHz $CDCl_3$): δ (ppm) = 2.37 (s, 12H, H-9), 3.69 (s, 2H, H-1), 6.84 (d, $^3J_{HF}$ =9.01 Hz, 2H, *H-3*), 7.01 (s, 2H, *H-8*), 7.10 (s, 4H, *H-6*).

^{13}C-NMR (101 MHz, $CDCl_3$): δ (ppm) = 155.8 (d, $^1J_{CF}$=236.9 Hz, C-4), 139.0 (C-5), 138.6 (C-7), 137.0 (d, $^4J_{CF}$=2.1 Hz, C-1), 129.4 (C-8), 129.3 (d, $^3J_{CF}$=7.3 Hz, C-2), 127.0 (C-6), 115.8 (d, $^2J_{CF}$=22.1 Hz, C-3), 21.5 (C-9).

^{19}F-NMR (376 MHz, $CDCl_3$): δ (ppm) = -128.06 (s).

Elemental Analysis (%) for $C_{22}H_{22}FN$: Found (Calculated): C 82.77 (82.72), H 6.65 (6.94), N 4.40 (4.39).

2,4,6-Tris(3,5-dimethylphenyl)aniline ($^{p(Ar-Me)}$2-NH_2)

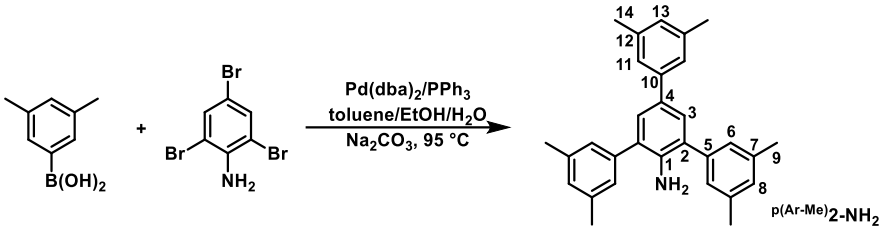

To a suspension of the 3,4,5-dimethylphenylboronic acid (3.0 g, 20 mmol, 4.5 eq), 2,4,6-tribromoaniline (1.45 g, 4.4 mmol, 1.0 eq), PPh_3 (53 mg, 203 µmol, 3.5 mol %), and $CaCO_3$ (2.5 g, 23.2 mmol, 4 eq) in 15 mL of toluene a solution of $Pd(dba)_2$ (50 mg, 87 µmol, 1.5 mol %) in 5 mL of toluene was added. The purple suspension was stirred for 10 minutes at room temperature to become orange. 4 mL of ethanol and 4 mL of water were added and the solution was heated for five days to 95 °C. After cooling to room temperature the reaction was stirred for one hour under air and then extracted with 75 mL of water and 75 mL of ether. The water phase was extracted three times with ether and the combined organic layers were dried over $MgSO_4$. After removal of the solvent the product was purified via recrystallization from pentane. $^{p(Ar-Me)}$**2-NH_2** was obtained as a white solid (1.5 g, 3.7 mmol, 84 %).

^{1}H-NMR (400 MHz, CD_2Cl_2): δ (ppm) = 7.38 (s, 2H, *H-3*), 7.21 (s, 2H, *H-11*), 7.18 (s, 4H, *H-6*), 7.02 (s, 2H, *H-8*), 6.93 (s, 1H, *H-13*), 3.99 (br, 2H, *NH_2*), 2.38 (s, 12H, *H-9*), 2.35 (s, 6H, *H-14*).
^{13}C-NMR (101 MHz, CD_2Cl_2): δ (ppm) = 140.8 (C-1), 139.3 (C-5), 138.7 (C-7), 138.3 (C-12), 132.8 (C-4), 129.9 (C-2), 129.7 (C-10), 129.3 (C-8), 128.3 (C-13), 128.3 (C-3), 127.3 (C-6), 124.6 (C-11), 21.6 (C-14), 21.5 (C-9).

2,4,6-[Tris(4-methoxy-3,5-dimethylphenyl)]aniline ($^{p(Ar-OMe)}$2-NH_2)

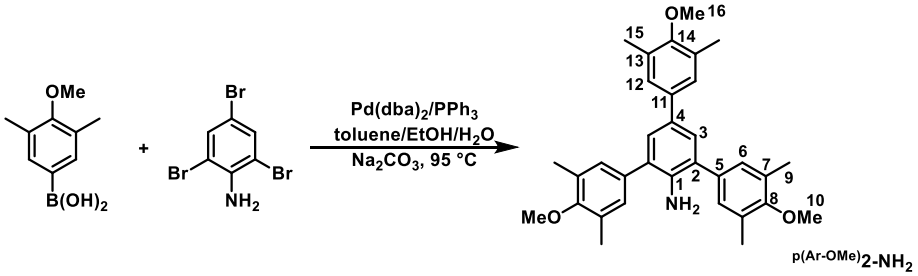

To a suspension of 3,5-dimethyl-4-methoxyphenylboronic acid (3.0 g, 16.7 mmol, 3.5 eq), 2,4,6-tribromoaniline (1.57 g, 4.8 mmol, 1.0 eq), PPh_3 (44 mg, 167 µmol, 3.5 mol %), and $CaCO_3$ (2.0 g, 19 mmol, 4 eq) in 15 mL of toluene a solution of $Pd(dba)_2$ (41 mg, 71 µmol, 1.5 mol %) in 10 mL of toluene was added. The purple suspension was stirred for 10 minutes at room temperature to become orange. 4 mL of ethanol and 4 mL of water were added and the solution was heated to 95 °C overnight. After cooling to room temperature the reaction was stirred for one hour under air and then extracted with 50 mL of water and 50 mL of ether. The water phase

was extracted three times with ether and the combined organic layers were dried over $MgSO_4$. After removal of the solvent the product was purified via column chromatography on silica using pentane/ether (3:1) as the eluent. **$^{p(Ar\text{-}OMe)}$2-NH$_2$** was obtained as a white solid (1.9 g, 3.8 mmol, 79 %).

^{1}H-NMR (400 MHz, CD_2Cl_2): δ (ppm) = 7.33 (s, 2H, *H-3*), 7.23 (s, 2H, *H-12*), 7.22 (s, 4H, *H-6*), 3.78 (s, 6H, *H-10*), 3.74 (s, 3H, *H-16*), 2.93 (br, 2H, *NH$_2$*), 2.34 (s, 12H, *H-9*), 2.31 (s, 6H, *H-15*).

N-[2,6-Bis(3,5-dimethylphenyl)-4-methylphenyl]-4,6-diiodosalicyl-aldimine (^{pMe}2-N^OH)

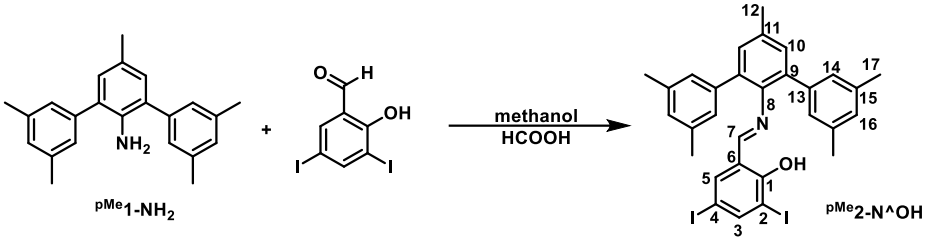

Under air, **^{pMe}1-NH$_2$** (3.16 g, 10 mmol, 1.0 eq), 3,5-diiodosalicylaldehyde (5.61 g, 15 mmol, 1.5 eq) and 0.4 mL of formic acid were suspended in 125 mL of methanol and heated to 60 °C for 2 hours while all starting materials dissolved. The reaction mixture was stirred for 20 hours at room temperature. After cooling the reaction to 0 °C, the yellow product was filtered off and washed with portions of cold methanol. After drying under vacuum, **^{pMe}2-N^OH** was obtained as a yellow solid (5.44 g, 8.1 mmol, 81 %).

^{1}H-NMR (400 MHz, CD_2Cl_2): δ (ppm) = 14.05 (s, 1H, *OH*), 7.98 (d, $^4J_{HH}$=2.1 Hz, 1H, *H-3*), 7.74 (s, 1H, *H-7*), 7.20 (s, 2H, *H-10*), 7.10 (d, $^4J_{HH}$=2.1 Hz, 1H, *H-5*), 6.98 (s, 4H, *H-14*), 6.93 (s, 2H, *H-16*), 2.43 (s, 3H, *H-12*), 2.28 (s. 12H, *H-17*).

^{13}C-NMR (101 MHz, CD_2Cl_2): δ (ppm) = 166.3 (C-7), 160.7 (C-1), 149.3 (C-3), 141.5 (C-), 140.5 (C-5), 139.8 (C-13), 138.5 (C-15), 136.8 (C-11), 135.8 (C-9), 131.3 (C-10), 129.1 (C-16), 128.1 (C-14), 120.8 (C-6), 87.3 (C-2), 79.7 (C-4), 21.6 (C-17), 21.3 (C-12).

N-[2,4,6-Tris(3,5-dimethylphenyl)phenyl]-4,6-diiodosalicyl-aldimine ($^{p(Ar\text{-}Me)}$2-N^OH)

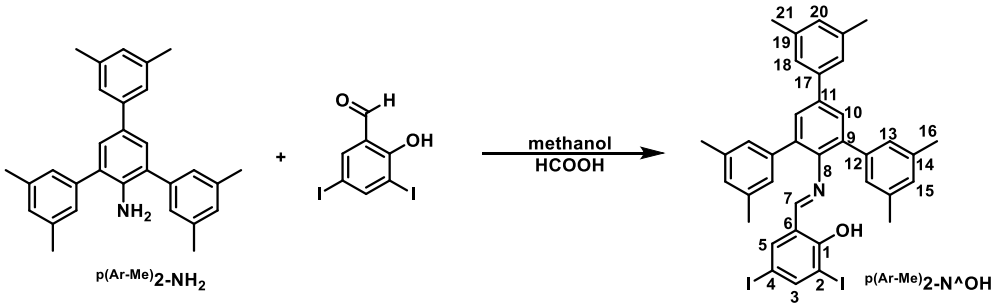

Under air, **$^{p(Ar\text{-}Me)}$2-NH$_2$** (507 mg, 1,25 mmol, 1.0 eq), 3,5-diiodosalicylaldehyde (701 mg, 1.87 mmol, 1.5 eq) and three drops of formic acid were suspended in 16 mL of methanol and

heated to 60 °C for 2 hours while all starting materials dissolved. The reaction mixture was stirred for 20 hours at room temperature. After cooling the reaction mixture to 0 °C, the orange product was filtered off and washed with small portions of cold methanol. After drying under vacuum, **$^{p(Ar\text{-}Me)}$2-N^OH** was obtained as an orange solid (750 mg, 0.98 mmol, 78 %).

^{1}H-NMR (400 MHz, CD_2Cl_2): δ (ppm) = 13.93 (s, 1H, *OH*), 8.00 (d, $^4J_{HH}$=1.8 Hz, 1H, *H-3*), 7.81 (s, 1H, *H-7*), 7.62 (s, 2H, *H-10*), 7.32 (s, 2H, *H-18*), 7.13 (d, $^4J_{HH}$=1.8 Hz, 1H, *H-5*), 7.04 (s, 4H, *H-13*), 7.03 (s, 1H, *H-20*), 6.96 (s, 2H, *H-15*), 2.38 (s, 6H, *H-21*), 2.30 (s. 12H, *H-16*).

^{13}C-NMR (101 MHz, CD_2Cl_2): δ (ppm) = 166.4 (C-7), 160.6 (C-1), 149.4 (C-3), 142.8 (C-8), 140.7 (C-5), 139.7 (C-11), 139.1 (C-19), 138.6 (C-14), 136.4 (C-9), 129.8 (C-17), 129.3 (C-15), 129.2 (C-10), 128.8 (C-12), 128.2 (C-13), 125.4 (C-18), 120.3 (C-6), 87.2 (C-2), 79.8 (C-4), 21.7 (C-21), 21.6 (C-16).

N-[2,4,6-Tris(4-methoxy-3,5-dimethylphenyl)phenyl]-4,6-diiodosalicyl-aldimine ($^{p(Ar\text{-}OMe)}$2-N^OH)

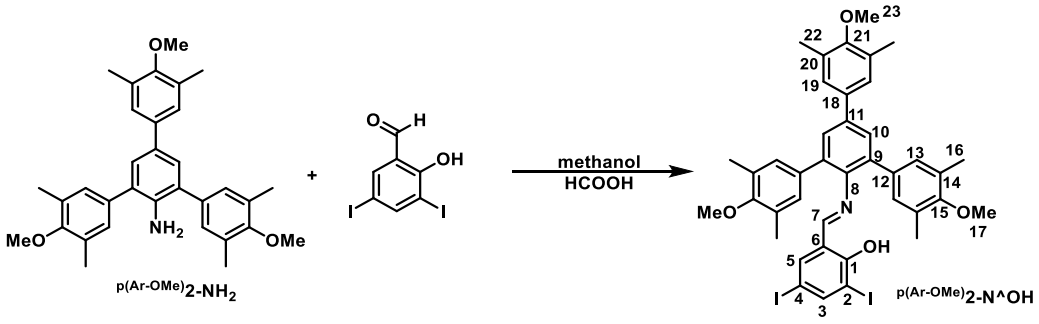

Under air **$^{p(Ar\text{-}OMe)}$2-NH$_2$** (698 mg, 1,41 mmol, 1.0 eq), 3,5-diiodosalicylaldehyde (1.05 g, 2.82 mmol, 2.0 eq) and ten drops of formic acid were suspended in 80 mL of methanol and heated to 60 °C for 2 hours while all starting materials dissolved. The reaction mixture was stirred at room temperature overnight. After cooling to 0 °C, the orange product was filtered off and washed with small portions of cold methanol. After drying under vacuum, **$^{p(Ar\text{-}OMe)}$2-N^OH** was obtained as an orange solid (1.06 g, 1.24 mmol, 88 %).

^{1}H-NMR (400 MHz, $CDCl_3$): δ (ppm) = 13.89 (s, 1H, *OH*), 7.97 (d, $^4J_{HH}$=2.1 Hz, 1H, *H-3*), 7.74 (s, 1H, *H-7*), 7.54 (s, 2H, *H-10*), 7.31 (s, 2H, *H-19*), 7.06 (d, $^4J_{HH}$=2.1 Hz, 1H, *H-5*), 7.03 (s, 4H, *H-13*), 3.77 (s, 3H, *H-23*), 3.74 (s, 6H, *H-17*), 2.35 (s, 6H, *H-22*), 2.27 (s, 12H, *H-16*).

^{13}C-NMR (101 MHz, $CDCl_3$): δ (ppm) = 165.5 (C-7), 160.0 (C-1), 157.0 (C-21), 156.4 (C-15), 148.8 (C-3), 142.4 (C-8), 140.0 (C-5), 139.1 (C-11), 135.6 (C-18), 135.5 (C-9), 134.8 (C-12), 131.5 (C-20), 131.1 (C-14), 130.3 (C-13), 128.4 (C-10), 127.6 (C-19), 120.4 (C-6), 87.1 (C-2), 79.5 (C-4), 60.0 (C-17), 60.0 (C-23), 16.4 (C-22), 16.3 (C-16).

{3,5-Diiodo-*N*-[2,6-Tris(3,5-dimethylphenyl)-4-methylphenyl]salicyl-aldiminato-κ^2-*N,O*}methylpyridinenickel(II) (^{pMe}2-pyr)

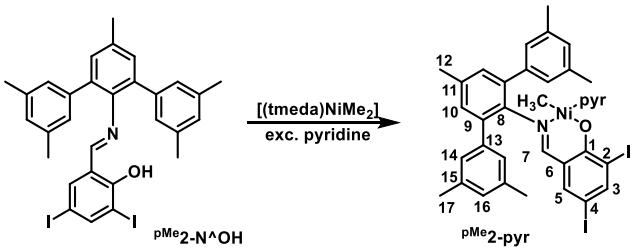

In a 25 mL Schlenk tube 134 mg (200 µmol, 1.0 eq) of **^{pMe}2-N^OH** and 45 mg (220 µmol, 1.1 eq) of [(tmeda)NiMe$_2$] were dissolved in 5 mL of benzene and 240 µL of pyridine (3.0 mmol, 2.5 eq). The dark red solution was stirred at room temperature for 1 hour. After filtration over a syringe filter, the solvent was removed by sublimation under vacuum. **^{pMe}2-pyr** was obtained as red-orange solid (150 mg, 182 µmol, 91 %).

^{1}H-NMR (400 MHz, CD_2Cl_2): δ (ppm) = 8.37 (dt, $^3J_{HH}$=5.0 Hz, $^4J_{HH}$=1.5 Hz, 2H, *o-H pyr*), 7.84 (d, $^4J_{HH}$=2.3 Hz, 1H, *H-3*), 7.61 (tt, $^3J_{HH}$=7.6 Hz, $^4J_{HH}$=1.5 Hz, 1H, *p-H pyr*), 7.46 (s, 1H, *H-7*), 7.22 (s, 4H, *H-14*), 7.16 (s, 2H, *H-10*), 7.11 (vt, $^3J_{HH}$=6.3 Hz, 2H, *m-H pyr*), 7.07 (s, 2H, *H-16*), 7.02 (d, $^4J_{HH}$=2.3 Hz, 1H, *H-5*), 2.41 (s, 3H, *H-12*), 2.37 (s, 12H, *H-17*), -1.03 (s, 3H, *Ni-CH$_3$*).

^{13}C-NMR (101 MHz, CD_2Cl_2): δ (ppm) = 167.5 (C-7), 163.4 (C-1), 152.2 (*o*-C pyr), 148.9 (C-3), 147.5 (C-8), 141.9 (C-5), 140.3 (C-13), 138.3 (C-15), 136.9 (*p*-C pyr), 136.1 (C-9), 136.1 (C-11), 130.9 (C-10), 129.2 (C-16), 128.8 (C-14), 123.7 (*m*-C pyr), 121.4 (C-6), 96.8 (C-2), 71.6 (C-4), 21.8 (C-17), 21.2 (C-12), -7.7 (Ni-CH$_3$).

{3,5-Diiodo-*N*-[2,6-Tris(3,5-dimethylphenyl)-4-fluorophenyl]salicyl-aldiminato-κ^2-*N,O*}methylpyridinenickel(II) (^{pF}2-pyr)

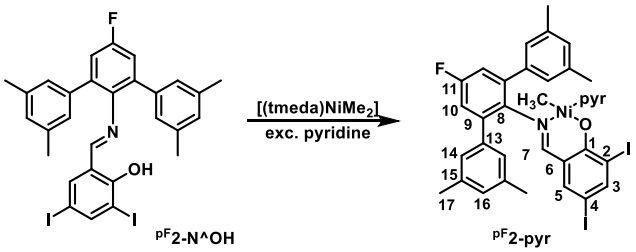

Catalyst precursor **^{pF}2-pyr** was kindly provided by Inigo Göttker-Schnetmann.

^{1}H-NMR (600 MHz, C_6D_6): δ (ppm) 8.16 (d, $^3J_{HH}$=5.1 Hz, 2H, *o-H pyr*), 7.97 (d, $^4J_{HH}$=2.2 Hz, 1H, *H-3*), 7.16 (s, 4H, *H-14*), 7.13 (d, $^3J_{HF}$=8.9 Hz, 2H, *H-10*), 7.09 (s, 1H, *H-7*), 6.91 (d, $^4J_{HH}$=2.2 Hz, 1H, *H-5*), 6.80 (s, 2H, *H-16*), 6.64 (t, $^3J_{HH}$=7.4 Hz, 1H, *p-H pyr*), 6.31 (vt, $^3J_{HH}$=6.6 Hz, 2H, *m-H pyr*), 2.19 (s, 12H, *H-17*), -0.62 (s, 3H, *Ni-CH$_3$*).

^{13}C-NMR (151 MHz, C_6D_6): δ (ppm) = 168.1 (C-7), 163.5 (C-1), 160.6 (d, $^2J_{CF}$=245.0 Hz, C-11), 151.9 (*o*-C pyr), 149.2 (C-3), 146.2 (d, $^4J_{CF}$=3.1 Hz, C-8), 142.0 (C-5), 139.2 (d, $^4J_{CF}$=1.4 Hz, C-13), 138.3 (d, $^3J_{CF}$=8.1 Hz, C-9), 138.1

(C-15), 135.9 (*p*-C pyr), 129.6 (C-16), 128.6 (C-14), 122.7 (*m*-C pyr), 121.1 (C-6), 116.5 (C-10), 97.3 (C-2), 72.0 (C-4), 21.5 (C-17), -7.6 (Ni-CH_3).

^{19}F NMR (376 MHz, C_6D_6) δ -116.82.

Elemental Analysis (%) $C_{35}H_{31}FI_2N_2NiO$: Found (calculated): C 50.93 (50.82), H 4.14 (3.78), N 3.69 (3.39).

{3,5-Diiodo-*N*-[2,4,6-Tris(3,5-dimethylphenyl)phenyl]salicylaldiminato-κ^2-*N,O*}methyl-pyridinenickel(II) ($^{p(Ar-Me)}$2-pyr)

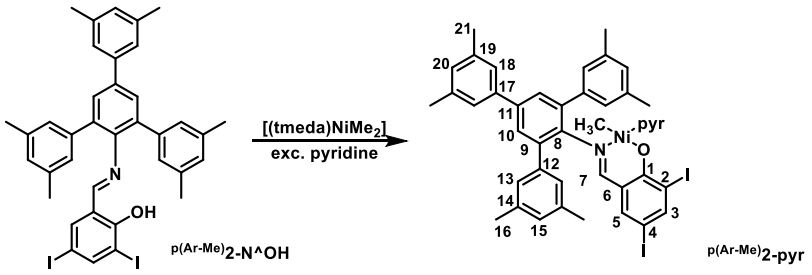

In a 25 mL Schlenk tube 152 mg (200 µmol, 1.0 eq) of **$^{p(Ar-Me)}$2-N^OH** and 45 mg (220 µmol, 1.1 eq) of [(tmeda)$NiMe_2$] were dissolved in 5 mL of benzene and 240 µL of pyridine (3.0 mmol, 2.5 eq). The dark red solution was stirred at room temperature for 1 hour. After filtration over a syringe filter, the solvent was removed by sublimation under vacuum. **$^{p(Ar-Me)}$2-pyr** was obtained as a red-orange solid (162 mg, 178 µmol, 89 %).

^{1}H-NMR (400 MHz, CD_2Cl_2): δ (ppm) = 8.39 (d, $^3J_{HH}$=5.0 Hz, 2H, *o-H pyr*), 7.86 (d, $^4J_{HH}$=2.3 Hz, 1H, *H-3*), 7.62 (br, 1H, *p-H pyr*), 7.59 (s, 2H, *H-10*), 7.53 (s, 1H, *H-7*), 7.31 (s, 2H, *H-18*), 7.29 (s, 4H, *H-13*), 7.12 (br, 2H, *m-H pyr*), 7.10 (s, 2H, *H-15*), 7.06 (d, $^4J_{HH}$=2.3 Hz, 1H, *H-5*), 7.02 (s, 1H, *H-20*), 2.40 (s, 12H, *H-16*), 2.37 (s, 6H, *H-21*), -0.96 (s, 3H, *Ni-CH_3*).

^{13}C-NMR (101 MHz, CD_2Cl_2): δ (ppm) = 167.4 (C-7), 163.4 (C-1), 152.1 (*o*-C pyr), 149.0 (C-3), 142.0 (C-5), 140.3 (C-8), 140.2 (C-12), 139.3 (C-11), 138.9 (C-19), 138.3 (C-14), 136.9 (*p*-C pyr), 136.7 (C-9), 129.6 (C-20), 129.3 (C-15), 128.8 (C-17), 128.8 (C-13), 125.3 (C-18), 123.6 (*m*-C pyr), 121.3 (C-6), 96.9 (C-2), 71.7 (C-4), 21.8 (C-16), 21.6 (C-21), -7.7 (Ni-CH_3).

Elemental Analysis (%) for $C_{43}H_{40}I_2N_2NiO$: Found (calculated): C 56.30 (56.55), H 4.76 (4.41), N 3.88 (3.07).

{3,5-Diiodo-*N*-[2,4,6-Tris(4-methoxy 3,5-dimethylphenyl)phenyl]salicyl-aldiminato-κ^2-*N,O*}methylpyridinenickel(II) ($^{p(Ar-OMe)}$2-pyr)

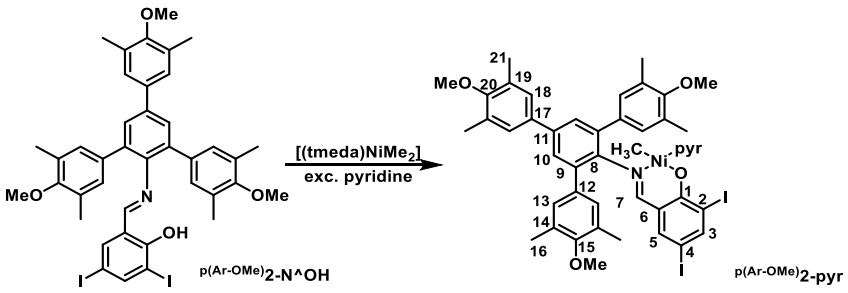

In a 25 mL Schlenk tube 200 mg (235 µmol, 1.0 eq) of $^{p(Ar-OMe)}$**2-N^OH** and 60 mg (294 µmol, 1.25 eq) of [(tmeda)$NiMe_2$] were dissolved in 10 mL of benzene and 850 µL of pyridine (10.6 mmol, 45 eq). The dark red solution was stirred at room temperature for 1 hour. After sublimation of all benzene under vacuum, the remaining orange solid was washed with pentane. The product was redissolved in benzene and filtered over a syringe filter. Sublimation of the solvent and drying under vacuum yielded $^{p(Ar-OMe)}$**2-pyr** as a red-orange solid (181 mg, 180 µmol, 77 %).

^{1}H-NMR (400 MHz, C_6D_6): δ (ppm) = 8.22 (d, $^3J_{HH}$=5.3 Hz, 2H, *o-H pyr*), 8.01 (d, $^4J_{HH}$=2.3 Hz, 1H, *H-3*), 7.90 (s, 2H, *H-10*), 7.51 (s, 4H, *H-13*), 7.41 (s, 2H, *H-18*), 7.24 (s, 1H, *H-7*), 6.96 (d, $^4J_{HH}$=2.3 Hz, 1H, *H-5*), 6.62 (t, $^3J_{HH}$=7.6 Hz, 1H, *p-H pyr*), 6.33 (vt, $^3J_{HH}$=6.5 Hz, 2H, *m-H pyr*), 3.43 (s, 3H, *OMe*), 3.41 (s, 6H, *OMe*), 2.32 (s, 12H, *H-16*), 2.26 (s, 6H, *H-21*), -0.45 (s, 3H, *Ni-CH_3*).

^{13}C-NMR (101 MHz, C_6D_6): δ (ppm) = 167.7 (C-7), 163.5 (C-1), 157.6 (C-20), 157.2 (C-15), 151.9 (o-C pyr), 149.1 (C-3), 148.9 (C-12), 148.8 (C-8), 142.0 (C-5), 139.4 (C-11), 136.6 (C-9), 136.3 (C-17), 135.9 (*p*-C pyr), 131.6 (C-13), 131.1 (C-14), 128.6 (C-19), 128.6 (C-11), 128.2 (C-18), 122.8 (*m*-C pyr), 121.5 (C-6), 100.4 (C-2), 71.9 (C-4), 59.5 (O-CH_3), 59.4 (O-CH_3), 16.5 (C-16), 16.4 (C-21), -7.5 (Ni-CH_3).

Elemental Analysis (%) for $C_{46}H_{46}I_2N_2NiO_4$: Found (calculated): C 56.79 (55.06), H 5.21 (4.62), N 3.04 (2.79).

3.4.4 Synthesis and Characterization of Naphthaldiminato Ni(II) Complexes

2-Hydroxy-*N*-[2,6-bis(3,5-dimethylphenyl)-4-fluorophenyl]-1-naphth-aldimine (^{pF}3-N^OH)

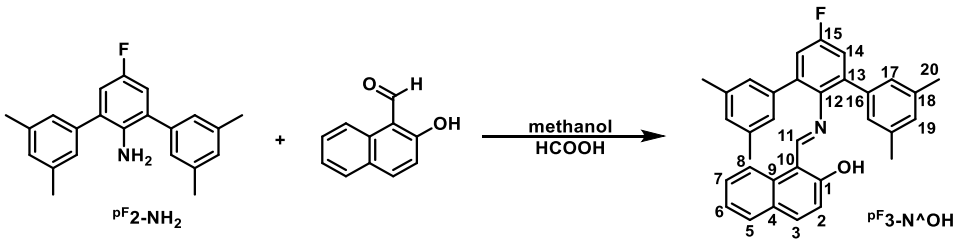

Under air, **^{pF}2-NH$_2$** (3.20 g, 10 mmol, 1.0 eq) and 2-hydroxynaphthaldehyde (2.07 g, 12 mmol, 1.2 eq) were suspended in 66 mL of methanol and 0.1 mL of formic acid was added. The mixture was heated to 65 °C for 1 hour while all starting material dissolved. After stirring for additional 4 hours at room temperature the suspension was cooled to 0 °C and the yellow precipitate filtered over a glass filter and washed with small portions of cold methanol. After drying under vacuum **^{pF}3-N^OH** was obtained as a yellow solid (4.47 g, 9.4 mmol, 94 %).

^{1}H-NMR (400 MHz, $CDCl_3$): δ (ppm) = 14.24 (d, $^{3}J_{HH}$=2.4 Hz, 1H, *OH*), 8.69 (d, $^{3}J_{HH}$=2.4 Hz, 1H, *H-11*), 7.66 (d, $^{3}J_{HH}$=9.1 Hz, 1H, *H-8*), 7.59 (dd, $^{3}J_{HH}$=7.7 Hz, $^{4}J_{HH}$=1.6 Hz, 1H, *H-7*), 7.22 (m, 2H, *H-5*, *H-6*), 7.13(d, $^{3}J_{HF}$=9.2 Hz, 2H, *H-14*), 7.06 (s, 4H, *H-17*), 7.03 (d, $^{3}J_{HH}$=8.1 Hz, 1H, *H-2*), 6.98 (d, $^{3}J_{HH}$=9.2 Hz, 1H, *H-3*), 6.91 (s, 3H, *H-19*), 2.26 (s, 12H, *H-20*).

^{13}C-NMR (101 MHz, $CDCl_3$): δ (ppm) = 166.3 (C-1), 163.1 (C-11), 160.2 (d, $^{1}J_{CF}$=245.6 Hz, C-15), 139.8 (d, $^{4}J_{CF}$=3.0 Hz, C-12), 138.8 (d, $^{4}J_{CF}$=1.6 Hz, C-16), 138.3 (C-17), 137.8 (d, $^{3}J_{CF}$=8.2 Hz, C-13), 135.4 (C-8), 133.2 (C-9), 129.3 (C-19), 129.0 (C-7), 127.5 (C-18), 127.4 (C-5), 127.3 (C-4), 123.2 (C-6), 121.0 (C-3), 119.2 (C-2), 116.8 (d, $^{2}J_{CF}$=22.3 Hz, C-14), 108.7 (C-10), 21.4 (C-20).

^{19}F-NMR (376 MHz, $CDCl_3$): δ (ppm) = -117.38 (s).

Elemental Analysis (%) for $C_{33}H_{28}FNO$: Found (calculated): C 83.79 (83.69), H 6.21 (5.95), N 2.95 (2.96).

{2-Hydroxy-*N*-[2,6-bis(3,5-dimethylphenyl)-4-fluorophenyl]-1-naphth-aldiminato-κ^2-*N,O*}methylpyridinenickel(II) (^{pF}3-pyr)

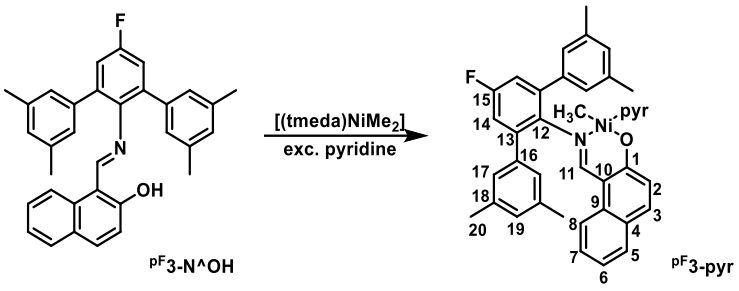

In a 25 mL Schlenk tube 476 mg (1 mmol, 1.0 eq) of **^{pF}3-N^OH** and 218 mg (1.06 mmol, 1.06 eq) of [(tmeda)$NiMe_2$] were cooled to -50 °C and dispersed in 5 mL of toluene and 200 µL of pyridine(2.5 mmol, 2.5 eq). The mixture was allowed to slowly warm to 0 °C over 45 min while the color changed to dark red. After removing all volatiles under vacuum, the red-orange solid was redissolved in benzene and filtered over a syringe filter. Sublimation of the benzene under vacuum yielded **^{pF}3-pyr** as a red-orange solid (549 mg, 0.9 mmol, 89 %).

^{1}H-NMR (400 MHz, C_6D_6): δ (ppm) = 8.18 (s, 1H, *H-11*), 8.11 (dd, $^3J_{HH}$=6.8 Hz, $^4J_{HH}$=1.6 Hz, 2H, *H-22*), 7.41 (dd, $^3J_{HH}$=8.0 Hz, $^4J_{HH}$=1.1 Hz, 1H, *H-8*), 7.34 7.19 (d, $^3J_{HF}$=8.9 Hz, 2H, *H-14*), (s, 4H, *H-17*), 7.34 (d, $^3J_{HH}$=9.0 Hz, 1H, *H-3*), 7.26 (dt, $^3J_{HH}$= 7.7 Hz, $^4J_{HH}$=1.4 Hz, 1H, *H-6*), 7.08 (dt, $^3J_{HH}$=7.4 Hz, $^4J_{HH}$=1.0 Hz, 1H, *H-7*), 6.95 (d, $^3J_{HH}$= 8.2 Hz, 1H, *H-5*), 6.85 (m, 3H, *H-19, H-2*), 6.56 (tt, $^3J_{HH}$=7.7 Hz, $^4J_{HH}$=1.6 Hz, 1H, *H-24*), 6.84 (dt, $^3J_{HH}$=6.3 Hz, $^4J_{HH}$=1.4 Hz, 2H, *H-23*), 2.22 (s, 12H, *H-20*), -0.56 (s, 3H, *H-21*).

^{13}C-NMR (101 MHz, C_6D_6): δ (ppm) = 167.6 (C-1), 163.2 (C-11), 160.5 (d, $^1J_{CF}$=243.8 Hz, C-15), 151.4 (C-22), 147.8 (d, $^4J_{CF}$=3.2 Hz, C-12), 140.5 (C-16), 139.1 (d, $^3J_{CF}$=8.0 Hz, C-13), 138.1 (C-18), 135.6 (C-4), 135.3 (C-24), 134.8 (C-3), 129.3 (C-19), 129.0 (C-8), 128.9 (C-17), 127.3 (C-6), 126.7 (C-9), 126.0 (C-2), 122.8 (C-23), 121.8 (C-7), 120.0 (C-5), 116.9 (d, $^2J_{CF}$=22.1 Hz, C-14), 112.0 (C-10), 21.6 (C-20), -7.8 (C-21).

^{19}F-NMR (376 MHz, C_6D_6): δ (ppm) = -118.12.

Elemental Analysis (%) for $C_{39}H_{35}FN_2NiO$: Found (calculated): C 74.16 (74.90), H 6.04 (5.64), N 4.50 (4.48).

{2-Hydroxy-*N*-[2,6-bis(3,5-dimethylphenyl)-4-methylphenyl]-1-naphth-aldiminato-κ^2-*N,O*}methylpyridinenickel(II) (^{pMe}3-pyr)

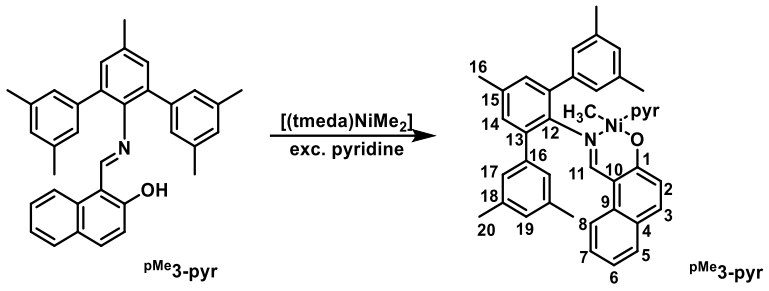

Catalyst precursor **^{pMe}3-pyr** was kindly provided by Inigo Göttker-Schnetmann.

^{1}H-NMR (400 MHz, CD_2Cl_2): δ (ppm) = 8.30 (d, $^3J_{HH}$=6.1 Hz, 2H, *o-H pyr*), 8.11 (s, 1H, *H-11*), 7.59 (t, $^3J_{HH}$=7.6 Hz, 1H, *p-H pyr*), 7.50 (d, $^3J_{HH}$=8.0 Hz, 1H, *H-5*), 7.47 (d, $^3J_{HH}$=9.2 Hz, 2H, *H-3*), 7.26 (s, 4H, *H-17*), 7.21 (s, 2H, *H-14*), 7.20 (vt, $^3J_{HH}$=8.3 Hz, 1H, *H-7*), 7.08 (m, 5H, *H-6/19/m-H pyr*), 6.86 (d, $^3J_{HH}$=8.4 Hz, 1H, *H-8*), 6.60 (d, $^3J_{HH}$=9.2 Hz, 1H, *H-2*), 2.43 (s, 3H, *H-16*), 2.38 (s, 12H, *H-20*), -1.08 (s, 3H, *Ni-CH$_3$*).

^{13}C-NMR (101 MHz, CD_2Cl_2): δ (ppm) = 167.0 (C-1), 162.7 (C-11), 151.6 (*o*-C pyr), 149.1 (C-12), 141.3 (C-16), 138.2 (C-18), 136.9 (C-13), 136.4 (*p*-C pyr), 135.3 (C-15), 135.2 (C-9), 134.3 (C-3), 130.8 (C-14), 128.9 (C-17), 128.8 (C-19), 128.7 (C-5), 127.3 (C-7), 126.3 (C-4), 125.9 (C-2), 123.8 (*m*-C pyr), 121.6 (C-6), 119.5 (C-8), 111.6 (C-10), 21.7 (C-20), 21.1 (C-16), -8.1 (Ni-CH_3).

Elemental Analysis (%) for $C_{40}H_{38}N_2NiO$: Found (calculated): C 77.47 (77.31), H 6.21 (6.16), N 4.87 (4.51).

3.4.5 Additional Spectra and Data

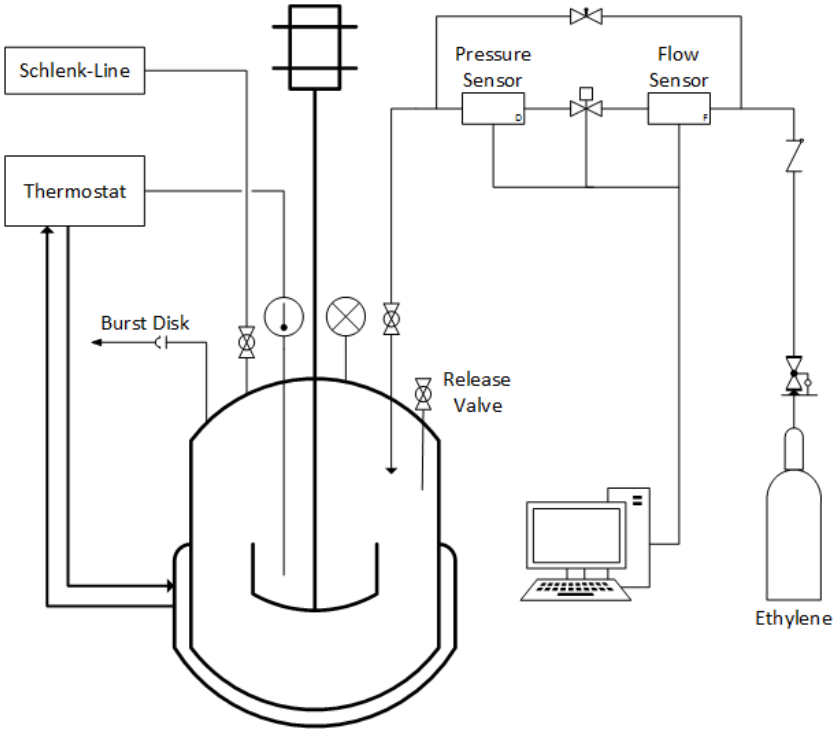

Figure 3.17: Flow chart of the *Büchi miniclave* reactor with a 200 mL steel vessel.

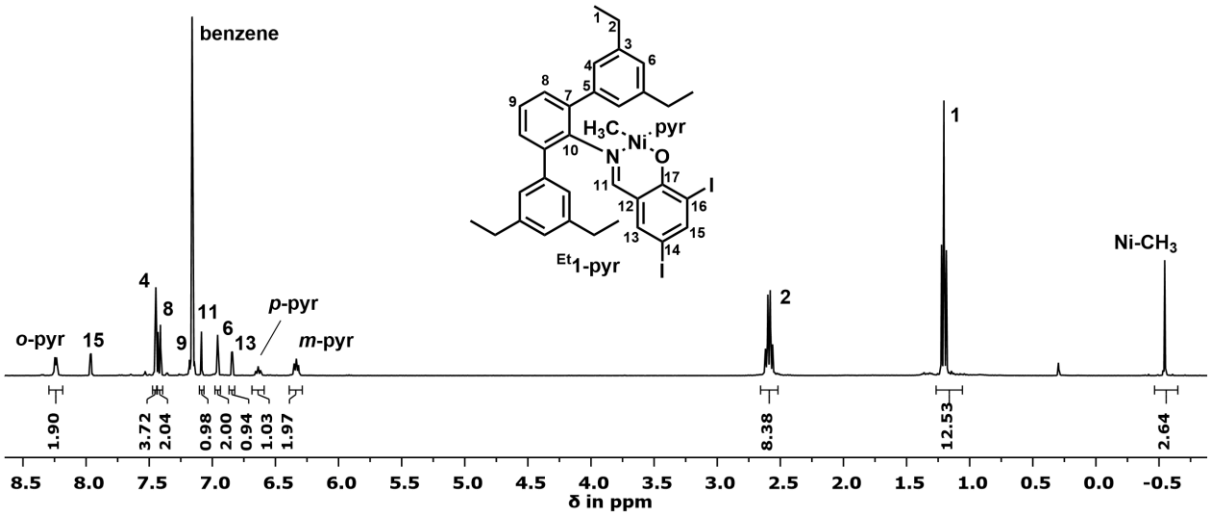

Figure 3.18: ^{1}H NMR spectrum (400 MHz, C_6D_6, 298 K) of complex ^{Et}**1-pyr**.

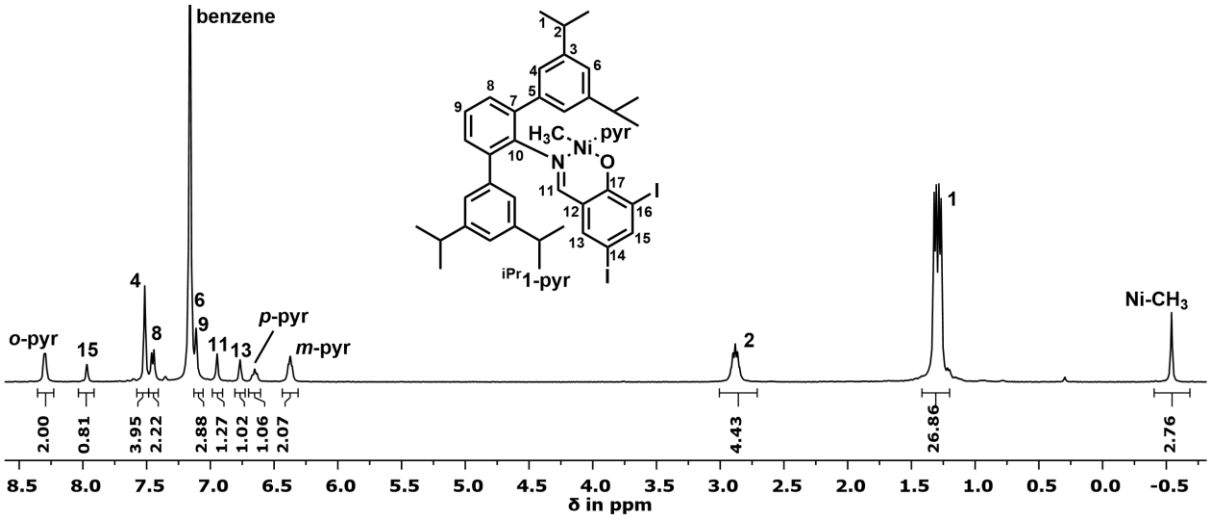

Figure 3.19: ^{1}H NMR spectrum (400 MHz, C_6D_6, 298 K) of complex ^{iPr}**1-pyr**.

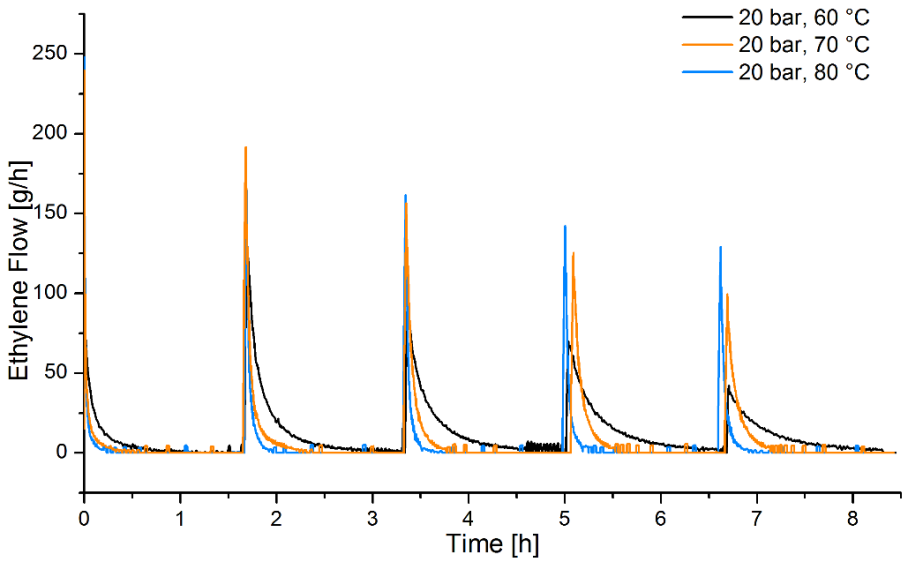

Figure 3.20: Mass flow traces for polymerizations with stepwise addition of ^{Me}**1-pyr** (120 µmol) via a pressure burette at different temperatures (60, 70, and 80 °C) at 20 bar.

Oligomerization Data

Table 3.11: Oligomerization results with complex ^{MeOMe}**2-pyr** at different reaction conditions.

entry	p [bar]	T [°C]	yield [g]	TON[a]	M_n (NMR) [g mol^{-1}][b]	M_n (GPC) [g mol^{-1}][c]	M_w/M_n (GPC)[c]	branches /1000 C[d]
1	40	40	0.4	1,400	1,400	3,000	1.7	80
2	35	40	5.5	19,600	1,400	3,100	1.7	79
3	30	40	5.8	20,700	1,400	3,100	1.7	79
4	25	40	5.1	18,200	1,400	3,100	1.7	79
5	20	40	4.2	15,000	1,400	3,000	1.7	79
6	15	40	4.5	16,100	1,300	2,900	1.7	82
7	10	40	3.0	10,700	1,200	2,800	1.6	83
8	20	20	0.7	2,500	2,100	4,600	1.8	79
9	20	30	2.1	7,500	1,700	3,900	1.7	79
10	20	40	4.2	15,000	1,400	3,000	1.7	79
11	20	50	6.9	24,600	1.100	1,500	2.4	81
12	20	60	3.0	10,700	900	2,100	1,5	81

reaction conditions: 10 µmol ^{MeOMe}**2-pyr** in 100 mL of toluene for 1 h. [a] TON x mol [C_2H_4] x mol^{-1} [Ni]. [b] molecular weights calculated from ^{1}H NMR intensity ratio of unsaturated end groups vs. overall integral. [c] in THF vs. polystyrene standards. [d] degree of branching calculated from ^{1}H NMR intensity ratio of methyl groups (corrected for saturated end groups) vs. overall integral.

Table 3.12: Microstructure analysis of an oligomer obtained with ^{MeOMe}**2-pyr** with fractional amount of different branch lengths.[a]

entry	p [bar]	T [°C]	branches /1000 C	methyl[a] [%]	ethyl[a] [%]	propyl[a] [%]	C_{4+}[a] [%]	*sec*-butyl[a] [%]
1	40	40	80	76	9	3	6	6
2	35	40	79	77	7	4	7	5
3	30	40	79	76	9	3	6	6
4	25	40	79	75	8	3	7	7
5	20	40	79	75	8	3	7	7
6	15	40	82	72	9	3	8	8
7	10	40	83	73	8	3	7	8
8	20	20	79	82	7	3	5	3
9	20	30	79	80	7	3	6	5
10	20	40	79	75	8	3	7	7
11	20	50	81	70	9	4	9	9
12	20	60	81	65	11	3	10	11

[a] percentage of different branch lengths can be calculated from relative intensity ratios of the corresponding signals ($1B_1$, $1B_2$, $1B_3$, $*B_{4+}$, B) of the respective branch in the ^{13}C NMR spectrum.

Table 3.13: Oligomerization results with complex $^{p(Ar\text{-}OMe)}$**2-pyr** at different reaction conditions.

entry	p [bar]	T [°C]	yield [g]	TON[a]	M_n (NMR) [g mol^{-1}][b]	M_n (GPC) [g mol^{-1}][c]	M_w/M_n (GPC)[c]	branches /1000 C[d]
1	40	40	5.7	20,400	1,300	2,800	1.7	80
2	35	40	6.0	21,400	1,300	2,900	1.6	81
3	30	40	7.0	25,000	1,300	2,900	1.7	81
4	25	40	3.1	11,100	1,300	2,900	1.7	81
5	20	40	5.8	20,700	1,300	2,800	1.7	81
6	15	40	4.3	15,400	1,200	2,700	1.6	82
7	10	40	3.3	11,800	1,200	2,600	1.6	85
8	20	20	0.7	2,500	2,000	4,200	1.7	82
9	20	30	2.6	9,300	1,500	3,400	1.7	82
10	20	40	5.8	20,700	1,300	2,800	1.7	81
11	20	50	6.8	24,300	1,000	2,300	1.6	81
12	20	60	5.0	17,900	900	1,900	1.5	81

reaction conditions: 10 µmol $^{p(Ar\text{-}OMe)}$**2-pyr** in 100 mL of toluene for 1 h. [a] TON x mol [C_2H_4] x mol^{-1} [Ni]. [b] molecular weights calculated from ^1H NMR intensity ratio of unsaturated end groups vs. overall integral. [c] in THF vs. polystyrene standards. [d] degree of branching calculated from ^1H NMR intensity ratio of methyl groups (corrected for saturated end groups) vs. overall integral.

Table 3.14: Microstructure analysis of an oligomer obtained with $^{p(Ar\text{-}OMe)}$**2-pyr** with fractional amount of different branch lengths.[a]

entry	p [bar]	T [°C]	branches /1000 C	methyl[a] [%]	ethyl[a] [%]	propyl[a] [%]	C_{4+}[a] [%]	*sec*-butyl[a] [%]
1	40	40	80	78	8	3	4	7
2	35	40	81	77	8	4	4	7
3	30	40	81	73	8	4	8	7
4	25	40	81	73	7	3	8	8
5	20	40	81	72	9	4	9	7
6	15	40	82	72	10	3	7	8
7	10	40	85	71	8	4	8	8
8	20	20	82	84	5	3	5	3
9	20	30	82	77	6	3	9	5
10	20	40	81	72	9	4	9	7
11	20	50	81	73	8	2	6	9
12	20	60	81	66	11	3	8	13

[a] percentage of different branch lengths can be calculated from relative intensity ratios of the corresponding signals ($1B_1$, $1B_2$, $1B_3$, $*B_{4+}$, B) of the respective branch in the ^{13}C NMR spectrum.

Table 3.15: Oligomerization results with complex $^{p(Ar\text{-}Me)}$**2-pyr** at different reaction conditions.

Entry	p [bar]	T [°C]	yield [g]	TON[a]	M_n (NMR) [g mol^{-1}][b]	M_n (GPC) [g mol^{-1}][c]	M_w/M_n (GPC)[c]	branches /1000 C[d]
1	40	40	1.7	6,100	1,400	2,400	2.3	70
2	30	40	7.5	26,800	1,400	3,300	1.7	74
3	20	40	5.5	19,600	1,400	3,100	1.8	78
4	10	40	3.5	12,500	1,200	2,800	1.7	78
5	20	60	4.9	17,500	900	2,100	1.6	81
6	20	50	2.5	8,900	1,200	2,600	1.7	79
7	20	40	5.5	19,600	1,400	3,100	1.8	78
8	20	30	0.9	3,200	1,700	4,300	1.6	76

reaction conditions: 10 µmol $^{p(Ar\text{-}Me)}$**2-pyr** in 100 mL of toluene for 1 h. [a] TON x mol [C_2H_4] x mol^{-1} [Ni]. [b] molecular weights calculated from ^1H NMR intensity ratio of unsaturated end groups vs. overall integral. [c] in THF vs. polystyrene standards. [d] degree of branching calculated from ^1H NMR intensity ratio of methyl groups (corrected for saturated end groups) vs. overall integral.

Table 3.16: Microstructure analysis of an oligomer obtained with **$^{p(Ar\text{-}Me)}$2-pyr** with fractional amount of different branch lengths.[a]

entry	p [bar]	T [°C]	branches /1000 C	methyl[a] [%]	ethyl[a] [%]	propyl[a] [%]	C_{4+}[a] [%]	*sec*-butyl[a] [%]
1	40	40	70	80	5	3	9	4
2	30	40	74	79	6	3	7	4
3	20	40	78	78	5	3	10	4
4	10	40	78	70	9	3	11	7
5	20	60	81	64	11	3	13	9
6	20	50	79	74	7	3	10	6
7	20	40	78	73	9	2	10	6
8	20	30	76	79	4	4	9	4

[a] percentage of different branch lengths can be calculated from relative intensity ratios of the corresponding signals ($1B_1$, $1B_2$, $1B_3$, $*B_{4+}$, B) of the respective branch in the ^{13}C NMR spectrum.

Table 3.17: Oligomerization results with complex **^{pMe}2-pyr** at different reaction conditions.

entry	p [bar]	T [°C]	yield [g]	TON[a]	M_n (NMR) [g mol^{-1}][b]	M_n (GPC) [g mol^{-1}][c]	M_w/M_n (GPC)[c]	branches /1000 C[d]
1	40	40	8.2	29,300	1,300	3,200	1.8	74
2	30	40	7.8	27,900	1,400	3,400	1.7	75
3	20	40	5.3	18,900	1,400	3,300	1.7	78
4	10	40	2.4	8,600	1,200	2,900	1.7	66
5	20	60	6.1	21,800	900	1,700	1.8	79
6	20	50	7.1	25,400	1,300	3,000	1.7	78
7	20	40	5.3	18,900	1,400	3,300	1.7	78
8	20	30	2.4	8,600	1,700	3,900	1.8	82

reaction conditions: 10 µmol **^{pMe}2-pyr** in 100 mL of toluene for 1 h. [a] TON x mol $[C_2H_4]$ x mol^{-1} [Ni]. [b] molecular weights calculated from ^1H NMR intensity ratio of unsaturated end groups vs. overall integral. [c] in THF vs. polystyrene standards. [d] degree of branching calculated from ^1H NMR intensity ratio of methyl groups (corrected for saturated end groups) vs. overall integral.

Table 3.18: Microstructure analysis of an oligomer obtained with ^{pMe}**2-pyr** with fractional amount of different branch lengths.[a]

entry	p [bar]	T [°C]	branches /1000 C	methyl[a] [%]	ethyl[a] [%]	propyl[a] [%]	C_{4+}[a] [%]	*sec*-butyl[a] [%]
1	40	40	74	75	8	5	9	5
2	30	40	75	77	6	4	9	4
3	20	40	78	78	6	4	11	4
4	10	40	66	72	6	6	12	6
5	20	60	79	72	11	3	6	8
6	20	50	78	78	6	3	8	5
7	20	40	78	78	6	4	11	4
8	20	30	82	74	8	3	11	4

[a] percentage of different branch lengths can be calculated from relative intensity ratios of the corresponding signals ($1B_1$, $1B_2$, $1B_3$, $*B_{4+}$, B) of the respective branch in the ^{13}C NMR spectrum.

4 Selective Oligomer Functionalization

4.1 Introduction

The functionalization of non-polar polyolefins is of great interest.[96] In comparison to unfunctionalized polymers, their functionalized analogues often benefit from better material properties regarding adhesion, paintability, and miscibility and give access to more complex macromolecular architectures such as *graft*- and *block*-copolymers. Especially lower molecular weight oligomers bearing a functional group are of interest for the applications as additives, surface modifiers, and lubricants.

Generally, several different strategies can be applied for the synthesis of functionalized polyolefins. One is the (co)polymerization of functional monomers by ROMP, ADMET or insertion (co)polymerization which results in the formation of multifunctional polymers in a single polymerization step with the functional groups incorporated into the polymer backbone.[19,20,97-99] The most common reaction for the commercial synthesis of functionalized polyolefins is the post-polymerization modification of the polymer backbone by radical reactions or by functionalization of unsaturated groups present in the polymer. This strategy takes advantage of the well-established polymerization reactions for non-polar olefins and offers great variability towards the functional groups accessible.[8,100,101] Here, an example is the ethylene chain growth on metallocenes with simultaneous chain transfer reactions as employed for the production of linear polyethylene waxes.[74] These are then functionalized by oxidation under severe conditions to yield linear oligoethylenes with an undefined number of different functional groups (primarily carboxylic acids) per chain.[74]

A strategy for a much more selective mono-functionalization of polymers involves the selective end-capping in living polymerizations which are mostly catalyzed by transition metal catalysts.[102,103] The Ziegler Alfol process is an illustrative and practically important example using a main group metal.[62] Chain-growth on aluminum yields longer chain aluminum alkyls. Subsequent oxidation and hydrolysis affords linear long-chain terminal alcohols in a reaction that is stoichiometric in aluminum. Due to the principle of one chain per active site, this method

is expensive when applied to transition metal catalysis because of the high amounts of catalyst required. This led to the development of a similar functionalization approach eliminating the need for stoichiometric amounts of metal catalyst. The use of less costly chain transfer agents (CTA) like AlR_3 or ZnR_2, and *in situ* chain transfer to these functional agents allows for a much more metal efficient reaction, since every active species generates a large number of polymer chains.[63,65-68] The major drawback of this reaction thus far is its limitation to the synthesis of linear, functionalized products and it has not yet been reported for the preparation of monofunctionalized, branched polymers. The selective introduction of a single functionality can also be carried out by post-polymerization functionalization of unsaturated chain ends. Again, this approach takes advantage of known polymerization procedures and gives access to a great variety of different polyolefins as a basis for the functionalization. Successful functionalization using this approach was reported for different reactions, involving e.g. hydroboration,[104,105] hydrosilylation,[106] and hydroalumination.[107,108] However, limitations can result from the poor solubility of the unfunctionalized polymer and the low concentration of double bonds present.

4.2 Results and Discussion

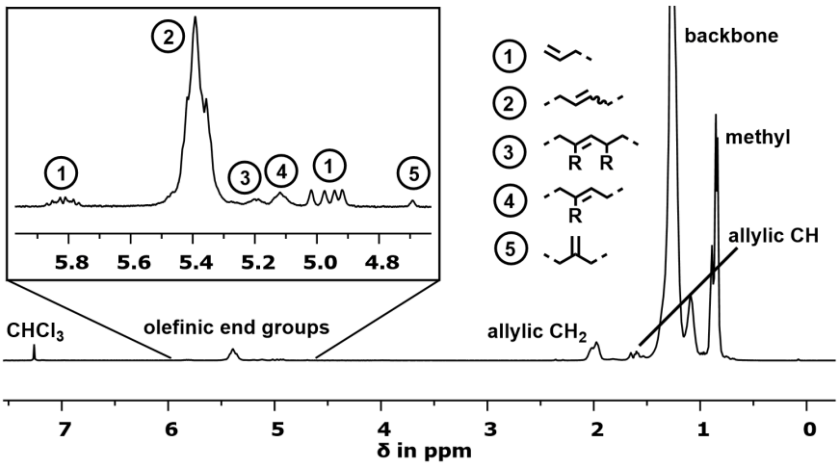

Figure 4.1: Representative ^{1}H-NMR spectrum of an unfunctionalized ethylene oligomer (cf. Chapter 3).

Considering that during the oligomerization reaction chain termination occurs via β-hydride elimination with the Ni(II)–salicylaldiminato complexes employed, every oligomer chain comprises an unsaturated end group. Therefore, the oligomers presented in the previous chapter exhibit potential for the synthesis of monofunctional, highly branched ethylene oligomers by post-polymerization functionalization.

Due to the extensive chain walking of the catalysts, most end groups found in these ethylene oligomers are internal double bonds and only minor amounts of terminal double bonds are

present (**Figure 4.1**). However, in terms of uniform reactivity properties of the resulting functionalized products, terminal functional groups are more preferable than a mixture of primary, secondary, and tertiary functional groups. An isomerization of the double bonds to the chain end prior to the functionalization step is one approach to achieve this aim.

4.2.1 Isomerizing Alkoxycarbonylation

A possible approach toward this issue is an isomerizing alkoxycarbonylation approach. It allows for a highly selective conversion of internal double bonds to terminal ester groups in a one-step reaction in the presence of carbon monoxide, an alcohol, and a Pd(II) catalyst.[109,110] The reaction is well established for the conversion of unsaturated fatty acids to the corresponding α,ω-diesters.[111-114] The isomerizing alkoxycarbonylation also allows for the isomerization and functionalization of trisubstituted double bonds. This was shown recently by Hanna Busch with the selective functionalization of terpenes.[115] However, the conversion of such trisubstituted double bonds was found to be considerably slower than the conversion of disubstituted or terminal double bonds. Overall, the isomerizing alkoxycarbonylation appears attractive for the synthesis of end-functionalized oligomers (**Scheme 4.1**). However, despite the extensive research dedicated to this reaction and its broad application in different chemical fields, the isomerizing alkoxycarbonylation has not yet been applied to such branched and structurally challenging polymers.

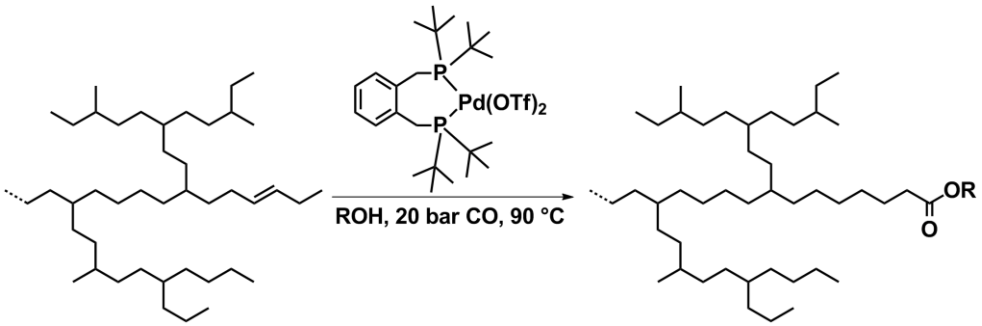

Scheme 4.1: Selective monofunctionalization of a hyperbranched ethylene oligomer by isomerizing alkoxycarbonylation.[85]

Typically, the methanol or ethanol co-reagent required for this reaction also serves as a solvent. However, this approach was not suitable for the functionalization of the non-polar oligomers due to their lack of solubility. After screening the solubility of the ethylene oligomers in a range of different solvent systems, a mixture of pentane and ethanol (1:1) proved to be most suited. However, this still did not result in a homogeneous solution of the oligomer, but rather a finely dispersed suspension. As the catalyst precursor, the well-established, isolated

[(dtbpx)Pd(OTf)2] complex (dtbpx = 1,2-bis[(di-tertbutylphosphino)methyl]benzene) was used.[111]

For the conversion of unsaturated fatty acid esters to the corresponding diester, very low catalyst loadings of down to 0.2 mol% can be sufficient. In order to map out the catalyst loadings required for the esterification of ethylene oligomers, the reaction was carried out with different amounts of catalyst. Addition of 2 mol%, 4 mol%, and 8 mol% of [(dtbpx)Pd(OTf)2] gave 30 %, 45 %, and 50 % conversion, respectively, within 5 days for a 1,300 g mol^{-1} oligomer (1 g oligomer, 20 bar of CO, 90 °C). Since the conversion could not be increased significantly by doubling the amount of catalyst from 4 to 8 mol%, a catalyst loading of 4 mol% was chosen as a compromise between catalyst efficiency and olefin conversion for all the following ethoxycarbonylation reactions of ethylene oligomers. Functionalization of the oligomers is evidenced by new signals appearing in the ^{1}H NMR spectra at 4.14 and 2.29 ppm for the methylene groups adjacent to the ester functionality (**Figure 4.2**).

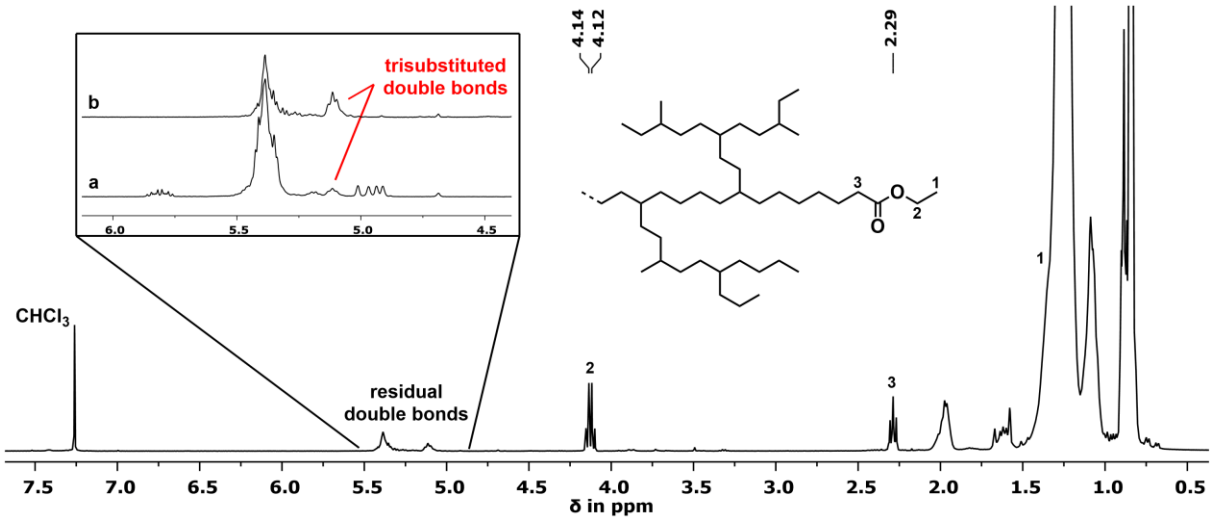

Figure 4.2: ^{1}H NMR spectrum of an ester-functionalized oligomer, with the olefinic region before (a) and after the isomerizing ethoxycarbonylation highlighted (entry 3, **Table 4.1**).

However, conversion is not complete, as indicated by the observation of signals in the olefinic region of the spectrum representing partially isomerized, but non-functionalized residual double bonds. To further investigate the scope of this reaction as a candidate for post polymerization functionalization, it was applied to oligomers with different molecular weights (**Table 4.1**).

Table 4.1: Conversions of the isomerizing alkoxycarbonylation of different molecular weight oligomers.[85]

entry	M_n (NMR)	branches/1000 C	conversion[a] (%)
1	850	80	50
2	1000	81	35
3	1300	75	35
4	2600	74	17

Reaction conditions: 1 g of oligomer, 4 mol% of [(dtbpx)Pd(OTf)$_2$], 10 mL of pentane/EtOH (1/1), 20 bar CO, 90 °C, 4 days. [a] To the primary ester.

The highest conversion to the ester was obtained using low-molecular-weight oligomers (850 g mol^{-1}, entry 4.1-1). For higher molecular weights the degrees of functionalization are significantly lower. Despite the incomplete conversion of the isomerizing ethoxycarbonylation when applied to the hyperbranched ethylene oligomers, it is still very selective and the primary esters are formed exclusively for all oligomers studied. No secondary esters are formed, as evidenced by NMR spectroscopy. In the ^{13}C NMR spectrum only one resonance for a carboxylic carbon atom is observed at 174.1 ppm. The lack of any cross signals of this carbon in the corresponding ^{1}H,^{13}C gHMBC NMR spectrum to any backbone CH groups confirmed this carbon atom to belong to a primary ester end group (**Figure 4.3**).

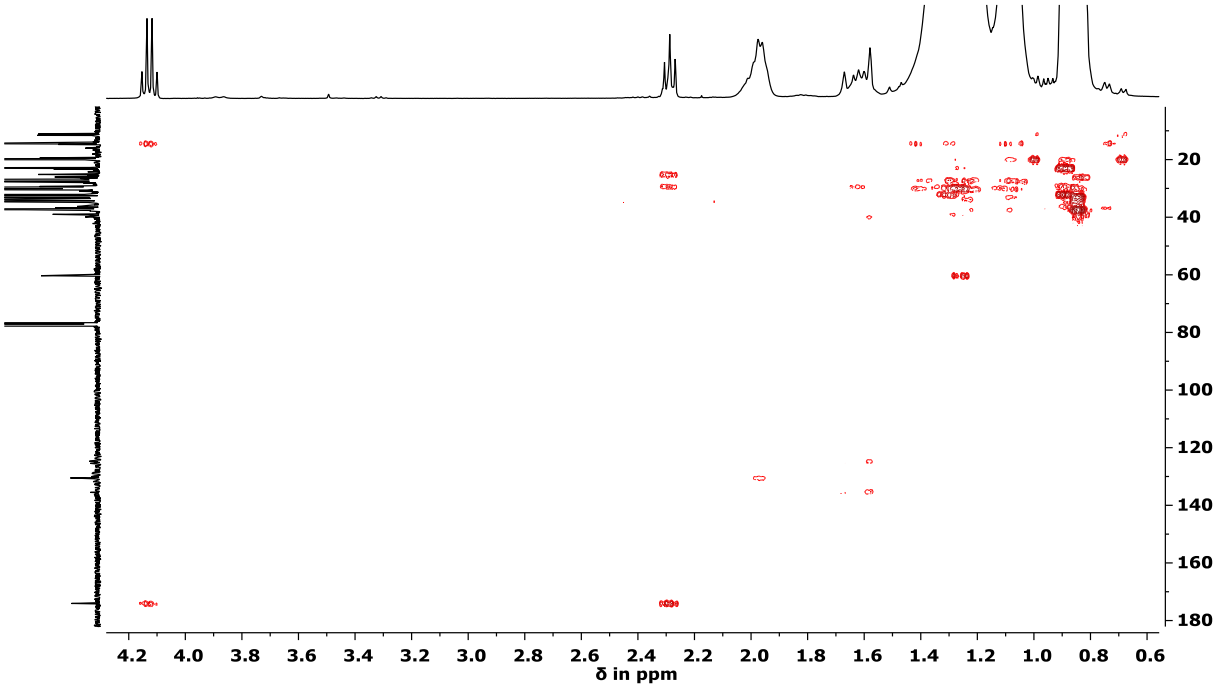

Figure 4.3: ^{1}H,^{13}C gHMBC NMR spectrum (400 MHz, 298 K, in $CDCl_3$) of a oligomer obtained by isomerizing ethoxycarbonylation (entry 3, **Table 4.1**).

Residual internal and trisubstituted double bonds are found after the reaction, while the terminal vinyl groups are fully converted. Notably, trisubstituted double bonds at a branching point are enriched during the reaction due to the high extent of isomerization (**Figure 4.2**). They appear poorly reactive for further conversion and thus represent a limiting factor for the degree of functionalization.[115] Additionally, the lower conversions of higher molecular weight oligomers can probably be attributed to limited solubility of the oligomers in the solvent mixture used for the reaction. However, decreasing the amount of ethanol to enhance the substrate solubility resulted in decreased degrees of functionalization. This is in agreement with previously published results, showing that the alcoholysis is the rate limiting step of the isomerizing alkoxycarbonylation.[116,117] Also, higher dilution or utilization of other solvent mixtures such as pentane/methanol and toluene/ethanol could not enhance conversion.

To further increase the degree of functionalization, a second repeated alkoxycarbonylation step of partially functionalized products was performed (**Table 4.1**, entry 4.1-3). This resulted in further conversion of internal double bonds with conversions similar to those of the first step, giving an overall degree of functionalization of 65 % (**Figure 4.4**). At the same time, the amount of trisubstituted double bonds remains unaltered suggesting a slow conversion of these double bonds to occur even in these sterically demanding oligomers. A complete lack of reactivity should rather be expected to result in a further enrichment by isomerization. In summary, isomerizing alkoxycarbonylation allows for a selective terminal post-functionalization of highly branched ethylene oligomers, though quantitative conversion could not be achieved. Nonetheless, 100 % ester functionalized product can be obtained by column chromatography where the functionalized chains are easily separated from the non-polar starting material (**Figure 4.5**).

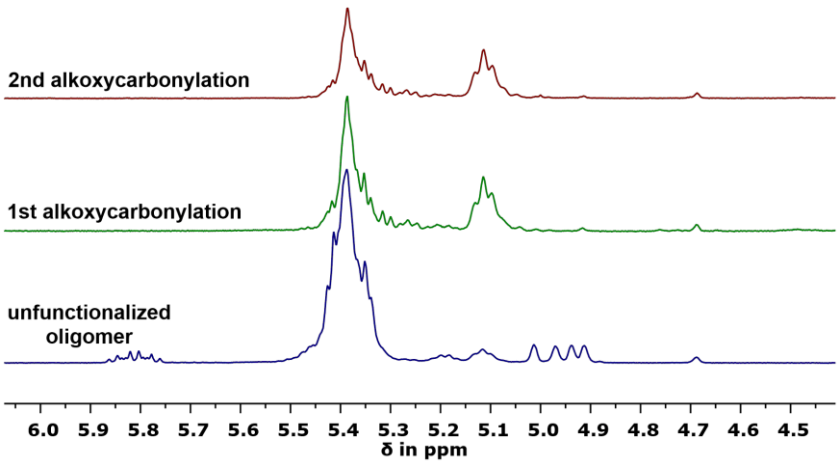

Figure 4.4: Olefinic region of the proton NMR spectrum of the unfunctionalized oligomer (bottom), after the first (center) and the second alkoxycarbonylation (top).

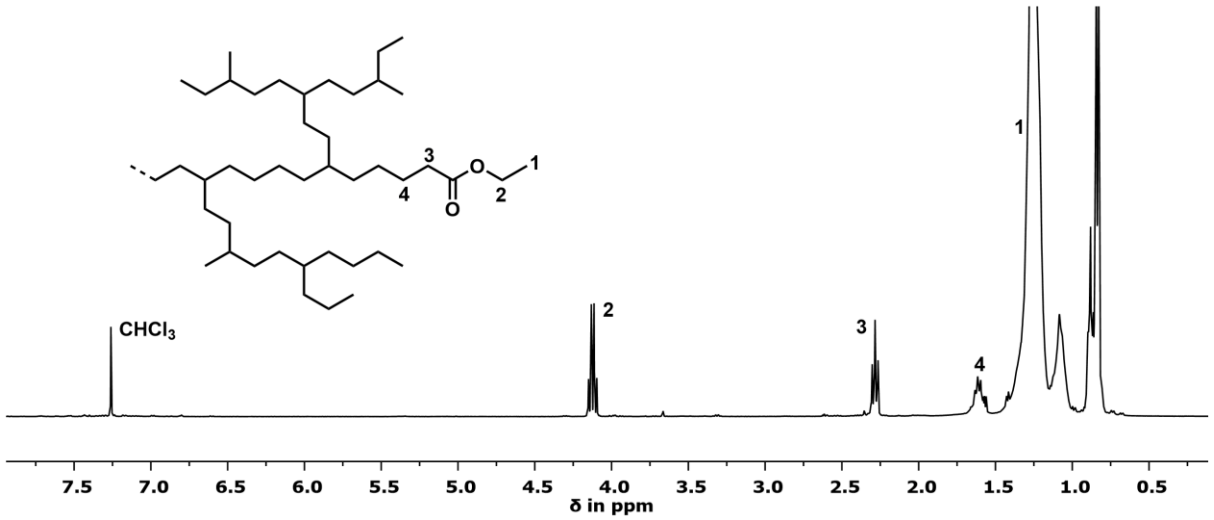

Figure 4.5: Ester functionalized ethylene oligomer from ethoxycarbonylation after column chromatography.

4.2.2 Functionalization via Cross Metathesis Reactions

An alternative approach to chain end functionalized oligomers is cross metathesis with functionalized olefins and subsequent hydrogenation of the double bond.[118-120] This is a promising reaction also in terms of large scale synthesis, considering the low catalyst loadings required. Furthermore, it has already been demonstrated by Coates *et al.* for the functionalization of polyolefins.[121] However, due to the high degrees of internal double bonds present in these oligomers, the reduction of molecular weight might be an issue. In order to obtain ester functionalized oligomers, the cross metathesis reaction of an ethylene oligomer (1,600 g mol^{-1}, 78 branches/1000 C atoms) was studied with 10 equiv of ethyl acrylate in the presence of 0.1 mol% Hoveyda-Grubbs second generation (HG II) catalyst precursor (**Scheme 4.2**). Excess ethyl acrylate was applied in order to suppress self-metathesis of the oligomers.

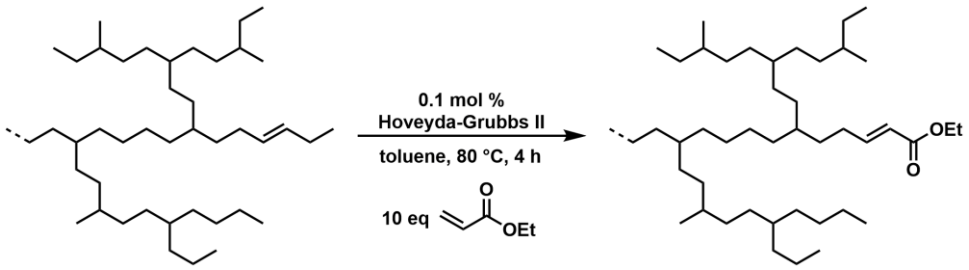

Scheme 4.2: Monofunctionalization with an ester group via cross metathesis.

Quantitative conversion of all double bonds occurred after 4 hours at 80 °C, as evidenced by key resonances at 6.97, 5.81, 4.18, and 2.19 ppm in the ^{1}H NMR spectrum – corresponding to

the unsaturated ester end group – and the absence of any olefinic resonances of the starting material (**Figure 4.6**).

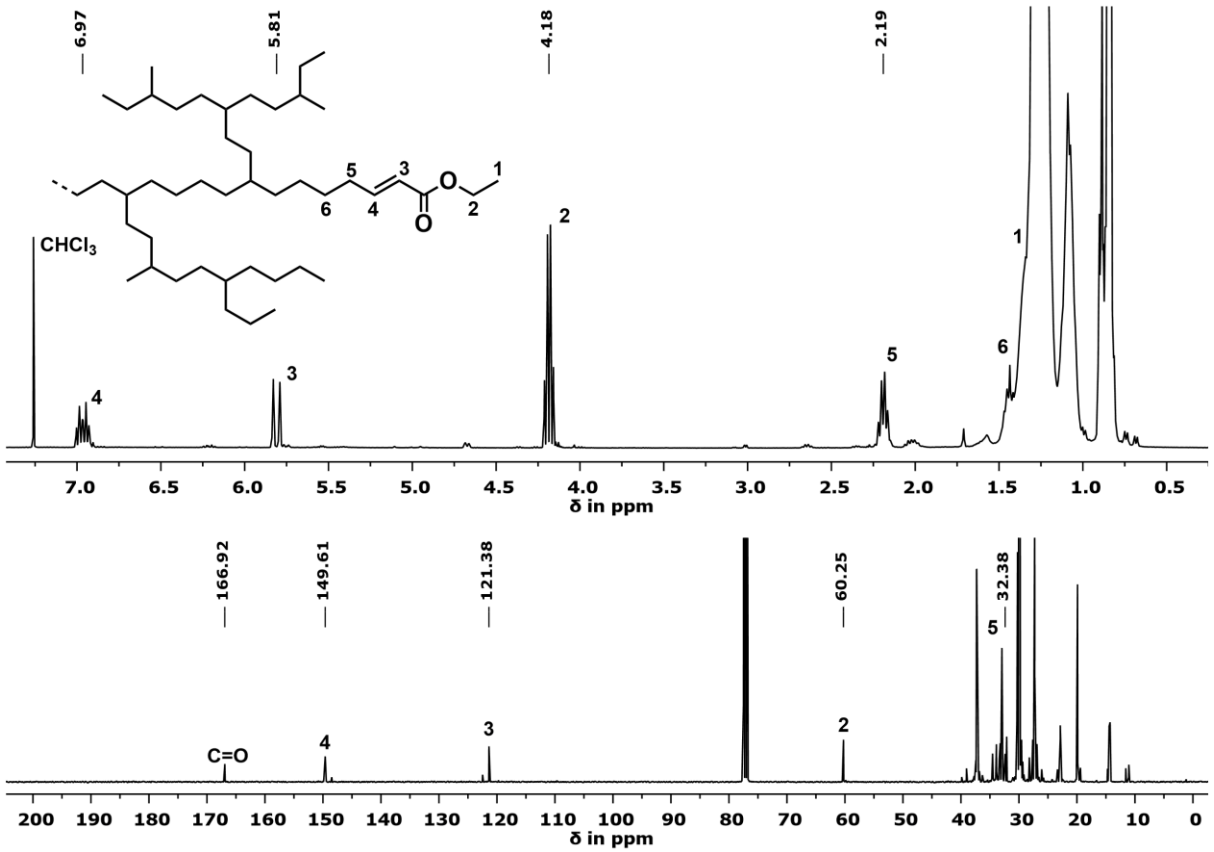

Figure 4.6: Proton (top) and carbon (bottom) NMR spectra of unsaturated ester functionalized oligomer after cross metathesis.

Identical results in terms of complete functionalization were observed for various other oligomers, independent of their molecular weights (1,000 – 3,000 g mol^{-1}) and degrees of branching (77 – 75 branches per 1000 C atoms). The synthesis was readily scalable up to 50 g batches. From these experiments, no limitation for further scale up is evident, such as a necessity of excessive solvent volumes or complicated workup procedures. ^{1}H NMR spectra and GPC measurements of the oligomers before and after metathesis revealed that molecular weights did not decrease, indicating that the internal double bonds are located close to a chain end. Thus, in addition to the functionalized oligomers, short-chained α,β-unsaturated ester fragments should be expected as additional metathesis products. To further illuminate this issue, all volatiles were removed after the metathesis reaction under high vacuum (0.01 mbar) at 80 °C and collected by condensation at -196 °C. This way, fragments with boiling points of up to bp = 330 °C can be collected. GC-MS analysis of this volatile fraction showed, aside from the self-metathesis products diethyl fumarate, the formation of the expected fragments from ethyl but-2-enoate to ethyl oct-2-enoate (bp = 216 °C), with the latter being the longest fragment observed

(**Figure 4.7**). These findings show that despite the distinct tendency of the Ni(II) salicylaldiminato complexes for chain walking during ethylene oligomerization, the major amount of internal double bonds is still located near the chain end and is not isomerized deep into the oligomer chain.

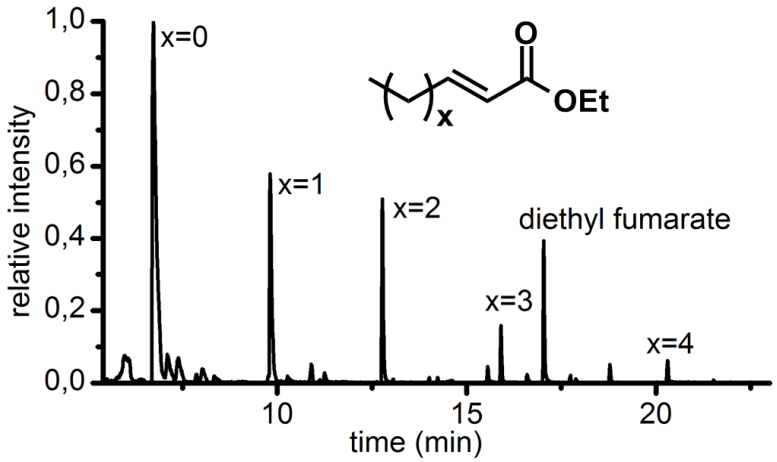

Figure 4.7: GC trace from GC-MS analysis of the volatile fragments after cross metathesis.[85] All minor signals without assignment originate from the column material of the GC.

The presented functionalization via cross metathesis shows great potential to introduce a range of other functionalities by using different acrylates or functional olefins. Hydroxyl end groups for example are desirable due to their high reactivity for further functionalization reactions. They can potentially be obtained directly by cross metathesis reaction with allylic alcohol circumventing the requirement for an additional reduction step after functionalization with an ester. Therefore, the scope of this reaction was studied with a range of different olefins (**Table 4.2**). The direct olefin functionalization with allylic alcohol or 1-butenol (entries 4.2-1 and 4.2-2) hardly resulted in any conversion which was attributed to a fast deactivation of the metathesis catalyst upon its addition as indicated by a rapid color change to yellow. Applying *cis*-butendiol under similar reaction conditions did not result in more than 5 % conversion either, even with a longer reaction time of 23 hours (entry 4.2-4). However, reducing the reaction temperature to 25 °C and using pentane as a solvent gave an increased conversion of 25 % (entry 4.2-5). The best result was obtained with allylic acetate under the same reaction conditions used for the cross metathesis reaction with ethyl acrylate giving 60 % conversion. Other functional olefins like dichloroethylene which would result in chloride end groups did not result in any conversion at all.

Table 4.2: Conversions of cross metathesis reactions with different functional olefins.

entry	olefin	T [°C]	time [h]	conversion
1		80	4	< 5 %
2		80	4	-
3		60	4	< 5 %
4		80	23	~ 5 %
5[a]	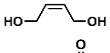	25	24	~ 25 %
6		80	4	~ 60 %
7		80	4	-

reaction conditions: 5 g of oligoethylene, 1 mol% HG II catalyst, 75 mL toluene; [a] reaction in 40 mL of pentane.

Since the complete functionalization via cross metathesis appeared to be limited to ethyl acrylate, alcohol terminated oligoethylenes were synthesized by hydrogenation of the unsaturated ester functionalized products and subsequent reduction of the corresponding saturated ester with $LiAlH_4$. Hydrogenation of the double bonds still present in the products was readily achieved with the Fischer carbene [$(PCy_3)_2Cl_2Ru$=CHOEt] (generated by quenching a Grubbs first generation catalyst precursor with a large excess of ethyl vinyl ether) in quantitative yield at 40 bar of H_2 and 75 °C after 24 hours (**Scheme 4.3**, first step). This complex is known to react with hydrogen to form [$RuHCl(H_2)(PCy_3)_2$] which performs as an excellent hydrogenation catalyst for double bonds.[122-125] Complete conversion was confirmed by the absence of any olefinic resonances in the proton NMR (**Figure 4.8**, center).

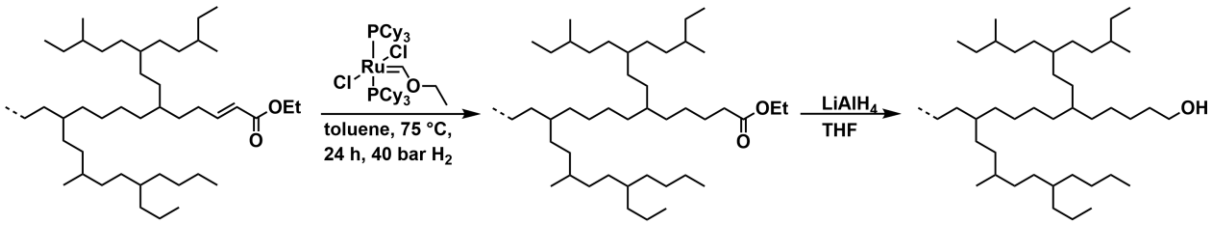

Scheme 4.3: Catalytic hydrogenation of the α,β-unsaturated ester functionalized oligomer with a quenched Grubbs first generation catalyst and subsequent reduction of the ester to the alcohol.

The saturated ester functionalized products could also be conveniently obtained in a one-pot reaction. An oligomer (molecular weight 1000 g mol^{-1}, 78 branches/1000 C) was therefore subjected to cross metathesis with ethyl acrylate using HG II in a stirred pressure reactor at 80 °C. After 4 hours the reaction was quenched with ethyl vinyl ether and pressurized with H_2 for 1 day. The saturated primary carboxylic acid ester product was formed as the only product, as evidenced by proton NMR spectroscopy (**Figure 4.8**, center). An incomplete metathesis functionalization prior to the pressurization with hydrogen would result in an apparent increase of molecular weight, as determined from NMR after hydrogenation, due to hydrogenation of

non-functionalized double bonds of the starting material. A found molecular weight of M_n(NMR) = 950 g mol^{-1} is further evidence of a complete metathesis step.

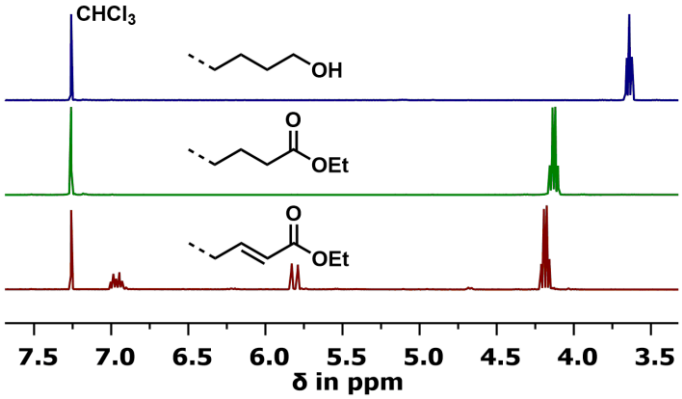

Figure 4.8: ^{1}H NMR spectra of the unsaturated ester (bottom), the saturated ester (center), and the hydroxyl-functionalized oligomer (top).[85]

From the new saturated ester functionalized, branched oligomers other functionalities like alcohols are easily accessible (**Scheme 4.3**). Reduction with an excess of $LiAlH_4$ quantitatively yielded the corresponding hydroxy-terminated oligomers (**Figure 4.8**, top). However, for a large scale synthesis (50 g batches) the utilization of $LiAlH_4$ would be disadvantageous due to cost, the hazardous nature of the reaction, and the tedious workup required for the removal of inorganic salts.

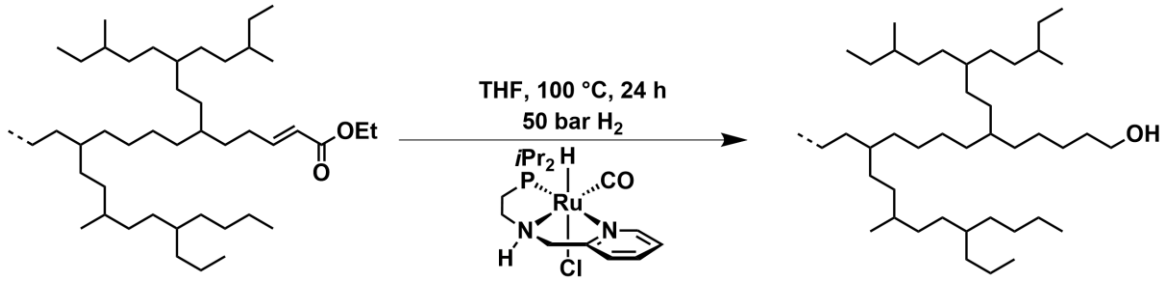

Scheme 4.4: One-step hydrogenation of the α,β-unsaturated ester functionalized oligomer to the saturated alcohol terminated product.

To resolve this issue, the ruthenium complex *trans*-RuHCl(CO)[PyCH$_2$NH(CH$_2$)P*i*Pr$_2$] (**Scheme 4.4**), reported by Gusev *et al.* for the conversion of α,β-unsaturated esters to the saturated alcohols, was found to be suited for the hydrogenation of the presented ester-functionalized oligomers.[126] The hydroxy-functionalized oligomers were obtained quantitatively in a one-step hydrogenation of the unsaturated ester products of the cross metathesis reaction after 1 day at 50 bar of H_2, as evidenced by NMR spectroscopy (**Figure 4.21**, p. 109).

4.2.3 Oligomer Epoxidation

In terms of further conversion or application of the highly branched oligomers, for example as macromonomers, reactive epoxide functional groups are of strong interest. They can be reacted with a wide range of different nucleophiles, giving access to various different functionalities. Furthermore, epoxidation of double bonds is well documented and has already been applied to polymers for post-polymerization functionalization.[127] In contrast to the aforementioned functionalization reactions with terminal functional groups, epoxidation mainly yields disubstituted ('internal') epoxides, corresponding to the distribution of double bonds present in the oligomers.

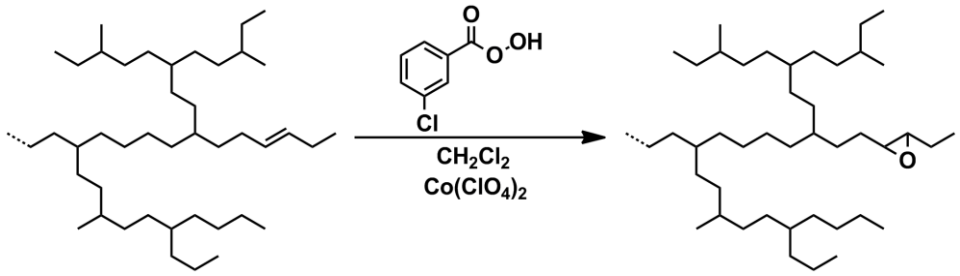

Scheme 4.5: Cobalt-catalyzed epoxy functionalization with *m*CPBA.

First epoxidation experiments were carried out according to a literature procedure reported by Kim *et al.* (**Scheme 4.5**).[128] This cobalt-catalyzed epoxidation with *meta*-chloroperoxybenzoic acid (*m*CPBA) yielded almost complete epoxidation of all olefins after 60 min at room temperature. Internal as well as terminal double bonds were converted, corresponding to degrees of functionalization of >95 %. Key proton NMR resonances from the epoxide products arise at 3.1 to 2.5 ppm, while only small amounts (<5 %) of terminal double bonds remain unreacted (**Figure 4.9**). Epoxide formation was also evidenced by a new resonance for the C–O stretching vibration of the epoxide at 895 cm^{-1} in the IR spectrum. As expected, a mixture of internal and terminal epoxides, reflecting the distribution of the double bonds generated in the branching ethylene oligomerization was obtained. However, using the procedure reported by Kim *et al.*, small amounts of ring opened diols were present in the products (broad signals between 4.2 and 3.1 ppm) originating from the acid catalyzed reaction with water. This resulted in a very tedious workup procedure due to poor phase separation while extracting the functionalized oligomers with toluene/water mixtures.

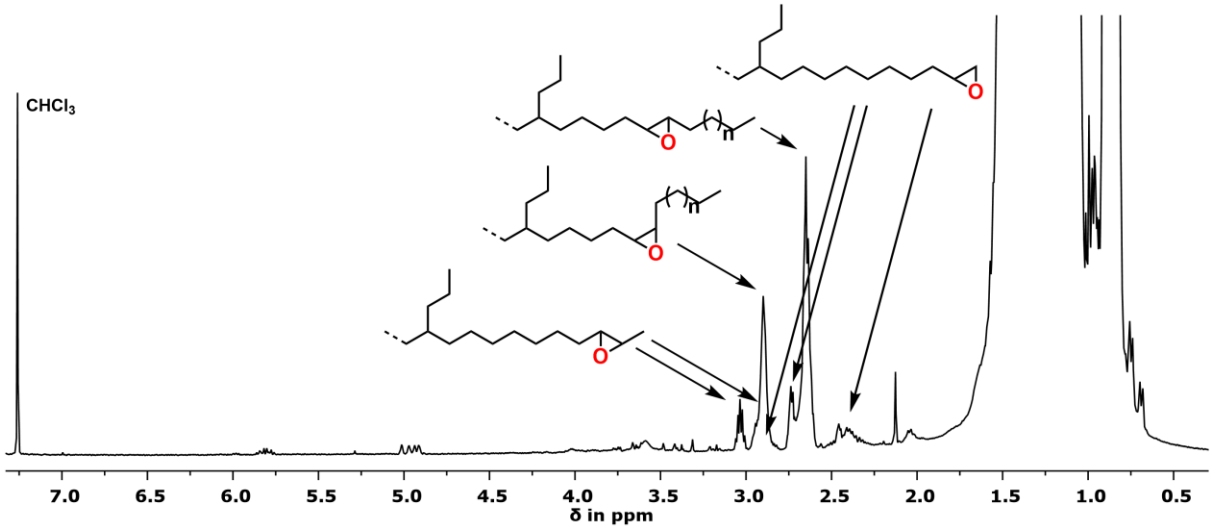

Figure 4.9: Representative ^{1}H NMR spectrum of epoxide oligomer after cobalt-catalyzed epoxidation with *m*CPBA.

Further investigation of the epoxidation reaction showed that no metal catalyst is required for a fast and quantitative epoxidation of the oligomers. Furthermore, a less harmful solution of peracetic acid (39 % in acetic acid) can be used instead of *m*CPBA. Additional dilution of the biphasic reaction mixture with water resulted in quantitative conversion of all double bonds and successfully suppressed the formation of the diol substituted side product due to a higher pH of the aqueous phase. Therefore, the epoxidized oligomers were obtained in very high purity and the workup procedure was simplified significantly by this improved procedure (**Figure 4.10**).

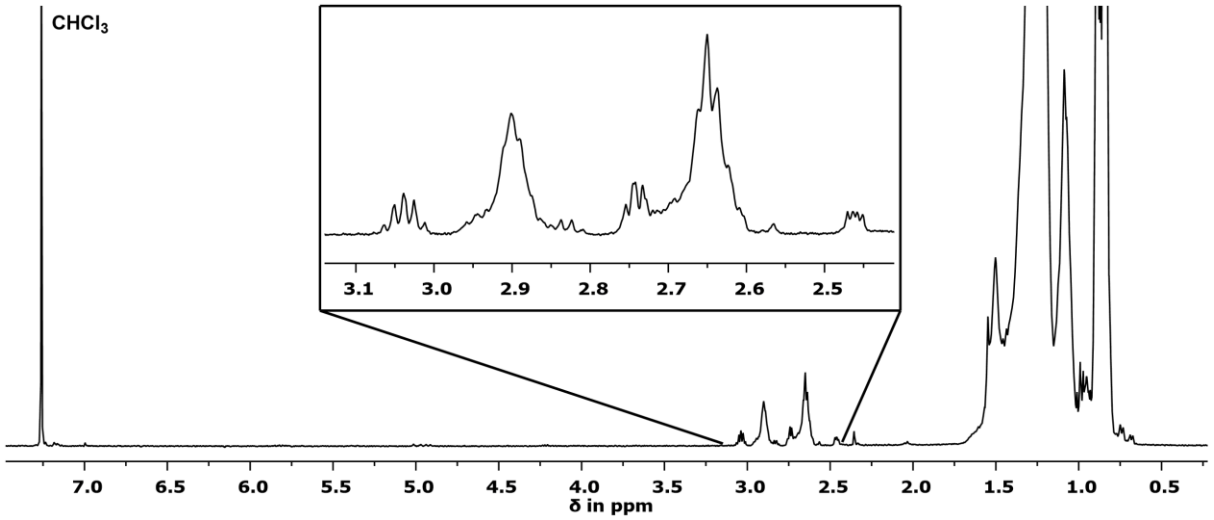

Figure 4.10: ^{1}H NMR spectrum of epoxy oligomer obtained with improved epoxidation procedure.

Epoxidation of the oligomers proved to be very robust and easily scalable. Functionalization could be performed on the branched oligoethylenes as obtained from oligomerization without further workup (involving e.g. removal of residual catalyst or its deactivation products) on a

100 g scale or larger. It is also applicable to a wide range of different oligomers independent of their molecular weight and degree of branching.

4.2.4 Synthesis of Hyperbranched Oligoethylene Macromonomers

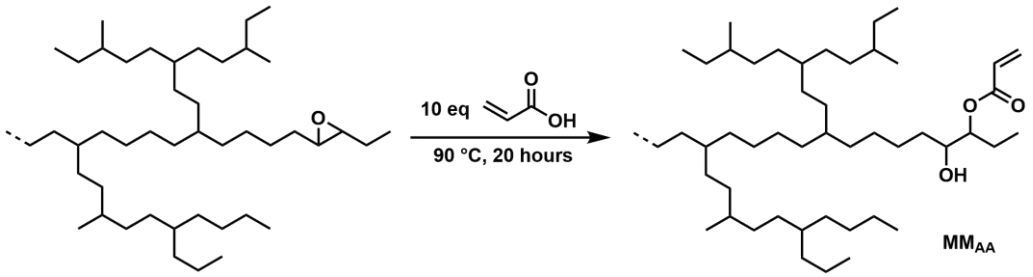

Figure 4.11: Macromonomer synthesis by epoxide ring-opening with an excess of acrylic acid.

Further conversion of the reactive epoxides was exemplified by the synthesis of acrylate functionalized macromonomers via ring-opening of the epoxides with acrylic acid and its derivatives. Such functionalized macromonomers carrying an acrylate end group are attractive e.g. for atom transfer radical (co-)polymerizations (ATRP). The ring-opening of epoxides with acrylic acid has been reported by Wool *et al*. and Bajpai *et al*. for the acrylate functionalization of epoxidized fatty acids.[129,130] In a similar approach, the epoxidized, highly branched oligomers could be readily opened with any strong acid like TsOH or hydrochloric acid according to reported procedures to give the tosylate or chloride substituted oligomers, respectively.[131] The addition of 2 equiv of acid at room temperature gave complete conversion of all the epoxides. Since acrylic acid is a much weaker acid compared to HCl or TsOH, harsher reaction conditions were required for the ring opening, however. The quantitative reaction was achieved by reacting the epoxy oligomers with 10 equiv of acrylic acid at 90 °C for 20 hours.

Quantitative conversion of the epoxy groups was confirmed by the absence of any epoxide resonances of the starting material in the ^{1}H NMR spectrum (**Figure 4.12**). Signals of the acrylate functionalized macromonomer arise at 6.41, 6.11, and 5.84 ppm for the acrylate double bond. Broad signals at 4.92 and 3.69 ppm correspond to the methine groups adjacent to the ester and the alcohol group, respectively.

However, two additional signals at 4.46 and 2.73 ppm are observed in the proton NMR spectrum which do not correspond to any protons of the expected product. 2D NMR spectroscopy revealed the presence of the structure with acrylic acid dimer opened epoxides depicted in **Figure 4.12**. The signals at 4.46 and 2.73 ppm were assigned to the methylene units 3 and 4 of the acrylic acid dimer (2-carboxyethyl acrylate).

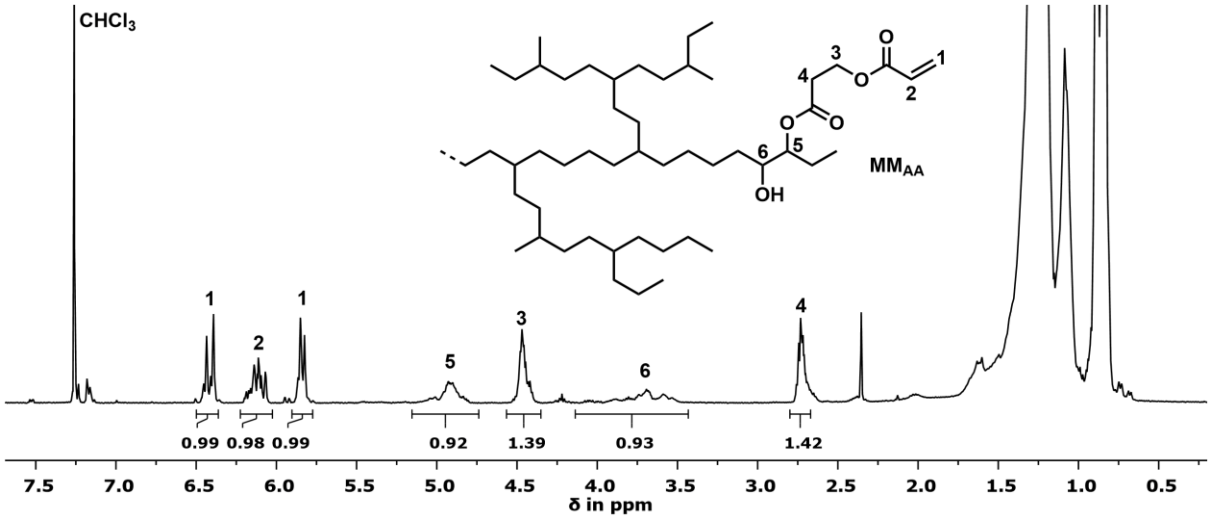

Figure 4.12: Representative ^{1}H NMR spectrum of the acrylate functionalized macromonomer.

It was found that the product (**MM_{AA}**) obtained is a mixture of the expected acrylate functionalized oligomer and the 2-carboxyethyl acrylate functionalized analogue. The major amount of epoxides (about 70 %) was opened by reaction with 2-carboxyethyl acrylate. This is formed *in situ* under the applied reaction conditions by a Michael addition based dimerization of acrylic acid (**Scheme 4.6**). However, this is not a problem since the diacrylic acid functionalized oligomer chains carry the same reactive acrylate end group.

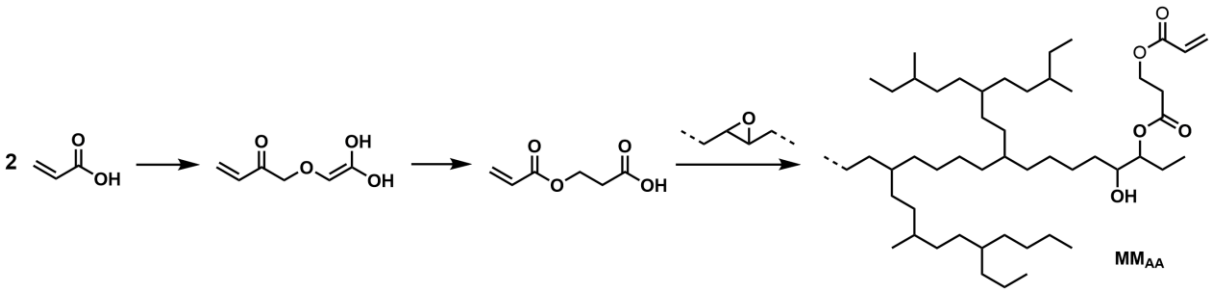

Scheme 4.6: Michael addition based dimerization of acrylic acid and subsequent epoxide ring opening by the product 2-carboxyethyl acrylate.

The epoxides can also be opened using methacrylic acid to yield the methacrylate functionalized oligomers (**MM_{MAA}**), although the reaction conditions had to be further optimized to reach satisfying conversions. Methacrylic acid proved to be significantly less reactive than acrylic acid and required a large excess (up to 100 equiv) and long reaction times of up to 3 days (**Table 4.3**).

Table 4.3: Reaction conditions for the epoxide ring opening of different oligomers in neat methacrylic acid.

entry	M_n (MM_{MAA}) [g mol^{-1}]	branches /1000 C (MM_{MAA})	MAA [equiv]	T [°C]	t [h]	conversion[a]
1	3,700	86	100	110	60	80 %
2	2,000	92	100	110	15	80 %
3	1,700	95	20	110	45	73 %

[a] Conversion of the epoxide to the methacrylate macromonomer calculated from the ^{1}H NMR intensity ratio of the epoxide signals before and after the functionalization.

Under harsh reaction conditions, conversions of up to 80 % were achieved. The polymerization of the methacrylic acid was found to be a major side reaction at the high temperatures required and therefore did not allow for even higher temperatures or longer reaction times. Even so, the methacrylate functionalized macromonomers were obtained in satisfying purity with a high degree of functionalization (**Figure 4.28**, p. 112). A range of macromonomers with different molecular weights ranging from 1,700 to 3,700 g mol^{-1} and degrees of branching between 86 and 95 branches per 1000 carbon atoms were obtained by this reaction.

4.2.5 Atom Transfer Radical Copolymerization of Macromonomers

ATRP with Methacrylate Functionalized Macromonomers MM_{MAA}

The acrylate groups provide a possibility for further application of the oligoethylenes for example as macromonomers in a radical polymerization. The copolymerization of macromonomers with low molecular weight comonomers by living polymerization processes is a well-established state of the art technique to synthesize *graft*-copolymers.[132-139] In such a polymerization, the molecular weight of the resulting copolymer as well as the average spacing between two macromonomers can be controlled by means of the reaction conditions.[133] Matyjaszewski *et al*. reported that in a free radical copolymerization of *n*BuA and PMMA-macromonomers the macromonomer incorporation is limited which they attributed to a diffusion control of its addition.[133,139] In a living ATRP however, they obtained a similar reactivity of the macromonomer to that of methyl methacrylate which was explained by different time scales of the monomer addition. In a free radical polymerization the frequency of monomer addition is in the range of milliseconds, while it is in the range of seconds for an ATRP.[133] Therefore, a living radical polymerization technique also seems promising for the copolymerization of the presented macromonomers. A different approach to synthesize poly(*n*-butyl acrylate)-*graft*-branched polyethylene was reported by Brookhart and coworkers.[135]

They applied methyacrylate terminated polyethylene macromonomers (PEMM with M_n = 10,000 to 14,000 g mol^{-1}) obtained from living polymerization of ethylene with a Pd(II) α-diimine catalyst in an ATRP with *n*-butyl acrylate (**Scheme 4.7**). While the macromonomer synthesis is elegant, it is limited due to the stoichiometric use of Pd(II). However, the conversion of the macromonomer was not complete, resulting in a blend of poly(*n*-butyl-acrylate)-*graft*-branched polyethylene and PEMM.

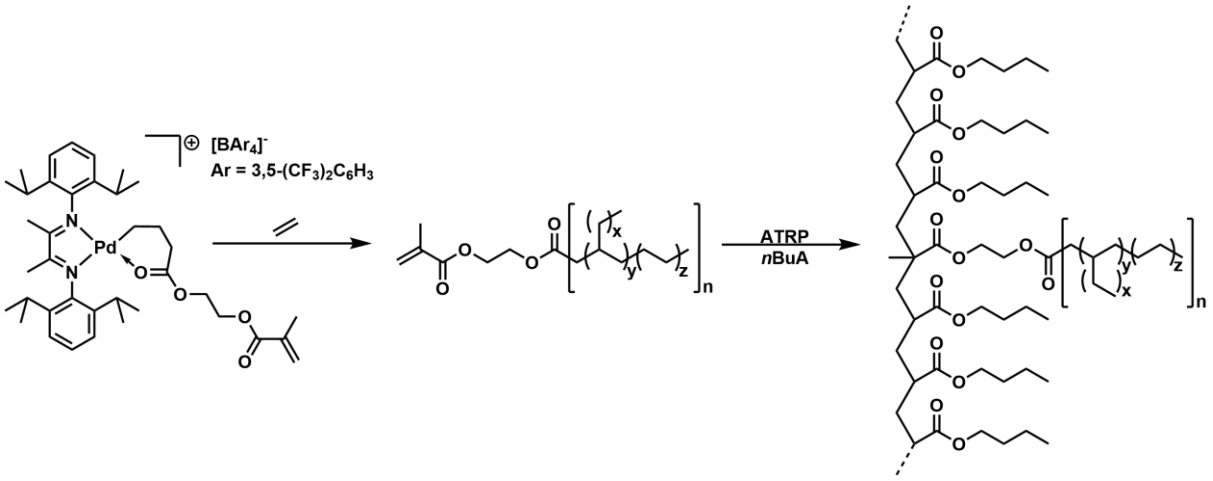

Scheme 4.7: Macromonomer synthesis via living ethylene polymerization with a functionalized Pd(II) α-diimine catalyst and subsequent copolymerization with *n*-butyl acrylate in an ATRP.[135]

Regarding the similarity of the macromonomers, the methacrylate functionalized macromonomers $\mathbf{MM_{MAA}}$ were subjected to the reaction conditions reported by Brookhart and Matyjaszewski *et al.* in order to study the atom transfer radical copolymerization of the macromonomers synthesized within this thesis. According to literature studies, the methacrylic acid functionalized macromonomers should be better suited for the copolymerization with *n*-butyl acrylate than the acrylate functionalized ones.[133,135,137] This was ascribed to the higher reactivity of the methacrylate end group in copolymerization which compensates for the generally lower reactivity of the macromonomers caused by its high mass and diffusion limitations. A monomer to initiator (methyl-2-bromo-propionate) ratio of 500:1 was chosen with 10 and 20 equiv of CuBr and dtbpy, respectively. Additionally, 10 equiv of Cu(0) was added in order to reduce Cu(II) which is potentially formed in the course of the reaction. All three macromonomers with different molecular weights and degrees of branching given in **Table 4.3** (p 92) were investigated in the radical copolymerization. Furthermore, different incorporation rates of the macromonomer in the *n*-butyl acrylate backbone were targeted for each macromonomer. Theoretical incorporations of 1 mol%, 2 mol% and 10 mol% were studied by changing the $[MM]_0$:$[n\text{BuA}]_0$ ratio from [1]:[99] to [1]:[49] and [1]:[9] while keeping the overall monomer to initiator ratio constant (500:1). A typical proton NMR spectrum of a copolymer

obtained by this procedure is shown in **Figure 4.13**. The spectrum shows all the signals expected for an *n*-butyl acrlyate polymer with additional signals of the aliphatic macromonomer side chains. The absence of any olefinic signals originating from the acrylate end group of $\mathbf{MM_{MAA}}$ is evidence of its complete conversion. The incorporation of the macromonomer in the product can be approximated by **Equation (4-1)**.

$$\text{MM incorporation} \approx \frac{(I_{aliph} - 9) \cdot 14\ \text{g mol}^{-1}}{2 \cdot M_n(\text{MM})} \cdot 100\ \% \qquad \textbf{(4-1)}$$

For the calculation, the isolated signal at 4.0 ppm, corresponding to the backbone methylene group, has to be normalized to an integral intensity of 2.00. In order to obtain the signal intensity of the incorporated macromonomer, 9 protons of the methylene and methyl groups of the *n*-butyl acrylate building block were subtracted from the overall integral of the aliphatic region I_{aliph} (0.6 to 2.0 ppm).

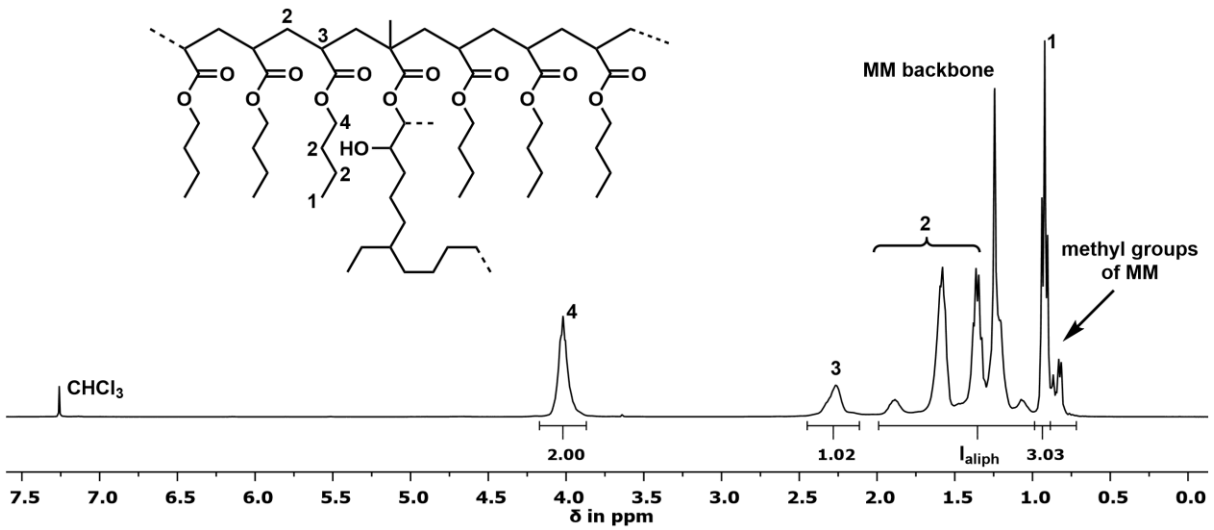

Figure 4.13: Proton NMR spectrum of copolymer 4.4-8 from **Table 4.4** (2 mol% MM incorporation, 1,700 g mol^{-1} MM).

The results of the different copolymerization experiments are depicted in **Table 4.4**. According to the NMR spectra of the product, copolymers of *n*BuA and the methacrylate functionalized macromonomer were obtained for all experiments. For the copolymerization experiments with the high molecular weight macromonomer (3,700 g mol^{-1}, entry 4.3-1, **Table 4.3**), complete conversion of the same was observed for low targeted incorporation rates of 1 mol% and 2 mol% (entries 4.4-1 and 4.4-2 in **Table 4.4**). Also, the macromonomer content found in the products is in good agreement with the expected values indicating a well-behaved, controlled radical polymerization. An exception is found for the copolymerization with a

targeted macromonomer incorporation of 10 mol%. An incorporation of 32.0 mol% was found in the product which exceeds the theoretical value by far, indicating a higher reactivity of $\mathbf{MM_{MAA}}$ compared to the *n*-butyl acrylate comonomer. This is in agreement with the generally higher reactivity of methacrylate monomers in a radical copolymerization with acrylates.[140] Although a MM incorporation of 1.3 mol% and 3.0 mol% may seem low, this corresponds to a high weight fraction of 28 wt% and 47 wt%, respectively, due to the high difference of molecular weights of the two comonomers. The molecular weights of the copolymers range from M_n = 26,800 to 57,700 g mol^{-1} and do not reach the theoretical values (99,700 and 242,900 g mol^{-1}, respectively) which were calculated from the initial initiator to monomer ratio not taking into account incomplete conversion of the monomers. However, GPC only yields apparent molecular weights since it is measured versus polystyrene standards. Molecular weight distributions M_w/M_n are between 2 and 3 for all copolymers obtained.

Table 4.4: Results of atom transfer radical copolymerizations of *n*-butyl acrylate and different methacrylate functionalized macromonomers.

entry	MM[a]	M_n (MM)	ratio $[MM]_0$:$[n\mathbf{BuA}]_0$	MM content[b] [mol%]	[wt%]	MM conversion[c]	M_n (GPC) [g mol^{-1}][d]	theoretical M_n [g mol^{-1}][e]
1	4.3-1	3,700	5:495	1.3	28	100	38,400	81,900
2	4.3-1	3,700	10:490	3.0	47	100	26,800	99,700
3	4.3-1	3,700	50:450	32.0	93	57	57,700[f]	242,600
4	4.3-2	2,000	5:495	5.6	48	100	10,000[f]	73,000
5	4.3-2	2,000	10:490	21.0	80	61	5,000[f]	82,700
6	4.3-2	2,000	50:450	60.0	96	52	4,200	157,600
7	4.3-3	1,700	5:495	1.5	17	100	33,800	71,900
8	4.3-3	1,700	10:490	2.0	21	100	27,300	79,600
9	4.3-3	1,700	50:450	28.0	84	65	34,500[f]	142,600

reaction conditions: in toluene at 90 °C for 20 h; initiator (bromopropionat) to monomer ration of 1:500, 10 eq CuBr, 20 eq dtbpx, 10 eq Cu (b. [a] $\mathbf{MM_{MAA}}$ macromonomer according to entries in **Table 4.3**. [b] $\mathbf{MM_{MAA}}$ incorporation calculated from the relative intensity ratios of the signals of incorporated nBuA and MM in the ^{1}H NMR spectra. [c] Conversion of the MM calculated from ^{1}H NMR intensity ratio of incorporated MM and residual olefinic signals. [d] in THF vs polystyrene standards. [e] Molecular weights calculated from the initial monomer to initiator ratio. [f] bimodal distribution according to GPC molecular weight determination.

The copolymerizations with $\mathbf{MM_{MAA}}$ 4.3-2 of **Table 4.3** (p. 92) did not proceed as well as the previous one. A complete conversion of this 2,000 g mol^{-1} macromonomer was only obtained for entry 4.4-4 with a targeted incorporation of 1 mol%. However, this seems to be a problem of this specific macromonomer batch since all copolymerization experiments with this compound gave exceptionally high incorporation ratios and resulted in very low molecular weights (4,200 g mol^{-1} to 10,000 g mol^{-1}).

For **MM_{MAA}** 4.3-3 (**Table 4.3**, p. 92), similar results compared to those with **MM_{MAA}** 4.3-1 were obtained. The macromonomer is completely consumed for low macromonomer incorporations while only a conversion of 65 % was reached for a targeted incorporation of 10 mol%. The macromonomer content in the product also corresponds well with the theoretical values for the first two copolymerizations (entries 4.4-7 and 4.4-8) while it exceeds the expected value for copolymerization 4.4-9 (28 mol% macromonomer instead of 10 mol%).

Conspicuously, for all copolymerization experiment which resulted in incomplete conversion of the macromonomer, the macromonomer content found in the product is higher than expected. This suggests a higher reactivity of the methacrylate functionalized macromonomer compared to the *n*-butyl acrylate comonomer which is in agreement with the generally higher reactivity of MMA in free radical copolymerization as well as in ATRP compared to *n*-butyl acrylate.[133,140]

Furthermore, a bimodal distribution of molecular weights was indicated by GPC results for several copolymers (entries 4.4-3/4/5 and 4.4-9) which might be caused by the formation of two homopolymers rather than a copolymer or by a mixture of copolymer and a homopolymer. This could also be accounted for by a higher reactivity of the macromonomer compared to *n*-butyl acrylate. However, in this case, for a controlled radical polymerization, block copolymers would be expected rather than two homopolymers. To further elucidate this issue, diffusion ordered DOSY NMR spectra of selected copolymers were recorded.

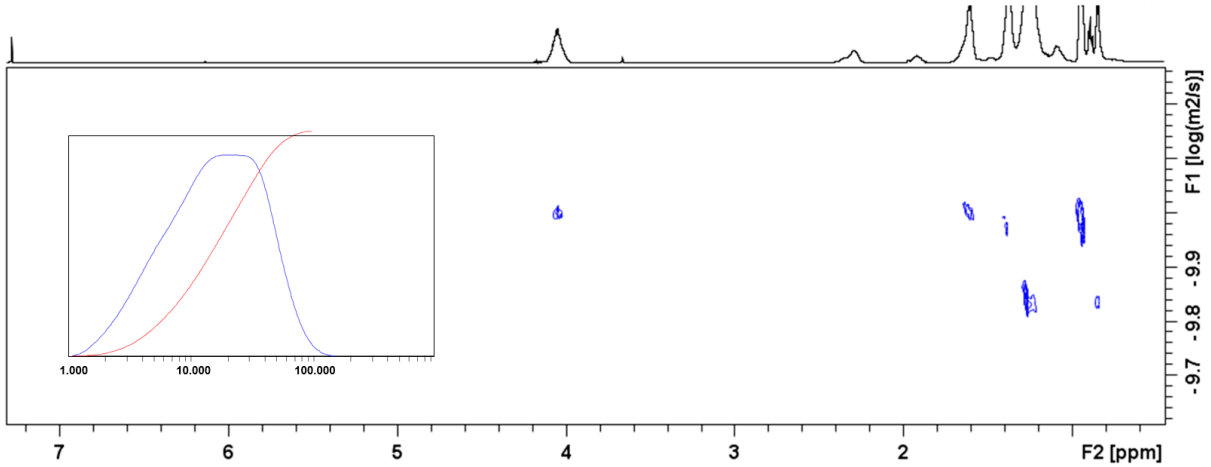

Figure 4.14: DOSY NMR spectrum and GPC trace of copolymer 4.4-4 indicating the presence of two homopolymers.

Although complete conversion of the macromonomer was observed for the copolymerization 4.4-4, the GPC traces indicated a bimodal molecular weight distribution of the product. **Figure 4.14** depicts the DOSY NMR spectrum which was recorded for copolymer 4.4-4 from **Table 4.4**. The spectrum clearly shows two distinct diffusion traces. The top trace which

corresponds to a slower diffusion, shows cross signals to all the proton resonances that originate from the polybutyl acrylate part while the bottom traces only displays cross signals to all the proton resonances which correspond to the hyperbranched oligomer side chains. The absence of any cross signals of the oligomer side chains in the diffusion trace of the polyacrylate and vice versa confirms the presence of two homopolymers instead of the desired copolymers. Similar results were found for copolymerizations 4.4-3,4,5 and 4.4-9 which also showed a bimodal molecular weight distribution in GPC measurements.

For the remaining experiments however, a monomodal molecular weight distribution was found by GPC measurements with M_n significantly exceeding that of the macromonomers **MM**$_{MAA}$. In these cases, the formation of copolymers was confirmed by the DOSY NMR spectra which showed a single diffusion traces with cross signals to the acrylate backbone as well as to the hyperbranched side chains. In **Figure 4.15**, a representative DOSY NMR spectrum for such a copolymer (copolymer 4.4-8, 2 mol% macromonomer content) is shown. The cross signals of the oligoethylene side chains are still slightly shifted to faster diffusion coefficients. This can perhaps be attributed to a higher flexibility of the side chains compared to the acrylate backbone which results in a higher overall diffusion speed.

The presented results show that the copolymerization of *n*-butyl acrylate and methacrylate functionalized oligoethylenes is possible in general. The desired *graft*-copolymers can be obtained for low macromonomer contents of 1 to 3 mol% which already translate to high weight fractions of up to 47 % macromonomer in the copolymer depending on the macromonomer molecular weight. Although contrary findings are reported in literature,[133,135] problems were observed due to the higher activity of the methacrylate moiety of the macromonomer compared to *n*-butyl acrylate.

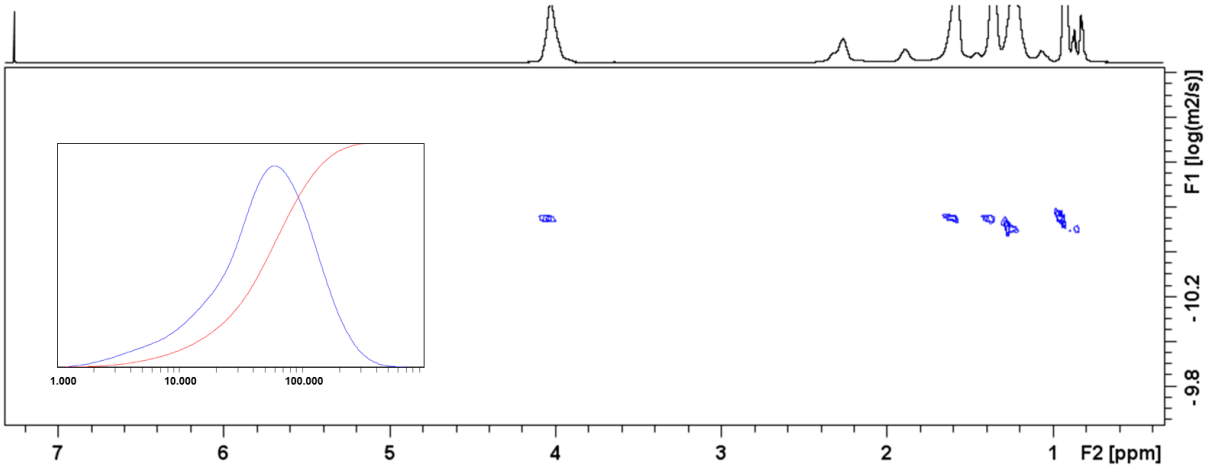

Figure 4.15: DOSY NMR spectrum and GPC trace of copolymer 4.4-8 with a single diffusion trace.

ATRP with Acrylate Functionalized Macromonomers MM_{AA}

To overcome this limitation, additional copolymerization experiments using the acrylate terminated macromonomer **MM_{AA}** (1,000 g mol^{-1}, 77 branches/1,000 C) were performed. The macromonomer was applied to the same reaction conditions, but using PMDETA (*N,N,N′,N″,N‴*-pentamethyldiethylenetriamine) as a ligand for copper instead of dtbipy. With the acrylate functionalized macromonomer also different contents of the same in the copolymer was targeted by varying the ratio of the two monomers from $[MM]_0$:$[n\text{BuA}]_0$ = [1]:[99] to [1]:[65.7] and [1]:[9]. The results are depicted in **Table 4.5**.

Table 4.5: Results of atom transfer radical copolymerizations of *n*-butyl acrylate and an acrylate functionalized macromonomer.

entry	ratio $[MM]_0$:$[n\text{BuA}]_0$	MM content[a] [mol%}	[wt%]	MM conversion[b]	M_n (GPC) [g mol^{-1}][c]	theoretical M_n [g mol^{-1}][d]
1	7.5:492.5	1.9	13	100	34,800	70,600
2	10:490	2.3	16	100	46,000	72,800
3	50:450	9.2	44	100	8,900	107,700

reaction conditions: 1 g MM (1,000 g mol^{-1}, 77 branches/1,000 C), 90 °C, 24 h, 20 mL of toluene [a] MM incorporation calculated from the relative intensity ratios of the signals of incorporated nBuA and MM in the ^{1}H NMR spectra. [b] Conversion of the MM calculated from ^{1}H NMR intensity ratio of incorporated MM and residual olefinic signals. [c] in THF vs polystyrene standards. [d] Molecular weights calculated from the initial monomer to initiator ratio.

All copolymerizations regardless of the monomer composition proceeded with quantitative consumption of the macromonomers which was evidenced by the absence of any olefinic signals in the proton NMR spectra. In the case of the acrylate functionalized macromonomer **MM_{AA}**, also higher macromonomer incorporation of up to 9.2 % was feasible. The macromonomer content in the copolymer corresponds well with the expected value for all products. Molecular weights (M^n = 8,900 – 46,000 g mol^{-1}) are in the same range as for the previous copolymers and no bimodal distributions were observed by GPC. DOSY NMR spectroscopy confirmed the formation of *graft*-copolymers for all copolymerization reactions with the acrylate functionalized macromonomer by the presence of a single diffusion traces with cross signals to all the proton resonances of the copolymer. This shows that due to a similar reactivity of the two monomers, the acrylate terminated macromonomer **MM_{AA}** is much better suited for a copolymerization with *n*-butyl acrylate than its methacrylate analogue **MM_{MAA}**.

4.3 Summary and Conclusion

Due to β–hydride elimination occurring as the major chain termination reaction in the oligomerization of ethylene with the Ni(II) salicylaldiminato complexes presented, every oligomer chain comprises an unsaturated end group. These double bonds exhibit potential for selective postpolymerization functionalization and for the synthesis of monofunctional hyperbranched ethylene oligomers. Due to the high amount of internal double bonds which are formed due to the extensive chain walking of the catalyst, an isomerization of the double bonds to the chain end is beneficial in order to ensure a high and uniform reactivity of the functional products for subsequent reactions. It was shown that the isomerizing ethoxycarbonylation is suited to obtain primary ester functionalized oligomers in a very selective manner. However, yields are limited to ca. 50 % which was attributed to the low solubility of the oligomers in the reaction media. It was found that trisubstituted double bonds are enriched in the course of the reaction and that they show very low reactivity for further reaction also limiting the overall conversion of this reaction.

As an alternative, the cross metathesis reaction of unsaturated hyperbranched ethylene oligomers with ethyl acrylate was studied. The reaction resulted in quantitative conversion of all double bonds. The molecular weight of the oligomers was retained and very little materials is lost. Hence, the internal double bonds must be located near a chain end in the oligomer starting material. This was also proven by GC-MS analysis of all volatile metathesis products which showed only small fragments. The double bond of the unsaturated ester product was readily catalytically hydrogenated. Subsequent reduction of the ester gave access to the hydroxyl terminated products. In an optimized procedure, the direct hydrogenation of the unsaturated esters from cross metathesis with *trans*-RuHCl(CO)[$PyCH_2NH(CH_2)PiPr_2$] allowed for the synthesis of the same products in a one-step reaction.

Epoxidation of the double bonds was achieved with peracetic acid in quantitative yield without the need for a transition metal catalyst. The epoxide groups lend themselves to further functionalization and for the synthesis of acrylate terminated macromonomers, e.g. for radical (co-)polymerization reactions. They were found to be readily opened by acids which was exemplified with acrylic and methacrylic acid, respectively. The macromonomers $\mathbf{MM_{AA}}$ and $\mathbf{MM_{MAA}}$ obtained this way were applied in a controlled radical copolymerization (ATRP) with *n*-butyl acrylate. A range of different poly-(*n*-butyl acrylate-*graft*-hyperbranched oligoethylene) copolymers were obtained with different macromonomer contents. The acrylate functionalized macromonomer $\mathbf{MM_{AA}}$ was found to be better suited for a radical copolymerization with *n*-butyl

acrylate than its methacrylate analogue $\mathbf{MM_{MAA}}$, which was attributed to the similar reactivity of the two comonomers. Copolymerizations with the methacrylate terminated macromonomer $\mathbf{MM_{MAA}}$ were found to be limited to low macromonomer incorporations and often resulted in the formation of two homopolymers instead of a copolymer. However, ATRP copolymerizations of $\mathbf{MM_{AA}}$ with *n*-butylacrylate were easily controllable with respect to macromonomer incorporation by adjusting the macromonomer : *n*-butyl acrylate ratio, and thus copolymers with macromonomer contents of up to 10 mol% (44 wt%) were synthesized.

Overall, all functionalization reactions presented are straightforward and readily scalable, which was demonstrated by the preparation of 50 g batches.

4.4 Experimental Section

4.4.1 Materials and General Considerations

Commercially available compounds were purchased from Aldrich, Acros, TCI or ABCR. Grubbs first generation and Hoveyda-Grubbs second generation catalyst precursors were purchased from Sigma Aldrich and stored under nitrogen prior to use. *n*-butyl acrylate (Sigma Aldrich) was degassed by repetitive freeze-pump cycles and stored under exclusion of light. CO and hydrogen were supplied by AirLiquid. All deuterated solvents were supplied by Eurisotop.

Toluene was dried over sodium and THF was distilled from blue sodium/benzophenone ketyl. [(dtbpx)Pd(OTf)$_2$] was available in in the group.[111] [$(PCy_3)_2Cl_2Ru$=CHOEt][125] and 2-(di-*iso*-propylphosphino)ethanamine were prepared according to a reported procedure.[141]

GC-MS Analysis

GC-MS spectra were recorded on a combination of an Agilent Technologies 7890A GC equipped with an Elite-5 crossbond 5 % diphenyl- 95 % dimethyl polysiloxane column of 30 m length and a 5975C inert MSD mass spectrometer with Triple-Axis detector.

IR Spectroscopy

IR spectra were recorded on a Perkin Elmer Spectrum 100 FT-IR spectrometer equipped with a Perkin Elmer Universal ATR unit. The absorption bands are given in wave numbers.

4.4.2 *trans*-RuHCl(CO)[PyCH$_2$NH(CH$_2$)P*i*Pr$_2$]

[RuHCl(CO)(AsPh$_3$)$_3$]

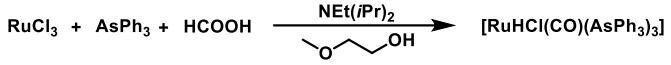

[RuHCl(CO)(AsPh3)3] was prepared according to a reported procedure.[126] A mixture of $RuCl_3 \cdot 3\ H_2O$ (523 mg, 2.0 mmol, 1.0 eq) and $AsPh_3$ (2.45 g, 8.0 mmol, 4.0 eq) was suspended in 50 mL of methoxyethanol. After addition of NEt(*i*Pr)$_2$ (2.0 g, 16 mmol, 8 eq) and 6 mL of HCOOH (80 mmol, 40 eq) the suspension was refluxed at 125 °C bath temperature for 4 h. After cooling to room temperature, the black/brown suspension was stirred additional 60 min. The gray solid was collected by filtration and washed with 5 mL of ethanol four times. After drying under vacuum, [RuHCl(CO)(AsPh$_3$)$_3$] was obtained as a gray solid (950 mg, 0.88 mmol, 44 %).

^{1}H NMR (400 MHz, CD_2Cl_2): δ (ppm) = 7.50 – 6.95 (m, 45 H, *Ar-H*), -8.67 (s, 1H, *Ru-H*).

PyCHN(CH$_2$)$_2$P*i*Pr$_2$

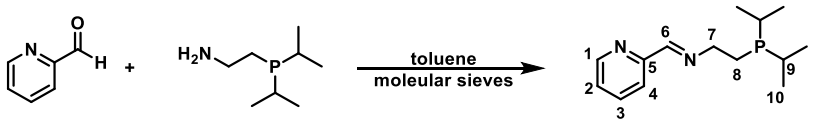

PyCHN(CH$_2$)$_2$P*i*Pr$_2$ was prepared according to a modification of reported procedures.[126,142] To a suspension of molecular sieves (powdered, 3 Å, 5 g) and 2-(di-*iso*-propylphosphino)ethanamine (1.6 g, 10 mmol, 1.0 eq) in 110 mL of toluene, a solution of pyridinealdehyde (1.1 g, 10 mmol, 1.0 eq) in 50 mL of toluene was added dropwise. After complete addition, the reaction mixture was stirred for 1 h at room temperature. Molecular sieves were filtered off and washed with toluene. After removing the solvent under vacuum, PyCHN(CH$_2$)$_2$P*i*Pr$_2$ was obtained as an orange oil (2.5 g, 10 mmol, 100 %).

^{1}H NMR (400 MHz, C_6D_6): δ (ppm) = 8.59 (s, 1H, *H-6*), 8.48 (d, $^3J_{HH}$ = 4.8 Hz, 1H, *H-1*), 8.20 (d, $^3J_{HH}$ = 7.9 Hz, 1H, *H-4*), 7.07 (vt, $^3J_{HH}$ = 7.4 Hz, 1H, *H-3*), 6.64 (dd, $^3J_{HH}$ = 4.8 Hz, $^3J_{HH}$ = 7.4 Hz, 1H, *H-2*), 3.76 (vq, $^3J_{HH}$ = 8.0 Hz, 2H, *H-7*), 1.72 (t, , $^3J_{HH}$ = 8.0 Hz, 2H, *H-8*), 1.57 (hept, $^3J_{HH}$ = 7.1 Hz, 2H, *H-9*), 0.99 (dd, $^3J_{HH}$ = 7.1 Hz, 12H, *H-10*).

^{13}C NMR (101 MHz, C_6D_6): δ (ppm) = 162.2 (C-6), 155.9 (C-5), 149.6 (C-1), 136.0 (C-3), 124.4 (C-2), 120.9 (C-4), 60.9 (C-7), 24.2 (C-8), 23.7 (C-9), 20.3 and 19.0 (C-10).

^{1}P NMR (161 MHz, C_6D_6): δ (ppm) = 0.14 (s).

$PyCH_2NH(CH_2)_2PiPr_2$

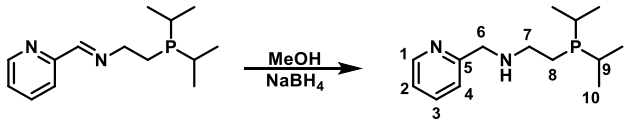

$PyCHN(CH_2)_2PiPr_2$ (2.5 g, 10 mmol, 1.0 eq) was dissolved in 50 mL of methanol and cooled to 0 °C. After addition of $NaBH_4$ (378 mg, 10 mmol, 1.0 eq) the reaction mixture was allowed to warm to room temperature (gas evolution). After stirring for 2 h at room temperature, the reaction was quenched with 1 mL of degassed water and stirred for additional 30 min. After removing the methanol under vacuum, the orange oil was redissolved in 20 mL of thf and dried over $MgSO_4$. After filtration, thf was removed under vacuum to yield $PyCH_2NH(CH_2)_2PiPr_2$ as an orange oil (2.3 g, 9.1 mmol, 91 %).

^{1}H NMR (400 MHz, C_6D_6): δ (ppm) = 8.49 (d, $^3J_{HH}$ = 4.9 Hz, 1H, *H-1*), 7.14 (d, $^3J_{HH}$ = 8.1 Hz, 1H, *H-4*), 7.11 (vt, $^3J_{HH}$ = 7.4 Hz, 1H, *H-2*), 6.65 (m, 1H, *H-3*), 3.93 (s, 2H, *H-6*), 2.81 (t, $^3J_{HH}$ = 7.5 Hz, 2H, *H-7*), 1.79 (br, 1H, *NH*), 1.53 (m, 4H, *H-8/9*), 0.99 (dd, $^3J_{HH}$ = 7.1 Hz, 12H, *H-10*).

^{13}C NMR (101 MHz, C_6D_6): δ (ppm) = 161.4 (C-5), 149.5 (C-1), 135.8 (C-3), 121.9 (C-2), 121.6 (C-4), 55.7 (C-6), 49.1 (C-7), 23.7 (C-8), 23.4 (C-9), 20.3 and 18.9 (C-10).

^{1}P NMR (161 MHz, C_6D_6): δ (ppm) = -1.98 (s).

trans-$RuHCl(CO)[PyCH_2NH(CH_2)PiPr_2]$

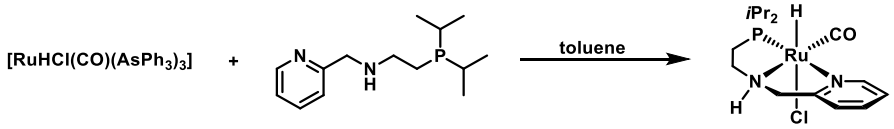

trans-$RuHCl(CO)[PyCH_2NH(CH_2)PiPr_2]$ was prepared according to a reported procedure.[126] In an 8 mL vial, $PyCH_2NH(CH_2)_2PiPr_2$ (116 mg, 460 µmol, 1.0 eq) and $[RuHCl(CO)(AsPh_3)_3]$ (500 mg, 460 µmol, 1.0 eq) were suspended in 6 mL of toluene and heated to 110 °C for 1 h. After cooling the brown suspension to -30 °C, the toluene was decanted off and the remaining brown solid was dried under vacuum. After repeated washing with diethylether (2 mL) and centrifugation, *trans*-$RuHCl(CO)[PyCH_2NH(CH_2)PiPr_2]$ was obtained as a brown solid (160 mg, 383 µmol, 83 %).

^{1}H NMR (400 MHz, CD_2Cl_2): δ (ppm) = 8.94 (d, $^3J_{HH}$ = 5.2 Hz, 1H, *pyr*), 7.69 (dt, $^3J_{HH}$ = 7.8 Hz, $^4J_{HH}$ = 1.6 Hz, 1H, *pyr*), 7.26 (m, 2H, *pyr*), 4.41 (m, 1H, CH_2), 4.08 (m, 2H, *NH/* CH_2), 3.52 (m, 1H, CH_2), 2.62 (m, 1H, CH_2), 2.52 (m, 1H, *CH*), 2.31 (m, 1H, CH_2), 2.19 (m, 1H, *CH*), 1.93 (m, 1H, CH_2), 1.22 (m, 1H, CH_3), -14.93 (s, 1H, *Ru-H*).

^{13}C NMR (101 MHz, CD_2Cl_2): δ (ppm) = 206.5 (C=O), 160.9 (pyr), 153.7 (pyr), 136.8 (pyr), 124.5 (pyr), 121.6 (pyr-CH_2), 59.8 (C-), 53.3 (N-CH_2), 32.6 (CH_2), 29.1 (CH), 25.0 (CH), 20.7 (2xCH_3), 19.1 (CH_3), 17.6 (CH_3).

^{1}P NMR (161 MHz, CD_2Cl_2): δ (ppm) = 93.64 (s).

4.4.3 General Procedure for the Isomerizing Ethoxycarbonylation

In a Schlenk flask, 1 g of ethylene oligomer was degassed in vacuo and 4 mol% of [(dtbpx)Pd(OTf)$_2$] in 10 mL of a 1:1 mixture of pentane and ethanol were added. The solution was transferred to an argon filled pressure reactor with magnetic stirring via syringe. The reactor was pressurized with CO to 20 bar and heated to 90 °C for 4 days. After cooling to room temperature the reactor was vented. Removal of the solvent under vacuum yielded ester functionalized ethylene oligomers.

4.4.4 General Procedure for the Oligomer Functionalization via Cross Metathesis with Ethyl Acrylate

Ethylene oligomer was degassed at 50 °C in a Schlenk flask and 5 mol % of 4-methoxyphenol and 10 equiv of ethyl acrylate were added. After dissolving all starting materials in toluene, the reaction mixture was heated to 80 °C and Hoveyda-Grubbs II catalyst (0.1 mol%) was added in toluene solution. After 4 hours, all volatiles were removed under vacuum. The crude product was redissolved in toluene and filtered over a short pad of silica. Clean ester functionalized oligomer was obtained after removal of the solvent under vacuum.

4.4.5 General Procedure for the Hydrogenation of Double Bonds with Quenched Grubbs I Catalyst

Under air, 1 g of ester functionalized oligomer from cross metathesis reaction was dissolved in toluene and 3 mg of [$(PCy_3)_2Cl_2Ru$=CHOEt] was added. The solution was transferred in a pressure reactor and pressurized to 40 bar with H_2 at 75 °C for 24 hours. The resulting solution was filtered over a short pad of silica to remove catalyst residues and dried under vacuum to yield the saturated ester functionalized oligomer.

4.4.6 General Procedure for the One-pot Synthesis of Saturated Ester Functionalized Oligomers

10 g of ethylene oligomer was degassed at 60 °C and 5 mol% of 4-methoxyphenol and 10 equiv of ethyl acrylate were added. After dissolving in 100 mL of toluene, the solution was transferred to a *Büchi Limbo* pressure reactor by cannula transfer and heated to 80 °C. A solution of Hoveyda-Grubbs II catalyst (0.1 mol%) in toluene was added and the reaction was stirred for

4 hours. The catalyst was quenched with 5 mL of ethyl vinyl ether and stirred for another 30 min at this temperature. The reactor was pressurized to 40 bar with H_2 for 24 hours. After cooling to 20 °C the reaction solution was filtered over a pad of silica and all volatiles were removed under vacuum to yield the saturated ester functionalized oligomers.

4.4.7 Reduction of Ester Terminated Oligomers with $LiAlH_4$

0.5 g of branched ethylene oligomer (2,000 g mol^{-1}, 250 µmol, 1.0 equiv) was degassed at 50 °C and dissolved in 25 mL of dry THF. A suspension of $LiAlH_4$ (23 mg, 600 µmol, 2.4 equiv) in THF (0.6 mL) was slowly added via syringe. The turbid mixture was stirred for 1 hour and subsequently quenched with 15 mL of a saturated aq. Rochelle salt solution (sodium potassium tartrate. The separated organic layer was washed three times with brine and dried over $MgSO_4$. Evaporation of the solvent under vacuum yielded the alcohol terminated oligomer as a colorless liquid in quantitative yield.

4.4.8 General Procedure for the Catalytic Hydrogenation of Unsaturated Esters

In a 25 mL Schlenk tube 0.5 g (500 µmol, 1 equiv) of unsaturated ester functionalized oligomer from cross metathesis was degassed at 50 °C. After addition of 4.2 mg (10 µmol, 1 mol%) of *trans*-$RuHCl(CO)[PyCH_2NH(CH_2)PiPr_2]$ and 22 mg (200 µmol, 20 mol%) of KOtBu, the oligomer was dissolved in 15 mL of THF and the solution was transferred to an argon filled pressure reactor via syringe. The reactor was pressurized with H_2 to 50 bar and heated to 100 °C for 24 hours. The reactor was vented and the solution was filtered over a short pad of silica. Removal of the solvent yielded saturated hydroxyl functionalized oligomer in quantitative yield.

4.4.9 General Procedures for the Epoxidation of Double Bonds

Procedure according to ref. [128]

In a round bottom flask, 50 g of ethylene oligomer was dissolved in 350 mL of dichloromethane and 200 mg $Co(ClO_4)_2$ in 25 mL of CH_3CN was added. After addition of 20 g of *m*CPBA (77 % in *meta*-chlorobenzoic acid), the mixture was stirred for 60 min at room temperature. After removal of the solvent the oligomer was dissolved in pentane and extracted repeatedly with methanol to yield epoxidized ethylene oligomers with high degrees of functionalization (>95 %).

Improved Epoxidation Procedure with Peracetic Acid

In a round bottom flask, 50 g of highly branched ethylene oligomer was dissolved in 350 mL of dichloromethane and 150 mL of water was added to result in a biphasic mixture. After addition of 50 mL of peracetic acid (37 % solution in acetic acid), the mixture was vigorously stirred for 1 hour at 40 °C. Dichloromethane was removed under vacuum and 150 mL of pentane was added to the resulting biphasic mixture. The organic layer was extracted three times with 50 mL of water and dried over $MgSO_4$. Removing the solvent under vacuum yielded the epoxide oligomers as a pale yellow oil.

4.4.10 General Procedure for the Synthesis of Macromonomers

In a round bottom flask 30 g of epoxidized oligomer was heated to 90 °C and 10 equiv of acrylic acid or 100 equiv of methacrylic acid were added, respectively. The reaction mixture was stirred until complete conversion of all epoxides was observed from monitoring of the reaction by NMR spectroscopy. The macromonomer was dissolved in toluene and extracted with water three times. The organic phase was dried over $MgSO_4$ and the solvent was removed under vacuum at 50 °C. The product was obtained as a colorless oil in quantitative yield and functionalization.

4.4.11 General Procedure for the Copolymerization of Hyperbranched Macromonomers with *n*-Butyl Acrylate

In a round bottom Schlenk flask, 5 to 50 equiv of macromonomer (depending on the desired macromonomer content of the product) were degassed at 50 °C. After addition of methyl-2-bromopropionate (1 equiv), CuBr (10 equiv), Cu powder < 10 µm (10 equiv), PMDETA (20 equiv) and 450 to 495 equiv of *n*-butyl acrylate (depending on the amount of macromonomer), the mixture was dissolved in 20 mL of toluene and stirred at 90 °C for 20 hours. After removing all volatiles under vacuum, the resulting green oil was dissolved in dichloromethane and filtered over a short plug of silica and a short plug of alumina to remove the copper residues. After removing the solvent under vacuum, the acrylate functionalized oligoethylene was obtained as a greenish, highly viscous oil.

4.4.12 Additional Spectra and Data

Ester Functionalized Oligomers from Isomerizing Alkoxycarbonylation

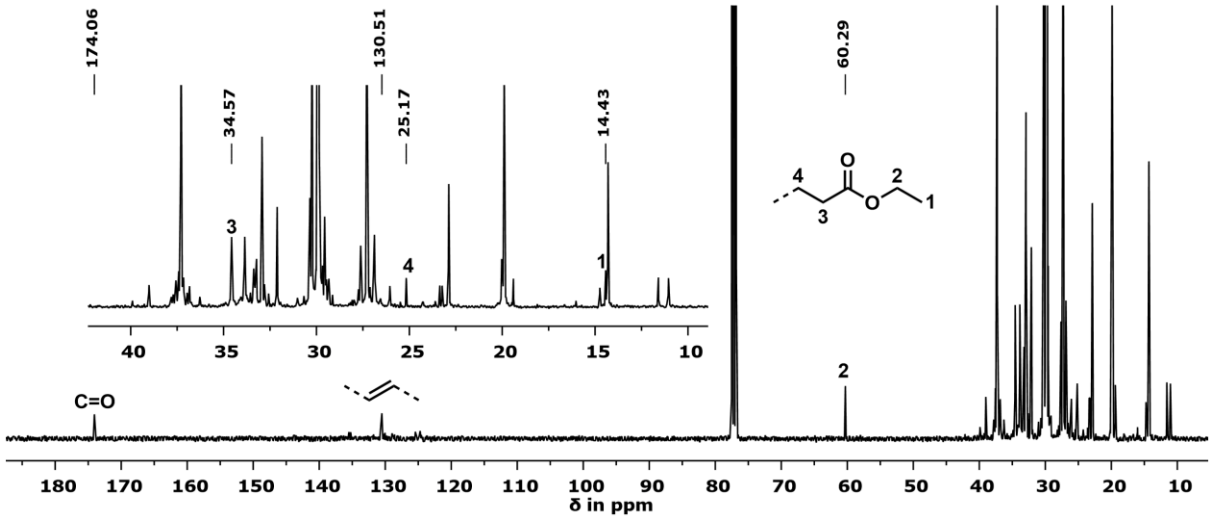

Figure 4.16: ^{13}C NMR spectrum (400 MHz, $CDCl_3$, 298 K) of partially functionalized oligomer obtained from isomerizing alkoxycarbonylation.

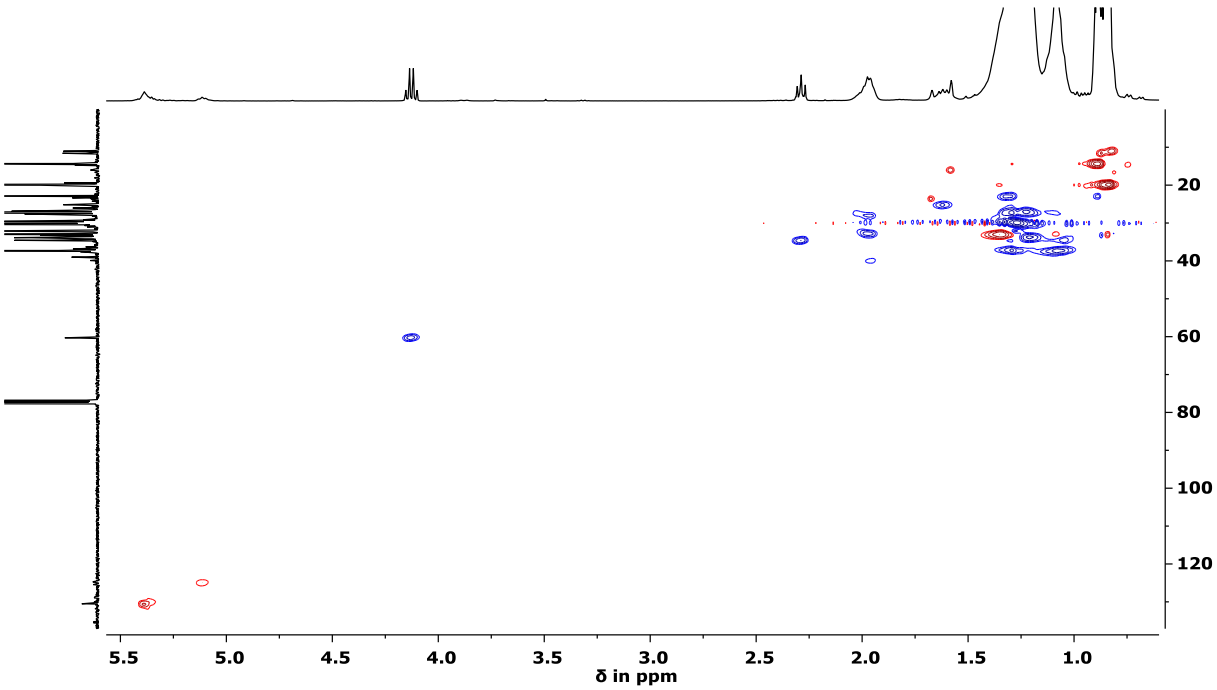

Figure 4.17: $^{1}H,^{13}C$ gHSQC NMR spectrum (400 MHz, 298 K, in CDCl3) of the oligomer obtained by isomerizing alkoxycarbonylation.

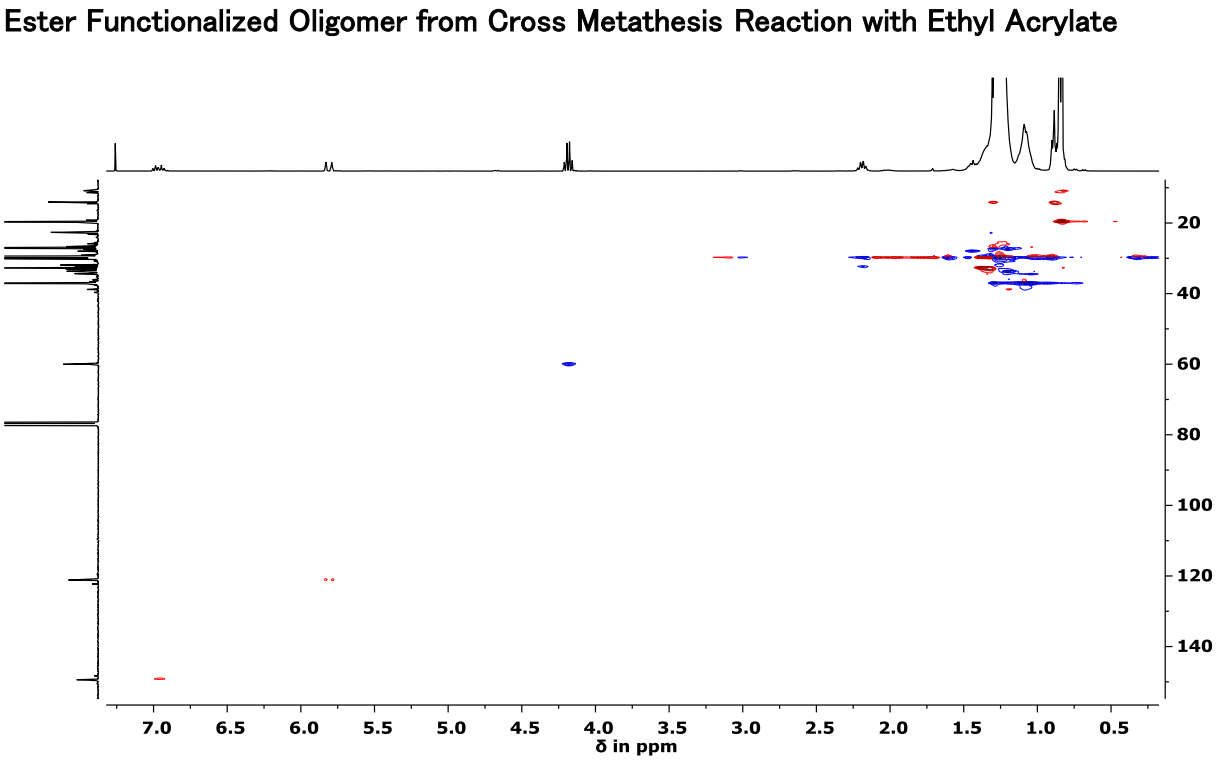

Figure 4.18: $^{1}H,^{13}C$ gHSQC NMR spectrum (400 MHz, 298 K, in $CDCl_3$) of the oligomer obtained by cross metathesis reaction with ethyl acrylate.

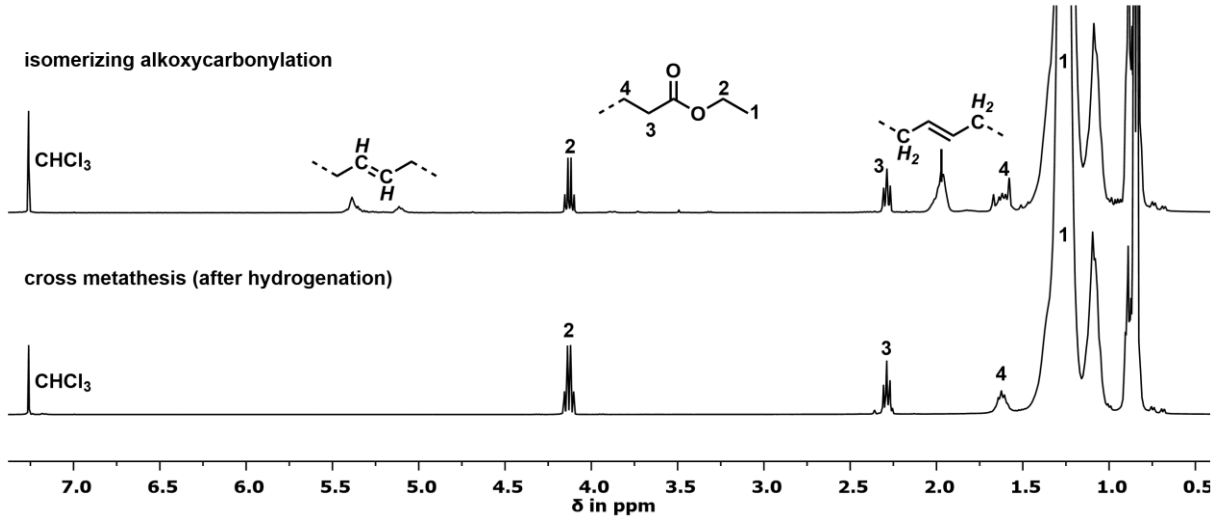

Figure 4.19: Comparison of ^{1}H NMR spectra of saturated ester functionalized oligomers obtained from isomerizing alkoxycarbonylation and cross metathesis (after hydrogenation).

Hydroxyl Terminated Oligoethylene

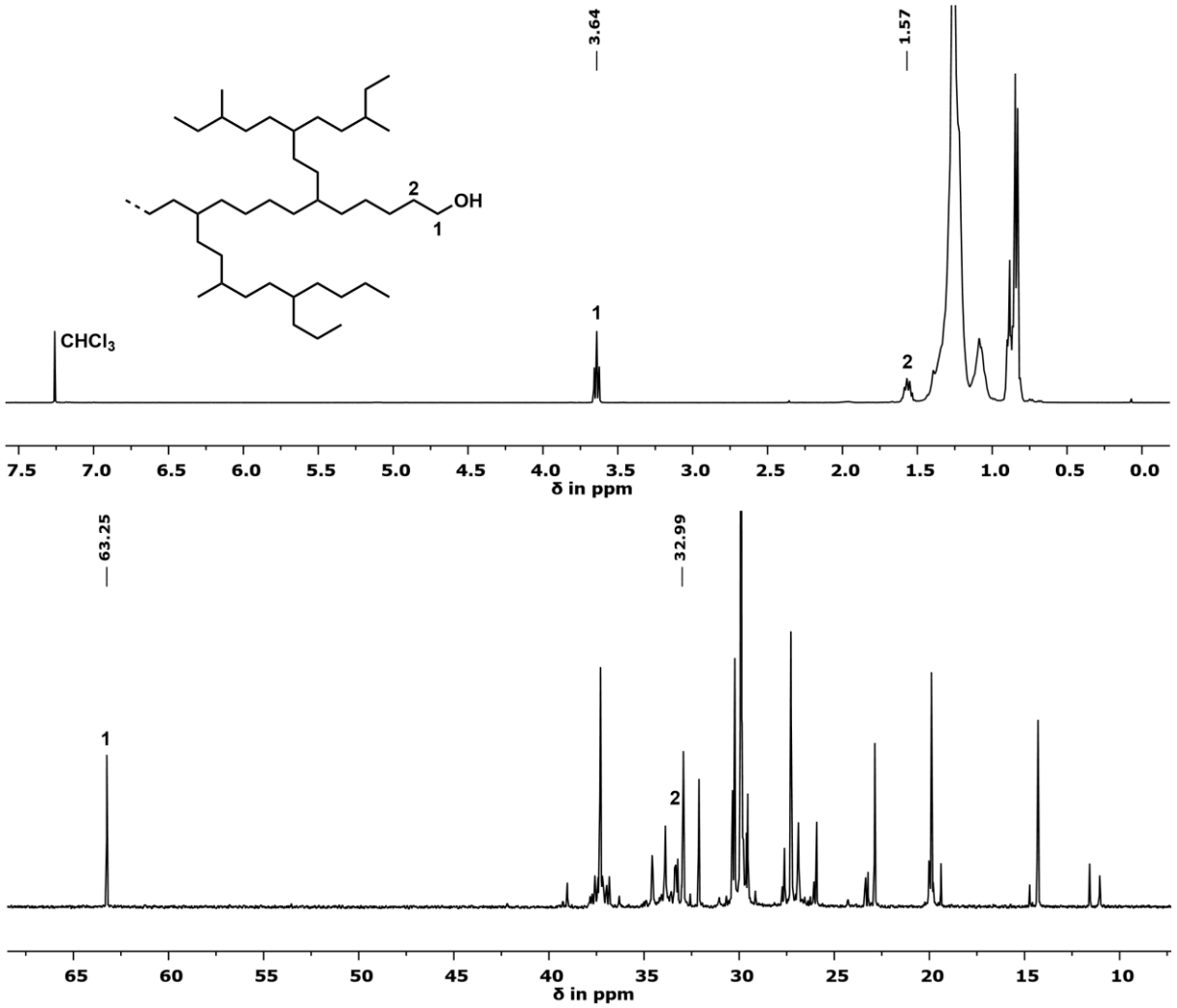

Figure 4.20: Proton (top) and carbon (bottom) NMR spectra of the alcohol terminated oligomer obtained by reduction of the saturated ester with $LiAlH_4$.

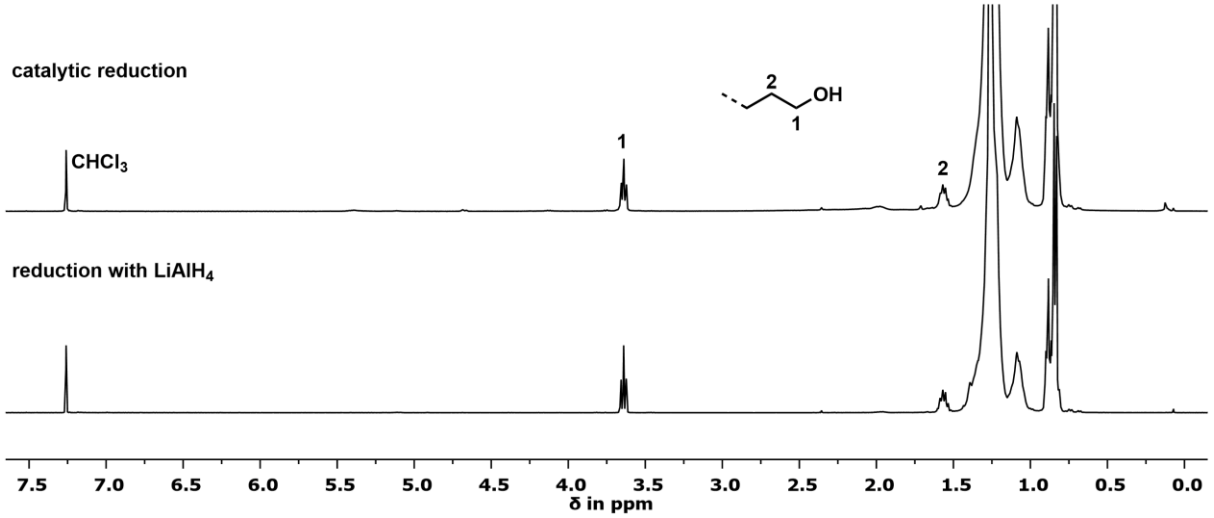

Figure 4.21: Comparison of ^{1}H NMR spectra of alcohol terminated products obtained from reduction of saturated ester with $LiAlH_4$ (bottom) and catalytic reduction of unsaturated ester with *trans*-$RuHCl(CO)[PyCH_2NH(CH_2)P\textit{i}Pr_2]$ in a one-step reaction (top).

Epoxide Oligomer

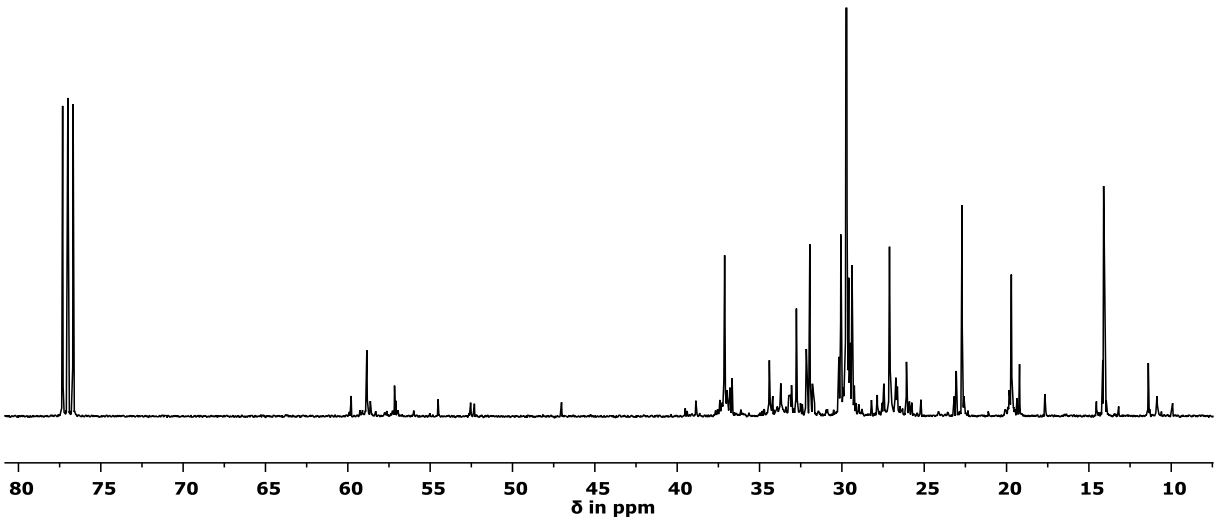

Figure 4.22: ^{13}C NMR spectrum (151 MHz, $CDCl_3$, 298 K) of functionalized oligomer obtained from epoxidation with *m*CPBA.

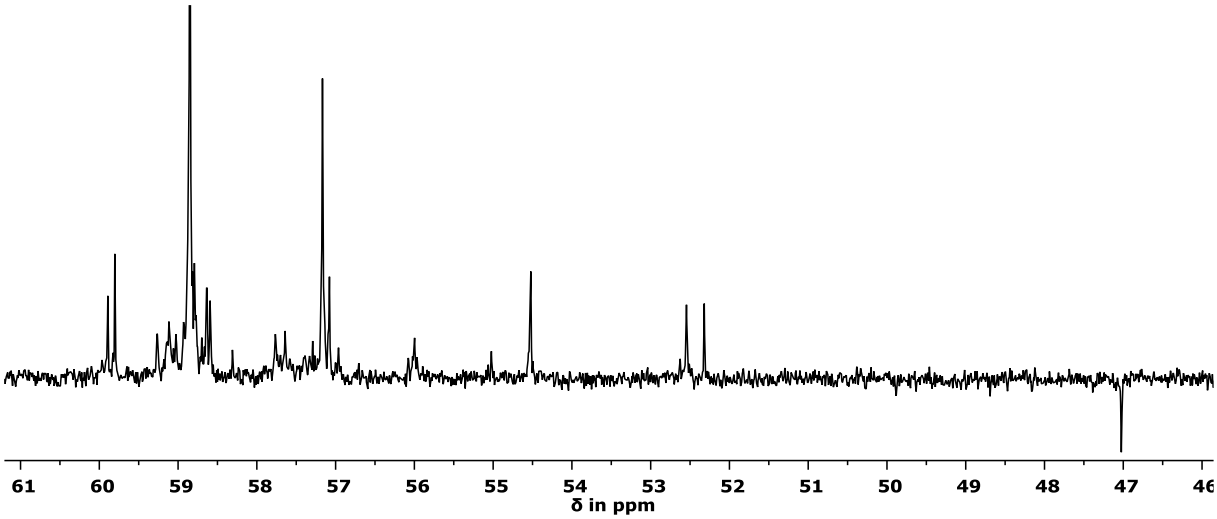

Figure 4.23: DEPT ^{13}C NMR spectrum (151 MHz, $CDCl_3$, 298 K) of relevant epoxy carbon signals obtained after epoxidation of oligomer with *m*CPBA.

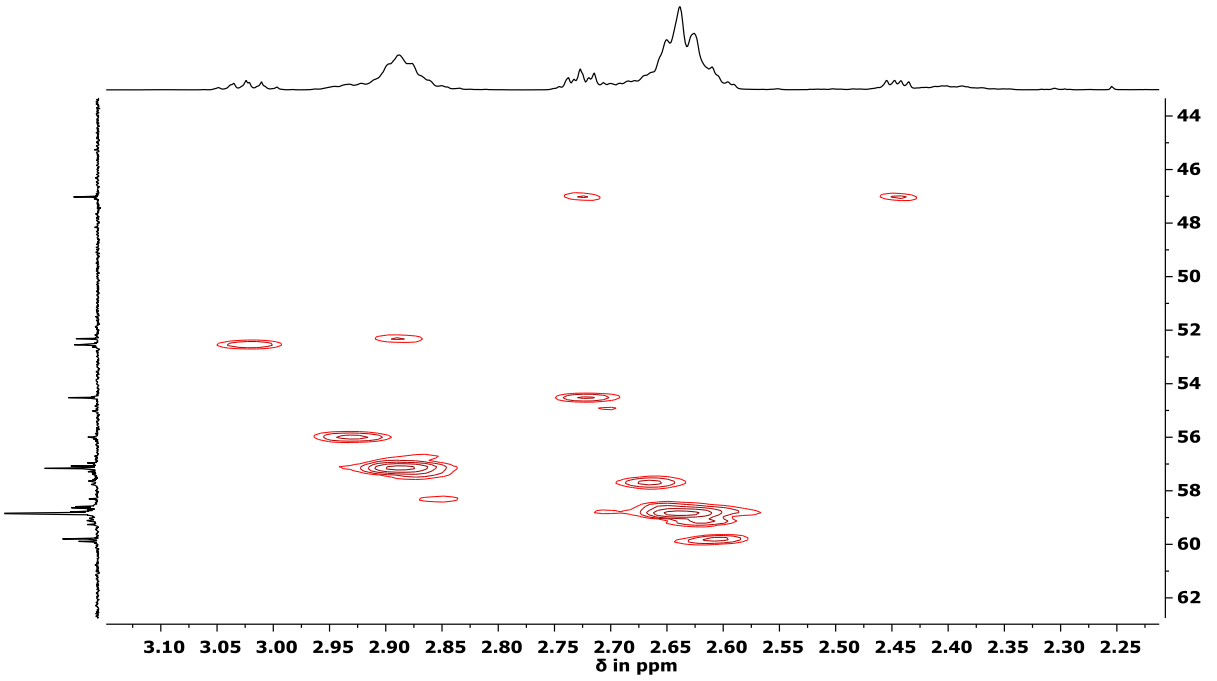

Figure 4.24: $^{1}H,^{13}C$ gHSQC spectrum (600 MHz, $CDCl_3$, 298 K) of functionalized oligomer obtained from epoxidation with *m*CPBA. ***Note:*** *Cross signals at 2.72 and 2.44 ppm for the CH_2 group of the terminal epoxy show the wrong phase correlation for CH/CH3 groups. However, the out of phase signal at 47.0 ppm in the DEPT ^{13}C NMR spectrum (**Figure 4.23**) proves this to be a methylene group.*

Acrylate Functionalized Macromonomer MM_{AA}

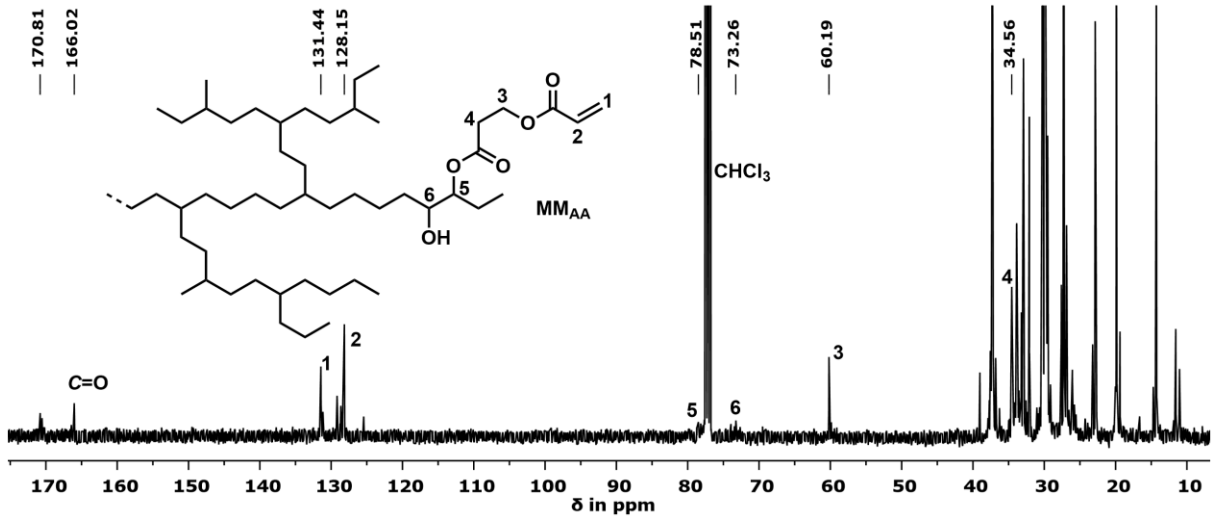

Figure 4.25: ^{13}C NMR spectrum (101 MHz, $CDCl_3$, 298 K) of the acrylate functionalized macromonomer **MM_{AA}**.

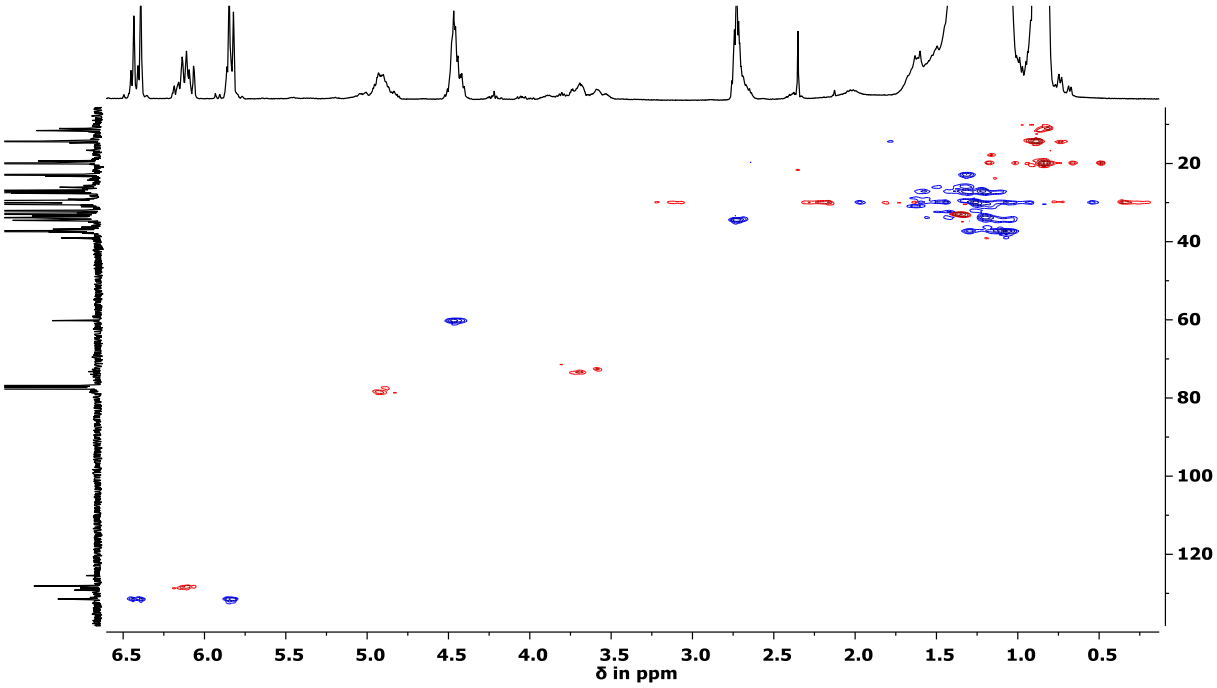

Figure 4.26: $^{1}H,^{13}C$ gHSQC spectrum (400 MHz, $CDCl_3$, 298 K) of the acrylate functionalized macromonomer **MM_{AA}**.

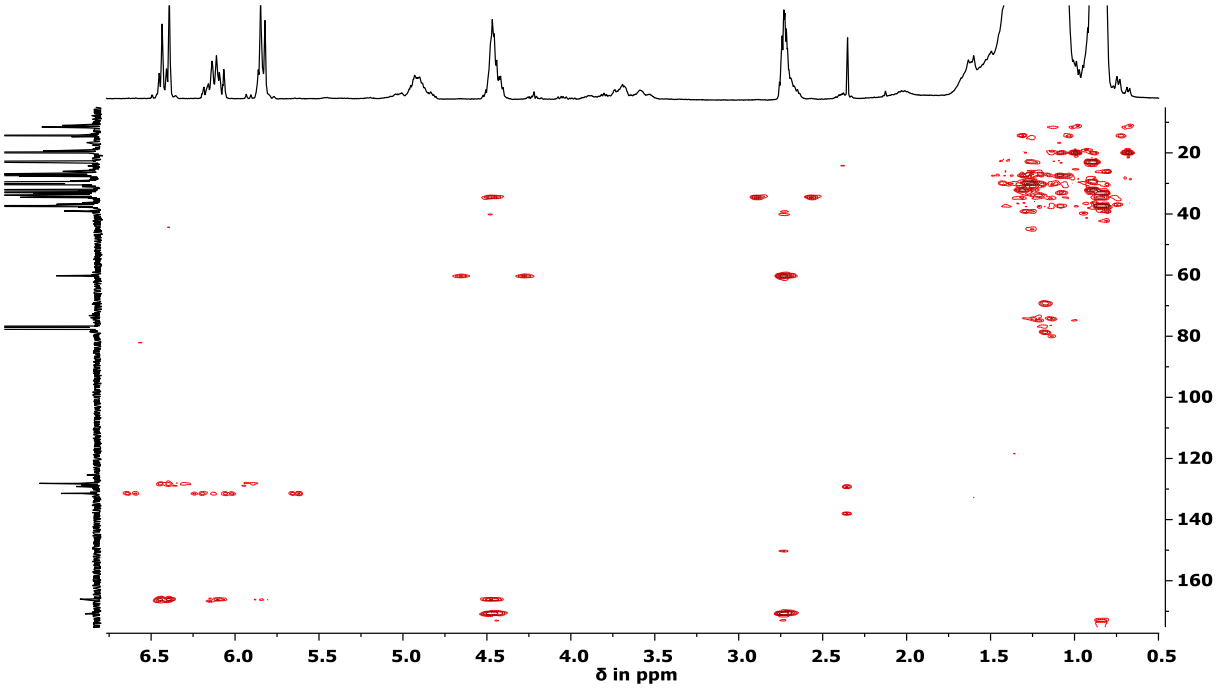

Figure 4.27: $^{1}H,^{13}C$ gHMBC spectrum (400 MHz, $CDCl_3$, 298 K) of the acrylate functionalized macromonomer **MM_{AA}**.

Methacrylate Functionalized Macromonomer MM_{MAA}

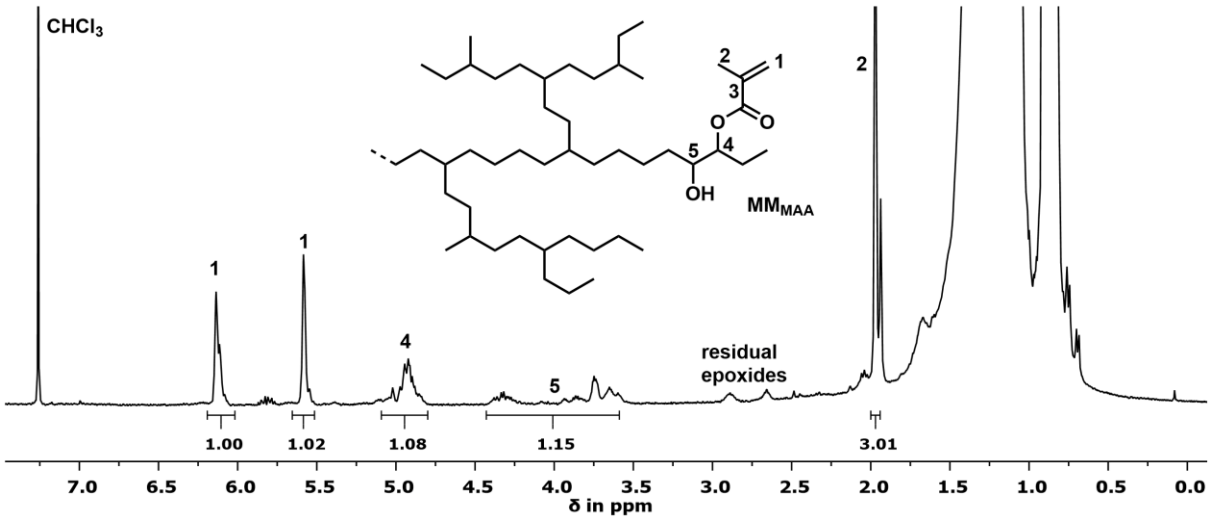

Figure 4.28: Characteristic ^{1}H NMR spectrum (400 MHz, $CDCl_3$, 298 K) of a methacrylate functionalized macromonomer **MM_{MAA}** (80 % methacrylate functionalization, **Table 4.3** entry 1).

5 Ethylene Oligomerization with Simplified Ni(II) Salicylaldiminato Complexes

5.1 Introduction

As shown in the previous chapters of this thesis, Ni(II) salicylaldiminato complexes present a unique possibility for the synthesis of highly branched ethylene oligomers by a chain walking insertion polymerization mechanism. The high degrees of branching obtained with this type of catalyst are unprecedented in the low molecular weight regime of < 5,000 g mol^{-1}. However, these high degrees of branching were thus far only obtained using *N*-terphenyl substituted Ni(II) salicylaldiminato complexes with electron donating substituents on the terphenyl moiety. The preparation of these very special catalysts, however, requires an elaborate synthesis procedure involving at least four reaction steps (cf. **Scheme 3.2**, p. 21). For a more detailed investigation and understanding of the practical scope of the Ni(II) salicylaldiminato catalyst system it is of strong interest to illuminate whether the synthesis of highly branched oligomers is a unique feature of catalysts with a 3,5,3',5'-substituted terphenyl moiety only. Therefore, the screening of new complexes with a simplified ligand structure with regard to their capability to afford highly branched oligoethylenes is of fundamental concern. Moreover, the highly branched oligomers are also of practical importance for commercial applications, for example as lubricants or defoamer additive.[73] For a prospective industrial scale synthesis of such products, the costly and elaborate synthesis of the required *N*-terphenyl Ni(II) salicylaldiminato catalyst would be a limitation. Hence, salicylaldiminato complexes with a simplified ligand structure based on inexpensive and abundantly available starting materials are desirable. Additionally, complexes with ligands accessible in a single reaction step from commercially available anilines and salicylaldehydes are of strong interest for a commercial application.

In the patent originally filed by DuPont for the newly developed neutral Ni(II) salicylaldiminato complexes, a variety of different nickel complexes with N^O-ligands were screened.[41] Revisiting this data, different complexes including ones with simplified ligand

structures – based on 2,6-dimethylaniline and 2,6-dibromoaniline – were reported to produce very short chain oligomers with high degrees of branching. However, the focus of this work was not on oligomerization and hence, there are only few examples described and the products were little characterized. Some of these potential oligomerization catalysts are depicted in **Figure 5.1**. Ethylene polymerization was carried out under harsh conditions at an ethylene pressure of 69 bar and 80 °C using Lewis acids as co-catalyst.

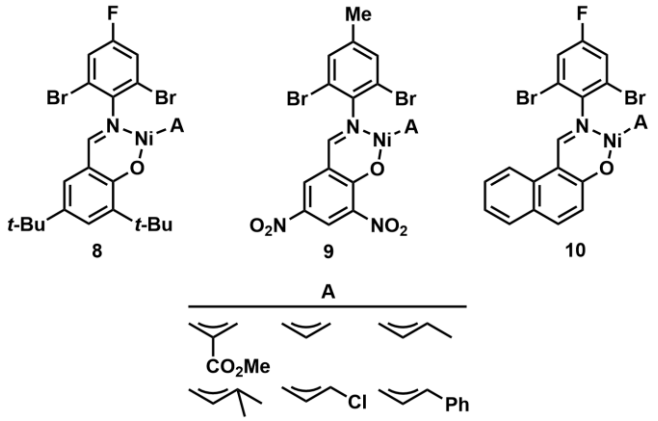

Figure 5.1: Ni(II)-N^O complexes reported to produce highly branched short chain oligomers.[41]

Under these conditions, **8** is reported to produce highly branched polyethylene with 4,700 g mol^{-1} and 137 branches per 1,000 carbon atoms at 80 °C and 69 bar ethylene. However, it has to be noted that the high degrees of branching are not corrected for saturated end groups and probably exceed the actual branch content. Similarly high degrees of branching of 135 and 99 branches per 1,000 C at molecular weights of 8,000 and 2,300 g mol^{-1} are reported for **9** and **10**, respectively. Furthermore, NMR spectroscopic analysis of selected oligomers revealed the presence of significant amounts of long chain branches. However, a detailed microstructure analysis is lacking and the activity of all three *in situ* generated catalysts is low and does not exceed several hundred turnovers per hour. Yet, these *in situ* generated, simplified catalyst structures generally appeared to be able to produce highly branched oligomers from ethylene and therefore represent an interesting lead structure.

5.2 Results and Discussion

On the basis of the results published by DuPont, 2,6-dibromoanilines were found to be one of the most promising aniline building blocks for the synthesis of oligomerization catalysts. The bromine substituents appear to introduce enough steric bulk in order to prevent excessive chain transfer reactions but are not as bulky as for example *iso*-propyl groups which lead to the formation of higher molecular weight polymers. Also, different 2,6-bromoanilines are

inexpensive and abundantly available. For a more systematic investigation of such simplified ligand structures, a small library of ligands was synthesized on the basis of different commercially available *para*-substituted 2,6-dibromoanilines and four aldehyde building blocks (**Figure 5.2**).

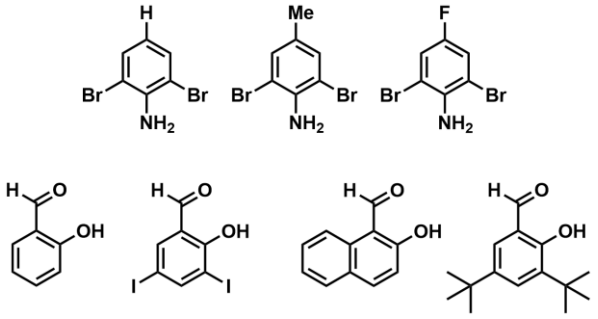

Figure 5.2: Building blocks for the synthesis of simplified salicylaldiminato ligands.

In contrast to the *in situ* generated allyl complexes reported in the patent by DuPont, defined nickel methyl pyridine complexes were synthesized which can be used as single-component catalyst without the need for a co-catalyst. These complexes were investigated with regard to their capability to produce highly branched oligomers under the mild reaction conditions using lower temperatures and ethylene pressures.

5.2.1 Ligand and Complex Synthesis

Synthesis of Simplified Salicylaldimines

The synthesis of new salicylaldiminato ligands based on commercially available amines and aldehydes was carried out following literature procedures for structurally related compounds.[50,51,53]

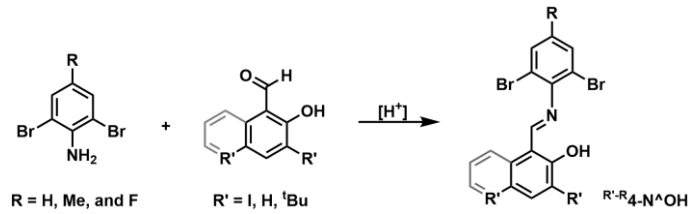

Scheme 5.1: Synthesis route for salicylaldimines based on para substituted 2,6-dibromoanilines and commercially available salicylaldehydes.

The salicylaldimines $^{I2\text{-}R}$**4-N^OH** (R' = I, R = H, Me, F) were synthesized via an acid catalyzed imine condensation reaction of 3,5-diiodosalicylaldehyde and the three different para-substituted 2,6-dibromoanilines. Due to incomplete conversion using a 1:1-mixture of the two starting compounds, a 2-fold excess of the aldehyde was applied in the preparation. Due to its

high solubility in methanol, it can easily be separated from the methanol insoluble product by filtration. All three salicylaldimines from 3,5-diiodosalicylaldehyde were obtained in high yields ($^{I2\text{-}R}$**4-N^OH**: R = H – 94 %, Me – 95 %, and F – 96 %) as yellow solids and were fully characterized by ^{1}H and ^{13}C NMR spectroscopy (cf. Experimental Section).

Salicylaldimines $^{Naph\text{-}R}$**4-N^OH** were synthesized following the same procedure using an excess of 2-hydroxynaphthaldehyde in order to assure complete conversion of the aniline. The products of the acid catalyzed imine condensation precipitated from the methanol solution and could be collected in high purity by filtration as yellow solids ($^{Naph\text{-}R}$**4-N^OH**: R = H – 80 %, Me – 89 %, and F – 88 %). All ligands were fully characterized by ^{1}H and ^{13}C NMR spectroscopy.

For salicylaldimines based on unsubstituted salicylaldehyde ($^{Sal\text{-}R}$**4-N^OH**), the standard procedure for imine condensations of the three anilines in methanol did not yield the desired products in high purity and yields. The ligands were synthesized instead by refluxing the starting compounds in toluene with a Dean-Stark apparatus for 2 days. After work-up and washing the final products with methanol all three salicylaldehyde based ligands were obtained in high purity and yield ($^{Sal\text{-}R}$**4-N^OH**: R = H – 95 %, Me – 97 %, and F – 93 %). Note that all three salicylaldimines were found to possess a limited stability in solution and slowly decompose via hydrolysis of the imine, forming the starting materials.

Imine condensations with 3,5-di-*tert*-butylsalicylaldehyde for the synthesis of the salicylaldimines $^{tBu\text{-}R}$**4-N^OH** also did not succeed in methanol. Instead, they were prepared by the same procedure used for the salicylaldehyde based ligands. Refluxing the starting materials in toluene using a Dean-Stark apparatus in the presence of p-toluenesulfonic acid yielded the desired ligands in low yields after work-up ($^{tBu\text{-}R}$**4-N^OH**: R = H – 31 %, Me – 29 %). $^{tBu\text{-}F}$**4-N^OH** could only be isolated as a mixture containing 40 % of 3,5-ditertbutylsalicylaldehyde and thus was not used for further complex synthesis.

Synthesis of Simplified Ni(II) salicylaldiminato Complexes

Complex syntheses with the simplified salicylaldimines were carried out using reported procedures at room temperature in benzene.[50]

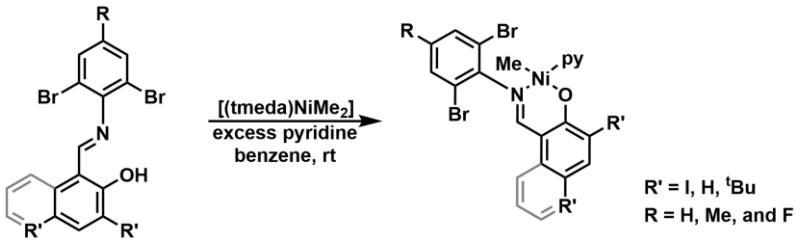

Scheme 5.2: Synthesis of simplified Ni(II) salicylaldiminato complexes.

The synthesis of $^{I2\text{-}R}$**4-pyr** was carried out by dissolving a mixture of the corresponding salicylaldimine and an equimolar amount of [(tmeda)$NiMe_2$] in benzene at room temperature in the presence of an excess of pyridine. An immediate change of color to dark red indicated the formation of the desired nickel methyl complexes. Washing the product with pentane and methanol to remove unreacted ligand present in the product however, resulted in decomposition of the complex and formation of nickel black. All three complexes could be obtained in an acid-base reaction of the salicylaldimine with a very small excess of the nickel precursor (1.05 to 1.10 equiv) in order to ensure full conversion of the salicylaldimine ($^{I2\text{-}R}$**4-pyr**: R = H – 89 %, Me – 92 %, and F – 90 %). The identity of the complexes $^{I2\text{-}R}$**4-pyr** was confirmed by ^{1}H NMR spectroscopy and the presence of signals for the Ni-Me group in the region of -1 ppm. These complexes were used as obtained from synthesis without removing residual nickel black traces.

The same problems described above were encountered while attempting to synthesize complexes $^{Naph\text{-}R}$**4-pyr** and therefore the identical synthesis procedure used for $^{I2\text{-}R}$**4-pyr** was applied. All complexes were obtained in very good yields and ^{1}H NMR spectroscopy proved the formation of clean nickel methyl complexes ($^{Naph\text{-}R}$**4-pyr**: R = H – 91 %, Me – 85 %, and F – 87 %).

The salicylaldimines $^{Sal\text{-}R}$**4-N^OH** based on salicylaldehyde were also applied to the same procedure using a small excess of [(tmeda)$NiMe_2$]. The two complexes $^{Sal\text{-}Me}$**4-pyr** and $^{Sal\text{-}F}$**4-pyr** could be obtained in high purity as evidenced by ^{1}H NMR spectroscopy ($^{Sal\text{-}Me}$**4-pyr**: X = Me – 83 %, F - 80 %). All attempts to synthesize $^{Sal\text{-}H}$**4-pyr** resulted in mixtures of the desired complex and free salicylaldimine. Due to low stability of the complex, the impurities of up to 50 % could not be removed and therefore this complex was not used for polymerization studies.

The synthesis of $^{tBu\text{-}R}$**4-pyr** with the procedure applied for the previous complexes resulted in the formation of a yellow-orange solid which is not the desired nickel methyl complex as indicated by the absence of a corresponding signal of the nickel methyl group in the ^{1}H NMR spectra. Attempted syntheses by dissolving [(tmeda)$NiMe_2$] and salicylaldimine in C_6D_6 in a NMR tube immediately resulted in the formation of a dark red solution. *In situ* NMR spectroscopy of the reaction however, did not confirm the formation of the nickel methyl pyridine complex regardless of the salicylaldimine applied.

Optimized Synthesis Procedure for $^{Naph\text{-}Me}$4-pyr

The complex synthesis procedure was optimized for complex $^{Naph\text{-}Me}$**4-pyr**. Dissolving the salicylaldimine and a stoichiometric amount of [(tmeda)$NiMe_2$] in benzene-d_6 in a NMR experiment did not result in clean formation of $^{Naph\text{-}Me}$**4-tmeda** but relative fast decomposition to the bischelated nickel complex. It was found that the presence of a coordinating solvent is

able to stabilize the desired methyl complex. The ^{1}H NMR spectrum after dissolving the salicylaldimine and nickel precursor in dmso-d_6 indicated the clean formation of the expected $^{Naph\text{-}Me}$**4-dmso** within 1 minute (**Figure 5.5**). However, all attempts to isolate the dmso coordinated complex by removing excess dmso resulted in decomposition and formation of bischelated nickel due to low stability in solution at room temperature. Synthesis of the pyridine coordinated $^{Naph\text{-}Me}$**4-pyr** in dmf as coordinating and stabilizing solvent was successful. However, after removal of the solvent under vacuum, the product was obtained as a sticky foam containing 1 equiv of dmf and removing all dmf by dissolving the product in benzene and subsequent sublimation under vacuum resulted in decomposition of the complex (**Figure 5.6**, p. 142).

Due to the limited stability of the complex in solution at room temperature, the synthesis was carried out in toluene at low temperatures. A small excess of [(tmeda)$NiMe_2$] precursor and the salicylaldimine were cooled to -60 °C and suspended in toluene and 2.5 equiv of pyridine were added. At this temperature, complexation does not occur. The suspension was slowly allowed to warm to 0 °C while the color gradually changed from yellow to dark red. After virtually complete reaction of all starting materials, the solvent was removed under vacuum at 0 °C. The orange solid was dissolved in cold benzene and quickly filtered via a syringe filter to remove nickel black. Subsequent removal of benzene by sublimation yielded $^{Naph\text{-}Me}$**4-pyr** in high yield (97 %) and high purity (**Figure 5.3**). This optimized procedure however, could not be applied successfully for the synthesis of any of the other simplified nickel salicylaldiminato complexes.

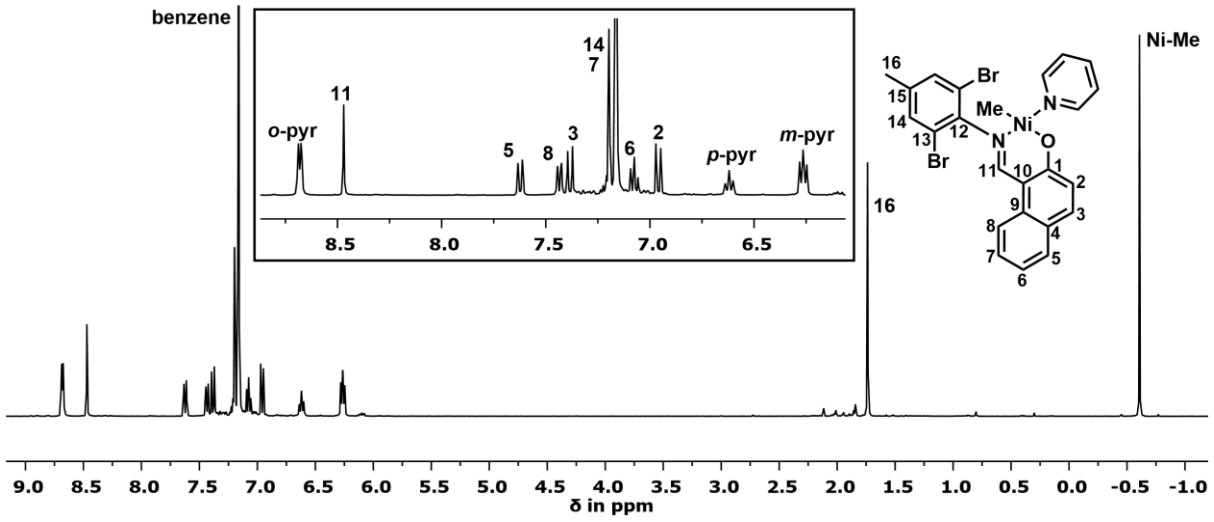

Figure 5.3: ^{1}H NMR spectrum (400 MHz, C_6D_6, 298 K) of $^{Naph\text{-}Me}$**4-pyr** from the optimized synthesis procedure.

All attempts to crystallize $^{Naph\text{-}Me}$**4-pyr** resulted in the crystallization of the bischelated decomposition product (**Figure 5.4**). Detailed information are listed in the Crystallography Appendix (**Table 8.2**, p. 199).

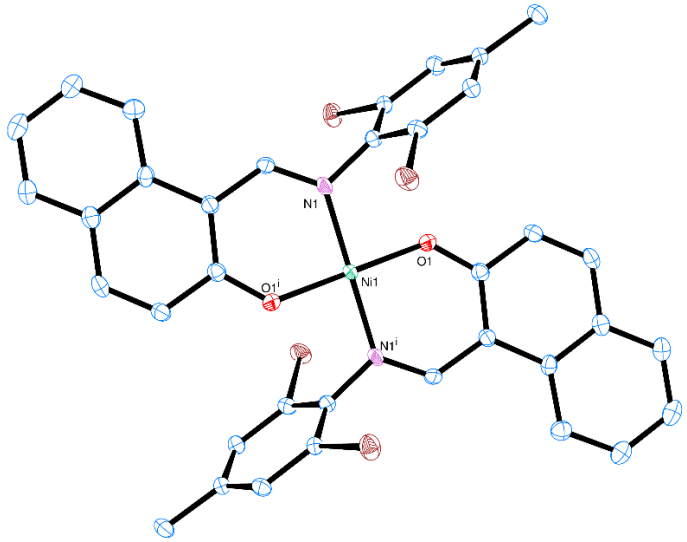

Figure 5.4: ORTEP of bischelated **[($^{Naph\text{-}Me}$N^O)$_2$Ni]** with 50 % probability ellipsoids. Hydrogen atoms and one co-crystallized dmso molecule are omitted for clarity.

5.2.2 Ethylene Oligomerization and Microstructure Analysis

The simplified nickel salicylaldiminato complexes based on different inexpensive, commercially available anilines and salicylaldehydes were subjected to the homopolymerization of ethylene. A special interest was dedicated to their potential capability to produce similar hyperbranched ethylene oligomers as their terphenyl amine based analogues. Since the previous oligomerization studies showed a much stronger dependence of the product properties like molecular weight, degree of branching and average branch length on the reaction temperature than on the ethylene pressure, only temperature dependent oligomerization studies were carried out. All simplified salicylaldiminato complexes were used as single component polymerization catalysts at 20, 40, and 60 °C at a constant ethylene pressure of 20 bar. The products obtained from the reactions were fully characterized and their molecular weights and microstructures were analyzed by ^{1}H and ^{13}C NMR spectroscopy as well as GPC. The activity and stability of all complexes was monitored by the ethylene uptake of the reactor during the polymerization. For comparison, ^{Me}**1-pyr** was used as a benchmark catalyst. It was applied under exactly the same reaction conditions and the products were also analyzed regarding their molecular weights, degree of branching, and exact microstructure (back-to-back experiments). The targeted structures should be in a molecular weight regime between 1,000 and 2,000 g mol^{-1} with degrees of branching greater than 70 branches per 1,000 carbon atoms including hyperbranching.

Ethylene Oligomerization with $^{I2-X}$4-pyr

The results of all polymerization runs at different temperatures with the three complexes $^{I2-H}$**4-pyr**, $^{I2-Me}$**4-pyr**, and $^{I2-F}$**4-pyr** are depicted in **Table 5.1**. Molecular weights and degrees of branching were calculated from intensity ratios in the proton NMR spectra according to **Equation (3-1)**, **(3-2)**, and **(3-3)** on p. 23. Remarkably, all three 3,5-diiodosalicylaldehyde based nickel salicylaldiminato complexes are capable of producing oligoethylenes in a low molecular weight regime between 1,800 and 5,000 g mol^{-1} with high degrees of branching of up to 66 branches per 1,000 carbon atoms. Molecular weight distributions of $M_w/M_n \approx 2$ indicate a well behaved single-site insertion polymerization. Note that GPC was measured against linear polyethylene standards and therefore underestimates the true molecular weight of the branched oligomers determined from the ^{1}H NMR spectra. The dependence of the product properties follows the same trends discussed for all previous nickel salicylaldiminato complexes. In general, the molecular weight of the oligomers decreases at higher temperatures, independent of the catalyst used, due to the higher degree of β-hydride elimination under such conditions. At the same time, the degree of branching increases for the same reason. Compared to the oligoethylenes produced by the benchmark catalyst ^{Me}**1-pyr** (entries 5.1.1-5.1.3, **Table 5.1**) the oligomers obtained with the three complexes with simplified ligands $^{I2-R}$**4-pyr** have higher molecular weights and lower degrees of branching. The lowest molecular weight products (2,200 – 3,600 g mol^{-1}) with the high degrees of branching between 51 and 63 branches per 1,000 carbon atoms are produced by $^{I2-H}$**4-pyr**. In terms of molecular weight, the fluorine and methyl substituted complexes $^{I2-F}$**4-pyr** and $^{I2-Me}$**4-pyr** produce similar products with molecular masses between 2,200 and 5,000 g mol^{-1} depending on the reaction temperature. However, oligomers obtained with $^{I2-F}$**4-pyr** exhibit a significantly lower amount of branches (55 per 1,000 C) than those produced by $^{I2-Me}$**4-pyr** (66 per 1,000 C) under identical reaction conditions (60 °C).

Table 5.1: Oligomerization results with complexes $^{I2\text{-}R}$**4-pyr** at different reaction temperatures.

entry	catalyst	T [°C]	yield [g]	TOF[a]	M_n (NMR) [g mol^{-1}][b]	M_n (GPC) [g mol^{-1}][c]	M_w/M_n (GPC)[c]	branches /1,000 C[d]
1	^{Me}**1-pyr**	20	2.1	3,800	2,600	1,700	2.3	78
2	^{Me}**1-pyr**	40	10.9	19,500	1,700	1,200	2.0	78
3	^{Me}**1-pyr**	60	9.0	16,200	1,100	800	2.0	80
4	$^{I2\text{-}H}$**4-pyr**	20	0.1	220	3,600	2,600	1.9	51
5	$^{I2\text{-}H}$**4-pyr**	40	5.0	8,900	3,700	2,700	2.2	54
6	$^{I2\text{-}H}$**4-pyr**	60	4.2	7,600	2,200	1,500	2.1	63
7	$^{I2\text{-}Me}$**4-pyr**	20	0.3	530	5,000	2,500	3.0	49
8	$^{I2\text{-}Me}$**4-pyr**	40	2.7	4,800	3,600	2,200	2.2	58
9	$^{I2\text{-}Me}$**4-pyr**	60	6.9	12,400	1,800	1,200	2.2	66
10	$^{I2\text{-}F}$**4-pyr**	20	0.1	150	-	2,300	1.8	-
11	$^{I2\text{-}F}$**4-pyr**	40	1.8	3,200	3,800	2,500	2.3	50
12	$^{I2\text{-}F}$**4-pyr**	60	9.1	16,300	2,500	1,600	2.4	55

reaction conditions: 20 µmol of catalyst in 100 mL of toluene for 1 h at 20 bar ethylene. [a] TOF x mol [C_2H_4] x mol^{-1} [Ni] h^{-1}. [b] molecular weights calculated from ^{1}H NMR intensity ratio of unsaturated end groups vs. overall integral. [c] in trichlorobenzene (160 °C) vs. polyethylene standards with linear calibration. [d] degree of branching calculated from ^{1}H NMR intensity ratio of methyl groups (corrected for saturated end groups) vs. overall integral.

Although the catalysts show faster decomposition and are less active than the terphenyl substituted analogs, mass flow traces collected during the polymerizations at constant pressure reveal a sufficient stability of all complexes for the one hour experiment conducted. Only at 60 °C, the initially very high ethylene uptake decreases very quickly due to catalyst decomposition. At 20 °C all the complexes $^{I2\text{-}R}$**4-pyr** are hardly active as evidenced by the low oligomer yield. The catalysts' activity clearly increases at higher temperature. However, the yields are limited by decomposition of the catalyst which is also favored under these conditions. $^{I2\text{-}F}$**4-pyr** appears to be the most active complex for ethylene oligomerization and reaches similar turnover frequencies as ^{Me}**1-pyr** (16,300). This is in agreement with previous findings, that a fluorine substituent in the *para*-position of the aniline increases the catalyst activity and productivity (Chapter 3.2).

A detailed investigation of the oligomer microstructures including the distribution of different branch lengths was carried out by analysis of the corresponding inverse gated decoupled ^{13}C NMR spectra. The results with fractional amounts of branches of different length are listed in **Table 5.2**.

Table 5.2: Microstructure analysis of oligomers obtained with $^{I2\text{-}R}$**4-pyr**.

entry	catalyst	T [°C]	branches /1,000 C	methyl[a] [%]	ethyl[a] [%]	propyl[a] [%]	C_{4+}[a] [%]	*sec*-butyl[a] [%]
1	^{Me}**1-pyr**	20	78	88	5	2	4	1
2	^{Me}**1-pyr**	40	78	79	7	3	7	4
3	^{Me}**1-pyr**	60	80	71	9	3	8	9
4	$^{I2\text{-}H}$**4-pyr**	20	51	85	6	3	4	2
5	$^{I2\text{-}H}$**4-pyr**	40	54	80	7	3	7	4
6	$^{I2\text{-}H}$**4-pyr**	60	63	75	10	3	8	5
7	$^{I2\text{-}Me}$**4-pyr**	20	49	88	3	1	5	2
8	$^{I2\text{-}Me}$**4-pyr**	40	58	79	7	4	7	4
9	$^{I2\text{-}Me}$**4-pyr**	60	66	71	12	3	8	6
10	$^{I2\text{-}F}$**4-pyr**	20	-	-	-	-	-	-
11	$^{I2\text{-}F}$**4-pyr**	40	50	84	7	1	7	1
12	$^{I2\text{-}F}$**4-pyr**	60	55	70	10	7	8	4

[a] percentage of different branch lengths can be calculated from relative intensity ratios of the corresponding signals ($1B_1$, $1B_2$, $1B_3$, $*B_{4+}$, B) of the respective branch in the ^{13}C NMR spectrum.

In addition to the high overall degrees of branching, all oligomers feature hyperbranched structures indicated by the presence of *sec*-butyl branches as the smallest and only detectable branch on branch motif. Notwithstanding, methyl branches represent the major amount of with more than 70 % of all branches. As expected from previous results, the amount of methyl branches decreases at higher temperatures in favor of longer chain branches and branch on branch structures. Therefore, oligomers with higher overall degrees of branching generally exhibit a longer average branch length with more long chain branches and hyperbranched structures.

Ethylene Oligomerization with $^{Naph\text{-}R}$4-pyr

The results of ethylene homopolymerization with the three 2-hydroxynaphthaldeyhde based complexes $^{Naph\text{-}R}$**4-pyr** are listed in **Table 5.3**. The molecular weights of the oligomers produced with $^{Naph\text{-}R}$**4-pyr** range from 2,100 to 6,400 g mol^{-1} and are higher when compared to the benchmark catalyst. Yet, extensive chain walking is observed for all three catalysts resulting in the very high degrees of branching of up to 86 branches per 1,000 carbon atoms ($^{Naph\text{-}Me}$**4-pyr**) found in all oligomers. The higher molecular weights compared to ^{Me}**1-pyr** along with the high degrees of branching are in agreement with the previous finding that 2-hydroxynaphthaldehyde (vide supra) based complexes produce longer chains with a high amount of branches. The degree of branching shows a much stronger dependence on the reaction temperature for $^{Naph\text{-}R}$**4-pyr** compared to ^{Me}**1-pyr** but follows the same trend with more branches at higher temperatures and

lower oligomer molecular weights. As observed for the 3,5-diiodosalicylaldimine based catalysts $^{I2\text{-}R}$**4-pyr**, the *para*-fluorine substituted complex $^{Naph\text{-}F}$**4-pyr** incorporates less branches in the oligomer than the methyl and proton substituted analogous.

Table 5.3: Oligomerization results with complexes $^{Naph\text{-}R}$**4-pyr** at different reaction temperatures.

entry	catalyst	T [°C]	yield [g]	TOF[a]	M_n (NMR) [g mol^{-1}][b]	M_n (GPC) [g mol^{-1}][c]	M_w/M_n (GPC)[c]	branches /1,000 C[d]
1	^{Me}**1-pyr**	20	2.1	3,800	2,600	1,700	2.3	78
2	^{Me}**1-pyr**	40	10.9	19,500	1,700	1,200	2.0	78
3	^{Me}**1-pyr**	60	9.0	16,200	1,100	800	2.0	80
4	$^{Naph\text{-}H}$**4-pyr**	20	0.1	140	6,400	5,000	2.1	65
5	$^{Naph\text{-}H}$**4-pyr**	40	4.0	7,200	4,100	3,200	1.9	73
6	$^{Naph\text{-}H}$**4-pyr**	60	2.5	4,500	2,400	1,700	2.1	84
7	$^{Naph\text{-}Me}$**4-pyr**	20	1.1	1,900	5,900	4,800	1.9	67
8	$^{Naph\text{-}Me}$**4-pyr**	40	4.1	7,300	2,500	2,800	2.0	77
9	$^{Naph\text{-}Me}$**4-pyr**	60	1.9	3,300	2,100	1,400	2.6	86
10	$^{Naph\text{-}F}$**4-pyr**	20	0.5	830	-	2,900	1.9	-
11	$^{Naph\text{-}F}$**4-pyr**	40	5.9	10,500	4,800	3,900	2.0	63
12	$^{Naph\text{-}F}$**4-pyr**	60	4.9	8,700	3,300	2,100	2.2	72

reaction conditions: 20 µmol of catalyst in 100 mL of toluene for 1 h at 20 bar ethylene. [a] TOF x mol [C_2H_4] x mol^{-1} [Ni] h^{-1}. [b] molecular weights calculated from ^{1}H NMR intensity ratio of unsaturated end groups vs. overall integral. [c] in trichlorobenzene (160 °C) vs. polyethylene standards with linear calibration. [d] degree of branching calculated from ^{1}H NMR intensity ratio of methyl groups (corrected for saturated end groups) vs. overall integral.

The activities of the 2-hydroxynaphthaldimine complexes are lower than for ^{Me}**1-pyr** which is also in agreement with results previously found for catalysts with an *N*-terphenyl-2-hydroxynaphthaldimine (vide supra). The highest activity is again found for the fluorine substituted complex at the highest reaction temperature studied (60 °C). Generally, the complexes are little active at 20 °C as indicated by the lack of significant ethylene uptake over the course of the polymerization. In strong contrast to $^{I2\text{-}R}$**4-pyr**, all $^{Naph\text{-}R}$**4-pyr** complexes exhibit maximum productivity at 40 °C. Though the activity increases at 60 °C, as indicated by the mass flow traces, catalyst deactivation is increased even more and results in lower oligomer yields.

The microstructure of all oligomers was investigated in detail by ^{13}C NMR spectroscopy and the results with the fractional amount of branches of different length are listed in **Table 5.4**. All oligomers obtained with $^{Naph\text{-}R}$**4-pyr** contain a significant amount of hyperbranched structures in the form of *sec*-butyl branches. With 64 to 80 %, the major amount of branches are methyl branches. Strikingly, the oligomers from $^{Naph\text{-}H}$**4-pyr**, $^{Naph\text{-}Me}$**4-pyr**, and $^{Naph\text{-}F}$**4-pyr** contain significantly more longer alkyl side chains (6 to 11 % C_{4+}) than those of the benchmark catalyst, thus substantiating the previous findings that with 2-hydroxynaphthaldehyde based catalysts

the average branch length is shifted from short methyl branches towards longer chain alkyl branches. As expected, the average branch length increases at higher temperatures since the higher propensity for chain walking favors the formation of alkyl branches and branches on branches over short methyl branches. Considering the high overall degrees of branching obtained with $^{Naph\text{-}H}$**4-pyr** and $^{Naph\text{-}Me}$**4-pyr** and the incorporation of a high amount of long chain branching and hyperbranching, these two complexes with a strongly simplified ligand are promising candidates for a potential replacement of the more complex terphenyl amine based Ni(II) salicylaldiminato catalysts for the branching oligomerization of ethylene.

Table 5.4: Microstructure analysis of oligomers obtained with $^{Naph\text{-}R}$**4-pyr**.

entry	catalyst	T [°C]	branches /1,000 C	methyl[a] [%]	ethyl[a] [%]	propyl[a] [%]	C_{4+}[a] [%]	*sec*-butyl[a] [%]
1	^{Me}**1-pyr**	20	78	88	5	2	4	1
2	^{Me}**1-pyr**	40	78	79	7	3	7	4
3	^{Me}**1-pyr**	60	80	71	9	3	8	9
4	$^{Naph\text{-}H}$**4-pyr**	20	65	77	8	5	7	2
5	$^{Naph\text{-}H}$**4-pyr**	40	73	74	9	4	9	5
6	$^{Naph\text{-}H}$**4-pyr**	60	84	64	12	7	10	7
7	$^{Naph\text{-}Me}$**4-pyr**	20	67	80	7	4	6	3
8	$^{Naph\text{-}Me}$**4-pyr**	40	77	70	9	8	8	5
9	$^{Naph\text{-}Me}$**4-pyr**	60	86	64	13	5	11	7
10	$^{Naph\text{-}F}$**4-pyr**	20	-	-	-	-	-	-
11	$^{Naph\text{-}F}$**4-pyr**	40	63	77	7	5	8	3
12	$^{Naph\text{-}F}$**4-pyr**	60	72	66	11	6	11	7

[a] percentage of different branch lengths can be calculated from relative intensity ratios of the corresponding signals ($1B_1$, $1B_2$, $1B_3$, $*B_{4+}$, B) of the respective branch in the ^{13}C NMR spectrum.

Ethylene Oligomerization with $^{Sal\text{-}R}$4–pyr

For the unsubstituted salicylaldimine based complexes, only $^{Sal\text{-}Me}$**4-pyr** and $^{Sal\text{-}F}$**4-pyr** were studied regarding their potential for ethylene oligomerization to highly branched products, since $^{Sal\text{-}H}$**4-pyr** could not be isolated in the desired purity. The results of all oligomerization reaction at different temperatures from 20 to 60 °C are listed in **Table 5.5**.

Both complexes $^{Sal\text{-}Me}$**4-pyr** and $^{Sal\text{-}F}$**4-pyr** produce ethylene oligomers that match the targeted structures in term of molecular weight and degree of branching. Particularly oligomers from $^{Sal\text{-}Me}$**4-pyr** show low molecular weights of 1,300, 1,400, and 2,200 g mol^{-1} at 60, 40, and 20 °C, respectively. These oligomers even contain a significantly higher amount of branches compared to those of the benchmark complex with up to 91 branches per 1,000 carbon atoms. In agreement with previous findings, the fluorine substituted complex produces fewer branches.

Table 5.5: Oligomerization results with complexes $^{Sal\text{-}R}$**4-pyr** at different reaction temperatures.

entry	catalyst	T [°C]	yield [g]	TOF[a]	M_n (NMR) [g mol^{-1}][b]	M_n (GPC) [g mol^{-1}][c]	M_w/M_n (GPC)[c]	branches /1,000 C[d]
1	^{Me}**1-pyr**	20	2.1	3,800	2,600	1,700	2.3	78
2	^{Me}**1-pyr**	40	10.9	19,500	1,700	1,200	2.0	78
3	^{Me}**1-pyr**	60	9.0	16,200	1,100	800	2.0	80
4	$^{Sal\text{-}Me}$**4-pyr**	20	0.4	750	2,200	1,500	2.3	73
5	$^{Sal\text{-}Me}$**4-pyr**	40	1.3	2,400	1,400	1,000	2.4	80
6	$^{Sal\text{-}Me}$**4-pyr**	60	1.4	2,500	1,300	800	2.1	91
7	$^{Sal\text{-}F}$**4-pyr**	20	0.6	1,000	3,700	2,900	2.1	62
8	$^{Sal\text{-}F}$**4-pyr**	40	1.9	3,400	2,300	1,700	2.2	69
9	$^{Sal\text{-}F}$**4-pyr**	60	1.8	3,200	1,400	1,000	2.5	75

reaction conditions: 20 µmol of catalyst in 100 mL of toluene for 1 h at 20 bar ethylene. [a] TOF x mol [C_2H_4] x mol^{-1} [Ni] h^{-1}. [b] molecular weights calculated from ^{1}H NMR intensity ratio of unsaturated end groups vs. overall integral. [c] in trichlorobenzene (160 °C) vs. polyethylene standards with linear calibration. [d] degree of branching calculated from ^{1}H NMR intensity ratio of methyl groups (corrected for saturated end groups) vs. overall integral.

A drawback of these two promising catalysts, however, is their considerably lower activity which is an order of magnitude lower than the ones of the corresponding terphenyl amine based complexes. The activity clearly increases at higher temperatures but is limited by a rapid catalyst decomposition. The lower stability could result from the aryl bromine bonds that might promote additional side reactions like oxidative addition to Ni(II).

The results of the detailed microstructure analysis by ^{13}C NMR spectroscopy of the oligomers are depicted in **Table 5.6**. In terms of distribution of branches of different length, $^{Sal\text{-}Me}$**4-pyr** and $^{Sal\text{-}F}$**4-pyr** produce similar oligomers compared to those of ^{Me}**1-pyr**. The oligoethylenes mainly contain methyl branches (60 – 80 %) but also exhibit longer ethyl, propyl, and alkyl branches as well as *sec*-butyl branches. The latter again prove a hyperbranched structure of the all oligomers. The distribution shows the same temperature dependence observed for the previously discussed catalysts. The amount of methyl branches decreases at higher reaction temperatures in favor of longer branches and hyperbranched structures.

Table 5.6: Microstructure analysis of oligomers obtained with $^{Sal\text{-}X}$**4-pyr**.

entry	catalyst	T [°C]	branches /1,000 C	methyl[a] [%]	ethyl[a] [%]	propyl[a] [%]	C_{4+}[a] [%]	*sec*-butyl[a] [%]
1	^{Me}**1-pyr**	20	78	88	5	2	4	1
2	^{Me}**1-pyr**	40	78	79	7	3	7	4
3	^{Me}**1-pyr**	60	80	71	9	3	8	9
4	$^{Sal\text{-}Me}$**4-pyr**	20	73	79	7	5	6	3
5	$^{Sal\text{-}Me}$**4-pyr**	40	80	72	9	5	7	7
6	$^{Sal\text{-}Me}$**4-pyr**	60	91	66	11	5	9	10
7	$^{Sal\text{-}F}$**4-pyr**	20	62	81	6	5	5	4
8	$^{Sal\text{-}F}$**4-pyr**	40	69	74	7	5	9	4
9	$^{Sal\text{-}F}$**4-pyr**	60	75	67	11	5	10	8

[a] percentage of different branch lengths can be calculated from relative intensity ratios of the corresponding signals ($1B_1$, $1B_2$, $1B_3$, $*B_{4+}$, B) of the respective branch in the ^{13}C NMR spectrum.

5.3 Summary and Conclusion

For a potential industrial application of Ni(II) salicylaldiminato complexes for the synthesis of highly branched oligoethylenes, the elaborate synthesis required for *N*-terphenyl amine based salicylaldiminato ligands would be a limitation. Especially the minimum of four reaction steps that is required for the catalyst synthesis represents a relevant effort. Therefore, low-cost catalysts with ligands accessible from inexpensive and commercially available compounds in a single reaction step would be beneficial.

To this end, a range of simplified salicylaldiminato ligands were synthesized by condensation of commercially available *para*-substituted 2,6-dibromoanlines with 3,5-substituted salicylaldehydes (**Scheme 5.3**). All ligands could be obtained in high purity and yield in a single reaction step. Complex synthesis according to known procedures yielded a range of eight strongly simplified Ni(II) salicylaldiminato methyl pyridine complexes. The synthesis of complexes based on 3,5-di-*tert*-butylsalicylaldehyde, however, was not successful.

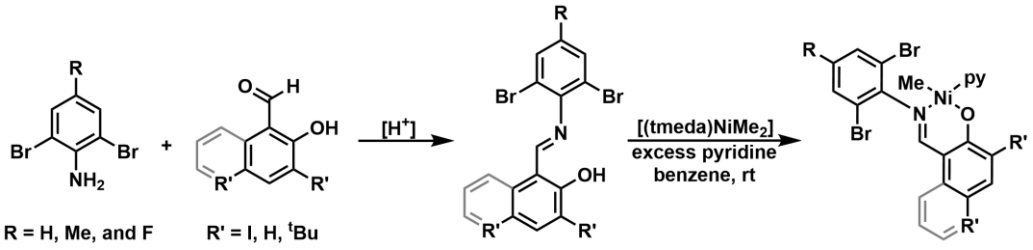

Scheme 5.3: Synthesis of simplified Ni(II) salicylaldiminato complexes based on commercially available anilines and salicylaldehydes.

All new simplified Ni(II) salicylaldiminato complexes were probed as single-component catalyst in the polymerization of ethylene regarding their ability to produce highly branched oligoethylenes. Remarkably, they are all capable of producing highly branched, low molecular weight ethylene oligomers at the reaction temperatures studied which included a wide range of oligomerization temperatures from 20 to 60 °C. The molecular weights of the oligomers produced with the new complexes are in the range of several 1,000 g mol^{-1}, but do not exceed 6,500 g mol^{-1}. Degrees of branching are between 50 and 90 branches per 1,000 carbon atoms depending on the reaction conditions and the catalyst applied. Therefore these strongly simplified complexes are promising candidates for the synthesis of similar products obtained with the more complex terphenyl amine based catalysts. The dependence of molecular weights and degrees of branching follow the same trends observed for all other Ni(II) salicylaldiminato complexes. Thus, lower molecular weight oligomers with higher degrees of branching are produced at higher temperatures and vice versa. Additionally, the *para*-fluorine substituent was found to increase the activity of the catalyst regardless of the salicylaldehyde used. At the same time, these catalysts are less prone to β-hydride elimination and incorporate fewer branches. All 2-hydroxynaphthaldehyde based complexes produced higher molecular weight oligomers with higher degrees of branching and significantly more of the longer chain alkyl branches.

Especially $^{Sal\text{-}Me}$**4-pyr** and $^{Naph\text{-}Me}$**4-pyr** are very promising catalysts for the synthesis of highly branched oligoethylenes. Both produce low molecular weight products with 1,300 and 2,100 g mol^{-1} and exceptionally high degrees of branching of 91 and 86 branches per 1,000 carbon atoms, respectively. Compared to the terphenyl amine based analogues, the simplified salicylaldiminato Ni(II) complexes exhibit lower activities especially at higher temperatures (2,400 and 7,300 mol [C_2H_4] x mol^{-1} [Ni] h^{-1} with $^{Sal\text{-}Me}$**4-pyr** and $^{Naph\text{-}Me}$**4-pyr**, respectively, compared to 19,500 mol [C_2H_4] x mol^{-1} [Ni] h^{-1} with). However, the lower activity is compensated for by the less costly starting materials and the single condensation step for the synthesis of the simplified salicylaldimines compared to an elaborated three step procedure required for the synthesis of the terphenyl amine based salicylaldimines.

5.4 Experimental Section

5.4.1 Materials and General Considerations

All complex syntheses were carried out under an argon or nitrogen atmosphere using standard Schlenk or glovebox techniques. Commercially available compounds were purchased from Aldrich, Acros, TCI or ABCR. Solvents were dried and degassed using standard laboratory

techniques.[94] Benzene and toluene were distilled from sodium and pyridine from KOH. Pentane, Et_2O and toluene used for complex syntheses and ethylene polymerization were dried by passing through columns equipped with aluminum oxide/molecular sieve 3 Å. Ethylene for polymerization (3.5 grade) was supplied by AirLiquide and used as received. All deuterated solvents were supplied by Eurisotop.

NMR-Spectroscopy

NMR spectra were recorded on a Varian Unity Inova 400 (^{1}H: 400 MHz, ^{13}C: 101 MHz, ^{19}F: 376 MHz), a Bruker Avance III 400 (^{1}H: 400 MHz, ^{13}C: 101 MHz, ^{19}F: 376 MHz), or a Bruker Avance III 600 spectrometer (^{1}H: 600 MHz, ^{13}C: 151 MHz, ^{19}F: 564 MHz). ^{1}H chemical shifts were referenced to the residual proton signal of the deuterated solvent. ^{13}C chemical shifts were referenced to the carbon signal of the deuterated solvent. Multiplicities are given as follows: s: singlet, d: doublet, t: triplet, q: quartet, quint: quintet, v: virtual multiplet, m: multiplet, br: broad signal or combination thereof. NMR spectra of polyethylenes were recorded at 130 °C with addition of 5 mg mL^{-1} of $Cr(acac)_3$ and CD_2Cl_4 as the solvent. For reliable integration all spectra were recorded inverse gated without NOE using a relaxation delay of 2s.

Gel Permeation Chromatography

High temperature gel permeation chromatography for PE molecular weight determination was carried out by Lars Bolk at the University of Konstanz in 1,2,4-trichlorobenzene at 160 °C at a flow rate of 1 mL min^{-1} on a 'Polymer Laboratories GPC 220' instrument equipped with 'PLgel Olexis' columns with differential refractive index-, viscostity- and light scattering- (15° and 90°) detectors. Data reported were determined via RI-detection against calibration with linear polyethylene standards.

Mass Spectroscopy

Electron spray ionization (ESI) mass spectra were recorded on a 'Bruker Esquire 3000+' instrument at the University of Konstanz.

Elemental Analyses

Elemental analyses were obtained by the Analytical Services at the Department of Chemistry, University of Konstanz. Elemental analyses were performed on an 'Elementar Vario MICRO cube' instrument.

Ethylene Polymerizations

Ethylene polymerizations were conducted in a 'Büchi *miniclave*' high pressure reactor equipped with a 200 mL steel vessel, with a mechanical stirrer and a cooling and heating jacket, supplied by a thermostat (Julabo FP 50) controlled by a thermocouple dipping into the polymerization mixture. Ethylene uptake of the reactor was monitored via Bronkhorst mass-flow meters.

5.4.2 Synthesis and Characterization of Simplified Salicylaldimines

3,5-Diiodo-*N*-[2,6-dibromophenyl]salicylaldimine ($^{I2-H}$4-N^OH)

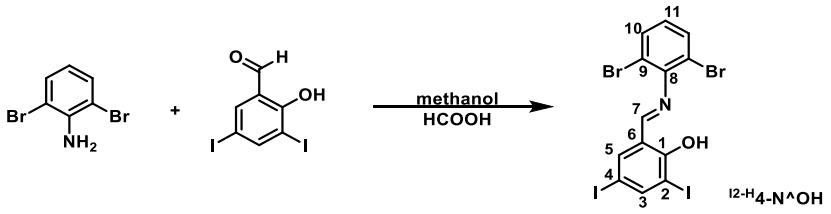

Under air 2,6-dibromoaniline (0.94 g, 3.7 mmol, 1.0 eq), 3,5-diiodosalicylaldehyde (2.75 g, 7.5 mmol, 2.0 eq) and 0.1 mL of formic acid were suspended in 45 mL of methanol and heated to 60 °C for 60 minutes while all starting materials dissolved. The reaction mixture was stirred for 19 hours at room temperature. After cooling to 0 °C, the yellow product was filtered off and washed with small portions of cold methanol. After drying under vacuum, **$^{I2-H}$4-N^OH** was obtained as a yellow solid (2.14 g, 3.5 mmol, 94 %).

^{1}H-NMR (400 MHz, $CDCl_3$): δ (ppm) = 13.39 (s, 1H, *OH*), 8.34 (s, 1H, *H-7*), 8.20 (d, $^{4}J_{HH}$=2.1 Hz, 1H, *H-3*), 7.71 (d, $^{4}J_{HH}$=2.1 Hz, 1H, *H-5*), 7.65 (d, $^{3}J_{HH}$=8.0 Hz, 2H, *H-10*), 7.00 (t, $^{3}J_{HH}$=8.0 Hz, 1H, *H-11*).
^{13}C-NMR (101 MHz, $CDCl_3$): δ (ppm) = 167.6 (C-7), 159.8 (C-1), 149.9 (C-3), 145.3 (C-8), 141.4 (C-5), 132.5 (C-10), 127.8 (C-11), 120.2 (C-6), 116.0 (C-9), 87.2 (C-2), 80.4 (C-4).
Elemental Analysis (%) for $C_{13}H_7Br_2I_2NO$: Found (Calculated): C 25.73 (25.68), H 1.16 (1.31), N 2.31 (2.70).
ESI-MS (positive) m/z = 609.0 ($C_{13}H_8Br_2I_2NO^+$).

3,5-Diiodo-*N*-[2,6-dibromo-4-methylphenyl]salicylaldimine ($^{I2-Me}$4-N^OH)

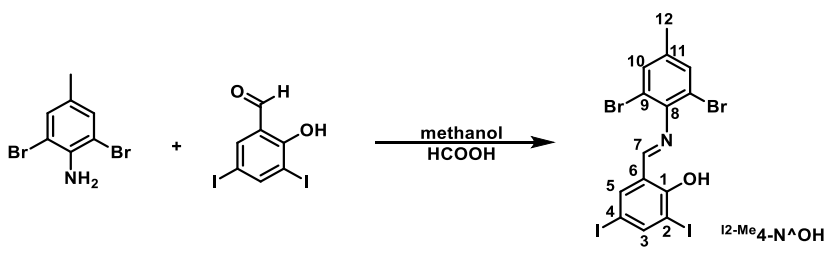

Under air 2,6-dibromo-4-methylaniline (0.95 g, 3.6 mmol, 1.0 eq), 3,5-diiodosalicylaldehyde (2.69 g, 7.2 mmol, 1.9 eq) and 0.1 mL of formic acid were suspended in 45 mL of methanol and heated to 60 °C for 60 minutes while all starting materials dissolved. The reaction mixture was stirred for 20 hours at room temperature. After cooling to 0 °C, the yellow product was filtered off and washed with small portions of cold methanol. After drying under vacuum, **$^{I2\text{-}Me}$4-N^OH** was obtained as a yellow solid (2.12 g, 3.4 mmol, 95 %).

^{1}H-NMR (400 MHz, $CDCl_3$): δ (ppm) = 8.31 (s, 1H, *H-7*), 8.16 (d, $^{4}J_{HH}$=2.1 Hz, 1H, *H-3*), 7.66 (d, $^{4}J_{HH}$=2.1 Hz, 1H, *H-5*), 7.43 (s, 2H, *H-10*), 2.34 (s, 3H, *H-12*).
^{13}C-NMR (101 MHz, $CDCl_3$): δ (ppm) = 167.7 (C-7), 160.2 (C-1), 150.1 (C-3), 143.1 (C-8), 141.2 (C-5), 138.5 (C-11), 133.2 (C-10), 120.0 (C-6), 115.9 (C-9), 87.4 (C-2), 80.4 C-4), 20.5 (C-12).
Elemental Analysis (%) for $C_{14}H_9Br_2I_2NO$: Found (Calcluated): C 27.08 (27.02), H 1.46 (1.55), N 2.26 (2.26).
ESI-MS (positive): m/z = 623.1 ($C_{14}H_{10}Br_2I_2NO^+$).

3,5-Diiodo-*N*-[2,6-dibromo-4-fluorophenyl]salicylaldimine ($^{I2\text{-}F}$4-N^OH)

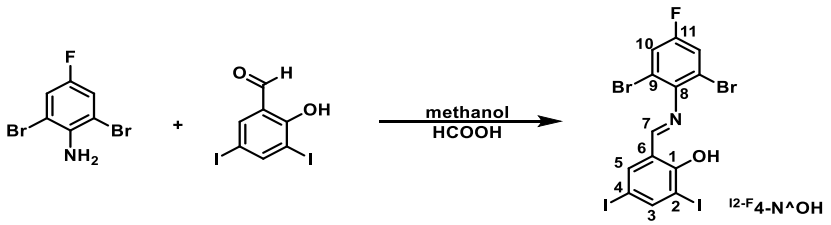

Under air 2,6-dibromo-4-fluoroaniline (1.00 g, 3.7 mmol, 1.0 eq), 3,5-diiodosalicylaldehyde (2.69 g, 7.2 mmol, 1.9 eq) and 0.1 mL of formic acid were suspended in 45 mL of methanol and heated to 60 °C for 60 minutes while all starting materials dissolved. The reaction mixture was stirred for 19 hours at room temperature. After cooling to 0 °C, the yellow product was filtered off and washed with small portions of cold methanol. After drying under vacuum, **$^{I2\text{-}F}$4-N^OH** was obtained as a yellow solid (2.32 g, 3.6 mmol, 96 %).

^{1}H-NMR (400 MHz, $C_2D_2Cl_4$): δ (ppm) = 13.26 (s, 1H, *OH*), 8.32 (s, 1H, *H-7*), 8.20 (d, $^{4}J_{HH}$=2.1 Hz, 1H, *H-3*), 7.71 (d, $^{4}J_{HH}$=2.1 Hz, 1H, *H-5*), 7.44 (d, $^{3}J_{HF}$=7.6 Hz, 2H, *H-10*).
^{13}C-NMR (101 MHz, $C_2D_2Cl_4$): δ (ppm) = 168.1 (C-7), 160.4 (C-1), 159.1 (d, $^{1}J_{CF}$=252.1 Hz, C-11), 150.1 (C-3), 142.2 (d, $^{4}J_{CF}$=4.0 Hz, C-8), 141.2 (C-5), 120.8 (d, $^{2}J_{CF}$=12.2 Hz, C-10), 119.9 (d, $^{3}J_{CF}$=25.5 Hz, C-9), 115.9 (C-6), 87.2 (C-2), 80.4 (C-4).
^{19}F-NMR (376 MHz, $CDCl_3$): δ (ppm) = -113.53 (t, $^{3}J_{FH}$=7.59 Hz).
Elemental Analysis (%) for $C_{13}H_6Br_2FI_2NO$: Found (Calculated) C 24.99 (24.94), H 0.97 (1.14), N 2.24 (2.76).
ESI-MS (positive): m/z = 627.0 ($C_{13}H_7Br_2FI_2NO^+$).

2-Hydroxy-*N*-[2,6-dibromophenyl]-1-naphthaldimine ($^{Naph-H}$4-N^OH)

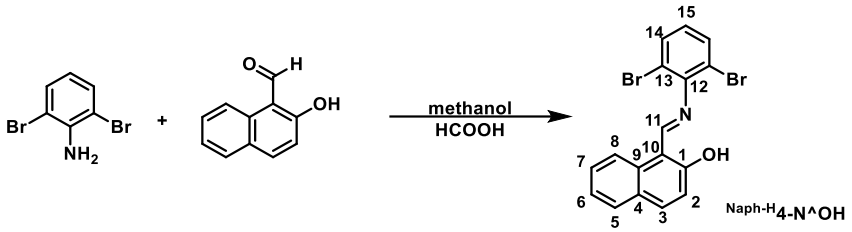

Under air 2,6-dibromoaniline (1.01 g, 4.0 mmol, 1.0 eq), 2-hydroxy-1-naphthaldehyde (1.34 g, 7.8 mmol, 1.9 eq) and 0.1 mL of formic acid were suspended in 45 mL of methanol and heated to 60 °C for 60 minutes while all starting materials dissolved. The reaction mixture was stirred for 23 hours at room temperature. After cooling to 0 °C, the yellow product was filtered off and washed with small portions of cold methanol. After drying under vacuum, $^{Naph-H}$**4-N^OH** was obtained as a yellow solid (1.28 g, 3.2 mmol, 80 %).

^{1}H-NMR (400 MHz, $CDCl_3$): δ (ppm) = 9.34 (s, 1H, *H-11*), 8.02 (dd, $^3J_{HH}$=8.3 Hz, $^4J_{HH}$=1.0 Hz, 1H, *H-8*), 7.84 (d, $^3J_{HH}$=9.1 Hz, 1H, *H-3*), 7.72 (dd, $^3J_{HH}$=8.1, $^4J_{HH}$=1.5 Hz, 1H, *H-5*), 7.56 (d, $^3J_{HH}$=8.1 Hz, 2H, *H-14*), 7.47 (ddd, $^3J_{HH}$=8.3, 6.9 Hz, $^4J_{HH}$=1.4 Hz, 1H, *H-7*), 7.31 (ddd, $^3J_{HH}$=8.1, 6.9 Hz, $^4J_{HH}$ = 1.0 Hz, 1H, *H-6*), 7.19 (d, $^3J_{HH}$=9.1 Hz, 1H, *H-2*), 6.87 (t, $^3J_{HH}$=8.0 Hz, 1H, *H-15*).

^{13}C-NMR (101 MHz, $CDCl_3$): δ (ppm) = 165.8 (C-11), 163.9 (C-1), 146.9 (C-12), 136.2 (C-3), 133.2 (C-9), 132.7 (C-14), 129.4 (C-5), 128.4 (C-7), 128.0 (C-4), 127.3 (C-15), 124.0 (C-6), 120.0 (C-2), 119.6 (C-8), 117.0 (C-13), 109.0 (C-10).

Elemental Analysis (%) for $C_{17}H_{11}Br_2NO$: Found (Calculated): C 50.40 (50.40), H 2.74 (2.86), N 3.88 (3.46).

ESI-MS (positive): m/z = 406.4 ($C_{17}H_{12}Br_2NO^+$).

2-Hydroxy-*N*-[2,6-dibromo-4-methylphenyl]-1-naphthaldimine ($^{Naph-Me}$4-N^OH)

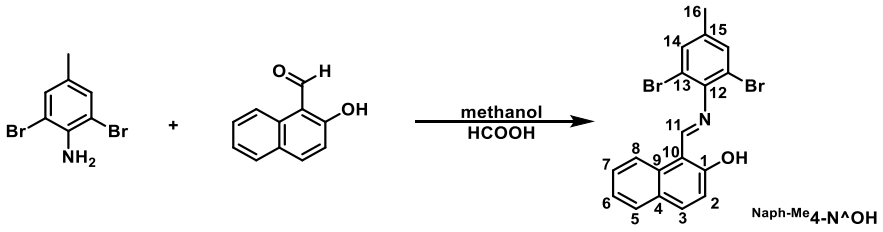

Under air 2,6-dibromo-4-methylaniline (0.95 g, 3.6 mmol, 1.0 eq), 2-hydroxy-1-naphthaldehyde (1.27 g, 7.4 mmol, 2.1 eq) and 0.1 mL of formic acid were suspended in 45 mL of methanol and heated to 60 °C for 60 minutes while all starting materials dissolved. The reaction mixture was stirred for 20 hours at room temperature. After cooling to 0 °C, the yellow product was filtered off and washed with small portions of cold methanol. After drying under vacuum, $^{Naph-Me}$**4-N^OH** was obtained as a yellow solid (1.35 g, 3.2 mmol, 89 %).

^{1}H-NMR (400 MHz, $CDCl_3$): δ (ppm) = 9.41 (s, 1H, *H-11*), 8.10 (d, $^3J_{HH}$=8.5 Hz, 1H, *H-8*), 7.92 (d, $^3J_{HH}$=9.0 Hz, 1H, *H-3*), 7.80 (d, $^3J_{HH}$=8.0, 1H, *H-5*), 7.56 (ddd, $^3J_{HH}$=8.5, 6.9 Hz, $^4J_{HH}$=1.4 Hz, 1H, *H-7*), 7.48 (s, 2H, *H-14*), 7.39 (ddd, $^4J_{HH}$=8.0, 6.9, 1.1 Hz, 1H, *H-6*), 7.31 (d, $^4J_{HH}$=9.1 Hz, 1H, *H-2*), 2.36 (s, 3H, *H-16*).
^{13}C-NMR (101 MHz, $CDCl_3$): δ (ppm) = 165.5 (C-11), 164.2 (C-1), 143.9 (C-12), 137.9 (C-15), 136.3 (C-3), 133.3 (C-14), 133.2 (C-9), 129.5 (C-5), 128.4 (C7), 128.0 (C-4), 123.9 (C-6), 120.1 (C-2), 119.6 (C-8), 116.5 (C-13), 108.9 (C-10), 20.5 (C-16).
Elemental Analysis (%) for $C_{18}H_{13}Br_2NO$: Found (Calculated) C 51.58 (51.47), H 3.13 (3.24), N 3.34 (3.73).
ESI-MS (positive): m/z = 420.4 ($C_{18}H_{14}Br_2NO^+$).

2-Hydroxy-*N*-[2,6-dibromo-4-fluorophenyl]-1-naphthaldimine ($^{Naph-F}$4-N^OH)

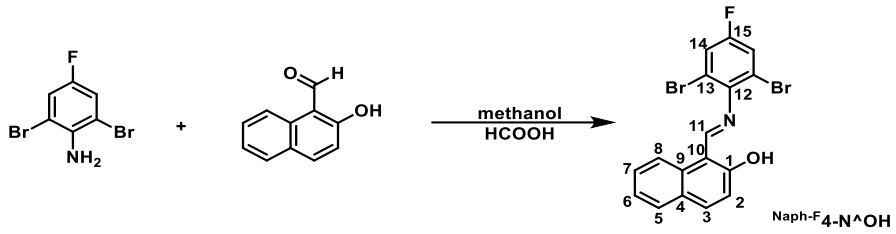

Under air 2,6-dibromo-4-fluoroaniline (0.96 g, 3.6 mmol, 1.0 eq), 2-hydroxy-1-naphthaldehyde (1.24 g, 7.2 mmol, 2.0 eq) and 0.1 mL of formic acid were suspended in 45 mL methanol and heated to 60 °C for 60 minutes while all starting materials dissolved. The reaction mixture was stirred for 20 hours at room temperature. After cooling to 0 °C, the yellow product was filtered off and washed with small portions of cold methanol. After drying under vacuum, **$^{Naph-F}$4-N^OH** was obtained as a yellow solid (1.33 g, 3.1 mmol, 88 %).

^{1}H-NMR (400 MHz, $CDCl_3$): δ (ppm) = 14.12 (s, 1H, *OH*), 9.40 (s, 1H, *H-11*), 8.09 (dd, $^3J_{HH}$=8.3 Hz, $^4J_{HH}$=0.9 Hz, 1H, *H-8*), 7.93 (d, $^3J_{HH}$=9.0 Hz, 1H, *H-3*), 7.81 (dd, $^3J_{HH}$=8.1, $^4J_{HH}$=1.4 Hz, 1H, *H-5*), 7.56 (ddd, $^3J_{HH}$=8.3, 6.9 Hz, $^4J_{HH}$=1.4 Hz, 1H, *H-7*), 7.44 (d, $^3J_{HF}$=7.6 Hz, 2H, *H-14*), 7.40 (ddd, $^3J_{HH}$=8.1, 6.9, $^4J_{HH}$ = 0.9 Hz, 1H, *H-6*), 7.28 (d, $^3J_{HH}$ = 9.0 Hz, 1H, *H-2*).
^{13}C-NMR (101 MHz, $CDCl_3$): δ (ppm) = 166.3 (d, $^6J_{CF}$=1.9 Hz, C-11), 163.9 (C-1), 159.1 (d, $^1J_{CF}$=252.4 Hz, C-15), 143.7 (d, $^4J_{CF}$=3.9 Hz, C-12), 136.4 (C-3), 133.2 (C-9), 129.5 (C-5), 128.5 (C-7), 128.1 (C-4), 124.1 (C-6), 120.1 (d, $^2J_{CF}$=24.9 Hz, C-14), 119.9 (C-2), 119.5 (C-8), 116.8 (d, $^3J_{CF}$=10.4 Hz, C-13), 108.9 (C-10).
^{19}F-NMR (376 MHz, $CDCl_3$): δ (ppm) = -114.58 (t, $^3J_{FH}$=7.56 Hz).
Elemental Analysis (%) for $C_{17}H_{10}Br_2NO$: Found (Calculated) C 48.26 (47.98), H 2.38 (2.61), N 3.31 (3.78).
ESI-MS (positive): m/z = 424.4 ($C_{17}H_{11}Br_2NO^+$).

N-[2,6-dibromophenyl]salicylaldimine ($^{Sal-H}$4-N^OH)

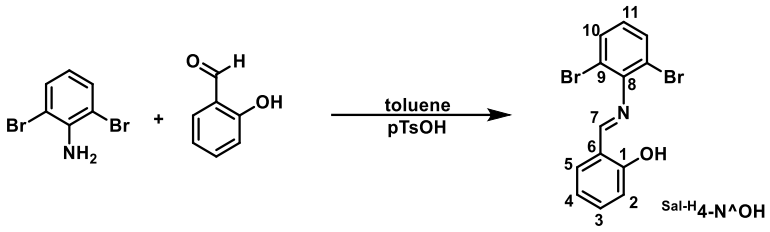

Under air 2,6-dibromoaniline (3.8 g, 15 mmol, 1.5 eq), salicylaldehyde (1.2 g, 15 mmol, 1.0 eq) and 5 mg of *p*-toluenesulfonic acid were dissolved in 100 mL of toluene and refluxed for 2 days with a Dean-Stark apparatus (150 °C bath temperature). The reaction mixture was cooled to room temperature and the solvent was removed under vacuum. The resulting yellow solid was washed with cold methanol to yield analytically pure **$^{Sal-H}$4-N^OH** (3.37 g, 9.5 mmol, 95 %).

^{1}H-NMR (400 MHz, $CDCl_3$): δ (ppm) = 8.46 (s, 1H, *H-7*), 7.60 (d, $^4J_{HH}$=8.0 Hz, 2H, *H-10*), 7.45 (ddd, $^3J_{HH}$=8.4, 7.5 Hz, $^4J_{HH}$=1.7 Hz, 1H, *H-3*), 7.40 (dd, $^3J_{HH}$=7.7 Hz, $^4J_{HH}$=1.7 Hz, 1H, *H-5*), 7.09 (dd, $^3J_{HH}$=8.4 Hz, $^4J_{HH}$=1.1 Hz, 1H, *H-2*), 6.98 (td, $^3J_{HH}$=7.5 Hz, $^4J_{HH}$=1.1 Hz, 1H, *H-4*), 6.93 (t, $^3J_{HH}$ =8.0 Hz, 1H, *H-11*).
^{13}C-NMR (101 MHz, $CDCl_3$): δ (ppm) = 169.8 (C-7), 161.5 (C-1), 146.9 (C-8), 134.4 (C-3), 133.1 (C-5), 132.5 (C-10), 127.2 (C-11), 120.0 (C-6), 119.5 (C-4), 118.3 (C-2), 116.4 (C-9).
Elemental Analysis (%) for $C_{13}H_9Br_2NO$: Found (calculated): C: 43.57 (43.98), H: 3.07 (2.56), N: 4.00 (3.95).
ESI-MS (positive) m/z = 356.0 ($C_{13}H_{10}Br_2NO^+$).

N-[2,6-dibromo-4-methylphenyl]salicylaldimine ($^{Sal-Me}$4-N^OH)

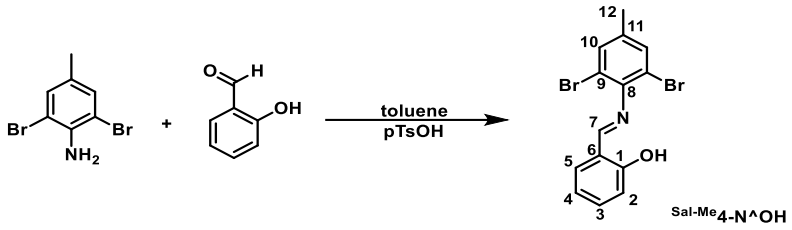

Under air 2,6-dibromo-4-methylaniline (4.0 g, 15 mmol, 1.5 eq), salicylaldehyde (1.2 g, 10 mmol, 1.05 eq) and 5 mg of *p*-toluenesulfonic acid were dissolved in 100 mL of toluene and refluxed for 2 days with a Dean-Stark apparatus (150 °C bath temperature). The reaction mixture was cooled to room temperature and the solvent was removed under vacuum. The resulting brown oil containing a yellow solid was suspended in methanol by ultra-sonication. The suspension was cooled, filtered over a Büchner funnel and the solid washed with cold methanol to yield **$^{Sal-Me}$4-N^OH** as a white solid. (3.56 g, 9.7 mmol, 97 %).

^{1}H-NMR (400 MHz, $CDCl_3$): δ (ppm) = 8.46 (s, 1H, *H-7*), 7.43 (m, 4H, *H-10/5/3/2*), 7.39 (dd, $^3J_{HH}$=7.7 Hz, $^4J_{HH}$=1.6 Hz, 1H, *H-5*), 7.07 (d, $^3J_{HH}$=8.4 Hz, 1H, *H-2*), 6.97 (td, $^3J_{HH}$=7.4 Hz, $^4J_{HH}$=1.0 Hz, 1H, *H-4*), 2.33 (d, $^4J_{HH}$=0.8 Hz, 3H, *H-12*).

^{13}C-NMR (101 MHz, $CDCl_3$): δ (ppm) = 169.8 (C-7), 161.6 (C-1), 144.1 (C-8), 137.8 (C-11), 134.3 (C-3), 133.1 (C-10/5), 119.4 (C-4), 118.4 (C-6), 117.7 (C-2), 116.0 (C-9), 20.4 (C-12).

Elemental Analysis (%) for $C_{14}H_{11}Br_2NO$: Found (calculated): C: 45.51 (45.56), H: 2.86 (3.00), N: 3.96 (3.80).

ESI-MS (positive): m/z = 370.2 ($C_{14}H_{12}Br_2NO^+$).

N-[2,6-dibromo-4-fluorophenyl]salicylaldimine ($^{Sal-F}$4-N^OH)

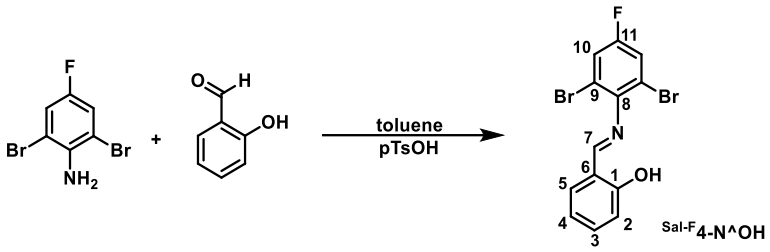

Under air 2,6-dibromo-4-fluoroaniline (4.0 g, 10 mmol, 1.5 eq), salicylaldehyde (1.2 g, 10 mmol, 1.0 eq) and 5 mg of *p*-toluenesulfonic acid were dissolved in 100 mL of toluene and refluxed for 2 days with a Dean-Stark apparatus (150 °C bath temperature). The reaction mixture was cooled to room temperature and the solvent was removed under vacuum. The resulting red solid was suspended in methanol by ultra-sonication. The suspension was cooled, filtered over a Büchner funnel and the solid washed with cold methanol to yield **$^{Sal-F}$4-N^OH** as a slight purple solid. (3.46 g, 9.3 mmol, 93 %).

^{1}H-NMR (400 MHz, $CDCl_3$): δ (ppm) = 8.45 (s, 1H, *H-7*), 7.45 (dt, $^3J_{HH}$=7.8 Hz, $^4J_{HH}$=1.7 Hz, 1H, *H-3*), 7.40 (m, 2H, *H-10/5*), 7.07 (d, $^3J_{HH}$=8.3 Hz, 1H, *H-2*), 6.98 (dt, $^3J_{HH}$=7.8 Hz, $^4J_{HH}$=1.1 Hz, 1H, *H-4*).

^{13}C-NMR (101 MHz, $CDCl_3$): δ (ppm) = 170.4 (d, $^6J_{CF}$=1.5 Hz, C-7), 161.5 (C-1), 159.1 (d, $^1J_{CF}$=252.4 Hz, C-11), 143.8 (d, $^4J_{CF}$=3.9 Hz, C-8), 134.5 (C-3), 133.2 (C-5), 120.0 (d, $^2J_{CF}$=24.9 Hz, C-10), 119.5 (C-4), 118.3 (C-), 117.8 (C-6), 116.2 (d, $^3J_{CF}$=10.3 Hz, C-9).

^{19}F-NMR (376 MHz, $CDCl_3$): δ (ppm) = -114.75 (t, $^3J_{FH}$=7.57 Hz).

Elemental Analysis (%) for $C_{13}H_8Br_2FNO$: Found (calculated): C: 41.80 (41.86), H: 1.90 (2.16), N: 3.94 (3.75).

ESI-MS (positive): m/z = 374.1 ($C_{13}H_9Br_2FNO^+$).

3,5-Di-*tert*-butyl-*N*-[2,6-dibromophenyl]salicylaldimine ($^{tBu-H}$4-N^OH)

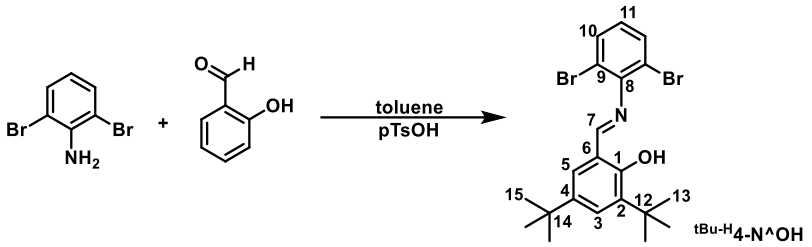

Under air 2,6-dibromoaniline (0.89 g, 3.55 mmol, 1.0 eq), 3,5-di-tert-butylsalicylaldehyde (0.84 g, 3.58 mmol, 1.0 eq) and 10 mg of *p*-toluenesulfonic acid were dissolved in 45 mL of toluene and refluxed for 4 hours with a Dean-Stark apparatus (150 °C bath temperature). The reaction mixture was cooled to room temperature and stirred for another 18 hours. After removing the solvent under vacuum, the resulting yellow oil was suspended in 10 mL pentane. The solid was filtered off with a Büchner funnel and washed with cold methanol. The filtrate was concentrated and suspended in 5 mL of methanol. The suspension was cooled to 0 °C, filtered and the solid washed with small portions of cold methanol. **$^{tBu-H}$4-N^OH** was obtained as a white solid (0.62 g, 1.33 mmol, 37 %).

^{1}H-NMR (400 MHz, $CDCl_3$): δ (ppm) = 8.46 (s, 1H, *H-7*), 7.60 (d, $^3J_{HH}$=8.0 Hz, 2H, *H-10*), 7.52 (d, $^4J_{HH}$=2.5 Hz, 1H, *H-3*), 7.19 (d, $^4J_{HH}$=2.5 Hz, 1H, *H-5*), 6.91 (t, $^3J_{HH}$=8.0 Hz, 1H, *H-11*), 1.49 (s, 9H, *H-15*), 1.33 (s, 9H, *H-13*).

^{13}C-NMR (101 MHz, $CDCl_3$): δ (ppm) = 170.8 (C-7), 159.8 (C-1), 147.2 (C-8), 140.9 (C-2), 137.5 (C-4), 132.5 (C-10), 129.4 (C-3), 127.5 (C-5), 119.6 (C-11), 117.4 (C-6), 116.6 (C-9), 35.4 (C-14), 34.4 (C-12), 31.6 (C-15), 29.6 (C-13).

Elemental Analysis (%) for $C_{21}H_{25}Br_2NO$: Found (calculated): C: 53.80 (53.98), H: 5.31 (5.39), N: 3.15 (3.00).

ESI-MS (positive) m/z = 468.7 ($C_{21}H_{26}Br_2NO^+$).

3,5-Di-*tert*-butyl-*N*-[2,6-dibromo-4-methylphenyl]salicylaldimine ($^{tBu-Me}$4-N^OH)

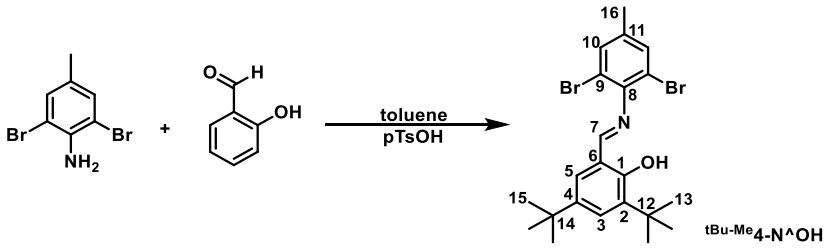

Under air 2,6-dibromo-4-methylaniline (1.91 g, 7.21 mmol, 1.0 equiv), 3,5-di-tert-butylsalicylaldehyde (2.09 g, 8.92 mmol, 1.2 eq) and 20 mg of *p*-toluenesulfonic acid were dissolved in 90 mL of toluene and refluxed for 4 hours with a Dean-Stark apparatus (150 °C bath temperature). The reaction mixture was cooled to room temperature and stirred for another 18 hours. After removing the solvent under vacuum, the resulting red oil was suspended in pentane.

The solid was filtered off with a büchner funnel and washed with cold methanol. The filtrate was concentrated and suspended in methanol. The suspension was cooled to 0 °C, filtered and the solid washed with small portions of cold methanol. **$^{tBu\text{-}Me}$4-N^OH** was obtained as a white solid. (1.02 g, 2.12 mmol, 29 %).

^{1}H-NMR (400 MHz, $CDCl_3$): δ (ppm) = 8.46 (s, 1H, *H-7*), 7.52 (d, $^4J_{HH}$=2.5 Hz, 1H, *H-3*), 7.42 (d, $^4J_{HH}$=0.8 Hz, 2H, *H-10*), 7.19 (d, $^4J_{HH}$=2.5 Hz, 1H, *H-5*), 2.33 (t, $^4J_{HH}$=0.8 Hz, 3H, *H-16*), 1.49 (s, 9H, *H-15*), 1.34 (s, 9H, *H-13*).
^{13}C-NMR (101 MHz, $CDCl_3$): δ (ppm) = 170.7 (C-7), 158.8 (C-1), 144.5 (C-8), 140.8 (C-2), 137.4 (C-11), 137.3 (C-5), 133.1 (C-10), 129.2 (C-3), 127.4 (C-5), 117.5 (C-6), 116.1 (C-9), 35.3 (C-14), 34.4 (C-12), 31.6 (C-15), 29.6 (C-13), 20.4 (C-16).
Elemental Analysis (%) for $C_{22}H_{27}Br_2NO$: Found (calculated): C: 55.26 (54.90), H: 5.46 (5.65), N: 3.09 (2.91).
ESI-MS (positive): m/z = 482.8 ($C_{22}H_{28}Br_2NO^+$).

3,5-Di-*tert*-butyl-*N*-[2,6-dibromo-4-fluorophenyl]salicylaldimine ($^{tBu\text{-}F}$4-N^OH)

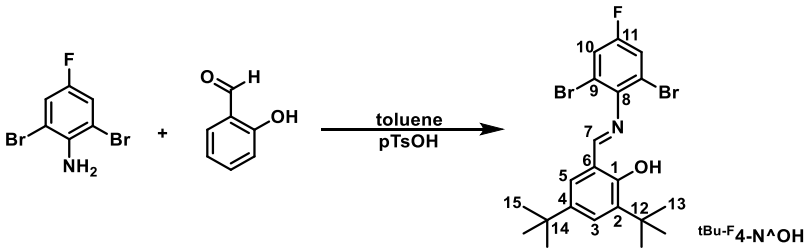

Under air 2,6-dibromo-4-fluoroaniline (0.97 g, 3.61 mmol, 1.0 eq), 3,5-di-tert-butylsalicylaldehyde (0.85 g, 3.63 mmol, 1.0 eq) and 10mg of *p*-toluenesulfonic acid were dissolved in 45 mL of toluene and refluxed for 4 hours with a Dean-Stark apparatus (150 °C bath temperature). The reaction mixture was cooled to room temperature and stirred for another 20 hours. The solvent was removed under vacuum to yield **$^{tBu\text{-}F}$4-N^OH** as a brown solid with 4 equivalents of the aldehyde starting material. (0.58 g, 1.2 mmol, 33 %).

^{1}H-NMR (400 MHz, $CDCl_3$): δ (ppm) = 12.76 (s, 1H, *OH*), 8.44 (s, 1H, *H-7*), 7.53 (d, $^4J_{HH}$=2.5 Hz, 1H, *H-3*), 7.40 (d, $^2J_{HF}$=7.7 Hz, 2H, *H-10*), 7.19 (d, $^4J_{HH}$=2.5 Hz, 1H, *H-5*), 1.48 (s, 9H, *H-15*), 1.33 (s, 9H, *H-13*).
^{13}C-NMR (101 MHz, $CDCl_3$): δ (ppm) = 171.3 (C-7), 159.2 (C-1), 158.9 (d, $^1J_{CF}$=252.4 Hz, C-11), 144.0 (d, $^4J_{CF}$=3.9 Hz, C-8), 141.0 (C-2), 137.5 (C-4), 129.5 (C-3), 127.5 (C-5), 119.9 (d, $^2J_{CF}$=24.9 Hz, C-10), 117.4 (C-6), 116.3 (d, $^3J_{CF}$=10.3 Hz, C-9), 35.3 (C-14), 34.4 (C-12), 31.6 (C-15), 29.6 (C-13).
^{19}F-NMR (376 MHz, $CDCl_3$): δ (ppm) = -115.26 (t, $^3J_{FH}$=7.59 Hz).
Elemental Analysis (%) for $C_{21}H_{24}Br_2FNO$: Found (calculated): C: 56.75 (51.98), H: 6.07 (4.99), N: 2.42 (2.89).
ESI-MS (positive): m/z = 486.6 ($C_{21}H_{25}Br_2FNO^+$).

5.4.3 Synthesis and Characterization of Simplified Complexes

[2,4-Diiodo-*N*-(2,6-dibromophenyl)salicylaldiminato-κ^2-*N,O*]methyl-pryidinenickel-(II) ($^{I2-H}$4-pyr)

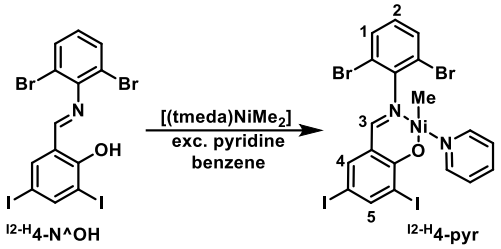

In a 25 mL Schlenk tube 90 mg (148 µmol, 1.0 eq) of $^{I2-H}$**4-N^OH** and 32 mg (158 µmol, 1.1 eq) of [(tmeda)$NiMe_2$] were dissolved in 10 mL of benzene and 80 µL (1 mmol, 6.8 eq) and stirred for 60 min at room temperature. The dark red solution was filtered over a syringe filter and the benzene was sublimated off under vacuum. $^{I2-H}$**4-pyr** was obtained as an orange/red powder (100 mg, 131 µmol, 89 %).

^{1}H-NMR (400 MHz, C_6D_6): δ (ppm) = 8.60 (s, br, 2H, *H-o-H pyr*), 8.10 (s, 1H, *H-3*), 7.20 (d, $^3J_{HH}$=8.0 Hz, 2H, *H-1*), 6.98 (d, $^4J_{HH}$=2.3 Hz, 1H, *H-3*), 6.76 (d, $^4J_{HH}$=2.3 Hz, 1H, *H-4*), 6.67 (s, br, 1H, *p-H pyr*), 6.31 (s, br, 2H, *m-H pyr*), 6.27 (t, $^3J_{HH}$=8.0 Hz, 1H, *H-2*), -0.74 (s, 3H, Ni-CH_3).

[2,4-Diiodo-*N*-(2,6-dibromo-4-methylphenyl)salicylaldiminato-κ^2-*N,O*]-methylpryidine-nickel-(II) ($^{I2-Me}$4-pyr)

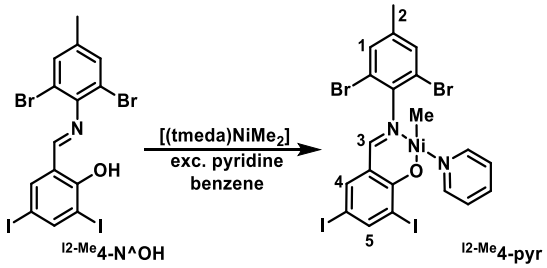

In a 25 mL Schlenk tube 63 mg (101 µmol, 1.0 eq) of $^{I2-Me}$**4-N^OH** and 22 mg (107 µmol, 1.05 eq) of [(tmeda)$NiMe_2$] were dissolved in 6 mL of benzene and 50 µL (630 µmol, 6.3 eq) and stirred for 60 min at room temperature. The dark red solution was filtered over a syringe filter and the benzene was sublimated off under vacuum. $^{I2-Me}$**4-pyr** was obtained as an orange/red powder (71 mg, 92 µmol, 92 %).

^{1}H-NMR (400 MHz, C_6D_6): δ (ppm) = 8.63 (s, br, 2H, *o-H pyr*), 8.11 (s, 1H, *H-3*), 7.10 (s, 2H, *H-1*), 7.00 (s, 1H, *H-4*), 6.88 (s, 1H, *H-5*), 6.67 (s, br, 1H, *p-H pyr*), 6.32 (s, br, 2H, *m-H pyr*), 1.70 (s, 3H, *H-2*), -0.68 (s, 3H, Ni-CH_3).

[2,4-Diiodo-*N*-(2,6-dibromo-4-fluorophenyl)salicylaldiminato-κ^2-*N,O*]-methylpryidine-nickel-(II) ($^{I2\text{-}F}$4-pyr)

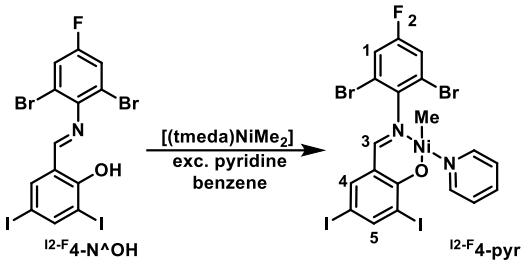

In a 25 mL Schlenk tube 62 mg (99 µmol, 1.0 eq) of $^{I2\text{-}F}$**4-N^OH** and 21 mg (103 µmol, 1.05 eq) of [(tmeda)NiMe$_2$] were dissolved in 6 mL of benzene and 50 µL (630 µmol, 6.3 eq) and stirred for 60 min at room temperature. The dark red solution was filtered over a syringe filter and the benzene was sublimated off under vacuum. $^{I2\text{-}F}$**4-pyr** was obtained as an orange/red powder (70 mg, 90 µmol, 90 %).

^{1}H-NMR (400 MHz, C_6D_6): δ (ppm) = 8.58 (s, 2H, *H-o-H pyr*, 8.10 (s, 1H, *H-3*), 7.01 (s, 1H, *H-4*), 6.94 (d, $^3J_{HF}$=7.5 Hz, 2H, *H-1*), 6.71 (s, 1H, *H-4*), 6.69 (s, br, 1H, *p-H pyr*), 6.33 (s, 2H, *m-H pyr*), -0.81 (s, 3H, Ni-CH_3).

[*N*-(2,6-dibromophenyl)-salicylaldiminato-κ^2-*N,O*]methylpryidinenickel-(II) ($^{Sal\text{-}H}$4-pyr)

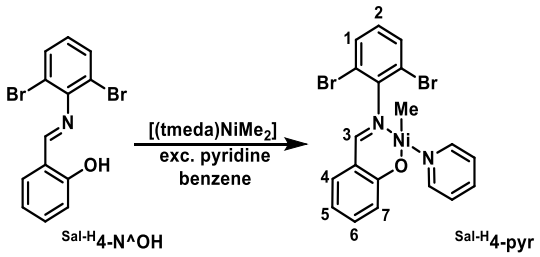

In a 25 mL Schlenk tube 82 mg (232 µmol, 1.0 eq) of $^{Sal\text{-}H}$**4-N^OH** and 47 mg (253 µmol, 1.05 eq) of [(tmeda)NiMe$_2$] were dissolved in 10 mL of benzene and 80 µL (1 mmol, 4.9 eq) and stirred for 60 min at room temperature. The dark red solution was filtered over a syringe filter and the benzene was sublimated off under vacuum. $^{Sal\text{-}H}$**4-pyr** was obtained as an orange/red powder (27 mg, 53 µmol, 26 %).

^{1}H-NMR (400 MHz, C_6D_6): δ (ppm) = 8.71 – 8.58 (m, 2H, *o-H pyr*), 7.70 – 5.70 (m, ~11 H), -0.77 (s, 3H, *Ni-CH_3*).

[*N*-(2,6-dibromo-4-methylphenyl)salicylaldiminato-κ^2-*N,O*]methylpryidine-nickel-(II) ($^{Sal-Me}$4-pyr)

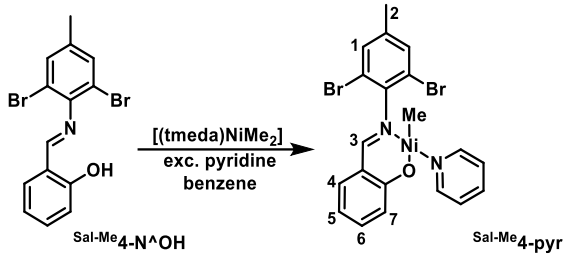

$^{Sal-Me}$4-N^OH $^{Sal-Me}$4-pyr

In a 25 mL Schlenk tube 55 mg (150 µmol, 1.0 eq) of $^{Sal-Me}$**4-N^OH** and 34 mg (165 µmol, 1.1 eq) of [(tmeda)NiMe$_2$] were dissolved in 10 mL of benzene and 80 µL (1 mmol, 6.7 eq) and stirred for 60 min at room temperature. The dark red solution was filtered over a syringe filter and the benzene was sublimated off under vacuum. $^{Sal-Me}$**4-pyr** was obtained as an orange/red powder (65 mg, 125 µmol, 83 %).

^{1}H-NMR (400 MHz, C_6D_6): δ (ppm) = 8.68 (s, 2H, *o-H pyr*), 7.37 (s, 1H, *H-3*), 7.35 (s, 1H, *H-4*), 6.99 – 6.92 (m, 3H, *H-1/6*), 6.44 (t, $^4J_{HH}$=7.3 Hz, 1H, *p-H pyr*), 6.29 – 6.15 (m, 4H, *H-5/7/m-H pyr*), 1.70 (s, 3H, *H-2*), -0.70 (s, 3H, *Ni-CH$_3$*).

[*N*-(2,6-dibromo-4-fluorophenyl)salicylaldiminato-κ^2-*N,O*]methyl-pryidinenickel-(II) ($^{Sal-F}$4-pyr)

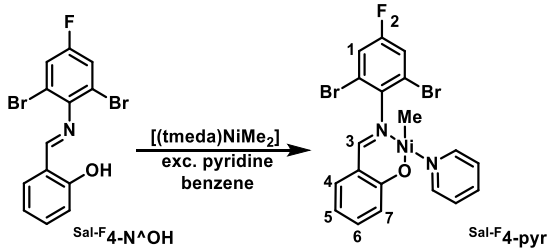

$^{Sal-F}$4-N^OH $^{Sal-F}$4-pyr

In a 25 mL Schlenk tube 57 mg (153 µmol, 1.0 eq) of $^{Sal-F}$**4-N^OH** and 31 mg (153 µmol, 1.0 eq) of [(tmeda)NiMe$_2$] were dissolved in 10 mL of benzene and 80 µL (1 mmol, 6.5 eq) and stirred for 60 min at room temperature. The dark red solution was filtered over a syringe filter and the benzene was sublimated off under vacuum. $^{Sal-F}$**4-pyr** was obtained as an orange/red powder (64 mg, 122 µmol, 80 %).

^{1}H-NMR (400 MHz, C_6D_6): δ (ppm) = 8.65 (s, br, 2H, *o-H pyr*), 7.34 (s, br, *H-3/4*), 6.96 (s, br, 3H, *H-1/6*), 6.60 (s, br, 1H, *H-7*), 6.45 (s, br, 1H, *p-H pyr*), 6.24 (s, br, 3H, *H-5/m-H pyr*), -0.82 (s, 3H, *Ni-CH$_3$*).

[2-Hydroxy-*N*-(2,6-dibromophenyl)-1-naphthaldiminato-κ^2-*N,O*]methyl-pryidinenickel-(II) ($^{Naph-H}$4-pyr)

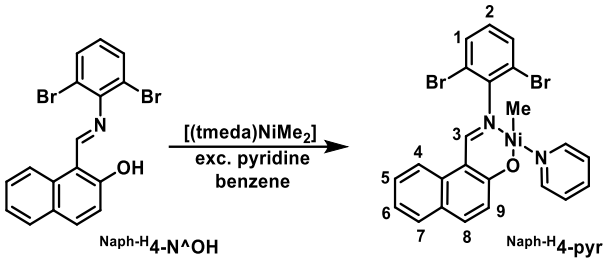

In a 25 mL Schlenk 61 mg (149 µmol, 1.0 eq) of $^{Naph-H}$**4-N^OH** and 35 mg (171 µmol, 1.1 eq) of [(tmeda)NiMe$_2$] were dissolved in 10 mL of benzene and 80 µL (1 mmol, 6.7 eq) and stirred for 60 min at room temperature. The dark red solution was filtered over a syringe filter and the benzene was sublimated off under vacuum. $^{Naph-H}$**4-pyr** was obtained as an orange/red powder (76 mg, 136 µmol, 91 %).

^{1}H-NMR (400 MHz, C_6D_6): δ (ppm) = 8.63 (t, $^4J_{HH}$=8.0 Hz, 2H, *o-H pyr*), 8.40 (s, 1H, *H-3*), 7.55 (d, $^3J_{HH}$=8.4 Hz, 1H, *H-4*), 7.42 (d, $^3J_{HH}$=7.9 Hz, 1H, *H-7*), 7.37 (d, $^4J_{HH}$=9.2 Hz, 1H, *H-8*), 7.31 (dd, $^3J_{HH}$=8.0 Hz, 2H, *H-1*), 7.07 (t, $^3J_{HH}$=7.9 Hz, 1H, *H-6*), 6.94 (d, $^3J_{HH}$=9.2 Hz, 1H, *H-9*), 6.66 (m, 1H, *H-5*), 6.60 (m, 1H, *p-H pyr*), 6.29 (t, $^3J_{HH}$=8.0 Hz, 1H, *H-2*), 6.25 (s, 2H, *m-H pyr*), -0.68 (s, 3H, *Ni-CH$_3$*).

[2-Hydroxy-*N*-(2,6-dibromo-4-methylphenyl)-1-naphthaldiminato-κ^2-*N,O*]methyl-pryidinenickel-(II) ($^{Sal-Me}$4-pyr)

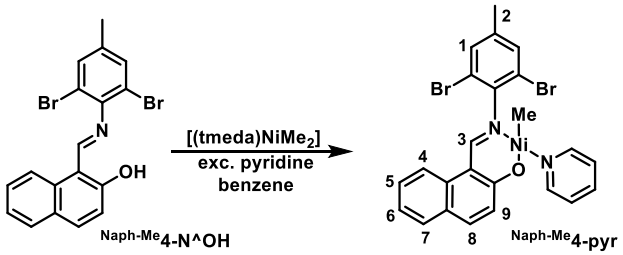

In a 25 mL Schlenk tube 63 mg (150 µmol, 1.0 eq) of $^{Naph-Me}$**4-N^OH** and 35 mg (170 µmol, 1.1 eq) of [(tmeda)NiMe$_2$] were dissolved in 10 mL of benzene and 80 µL (1 mmol, 6.7 eq) and stirred for 60 min at room temperature. The dark red solution was filtered over a syringe filter and the benzene was sublimated off under vacuum. $^{Naph-Me}$**4-pyr** was obtained as an orange/red powder (73 mg, 127 µmol, 85 %).

^{1}H-NMR (400 MHz, C_6D_6): δ (ppm) = 8.68 (d, $^3J_{HH}$=5.9 Hz, 2H, *o-H pyr*), 8.46 (s, 1H, *H-3*), 7.62 (d, $^3J_{HH}$=8.4 Hz, 1H, *H-4*), 7.44 (dd, $^3J_{HH}$=7.4 Hz, $^4J_{HH}$=1.4 Hz, 1H, *H-7*), 7.38 (d, $^3J_{HH}$=9.2 Hz, 1H, *H-8*), 7.20 (s, 2H, *H-1*), 7.18 – 7.14 (m, 1H, *H-5*), 7.08 (td, $^3J_{HH}$=7.4 Hz, $^4J_{HH}$=1.0 Hz, 1H, *H-6*), 6.96 (d, $^3J_{HH}$=9.2 Hz, 1H, *H-9*), 6.61 (t, $^3J_{HH}$=7.6 Hz, 1H, *p-H pyr*), 6.26 (t, $^3J_{HH}$=6.8 Hz, 2H, *m-H pyr*), 1.74 (s, 3H, *H-2*), -0.61 (s, 3H, *Ni-CH$_3$*).

Elemental Analysis (%) for $C_{24}H_{20}Br_2N_2NiO$: Found (Calculated): C 51.34 (50.49); H 3.71 (3.53); N 5.28 (4.91).

[2-Hydroxy-*N*-(2,6-dibromo-4-methyl-phenyl)-1-naphthaldiminato-κ^2-*N,O*]-methyl-pryidinenickel-(II) ($^{Naph-F}$4-pyr)

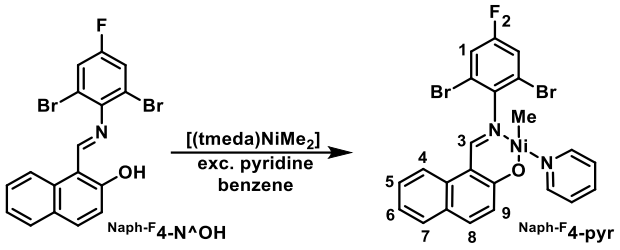

In a 25 mL Schlenk tube 65 mg (154 µmol, 1.0 eq) of $^{Naph-F}$**4-N^OH** and 38 mg (187 µmol, 1.2 eq) of [(tmeda)$NiMe_2$] were dissolved in 10 mL of benzene and 80 µL (1 mmol, 6.5 eq) and stirred for 60 min at room temperature. The dark red solution was filtered over a syringe filter and the benzene was sublimated off under vacuum. $^{Naph-F}$**4-pyr** was obtained as an orange/red powder (77 mg, 134 µmol, 87 %).

^{1}H-NMR (400 MHz, C_6D_6): δ (ppm) = 8.66 – 8.60 (m, 2H, *o-H pyr*), 8.31 (s, 1H, *H-3*), 7.61 (d, $^3J_{HH}$=8.4 Hz, 1H, *H-4*), 7.42 (dd, $^3J_{HH}$=7.8 Hz, $^4J_{HH}$=1.4 Hz, 1H, *H-7*), 7.37 (d, $^3J_{HH}$=9.3 Hz, 1H, *H-8*), 7.21 (ddd, $^3J_{HH}$=8.5, 7.0 Hz, $^4J_{HH}$=1.5 Hz, 1H, *H-5*), 7.08 (t, $^4J_{HH}$=7.4 Hz, 1H, *H-6*), 7.03 (d, $^3J_{HF}$=7.6 Hz, 2H, *H-1*), 6.93 (d, $^3J_{HH}$=9.2 Hz, 1H, *H-9*), 6.62 (td, $^3J_{HH}$=7.6 Hz, $^4J_{HH}$=3.3 Hz, 1H, *p-H pyr*), 6.32 – 6.22 (m, 2H, *m-H pyr*), -0.74 (s, 3H, *Ni-CH_3*).

5.4.4 Ethylene Oligomerization

The reactor (*Büchi Miniclave*) was heated to 60 °C and evacuated and refilled with argon repeatedly and 100 mL of toluene was added by cannula transfer. After heating to the desired temperature under stirring with 1000 rounds per minute (rpm) 20 µmol of catalyst in 2 mL of toluene was added and the reactor was pressurized with ethylene to 20 bar. Polymerization was conducted at constant pressure for 60 min. The reactor was vented and the reaction mixture obtained was washed several times with 3 M HCl. The organic layer was dried over $MgSO_4$ and the solvent was removed under vacuum to yield the product as a pale yellow oil.

5.4.5 Additional Spectra

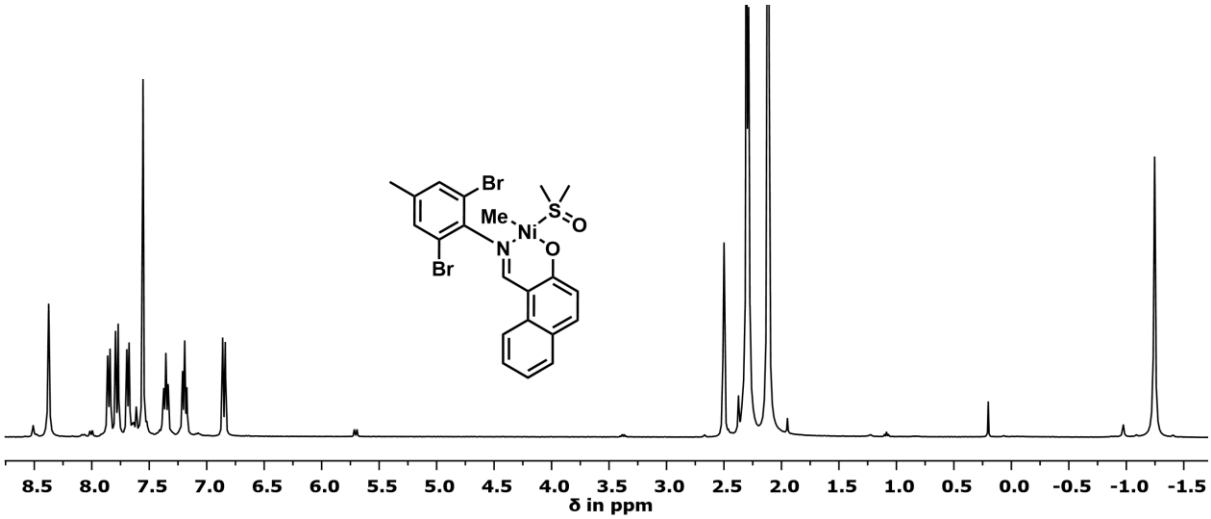

Figure 5.5: ^{1}H NMR spectrum (400 MHz, dmso-d6) of $^{\text{Naph-Me}}$**4-dmso**.

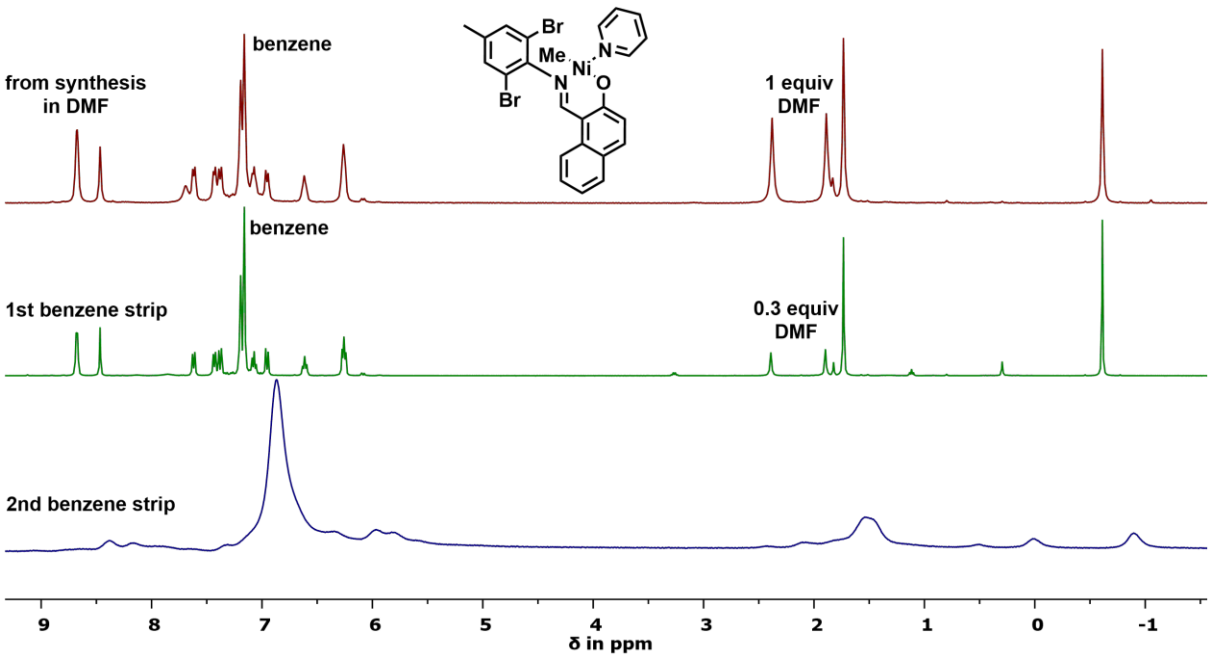

Figure 5.6: ^{1}H NMR spectra (400 MHz, C_6D_6, 298 K) of $^{\text{Naph-Me}}$**4-pyr** from synthesis in dmf (top), after one benzene strip (center), and after a second benzene strip (bottom).

6 Origin of the Remote Substituent Effect

6.1 Introduction

The remarkable influence of the remote substituents of Ni(II) salicylaldiminato complexes with a 3,5,3',5'-substituted *N*-terphenyl moiety on the polymerization has been further demonstrated in detail in this thesis. Although sterics influence the molecular weight and degrees of branching of the polymers formed to some extent (cf. Chapter 3.2, p. 20), these product properties are mainly governed by the electronic nature of the remote substituents. Systematic investigations with a variety of different substituents on the terphenyl amine were carried out by Martin Zuideveld and Amaia Bastero.[51,53] It was shown, that the molecular weight of the polymer produced by a given catalyst correlates with the Hammet constant of its substituents. Despite these systematic investigations, the origin of this remote substituent effect, especially how the electronic influence of the substituents is transferred to the active nickel center, remained elusive. Marks and coworkers suggested a fluorine effect (interaction of the fluorine substituents with the β-hydrogen of the growing polymer chain) that disfavors β-hydride elimination to be the origin of the high molecular weights and high activities obtained with ^{CF_3}**1-L** in contrast to ^{Me}**1-L**.[82] Similar fluorine interactions were discussed to be the origin for the living polymerization behavior of Fujita type early transition metal complexes with fluorinated enolatoimine ligands.[143,144] However, detailed NMR spectroscopic investigations showed that for the titanium complexes an interaction of the *ortho*-fluorine substituents with the active Ti center instead of the hydrogen of the growing polymer chain is the origin of the living nature of the polymerization.[145,146] Also, such fluorine interactions cannot explain the significant changes in polymer molecular weight depending on the electronic nature of different non-fluorinated catalysts observed for the nickel salicylaldiminato complexes. Furthermore, Anna Osichow recently showed that the NO_2-substituted electron poor analogue of ^{CF_3}**1-pyr** produces similar high molecular weight polymers with low degrees of branching (**Figure 6.1**). These findings show that the electronic character of the remote substituents is indeed decisive for the control of the microstructure rather than a weak fluorine interaction.[52]

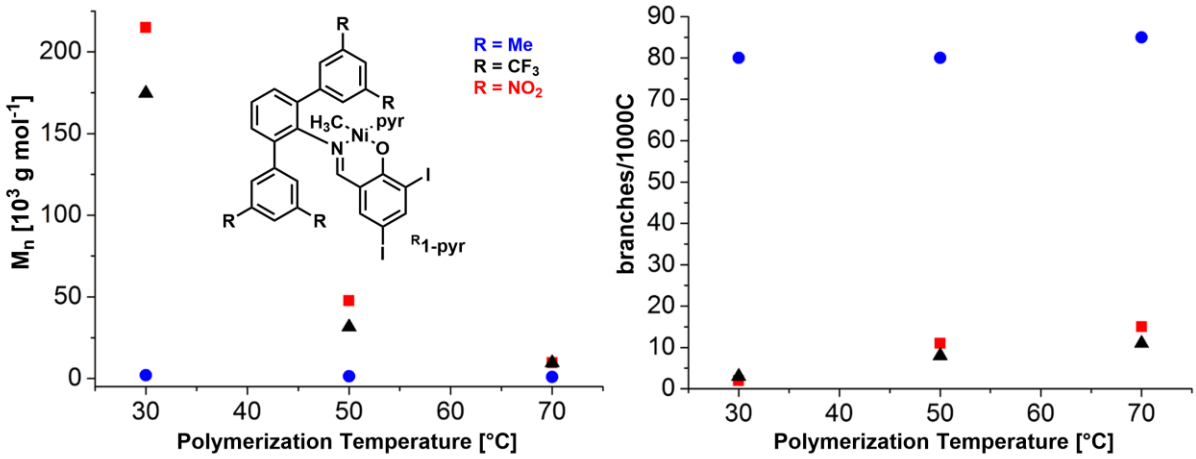

Figure 6.1: Polymer molecular weights (left) and degrees of branching (right) for complexes with different substituents (Me, CF_3, and NO_2) at various polymerization temperatures (at 40 bar of ethylene pressure. Figure adopted from ref. 52.

Phenomenologically, electron rich substituents in the 3,5-positions of the *N*-terphenyl moiety make the nickel center more prone for β-hydride elimination. This increases chain walking and chain transfer reactions explaining the lower molecular weight oligomers with high degrees of branching produced by these complexes. However, the underlying mechanism how the electronic character of the substituents translates to the nickel center remains uncertain. One possibility is a transfer of electron density via increasing the overall electron density of the conjugated system of the salicylaldiminato ligand. A second scenario comprises additional discrete interactions of the salicylaldiminato ligand with the nickel center, e.g. by direct π-interaction between the ligand aryl moieties and the metal center. Indications for such additional ligand-nickel interactions can be deduced from X-Ray diffraction analyses of *N*-terphenyl salicylaldiminato nickel complexes: in the solid state structures, one of the terminal aryl rings of the terphenyl moiety occupies space close to the axial position of the nickel center with typical nickel-aryl distances in the range of 3.05 to 3.47 Å (**Figure 6.2**, left and center).[50,51] These short nickel aryl distances allow for a potential π-interaction. The remote aryl moiety is tilted towards the nickel center in all solid state structure with the *ortho*-carbon atom having the shortest distance to the nickel. Thus, only one C=C double bond is in close proximity to the nickel center and the proposed interaction is most likely a weak η^2-π-coordination of the ligand aryl group to the nickel center. Changing the electron density of the aryl rings with different substituents might result in a stronger or weaker interaction and thereby – by a mechanism to be discussed – influence the ratio of chain propagation to chain walking and transfer, explaining the completely different materials obtained with ^{CF_3}**1-pyr** and ^{Me}**1-pyr**.

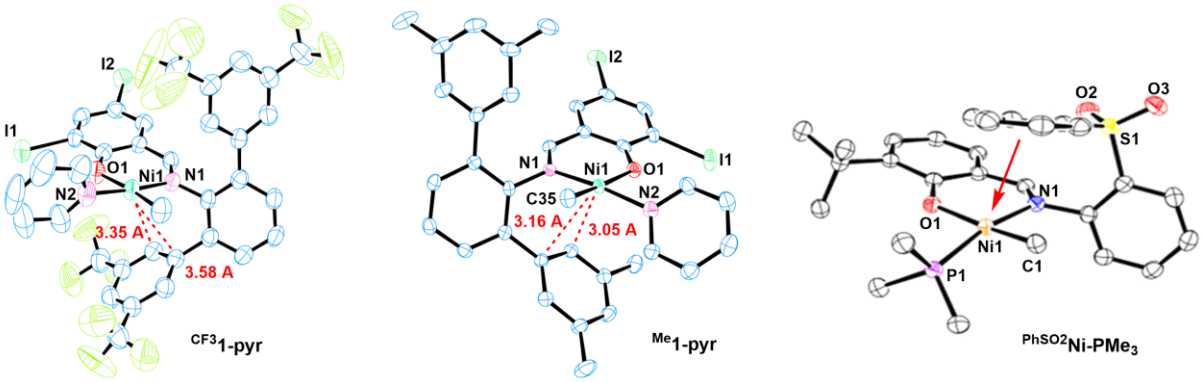

Figure 6.2: Comparison of X-ray crystal structures (50 % probability ellipsoids, H atoms omitted for clarity) of ^{CF_3}**1-pyr**, ^{Me}**1-pyr**, and ^{PhSO_2}**Ni-PMe$_3$** (taken from ref. [147]) with aryl groups in the axial position of the nickel center.

Recently, Marks *et al.* reported a nickel salicylaldiminato complex with a potentially coordinating sulfonyl moiety bound to the N-aryl of the salicylaldiminato ligand (**Figure 6.2** and **Figure 6.3**)[147] Compared to a catalyst with a –CH_2- group, the sulfonyl complex exhibits an activity that is 18 times higher. Additionally, it produces higher molecular weight polyethylene with 1.5 times more branches and is thermally more stable. By the authors this was attributed to a hemilabile coordination of the ligand sulfonyl group to the nickel center.

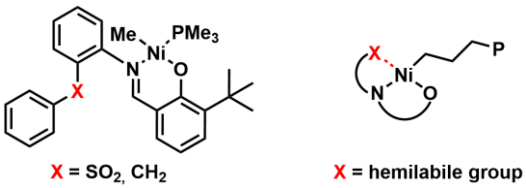

Figure 6.3: Stabilization of three coordinate intermediates by the hemilabile coordination of a sulfonyl moiety of the salicylaldiminato ligand.

The concept of such a hemilabile coordination of ligands to the metal center is well known.[148-151] Multifunctional ligands including one weakly coordinating moiety were found to provide a coordination site for other incoming ligands and at the same time allow for stabilization of reactive intermediates by reversible coordination. DFT calculations carried out by Marks and coworkers indicate that the better thermal stability of ^{PhSO_2}**Ni-PMe$_3$** also arises from the ability of the weakly coordinating, hemilabile sulfonyl group to stabilize three coordinate intermediates in the catalytic cycle. Marks *et al.* suggest that this suppresses chain transfer reactions and favors chain propagation and branch formation but unfortunately the authors did not support their hypothesis with additional calculations. Furthermore, also a short aryl-nickel contact (partial aryl-π interaction with the nickel center) is present in the solid state structure recently published by Marks and coworkers (**Figure 6.2**, right) and might also

constitute a weak interaction to the nickel center similar to that proposed for *N*-terphenyl salicylaldiminato nickel complexes.

Considering the effect of the sulfonyl group on catalytic behavior, it also has to be taken into account that replacement of the $-CH_2-$ group by $-SO_2-$ significantly alters the electronic nature of the ligand.

6.2 Results and Discussion

Despite extensive research dedicated to nickel salicylaldiminato complexes, the origin of the remote substituent effect remains elusive. A potential weak bonding interaction as the origin of the remarkable effect of remote substituents was investigated in this chapter. Especially the proposed concept of a weak π-interaction of the ligand with the nickel center was studied. For this purpose, a series of Ni(II) salicylaldiminato complexes with new aryl substituents on the aniline, including asymmetric terphenyl amines, and complexes with potential weakly coordinating moieties were synthesized.

6.2.1 Catalysts with Coordinating Motifs on the Salicylaldiminato Ligand

To investigate the concept of stabilizing the catalyst by weakly coordinating motifs in the ligand backbone, the synthesis of the complexes illustrated in **Figure 6.4** was targeted. In all complexes potential coordinating aryl motifs are introduced by substitution of the aniline with heterocycles. Furan and thiophene are promising because the heteroatom should be directed towards the metal center in the final complex facilitating a potential interaction. The 2-methylfuran substituted analogue was targeted in order to introduce additional steric bulk in the ligand. Finally, the synthesis of two pyridine derivatives was intended. **^{Pyr}5-pyr** exhibits nitrogen atoms directed towards the nickel center, while an interaction involving the lutidine N-atom is not likely in **^{Lut}5-pyr**. Furthermore, the latter complex is very similar to the structure of **^{Me}1-pyr** but also exhibits heterocyclic substituents on the aniline moiety.

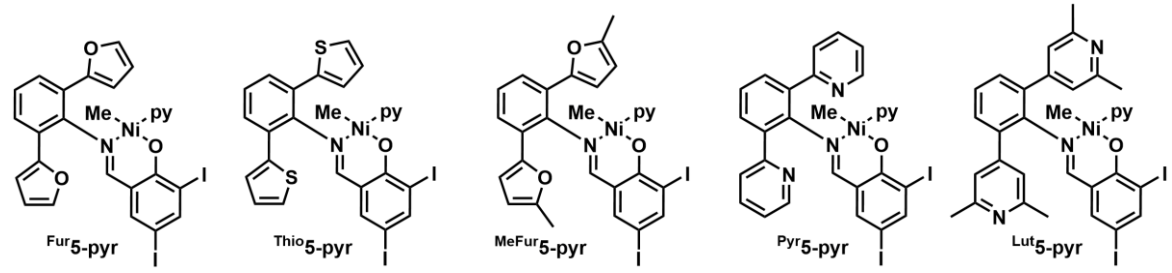

Figure 6.4: Targeted complexes with additional potentially coordinating motifs in the salicylaldiminato ligand.

Complex Synthesis

The synthesis of five new heteroatom containing Ni(II) salicylaldiminato complexes was accomplished following known procedures already presented in Chapter 3. Full synthetic procedures and characterization of all complexes and intermediates are discussed in detail in Chapter 6.4 Experimental Section. Starting from 2,6-dibromoaniline and the corresponding aryl boronic acid or boronic acid ester, 2,6-aryl substituted anilines were obtained by Suzuki coupling reactions. While furan boronic acid is commercially available and pyridine-2-boronic acid was available in the group, all other boronic acid ester starting materials were synthesized by iridium catalyzed borylation of thiophene, 2-methylfuran, or lutidine, respectively.[152] All Suzuki coupling reactions involving heteroareneboronic acid esters turned out to be tedious due to deactivation of the bromine component after the first coupling step. The desired symmetrical, disubstituted products could only be isolated in low yields and the 2-bromo-6-areneanilines were the main products of the reaction. In the case of 2-methylfuran, the mono-coupling product was formed exclusively, while no coupling was observed when using pyridine-2-boronic acid. The mono-coupling product ^{BrMeFur}**5-NH$_2$** was still useful for ligand and complex synthesis in order to target the unsymmetrical complex ^{BrMeFur}**5-pyr**.

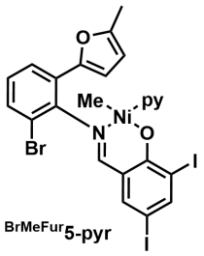

Figure 6.5: Complex ^{BrMeFur}**5-pyr** obtained instead of ^{MeFur}**5-pyr** due to an incomplete Suzuki coupling reaction (cf. Complex Synthesis).

Salicylaldiminato ligands ^{X}**5-N^OH** were obtained in good yields by condensation of the anilines with 3,5-diiodosalicylaldehyde. Also complex synthesis with [(tmeda)NiMe$_2$] as the nickel precursor gave the desired complexes in good yields following known procedures.[50,85] Reaction of ^{Lut}**5-N^OH** with the nickel precursor resulted in formation of a nickel methyl complex as evidenced by the presence of corresponding signals of the methyl group at -1.0 to -1.5 ppm in the ^{1}H NMR spectrum. However, the signals are broad and the presence of several sets of signals indicates the formation of a number of different species. This was attributed to the formation of multinuclear species via intermolecular coordination of the lutidine moieties of the ligand to the nickel center, replacing pyridine. Additionally, methyl pyridine ligated complex ^{PhSO_2}**Ni-pyr** was synthesized to enable a back-to-back comparison of

the catalytic behavior with the phenyl triphenylphosphine ligated analogue ^{PhSO_2}**Ni-PMe$_3$** reported by Marks *et al*. Synthesis of the salicylaldimine was carried out according to the procedure already reported.[147] Complexation with [(tmeda)NiMe$_2$] in the presence of excess pyridine yielded the desired methyl pyridine Ni(II) salicylaldiminato complex ^{PhSO_2}**Ni-pyr**.

Ethylene Oligomerization and Microstructure Analysis

The three complexes ^{Fur}**5-pyr**, ^{Thio}**5-pyr**, and ^{BrMeFur}**5-pyr** were subjected to ethylene polymerization as single component catalysts. Remarkably, all complexes exhibit high activities and produce low molecular weight polyethylene. The resulting molecular weight and degrees of branching are listed in **Table 6.1**.

Table 6.1: Polymerization results with complexes bearing potential coordinating motifs in the ligand backbone.

entry	catalyst	T [°C]	yield [g]	TOF[a]	M_n (NMR) [g mol^{-1}][b]	M_n (GPC) [g mol^{-1}][c]	M_w/M_n (GPC)[c]	branches /1,000 C[d]
1	^{Fur}**5-pyr**	40	9.9	17,700	4,800	5,900	1.9	109
2	^{Fur}**5-pyr**	60	6.2	11,100	2,600	5,100	2.0	115
3	^{Fur}**5-pyr**	80	1.8	3,200	1,200	1,800	2.5	112
4	^{Thio}**5-pyr**	40	2.2	3,900	4,100	8,600	1.7	127
5	^{Thio}**5-pyr**	60	0.3	550	2,200	3,500	1.7	123
6	^{BrMeFur}**5-pyr**	40	3.7	6,600	2,900	6,200	1.7	111
7	^{PhSO_2}**Ni-pyr**	40	2.1	3,800	1,500	2,200	1.9	124
8[e]	^{PhSO_2}**Ni-PMe$_3$**	40	2.8	10,000	1,600	2,800	1.9	145[f]

reaction conditions: 20 µmol of catalyst in 100 mL of toluene for 1 h at 20 bar of ethylene. [a] TOF x mol [C_2H_4] x mol^{-1} [Ni] h^{-1}. [b] molecular weights calculated from ^{1}H NMR intensity ratio of unsaturated end groups vs. overall integral. [c] in THF vs. polystyrene standards. [d] degree of branching calculated from ^{1}H NMR intensity ratio of methyl groups (corrected for saturated end groups) vs. overall integral. [e] data from ref. [147]: 10 µmol of catalyst, [Ni(cod)$_2$] as cocatalyst at 8 bar for 40 min. [f] not corrected for endgroups

It is striking, that all three complexes produce polymers with extremely high degrees of branching which exceed those of any terphenyl amine based catalyst by far. At 40 °C and 20 bar of ethylene, ^{Fur}**5-pyr** yields polyethylene with 109 branches per 1,000 carbon atoms and M_n = 4,800 g mol^{-1}. In detail, the high amount of branches goes along with a rather high molecular weight of the product. In general, high degrees of branching go along with low molecular weights and the ratio of both values was always found to vary only within a certain range. This was found to hold true independent of the catalyst used (Chapters 3 and 5). For a molecular weight of 5,000 g mol^{-1}, a degree of branching of about 50-60 branches per 1,000 carbon atoms would be expected for the 3',5',3'',5''-substituted terphenyl. Alongside the high

amount of branches introduced in the polymer by ^{Fur}**5-pyr**, this catalyst also exhibits a remarkably high activity which rivals that of the terphenyl based complexes. At 60 and 80 °C, the molecular weight of the products decrease to 2,600 and 1,200 g mol^{-1}, respectively. At the same time, the degree of branching cannot be pushed any further and stays more or less constant with 115 and 112 branches per 1,000 carbon atoms. Remarkably, ^{Fur}**5-pyr** exhibits a high activity with 17,700 turnovers per Ni center at 40 °C (average activity over an one hour experiment). Usually, catalysts with a distinct tendency for β-hydride elimination are less stable and active compared to their analogues which afford linear polyethylene. ^{Fur}**5-pyr** clearly does not follow this trend with its high activity in combination with the unusually high degrees of branching. Substituting the oxygen atom of the furan for sulfur atoms in ^{Thio}**5-pyr** results in the formation of a polymer with an even higher degree of branching (127 per 1,000 C) and a similar molecular weight of M_n = 4,100 g mol^{-1}. At the same time, the activity of ^{Thio}**5-pyr** is considerably lower than that of ^{Fur}**5-pyr** and the terphenyl amine based complexes. At 60 °C, the molecular weight of the polymer decreases to 3,500 g mol^{-1} and the activity drops to only 550 turnovers per hour. As observed for the furan substituted catalyst ^{Fur}**5-pyr**, the degree of branching cannot be increased further at higher temperatures and stays constant within the error of determination.

At 40 °C, the unsymmetrical complex ^{BrMeFur}**5-pyr** produces a similar polymer compared to that obtained with ^{Fur}**5-pyr** under the same conditions. The molecular weight of M_n = 2,900 g mol^{-1} is slightly lower while the amount of branches is the same (111 branches per 1,000 C). However, ^{BrMeFur}**5-pyr** is also significantly less active which can be attributed to the fast deactivation within the course of the reaction as observed by mass flow data. This could be explained by a less effective stabilization because it only contains one potentially coordinating moiety. More likely, this can be accounted for by the presence of an aryl-bromine group which can give access to new deactivation pathways. A significantly reduced stability of complexes with bromine substituents in this position was already observed in Chapter 5.2.2. For comparison, an additional polymerization experiment was carried out using complex ^{PhSO_2}**Ni-pyr** – the methyl pyridine analogue of the phenyl triphenylphosphine complex ^{PhSO_2}**Ni-PMe$_3$** reported by Marks and coworkers (entries 6.1-7 and 6.1-8).[147] Both ^{PhSO_2}**Ni-pyr** and ^{PhSO_2}**Ni-PMe$_3$** yield identical oligomers in terms of molecular weight and degree of branching. Note that the degree of branching from literature only appears to be higher because it is not corrected for end groups (cf. Chapter 3.2.1).

To further examine the catalytic behavior of these new complexes, the microstructure analysis with the amount of different branch lengths by ^{13}C NMR spectroscopy is illustrative. From the results listed in **Table 6.2** it becomes evident that the chain architecture of the polymers produced with complexes ^{Fur}**5-pyr**, ^{Thio}**5-pyr**, and ^{BrMeFur}**5-pyr** containing coordinating

motifs in the ligand backbone differs significantly from those of other oligomers synthesized with terphenyl amine based Ni(II) salicylaldiminato complexes. All oligomers obtained at 40 °C comprise unexpectedly high amounts of methyl branches (up to 88 % for ^{Fur}**5-pyr**). However, also small amounts of longer branches (ethyl, propyl, butyl,) and hyperbranched structures (*sec*-butyl) are present. By comparison, ^{PhSO_2}**Ni-pyr** and ^{PhSO_2}**Ni-PMe$_3$** afford highly branched oligomers that comprise high amounts of longer chain branches (C_{4+}) and branch on branch structures (*sec*-butyl branches), like found for ^{Me}**1-pyr** (**Table 3.4**, p 34).

Table 6.2: Fractional amounts of different branch lengths of polymers obtained with complexes containing coordinating motifs.

entry	catalyst	T [°C]	branches /1,000 C	methyl[a] [%]	ethyl[a] [%]	propyl[a] [%]	C_{4+}[a] [%]	*sec*-butyl[a] [%]
1	^{Fur}**5-pyr**	40	109	88	6	3	2	2
2	^{Fur}**5-pyr**	60	115	83	8	3	2	4
3	^{Fur}**5-pyr**	80	112	75	10	4	3	8
4	^{Thio}**5-pyr**	40	127	79	7	5	4	5
5	^{Thio}**5-pyr**	60	123	73	10	3	6	8
6	^{BrMeFur}**5-pyr**	40	111	80	8	3	3	5
7	^{PhSO_2}**Ni-pyr**	40	124	65	9	2	7	17
8[b]	^{PhSO_2}**Ni-PMe$_3$**	40	145[c]	44	9	2		23[d]

[a] percentage of different branch lengths can be calculated from relative intensity ratios of the corresponding signals ($1B_1$, $1B_2$, $1B_3$, $*B_{4+}$, B) of the respective branch in the ^{13}C NMR spectrum. [b] data from ref. [147]. [c] not corrected for endgroups [d] overall butyl branches: *n*-butyl + *sec*-butyl

Apart from this, the distribution of different branch lengths follows the expected trends and the amount of methyl branches decreases at higher temperatures in favor of longer chain branches and hyperbranched structures.

In summary, the introduction of potentially weakly coordinating electron rich motifs in the salicylaldiminato ligand results in unexpected catalytic behavior of the corresponding nickel salicylaldiminato complexes. Not only are these catalysts capable of producing oligoethylenes with surprisingly high degrees of branching indicating a high propensity for β-hydride elimination and chain walking, they still incorporate mostly methyl branches and hardly any longer chain branches. Although the underlying mechanism for this unexpected behavior of ^{Fur}**5-pyr** and ^{Thio}**5-pyr** remains an open issue, these new complexes produce polyethylene with an unprecedented microstructure in terms of branching and molecular weight combination.

Polymerizations carried out with ^{Lut}**5-pyr** showed that the suggested formation of multinuclear species renders this complex almost completely inactive as single-component catalyst. The activity could be increased with the addition of $B(C_6F_5)_3$ for sequestration of the

potentially coordinated lutidine moieties of the ligand. The polymerization results with different amounts of borane are listed in **Table 6.3**.

Table 6.3: Polymerization results with complex ^{Lut}**5-pyr**.

entry	catalyst	$B(C_6F_5)_3$ [equiv]	yield [g]	TOF[a]	M_n (NMR) [g mol^{-1}][b]	M_n (GPC) [g mol^{-1}][c]	M_w/M_n (GPC)[c]	branches /1,000 C[d]
1	^{Lut}**5-pyr**	-	0.4	700	2,800	1,600	2.0	65
2	^{Lut}**5-pyr**	0.5	1.1	2,000	2,400	1,600	2.1	60
3	^{Lut}**5-pyr**	1	1.5	2,700	3,700	2,000	2.2	56
4	^{Lut}**5-pyr**	2	1.4	2,500	11,300	6,200	2.3	35

reaction conditions: 20 µmol of catalyst in 100 mL of toluene for 1 h at 20 bar of ethylene at 60 °C. [a] TOF x mol $[C_2H_4]$ x mol^{-1} [Ni] h^{-1}. [b] molecular weights calculated from ^{1}H NMR intensity ratio of unsaturated end groups vs. overall integral. [c] in trichlorobenzene (160 °C) vs. polyethylene standards with linear calibration. [d] degree of branching calculated from ^{1}H NMR intensity ratio of methyl groups (corrected for saturated end groups) vs. overall integral.

Addition of $B(C_6F_5)_3$ significantly increases the catalytic activity but it still remains limited with a maximum of 2,700 turnovers h^{-1}. Abstraction of the labile ligand pyridine and the lutidine of the ligand backbone also strongly affects the microstructure of the resulting product. With increasing amounts of borane, higher molecular weight polyethylene is obtained. Additionally, the degree of branching decreases from 65 to 35 branches per 1,000 carbon atoms without and with 2 equiv of $B(C_6F_5)_3$, respectively. Analysis of the branching pattern of the polymers with ^{13}C NMR spectroscopy revealed that all products only contain methyl branches and no longer chain alkyl or *sec*-butyl branches.

6.2.2 Catalysts with New Aryl Substitution Patterns

To further elucidate the hypothesis of a weak π-interaction of the terphenyl moiety with the catalytically active nickel center, complexes with new aryl substitution patterns were synthesized (**Figure 6.6**). New aryl groups were targeted with the introduction of naphthyl substituents instead of the known 3,5-substituted phenyl groups. Additionally, the introduction of cyclopentadienyl rings with the ability for a stronger interaction was targeted with ferrocenyl substituents on the aniline. A special interest was dedicated to 3,5-substituted terphenyl amine based complexes with a mixed substitution pattern $^{Me/CF_3}$**1-pyr** and $^{(MeCF_3)}$**1-pyr**.

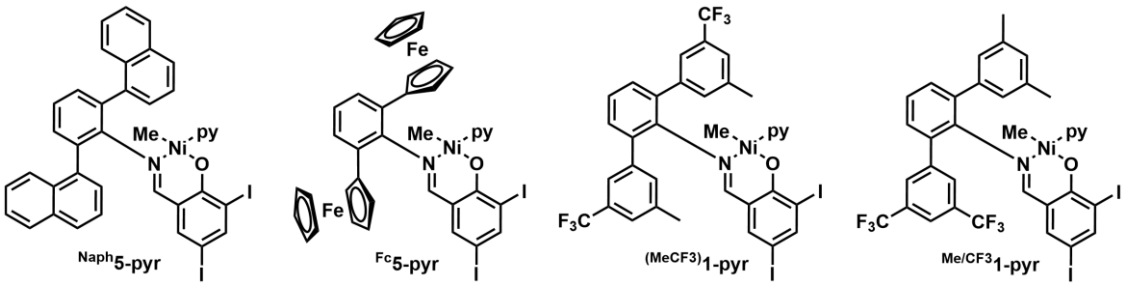

Figure 6.6: Targeted Ni(II) salicylaldiminato complexes with new aryl substitution patterns.

Assuming a π-interaction is involved, $^{Me/CF_3}$**1-pyr** exhibits two different aryl moieties for such an interaction and should therefore produce a different polymer compared to the mixed, symmetrical complex $^{(MeCF_3)}$**1-pyr** with methyl and CF_3 groups on both phenyl rings. Depending on the mechanism involved, as an extreme scenario, this could even result in the formation of reactor blends of linear polyethylene and branched oligoethylenes depending on which phenyl group temporarily interacts with the nickel center (**Scheme 6.1**).

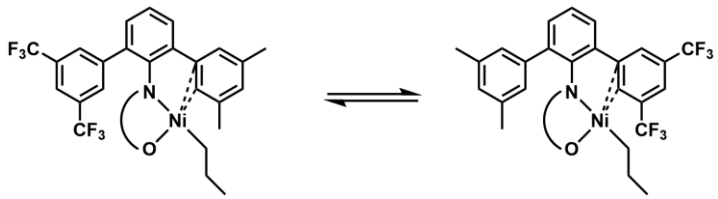

Scheme 6.1: Potential exchange between weak interaction of the nickel center with the methyl or the trifluoromethyl substituted aryl moiety, respectively.

Complex Synthesis

All four complexes are accessible following known procedures for similar Ni(II) salicylaldiminato complexes. Detailed synthetic procedures and characterization of all products and intermediates are provided in Chapter 6.4 Experimental Section. Commonly, 3,5-substituted anilines were synthesized by Suzuki coupling reaction of 2,6-dibromoaniline with the corresponding arylboronic acid ester or ferrocenylboronic acid, respectively (**Scheme 6.2**).

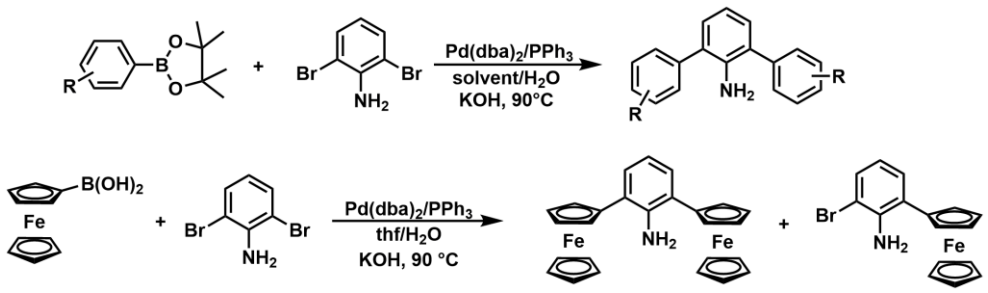

Scheme 6.2: Aniline Synthesis via Pd-catalyzed Suzuki coupling. For Suzuki coupling with ferrocenylboronic acid, the monosubstituted aniline is the main product.

3,5-Substituted phenylboronic acid esters which are not commercially available were synthesized by an iridium catalyzed borylation via C-H activation reported by Hartwig and coworkers (**Scheme 6.3**).[152-155]

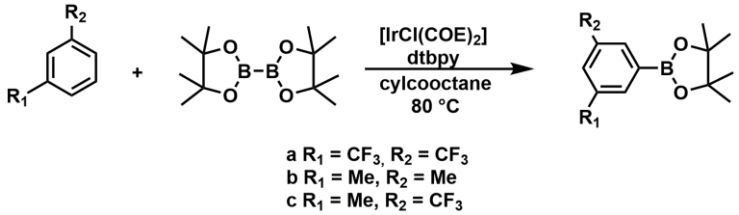

Scheme 6.3: Synthesis of 3,5-substituted phenylboronic acid esters by iridium catalyzed borylation.

The terphenyl amine ^{Fc}**5-NH$_2$** was isolated with a very low yield of 10 %. Due to a deactivation of the bromine component after the first coupling step the monosubstituted 2-bromo-6-ferrocenylaniline is the main product of this Suzuki coupling reaction (**Scheme 6.2**, bottom). For the synthesis of $^{Me/CF3}$**1-NH$_2$**, 2,6-dibromoaniline was reacted with equimolar amounts of 3,5-dimethyl- and 3,5-di(trifluoromethyl)phenylboronic acid pinacol ester. The unsymmetrically substituted product could be isolated from the reaction mixture, which also contained the two symmetric terphenyl amines, by column chromatography in 38 % yield.

The salicylaldiminato ligands were obtained by condensation of the anilines with 3,5-diiodosalicylaldehyde in good yields. An acid base reaction of the corresponding ligand with [(tmeda)NiMe$_2$] as a nickel precursor in the presence of excess pyridine gave the desired nickel methyl pyridine complexes in high purities. For ^{Naph}**5-pyr**, two isomers with Ni-Me resonances arising at -0.75 and -0.93 ppm were formed according to ^{1}H NMR spectroscopy in a ratio of 1 : 1.6. The two signals probably correspond to different rotamers due to hindered rotation of the naphthyl groups.

Ethylene Oligomerization and Microstructure Analysis

The four new Ni(II) salicylaldiminato complexes with alternative aryl substitution patterns were studied in ethylene oligomerization. The products were analyzed with regard to their molecular weight and degree of branching by ^{1}H NMR spectroscopy (vide supra) and GPC. The results are listed in **Table 6.4**. For comparison, results of similar polymerization runs with the exclusively methyl and CF_3-substituted complexes ^{Me}**1-pyr** and ^{CF3}**1-pyr**, respectively, are also listed (entries 6.1-1 and 6.1-2). Under the reaction conditions of 40 °C at an ethylene pressure of 20 bar, ^{Me}**1-pyr** yields a highly branched (77 branches per 1,000 C) oligomer with 1,600 g mol^{-1}.

Table 6.4: Polymerization results with ^{X}**5-pyr** at 40 °C and 20 bar of ethylene.

entry	catalyst	yield [g]	TOF[a]	M_n (NMR) [g mol^{-1}][b]	M_n (GPC) [g mol^{-1}][c]	M_w/M_n (GPC)[c]	branches /1,000 C[d]	T_m [°C]
1	^{Me}**1-pyr**	10.9	19,500	1,600	3,500[f]	1,7	77	-
2[e]	^{CF_3}**1-pyr**	23.4	41,800	-	19,000	5.1	10	123
3	^{Fc}**5-pyr**	2.1	3,800	56,900	32,400	2.8	11	126
4	^{Naph}**5-pyr**	2.7	4,800	2,000	1,600	1.6	59	-
5	$^{Me/CF_3}$**1-pyr**	6.1	10,900	4,700	5,100	1.9	39	100[g]
6	$^{(MeCF_3)}$**1-pyr**	7.7	13,800	5,500	13,100	1.6	35	99[g]

reaction conditions: 20 µmol of catalyst in 100 mL of toluene for 1 h at 40 °C and 20 bar of ethylene. [a] TOF mol [C_2H_4] mol^{-1} [Ni] h^{-1}. [b] molecular weights calculated from ^{1}H NMR intensity ratio of unsaturated end groups vs. overall integral. [c] in trichlorobenzene at 160 °C vs. polyethylene standards with linear calibration. [d] degree of branching calculated from ^{1}H NMR intensity ratio of methyl groups (corrected for saturated end groups) vs. overall integral. [e] 40 µmol of catalyst for 30 min at 40 bar and 40 °C from ref. 53. [f] in THF vs. polystyrene standards. [g] broad melting endotherms.

As expected, much higher molecular weight polyethylene with 19,000 g mol^{-1} with only 10 branches per 1,000 carbon atoms is obtained with ^{CF_3}**1-pyr** at slightly different conditions (result adopted from ref. 53)**.** This product is a semicrystalline solid with a melting temperature of 123 °C while the highly branched oligoethylene from ^{Me}**1-pyr** is a completely amorphous, highly viscous liquid.

Despite the anticipated rather electron donating nature of the ferrocenyl group, the bis-ferrocenyl substituted complex ^{Fc}**5-pyr** yields very high molecular weight polyethylene with 56,900 g mol^{-1} with few branches (11 per 1,000 C). Overall, the polymer properties, including a melting point of T_m = 126 °C, are very similar to those of the polymer produced by ^{CF_3}**1-pyr**. This can probably be attributed to the high steric demand of the ligand rather than its electronic properties, though such an assumed steric influence would be much more pronounced than expected. In contrast to ^{Fc}**5-pyr**, the naphthyl-substituted complex ^{Naph}**5-pyr** yields highly viscous liquid product with a low molecular weight of 2,000 g mol^{-1}. Due to the high degree of branching with 59 branches per 1,000 carbon atoms, it is completely amorphous.

Both mixed complexes with methyl and trifluoromethyl substituents yield similar products regarding molecular weights and degrees of branching. $^{Me/CF_3}$**1-pyr** and $^{(MeCF_3)}$**1-pyr** produce polyethylene with moderate degrees of branching of 39 and 35 branches per 1,000 carbon atoms and molecular weights of 4,700 and 5,500 g mol^{-1}, respectively. Both polymers are semi-crystalline solids and have melting transitions at about T_m = 100 °C. However, aside from this relatively narrow melting transition, the melting endotherms are very broad over a temperature range between 30 and 100 °C (cf. DSC traces in Experimental Section, **Figure 6.12** and **Figure 6.13**). Neither of the catalysts shows unexpected behavior and both instead yield products with properties (M_n, T_m, degree of branching) which are intermediate to the two completely methyl

or trifluoromethyl, respectively, substituted complexes ^{Me}**1-pyr** and ^{CF_3}**1-pyr**. Hence, these observations are not further conclusive concerning the nature of interactions between the N-terphenyl moiety and the metal center. Also, molecular weight distributions of $M_w/M_n \approx 2$ indicate a well-behaved single-site polymerization behavior and neither GPC nor DSC results suggest the presence of e.g. block-copolymers or a blend of homopolymers.

The results of the microstructure analysis via ^{13}C NMR spectroscopy are listed in **Table 6.5**. In agreement with the high molecular weight and low overall degree of branching of the polymer produced with ^{Fc}**5-pyr**, it only contains short methyl branches. For the oligomer obtained with the naphthyl substituted complex ^{Naph}**5-pyr** the distribution of different branch lengths also follows the expectations for a product with an intermediate molecular weight and degree of branching. It mainly contains methyl branches but also exhibits significant amounts of longer alkyl branches (C_{4+}) and branch on branch motifs (*sec*-butyl).

Table 6.5: Fractional amount of different branch lengths of polymers obtained with complexes containing new aryl substitution patterns.

entry	catalyst	branches /1,000 C	methyl[a] [%]	ethyl[a] [%]	propyl[a] [%]	C_{4+}[a] [%]	*sec*-butyl[a] [%]
1	^{Me}**1-pyr**	77	71	8	3	12	6
2	^{CF_3}**1-pyr**	11	100	-	-	-	-
3	^{Fc}**5-pyr**	11	100	-	-	-	-
4	^{Naph}**5-pyr**	59	83	4	2	8	3
5	$^{Me/CF_3}$**5-pyr**	39	88	5	2	5	-
6	$^{(MeCF_3)}$**5-pyr**	35	91	3	2	4	-

[a] percentage of different branch lengths can be calculated from relative intensity ratios of the corresponding signals ($1B_1$, $1B_2$, $1B_3$, $^*B_{4+}$, B) of the respective branch in the ^{13}C NMR spectrum.

The two complexes $^{Me/CF_3}$**5-pyr** and $^{(MeCF_3)}$**5-pyr** with mixed substituents also produce similar products in terms of their detailed microstructure and distribution of different branch lengths. Neither one of the catalysts produces substantial amounts of hyperbranched structures as indicated by the absence of *sec*-butyl groups. Longer alkyl branches are produced to a small extent (4 – 5 %) but methyl branches represent the majority of all the polymers branches (88 and 91 %, respectively). Finally, the products and their respective microstructure match the expectation of a polymer produced by a catalyst with an intermediate behavior between the fully methyl and fully CF_3-substituted complexes. However, an averaged influence of the 3,5-dimethylphenyl and the 3,5-bis(trifluoromethyl) group in $^{Me/CF_3}$**5-pyr** could also be caused by a reversible exchange of interaction between the two aryl moieties which is fast on the time scale of the polymerization.

In summary, except for the surprisingly high molecular weight and linear polyethylene produced by ^{Fc}**5-pyr**, the four complexes with new aryl substitution patterns did not show any distinct behavior which would allow for further conclusions.

6.2.3 Cyclic Voltammetry

To further illuminate the electronic properties of the nickel center in this type of polymerization catalysts, cyclic voltammetry measurements were conducted. The focus was put on the investigation of the electron density of the nickel depending on the substitution pattern of the corresponding ligand.

Figure 6.7 depicts the complexes which were selected for the investigation of their electronic properties. ^{CF_3}**1-pyr** and ^{Me}**1-pyr** were selected as extreme cases with very electron withdrawing and electron donating substituents, respectively. The two mixed complexes $^{(MeCF_3)}$**1-pyr** and $^{Me/CF_3}$**1-pyr** contain both electron donating as well as electron withdrawing substituents but differ in their constitution. In addition to these four terphenyl amine based complexes, also the two catalyst precursors ^{Fur}**5-pyr** and ^{Thio}**5-pyr** were investigated since they gave remarkable results in ethylene oligomerization experiments.

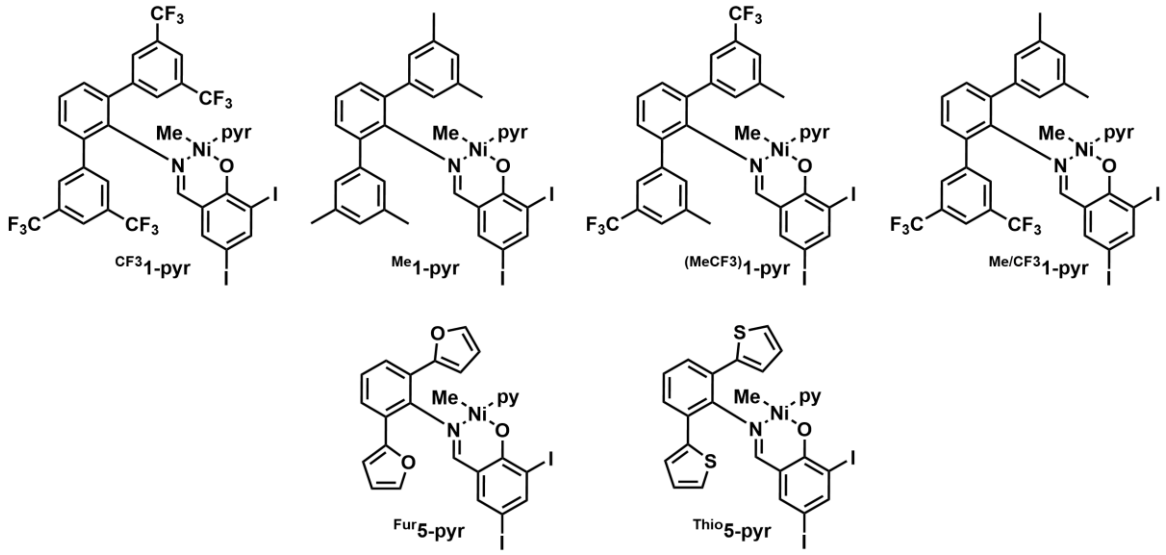

Figure 6.7: Complexes used for cyclic voltammetry measurements.

All complexes showed one oxidation process during cyclic voltammetry measurements in the potential range expected for a four coordinate square planar Ni(II)/Ni(III) pair. Measurements were carried out using different scan rates from 25 to 2,000 mV s^{-1} and the half-wave potential was found to be independent of the scan rate. The oxidation of all complexes is only partially reversible which is attributed to a relatively fast decomposition of the Ni(III)-species. Cyclic voltammograms of the corresponding ligands did not show any redox

transitions at the potentials observed for the complex. Therefore, the oxidation and reduction processes during cyclic voltammetry measurements are assumed to be metal centered. EPR measurements conducted with the chemically oxidized ^{Me}**1-pyr** (*in situ* oxidation with [1,1'-diacetylferrocenium]SbF_6) did not provide further information concerning the exact location of the electron within the complex structure since no EPR signal could be detected. Representative referenced cyclic voltammograms of all complexes are provided in the experimental section of this chapter.

In **Table 6.6** the half-wave potentials of the six different complexes determined from the cyclic voltammograms are listed. Complex ^{Me}**1-pyr** bearing electron donating substituents was found to be oxidized most easily as evidenced by the lowest (most negative) $E_{1/2}$ value. Electron withdrawing substituents hinder the oxidation of the nickel center which is displayed by the highest half-wave potential of $E_{1/2}$ = 306 mV found for ^{CF_3}**1-pyr** as compared to $E_{1/2}$ = -33 mV found for ^{Me}**1-pyr**. This translates to a higher electron density of the nickel atom in the electron donating methyl substituted complex ^{Me}**1-pyr** compared to that of ^{CF_3}**1-pyr**. This result follows the expected behavior and strongly supports the hypothesis of an electronic influence of the remote substituents on the active nickel center.

Table 6.6: Half-wave potentials of selected catalysts according to cyclic voltammetry measurements.

entry	complex	$E_{1/2}$ [mV][a]
1	^{CF_3}**1-pyr**	306
2	^{Me}**1-pyr**	-33
3	$^{(MeCF_3)}$**1-pyr**	91
4	$^{Me/CF_3}$**1-pyr**	164
5	^{Fur}**5-pyr**	84
6	^{Thio}**5-pyr**	76

[a] determined from referenced cyclic voltammograms

The half-wave potentials of both complexes $^{(MeCF_3)}$**1-pyr** and $^{Me/CF_3}$**1-pyr** with mixed substituents are intermediate to the most extreme values of the fully methyl and CF_3-substituted complexes. In agreement with their oligomerization behavior observed in Chapter 6.2.2, producing oligomers with intermediate properties, the electron density of the nickel center also appears to be inbetween those of ^{CF_3}**1-pyr** and ^{Me}**1-pyr** for both complexes. Though the symmetrical mixed complex $^{(MeCF_3)}$**1-pyr** exhibits a slightly lower half-wave potential than the asymmetrical complex $^{Me/CF_3}$**1-pyr** (91 mV vs. 164 mV), the electronic influence of the CF_3 and methyl substituents seem to level each other out in both complexes. For the two complexes ^{Fur}**5-pyr** and ^{Thio}**5-pyr** bearing electron rich motifs on the salicylaldiminato ligand with

coordinating motifs, the redox potentials of $E_{1/2}$ = 84 and 76 mV, respectively, are in the range of the mixed complexes and significantly higher than the one of the electron rich complex ^{Me}**1-pyr**.

Given that the electronic nature of the remote substituents correlates with polymer molecular weight on the one hand and the half-wave potential on the other hand, the half-wave potential of the complexes was found to correlate with the molecular weight of the polyethylene they produce under given reaction conditions (**Figure 6.8**, orange). Complexes with a higher half-wave potential produce higher molecular weight polymer and vice versa. This does not only hold true for the two benchmark complexes ^{CF3}**1-pyr** and ^{Me}**1-pyr** but also for the two mixed complexes and those bearing coordinating motifs, having half-wave potentials and molecular weights in between the extreme values.

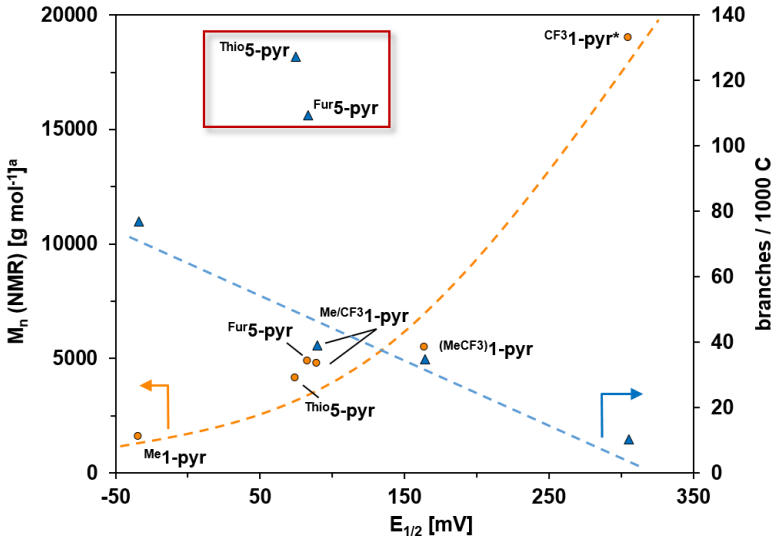

Figure 6.8: Correlation of the catalysts half-wave potential vs. polymer molecular weight and degree of branching. [a] molecular weight of polymers synthesized at 40 °C and 20 bar of ethylene; * polymer obtained at 40 °C and 40 bar of ethylene according to ref. 53. Dashed lines are merely a guide to the eye.

For the four different terphenyl amine based nickel salicylaldiminato complexes, also the overall degree of branching of the polymers correlates with the catalysts' half-wave potential. This is in agreement with a higher propensity of a more electron rich nickel center for β-hydride elimination as fundamental step for both chain transfer and chain walking. While this experimental correlation (linear) is even quantitative, ^{Fur}**5-pyr** and ^{Thio}**5-pyr** with coordinating motifs also fit the trend but not quantitatively (red box in **Figure 6.8**). Both exhibit half-wave potentials similar to the one of $^{(MeCF3)}$**1-pyr** ($E_{1/2}$ = 84 and 76 mV vs. 91 mV) but produce polymers with a three times higher degree of branching. In summary, these CV studies show that the nature of the remote substituents impacts the electronic nature of the nickel center, as observed by the different ease of oxidation of the nickel catalyst precursors.

6.2.4 Density Functional Theory Calculations (Performed by Prof. Dr. Lucia Caporaso and Dr. Laura Falivene)

In order to gain a more fundamental insight in the catalytic behavior and the selectivity for branch formation or linear chain growth of *N*-terphenyl Ni(II) salicylaldiminato complexes, ^{Me}**1-pyr** and ^{CF3}**1-pyr** were studied theoretically by density functional theory calculations. All computational details of these investigations are provided in the Chapter 6.4 Experimental Section. Given the major differences of product properties obtained with ^{Me}**1-pyr** and ^{CF3}**1-pyr**, significant differences of the overall barriers for linear chain growth and branch formation for the two complexes are expected. The calculations include Gibbs free energies (ΔG in kcal mol^{-1}) of all important intermediates and transition states involved in the branch formation and linear chain growth during the polymerization as well as for relevant intermediates of the initiation and termination reactions.

Initiation and Ethylene Insertion

Two different isomers for the Ni-methyl fragment formed by dissociation of the labile pyridine ligand were found to be viable (**Figure 6.9**). In **1-Me-T**, the methyl group is located *trans* to the oxygen of the salicylaldiminato ligand. In **1-Me-C**, the methyl group is in the *cis* position to the oxygen ligand which allows for a stabilizing η^2-interaction of one of the aromatic rings of the terphenyl moiety of the ligand to the metal center. For such an interaction to be possible, a rotation of the terphenyl moiety around the N-C axis and a *cis*/*trans* isomerization is required.

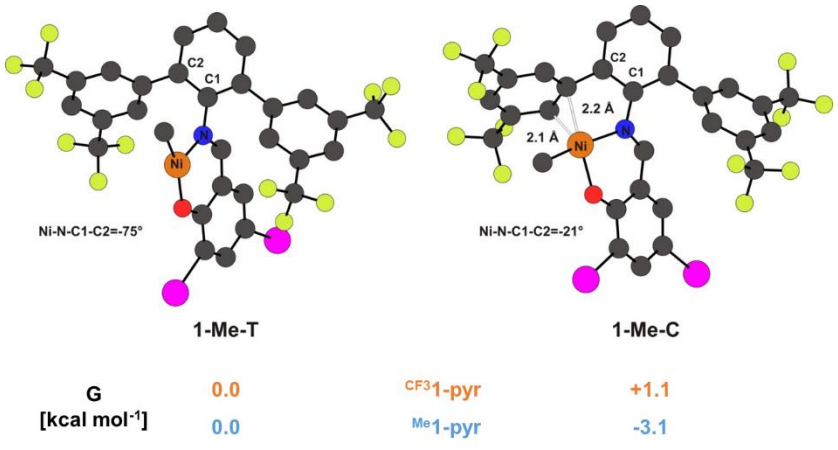

Figure 6.9: Two possible isomers **1-Me-T** and **1-Me-C** of the dissociated three coordinate nickel-methyl starting species.

The calculations reveal, that for the two complexes ^{Me}**1-pyr** and ^{CF_3}**1-pyr** different isomers from **Figure 6.9** are favored. While for ^{Me}**1-pyr** there is a preference of -3.1 kcal mol^{-1} for the **1-Me-C** isomer which includes the η²-interaction of the aryl ring of the terphenyl moiety, ^{CF_3}**1-pyr** shows a small preference of -1.1 kcal mol^{-1} for the *trans*-isomer **1-Me-T**. This difference is accounted for by the presence of the different substituents on the coordinating aromatic ring of the ligand, with the electron donating methyl group in ^{Me}**1-pyr** resulting in a stronger interaction with the nickel center compared to the electron withdrawing CF_3 substituents in ^{CF_3}**1-pyr**. This is already a first indication that the proposed, weak π-interaction of the aryl groups of the ligand with the nickel center might play a role in the catalytic cycle of the ethylene polymerization and that it can possibly explain the different behavior observed for ^{Me}**1-pyr** and ^{CF_3}**1-pyr**.

Moving to the ethylene coordination and the subsequent insertion step, two different pathways can be considered (**Scheme 6.4**). Starting from the three coordinate intermediate **1-Me-T** after pyridine dissociation, only for ^{Me}**1-pyr** stabilization by rotation of the terphenyl and interaction of the aryl with the nickel center is favored. However, for both ^{Me}**1-pyr** and ^{CF_3}**1-pyr** starting from **1-Me-T**, ethylene coordination to form **1-Coor-T** is the energetically most favorable pathway with a gain in energy of $\Delta G^{\neq}$ = 8.5 and 11.0 kcal mol^{-1}, respectively.

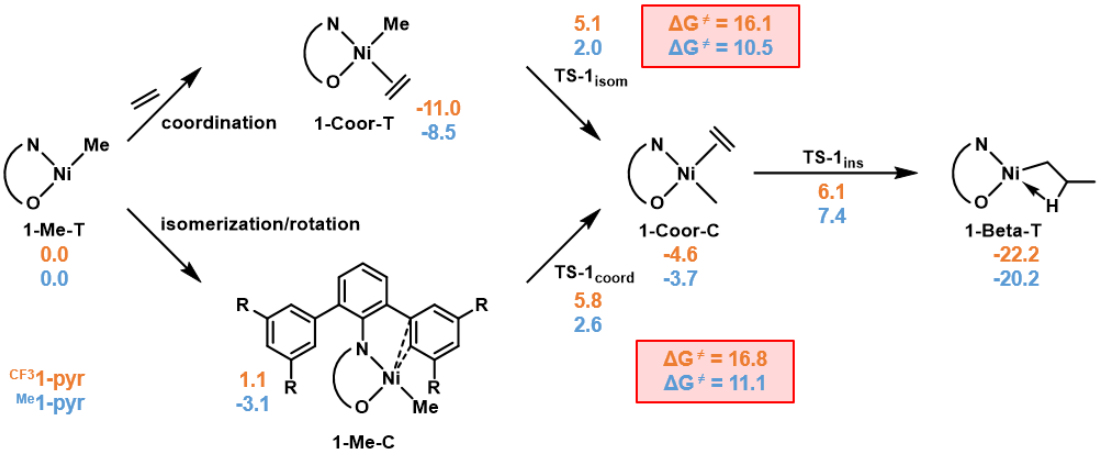

Scheme 6.4: Two potential pathways for ethylene coordination to the starting species **1-Me-T** and subsequent insertion with the corresponding Gibbs free energies (G in kcal mol^{-1}) of all intermediates for ^{Me}**1-pyr** (blue) and ^{CF_3}**1-pyr** (orange)

The calculations show that for these *N*-terphenyl Ni(II) salicylaldiminato complexes insertion can only take place from the *cis* coordinated species **1-Coor-C**. Therefore, prior to insertion, an isomerization from **1-Coor-T** to **1-Coor-C** is necessary. This step proceeds via a tetrahedral four coordinate transition state **TS-1$_{isom}$** which involves a rather high energy barrier of $\Delta G^{\neq}$ = 10.5 and $\Delta G^{\neq}$ = 16.1 kcal mol^{-1} for ^{Me}**1-pyr** and ^{CF_3}**1-pyr**, respectively. Considering the ethylene coordinated **1-Coor-T** as the starting species due to its low energy, the alternative

pathway to its *cis* isomer **1-Coor-C** via the aryl coordinated intermediate **1-Me-C** involves slightly higher overall barriers of $\Delta G^{\neq}$ = 11.1 and 16.8 kcal mol^{-1} for the two complexes. From **1-Coor-C**, the subsequent migratory insertion via the transition state **TS-1$_{ins}$** proceeds with similar barriers of $\Delta G^{\neq}$ = 11.1 kcal mol^{-1} and $\Delta G^{\neq}$ = 10.7 kcal mol^{-1} for both complexes to result in the most stable β-agostic intermediate **1-Beta-T**. The overall barrier for the first ethylene insertion for ^{Me}**1-pyr** is $\Delta G^{\neq}$ = 15.9 kcal mol^{-1} and therefore lower than that of ^{CF3}**1-pyr** which is $\Delta G^{\neq}$ = 17.1 kcal mol^{-1}.

Linear Chain Growth

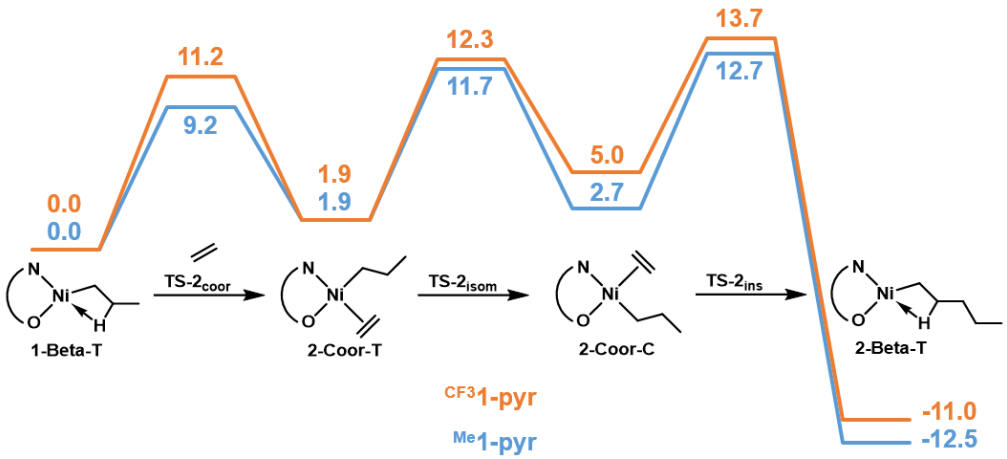

Scheme 6.5: Energy profile (G in kcal mol^{-1}) for the catalytic ethylene insertion with complexes ^{Me}**1-pyr** (blue) and ^{CF3}**1-pyr** (orange). Energies relative to the energy of the β-agostic *trans*-polymeryl nickel complex **1-Beta-T** as a reference, set to zero.

Starting from **1-Beta-T**, the further catalytic chain growth was calculated. An energy profile of all steps involved in the second insertion reaction is depicted in **Scheme 6.5**. **1-Beta-T** as a suitable model for the generic insertion resting state was fixed as the zero energy point. For an ethylene coordination to occur, the β-agostic interaction of **1-Beta-T** has to be cleaved. Therefore, ethylene coordination requires a high energy barrier of $\Delta G^{\neq}$ = 9.2 kcal mol^{-1} and $\Delta G^{\neq}$ = 11.2 kcal mol^{-1} to be overcome for the two complexes ^{Me}**1-pyr** and ^{CF3}**1-pyr**, respectively. For both complexes, the resulting **2-Coor-T** is not favored and1.9 kcal mol^{-1} higher in energy. From there, the system isomerizes via the tetrahedral four-coordinate transition state **TS-2$_{isom}$** to the even less favored **2-Coor-C**. Migratory insertion via **TS-2$_{ins}$** gives again the β-agostic complex **2-Beta-T**.

Both complexes behave similar in this sequence which represents linear chain growth, with the fluorine substituted ^{CF3}**1-pyr** having slightly higher barriers and a profile that is overall higher in energy. Ethylene coordination is not favored for both systems. While **1-Coor-T** has the same energy for both complexes, the isomerization to **2-Coor-C** results in a stronger destabilization

of ^{CF_3}**1-pyr** compared to ^{Me}**1-pyr**. This can be explained by the slightly different steric hindrance of the two systems with the CF_3 substituted complex being the more sterically hindered one. **Figure 6.10** depicts the topographic steric maps and quadrant $\%V_{Bur}$ of the fragment **1-Me-T** of both systems. The main steric hindrance of the two systems is located in the north and south east quadrants, the quadrants where the monomer is directed to in the **2-Coor-C** intermediates. Consequently, the effect of the higher steric hindrance of ^{CF_3}**1-pyr** is more pronounced when the monomer is located in the more crowded site *trans* to the oxygen atom.

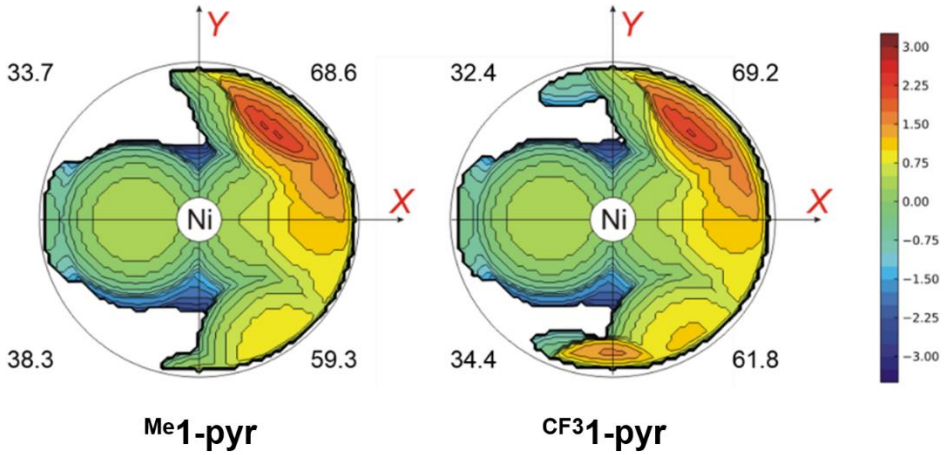

Figure 6.10: Topographic steric maps of the fragment **1-Me-T** of ^{Me}**1-pyr** and ^{CF_3}**1-pyr**.

Branch Formation and Chain Transfer Reactions

Both for branch formation via chain walking and for the common chain transfer reactions, the catalyst has to undergo β-hydride elimination first. Starting from **1-Beta-T**, the β-hydride elimination was calculated to form the nickel hydride species **1-βEl-T** with coordinated propene in the *trans* position of the oxygen atom. This reaction is less favored for ^{CF_3}**1-pyr** compared to ^{Me}**1-pyr** from a kinetic as well as a thermodynamic point of view (cf. overview **Scheme 6.8**, p. 166). A direct β-hydride elimination from the insertion product **1-Beta-T** was ruled out as a viable pathway for both complexes due to the high energy of the product **1-βEl-T** with the coordinated olefin in the more sterically crowded *cis* position of the oxygen atom. Hence, β-hydride elimination has to occur from the *cis* isomer **1-Beta-C** which would give the sterically less crowded and energetically favored isomer **1-βEl-C**. However, all potential pathways for a direct *cis*/*trans* isomerization of the β-agostic complex were calculated to involve transition states with extremely high Gibbs free energies (> 20 kcal mol^{-1}) and therefore could be ruled out.

An alternative pathway for *cis*/*trans* isomerization that was already shown to be low in energy is the one following ethylene coordination to give **2-Coor-C** (**Scheme 6.5**). Especially at

high ethylene pressure, this reaction is favored over the alternative direct pathways. Reaching **2-Coor-C** via the pathway shown in **Scheme 6.5**, ethylene can be inserted as described, or ethylene can be released again by decoordination to form the β-agostic intermediate **1-Beta-C** (**Scheme 6.6**).

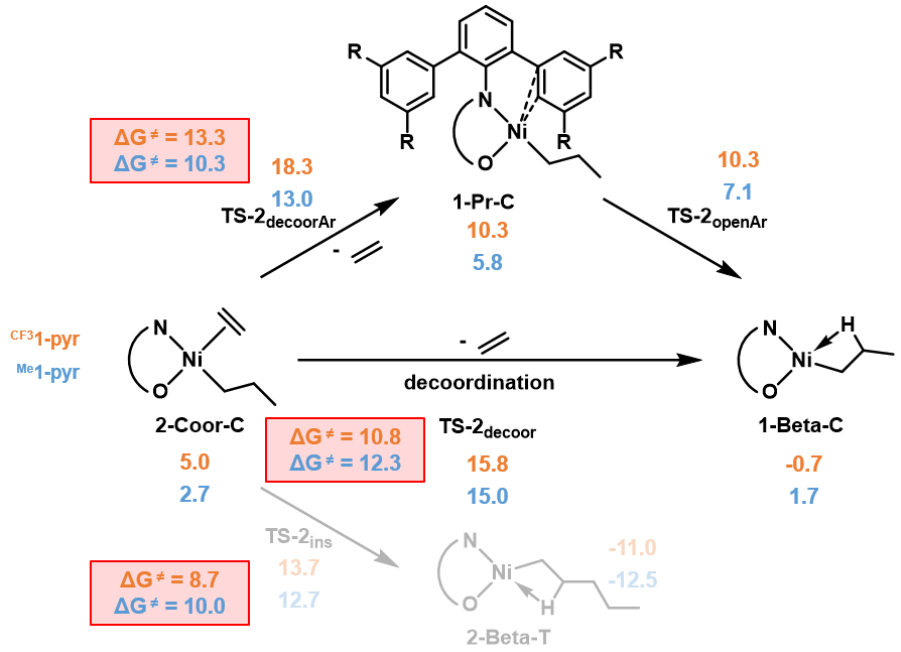

Scheme 6.6: Two potential pathways for the decoordination of ethylene to form **1-Beta-C**. Gibbs free energies (G in kcal mol^{-1}) of all intermediates for ^{Me}**1-pyr** (blue) and ^{CF_3}**1-pyr** (orange).

For this reaction, also two competitive pathways were found to be accessible. One pathway is the direct decoordination of ethylene via **TS-2**$_{decoor}$ to **1-Beta-C**. An alternative pathway involves a two-step reaction where ethylene is first replaced by η²-interaction of the aryl ring of the terphenyl moiety followed by subsequent opening and formation of the β-agostic complex. As revealed by the Gibbs free energies in **Scheme 6.6**, the direct pathway is favored for ^{CF_3}**1-pyr** by $\Delta\Delta G^{\neq}$ = 2.5 kcal mol^{-1} with respect to the indirect one. Remarkably, the pathway mediated by the aryl interaction is favored for ^{Me}**1-pyr** and by $\Delta\Delta G^{\neq}$ = 2.0 kcal mol^{-1} lower in energy compared to the direct one. Due to the stronger interaction of the more electron rich methyl substituted aryl rings of ^{Me}**1-pyr**, the intermediate η²-interaction was found to be able to significantly reduce the overall energy required for ethylene release. In agreement with experimental results that yield lower molecular weight products with higher degrees of branching with ^{Me}**1-pyr**, the release of ethylene is favored by $\Delta\Delta G^{\neq}$ = 0.5 kcal mol^{-1} for ^{Me}**1-pyr** with respect to ^{CF_3}**1-pyr**. Furthermore, the alternative, ligand assisted pathway makes ethylene release even more competitive compared to ethylene insertion for ^{Me}**1-pyr** with a difference in energy of only $\Delta\Delta G^{\neq}$ = 0.3 kcal mol^{-1} with respect to linear chain growth to **2-Beta-T** (**Scheme 6.5**). For

comparison, for ^{CF_3}**1-pyr**, ethylene insertion remains favored over ethylene release by $\Delta\Delta G^{\neq}$ = 2.1 kcal mol^{-1}.

Having found an accessible pathway for the formation of **1-Beta-C**, the subsequent β-hydride elimination reaction was calculated. This is the key step for all branch formation and chain transfer reaction pathways (**Scheme 6.7**). After formation of **1-Beta-C**, as expected, both systems can undergo β-hydride elimination to form the stable **1-βEl-C** with the coordinated propene directed away from the area of high steric hindrance. In agreement with the experimental results, the β-hydride elimination is favored for ^{Me}**1-pyr** with respect to ^{CF_3}**1-pyr**. From the propene coordinated hydride complex, again two different pathways are accessible: chain transfer or branch formation via chain walking.

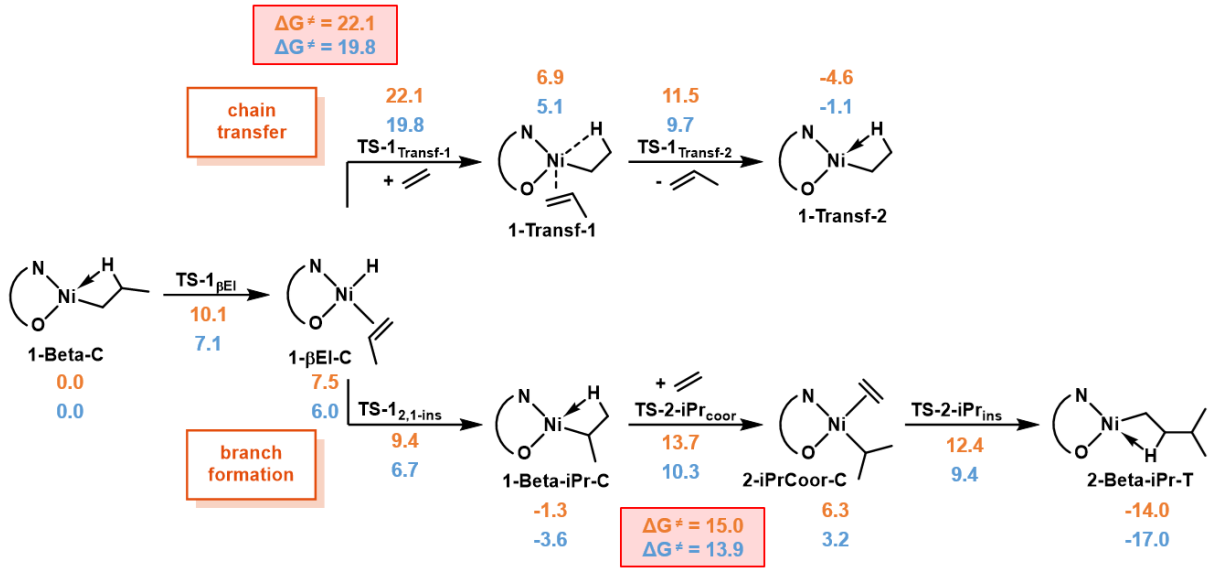

Scheme 6.7: Gibbs free energies (G in kcal mol^{-1}) of all important intermediates for chain transfer and branch formation with ^{Me}**1-pyr** (blue) and ^{CF_3}**1-pyr** (orange).

1. Chain transfer (**Scheme 6.7**, top) proceeds via ethylene coordination and subsequent insertion to form the five coordinate intermediate **1-Transf-1** with a very high overall barrier of $\Delta G^{\neq}$ = 19.8 kcal mol^{-1} and $\Delta G^{\neq}$ = 22.1 kcal mol^{-1} for ^{Me}**1-pyr** and ^{CF_3}**1-pyr**, respectively. After release of propene, the β-agostic complex **1-Transf-2** is formed to start the growth of a new polymer chain. The rate determining step of the chain termination reaction is the ethylene coordination and insertion which is not surprising, considering the high steric demand of the five coordinate intermediates involved. Overall, the rate determining step for the chain transfer reaction is about $\Delta\Delta G^{\neq}$ = 2.3 kcal mol^{-1} lower for ^{Me}**1-pyr** compared to ^{CF_3}**1-pyr**. In combination with the lower barrier calculated for ^{Me}**1-pyr** to access these pathways via **1-Beta-C**, this finding nicely explains the low molecular weight oligomers obtained by ^{Me}**1-pyr** in contrast to the high molecular weight polyethylene produced by ^{CF_3}**1-pyr**.

2. Branch formation as an alternative pathway (**Scheme 6.7**, bottom) starts with reinsertion of the coordinated propene in a 2,1-fashion (**TS-1$_{2,1\text{-ins}}$**). This is energetically favored for both ^{Me}**1-pyr** and ^{CF_3}**1-pyr** compared to chain transfer and results in the formation of the β-agostic resting state **1-Beta-iPr-C**. The branch formation proceeds with the ethylene coordination in the *trans* position to the oxygen atom through the displacement of the agostic interaction of the polymeryl chain and the metal center (**2-iPrCoor-C**). In a last step, the monomer insertion into the nickel isopropyl bond takes places via the **TS-2-iPr$_{ins}$** transition state leading to the methyl branched product **2-Beta-iPr-T** which is stabilized by a β-agostic interaction. The rate determining step for branch formation is the cleavage of the agostic interaction by ethylene coordination. This step is also favored for ^{Me}**1-pyr** with an overall barrier of $\Delta G^{\neq}$ = 13.9 kcal mol^{-1} compared to a barrier of $\Delta G^{\neq}$ = 15.0 kcal mol^{-1} for ^{CF_3}**1-pyr**. This is in agreement with the much higher degree of branching of products obtained by ^{Me}**1-pyr** compared to those of ^{CF_3}**1-pyr**.

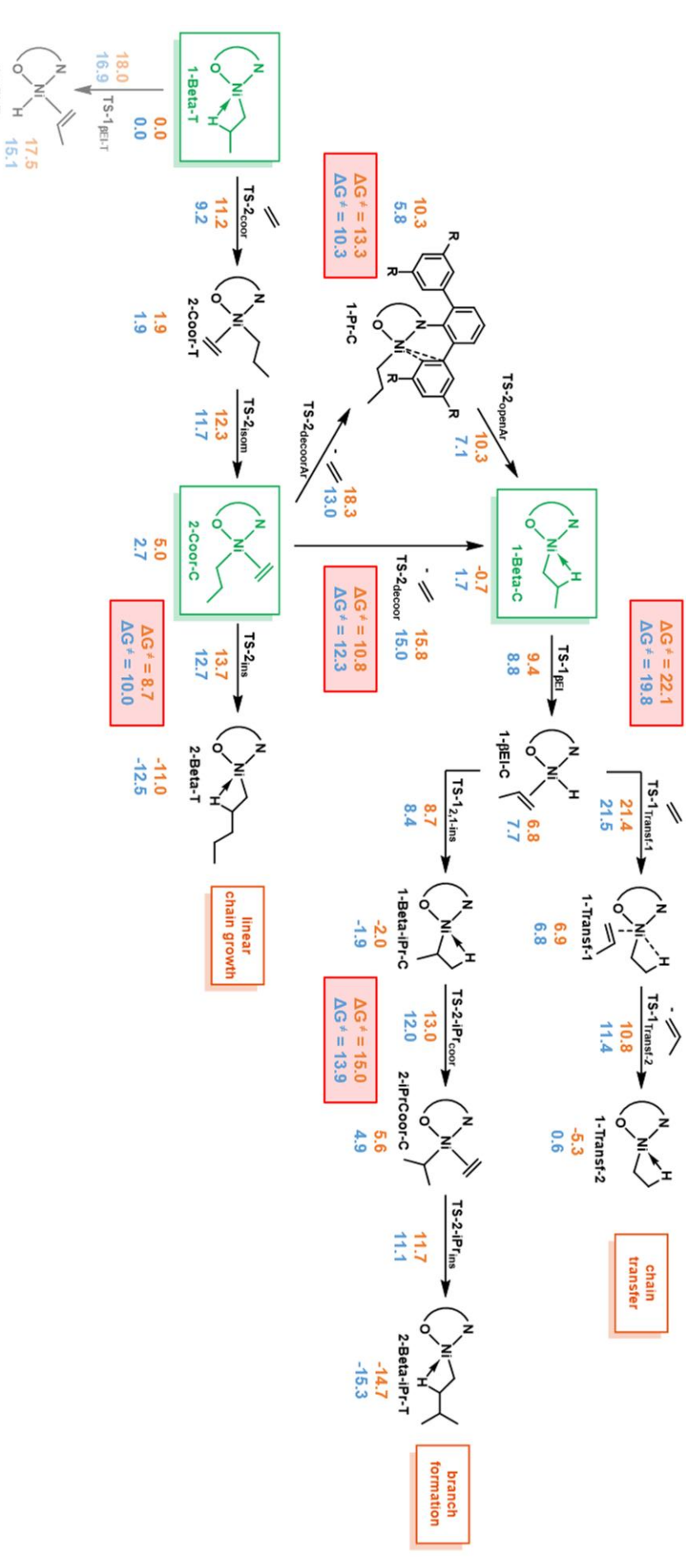

Scheme 6.8: Complete mechanistic picture for branching ethylene oligomerization obtained from DFT calculations with Gibbs free energies (G in kcal mol^{-1}) of all important intermediates and transition states for ^{Me}**1-pyr** (blue) and ^{CF_3}**1-pyr** (orange).

Scheme 6.8 gives a complete overview of all important mechanistic pathways obtained from DFT calculations involved in the branching ethylene oligomerization with ^{Me}**1-pyr** and ^{CF_3}**1-pyr**. In conclusion, both the linear propagation as well as the chain transfer and branch formation mechanisms start from **1-Beta-T** and overlap until the formation of **2-Coor-C**. For linear chain growth, the two catalysts systems ^{Me}**1-pyr** and ^{CF_3}**1-pyr** were found to behave very similar with similar overall barriers of $\Delta G^{\neq}$ = 12.7 kcal mol^{-1} and $\Delta G^{\neq}$ = 13.7 kcal mol^{-1}, respectively. The results indicate that **2-Coor-C** is the key intermediate of the entire catalytic cycle in that it gives access to branch formation and chain transfer as the side reactions governing the product molecular weight and the degree of branching. In line with its decisive role in the catalytic cycle this is where the main differences between the two catalyst systems can be found. For both catalysts, linear chain growth has the lowest barrier starting from **2-Coor-C**. This is in agreement with the experimental results since both systems provide long chain products including linear sequences. However, only for ^{Me}**1-pyr**, branch formation and chain transfer pathways are accessible with a similar barrier of only $\Delta\Delta G^{\neq}$ = 0.3 kcal mol^{-1} higher than that of linear chain growth. The theoretical studies also show that a metal-ligand π-interaction proposed in this thesis indeed might play a key role in the catalytic cycle and is responsible for the different catalytic behavior of ^{Me}**1-pyr** and ^{CF_3}**1-pyr** during ethylene polymerization. The key difference was found to be the aryl coordinated intermediate **1-Pr-C** which is able to significantly reduce the barrier for ethylene release from ^{Me}**1-pyr** to form the important intermediate **1-Beta-C**. Due to the weaker aryl-metal interaction, this alternative pathway does not occur to a larger extent for ^{CF_3}**1-pyr**. These findings nicely support the mechanism of a weak π-interaction proposed in this thesis to govern the selectivity of ^{Me}**1-pyr** for highly branched low molecular weight products. Furthermore, in line with experimental results, a lower overall barrier for β-hydride elimination as well as chain transfer and chain walking was found for ^{Me}**1-pyr** compared to ^{CF_3}**1-pyr** which explains the lower molecular weight products with higher degrees of branching obtained.

6.3 Summary and Conclusion

Ni(II) salicylaldiminato complexes represent a unique and versatile class of ethylene polymerization catalysts. Especially with *N*-terphenyl based complexes, the variation of the electronic nature of remote substituents allows for a fine tuning of the resulting polymer properties in a wide range.[50,51] Electron donating substituents result in the formation of highly branched oligomers while catalysts with electron withdrawing substituents produce linear, semi-crystalline polyethylene. However, the origin of this remote substituent effect remained

elusive and the mechanism how the electronic information of the substituents is transferred to the catalytically active nickel center is unclear.

A weak π-interaction of the ligand aryl groups with the nickel center could account for the remarkable influence of the remote substituents in terphenyl amine based complexes. Corresponding short aryl-nickel distances are observed in all single crystal structures of *N*-terphenyl Ni(II) salicylaldiminato complexes. This concept was further investigated in detail with the synthesis of a series of catalysts with new substitution patterns (**Figure 6.11**).

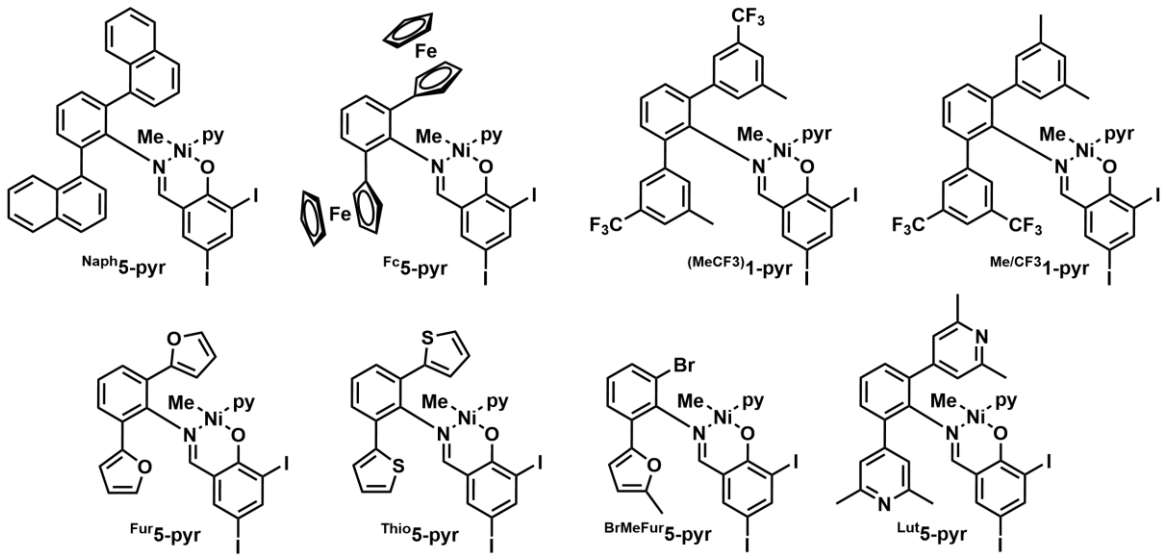

Figure 6.11: New complexes synthesized for the investigation of the remote substituent effect.

An additional weak interaction of the salicylaldiminato ligand was studied via introduction of heteroarenes like furan and thiophene as potentially coordinating motifs. Both complexes **^{Fur}5-pyr** and **^{Thio}5-pyr** show a remarkable polymerization behavior. Though they produce polymers with significantly higher molecular weights compared to **^{Me}1-pyr**, the products contain unprecedentedly high amounts of branches of up to 127 per 1,000 carbon atoms. At the same time both catalysts mainly produce methyl branches and only few longer alkyl branches or branch on branch motifs. A similar weak interaction of the 3,5-substituted aryl rings in *N*-terphenyl based salicylaldiminato Ni(II) complexes, was investigated with the two complexes **$^{Me/CF_3}$1-pyr** and **$^{(MeCF_3)}$1-pyr** that combine electron withdrawing and electron donating properties by having methyl and CF_3 substituents (one asymmetric and one symmetric complex). Both produce polymers with intermediate molecular weights and degrees of branching. These experimental results do not directly support or contradict the presence of an additional weak π-interaction between the salicylaldiminato ligand and the nickel center.

Cyclic voltammetry measurements of all new complexes show that the different peripheral aryl moieties impact the electronic situation of the nickel center. For terphenyl amine based

catalysts, the half-wave potential of the complex was found to follow the trend of the electronic nature of its substituents. Electron withdrawing substituents in complex ^{CF_3}**1-pyr** hinder the oxidation as indicated by the highest half-wave potential found for this complex, while the electron rich substituted complex ^{Me}**1-pyr** exhibits a small potential and is oxidized most easily. Given the observed correlation between the nature of the remote substituents and the polymer microstructure and molecular weights, also high half-wave potentials appear to go along with high molecular weight and low degrees of branching and vice versa. Complexes ^{Fur}**5-pyr** and ^{Thio}**5-pyr** containing potential coordinating motifs in the ligand backbone also follow this trend but not quantitatively. Although they show similar half-wave potential as observed for $^{(MeCF_3)}$**1-pyr**, these complexes produce three times more branches at the same polymer molecular weight.

A further fundamental insight in the mechanism underlying the catalytic ethylene polymerization with ^{CF_3}**1-pyr** and ^{Me}**1-pyr** was gained by density functional theory calculations carried out by Lucia Caporaso and Laura Falivene. The detailed calculations include energies and energy barriers of all relevant intermediates and reaction steps involved in the catalytic cycle. The calculations are in agreement with experimental results and can explain the different microstructures of the products obtained with the two different catalysts. Remarkably, the calculations support the hypothesis of a π-interaction of the aryl groups of the ligand with the nickel center. It was shown that for the fully methyl substituted complex ^{Me}**1-pyr** an aryl coordinated intermediate indeed plays a key role in the catalytic cycle since it reduces the overall energy barrier of the reaction step that is critical for both branch formation and chain transfer pathways. For ^{CF_3}**1-pyr** this π-interaction was calculated to be much weaker due to the lower electron density of the ligand aryl rings. Therefore, branch formation and chain transfer pathways are not as readily accessible with ^{CF_3}**1-pyr** explaining the more linear, higher molecular weight polyethylene obtained.

6.4 Experimental Section

6.4.1 General Considerations and Materials

All complex syntheses were carried out under an argon or nitrogen atmosphere using standard Schlenk or glovebox techniques. Solvents were dried and degassed using standard laboratory techniques.[94] Benzene and toluene were distilled from sodium, methylene chloride was distilled from CaH_2, pyridine from KOH and THF and Et_2O were distilled from blue sodium/benzophenone ketyl. Pentane, Et_2O and toluene used for complex syntheses and

ethylene polymerization were dried by passing through columns equipped with aluminum oxide/molecular sieve 3 Å. Ethylene for polymerization (3.5 grade) was supplied by AirLiquide and used as received. [(tmeda)$NiMe_2$] was purchased from MCAT. $^{Naph}\mathbf{NH_2}$ was available in the group and was synthesized according to procedures reported for similar compounds.[50] Thiophene was degassed prior to use. All commercially available compounds and starting materials were purchased from Aldrich, Acros, TCI, ABCR, or ApolloScientific. All deuterated solvents were supplied by Eurisotop.

NMR-Spectroscopy

NMR spectra were recorded on a Varian Unity Inova 400 (^{1}H: 400 MHz, ^{13}C: 101 MHz, ^{19}F: 376 MHz), a Bruker Avance III 400 (^{1}H: 400 MHz, ^{13}C: 101 MHz, ^{19}F: 376 MHz), or a Bruker Avance III 600 spectrometer (^{1}H: 600 MHz, ^{13}C: 151 MHz, ^{19}F: 564 MHz). ^{1}H chemical shifts were referenced to the residual proton signal of the deuterated solvent. ^{13}C chemical shifts were referenced to the carbon signal of the deuterated solvent. Multiplicities are given as follows: s: singlet, d: doublet, t: triplet, q: quartet, quint: quintet, v: virtual multiplet, m: multiplet, br: broad signal or combination thereof. NMR spectra of polyethylenes insoluble in chloroform at room temperature were recorded at 130 °C with addition of 5 mg mL^{-1} of $Cr(acac)_3$ and CD_2Cl_4 as the solvent. For reliable integration all spectra were recorded inverse gated without NOE using a relaxation delay of 2s.

Differential Scanning Calorimetry

Differential scanning calorimetry (DSC) was carried out in Netzsch DSC 204 F1 in closed 40 µL pan alumina crucible under a nitrogen atmosphere. The samples were heated with a bicylclic temperature program from -50 °C to 160 °C with heating and cooling rates of 10 K min^{-1}. For determination of melting temperatures and degrees of crystallization, the second heating curve was used. For determination of the degree of crystallization, the enthalpy of fusion of the measured polymer was compared to 100 % crystalline PE (293 J g^{-1}).[95]

Gel Permeation Chromatography

High temperature gel permeation chromatography for PE molecular weight determination was carried out by Lars Bolk at the University of Konstanz in 1,2,4-trichlorobenzene at 160 °C at a flow rate of 1 mL min^{-1} on a 'Polymer Laboratories GPC 220' instrument equipped with 'PLgel Olexis' columns with differential refractive index-, viscostity- and light scattering- (15° and 90°) detectors. Data reported were determined via RI-detection against calibration with linear

polyethylene standards. For oligomers soluble in THF at 50 °C, molecular weight determination was carried out on a Polymer Laboratories PL-GPC 50 instrument with two PLGel 5 µm MIXED-C columns and an RI-detector in THF against polystyrene standards.

Elemental Analyses

Elemental analyses were obtained by the Analytical Services at the Department of Chemistry, University of Konstanz. Elemental analyses were performed on an 'Elementar Vario MICRO cube' instrument.

Ethylene Oligomerization

All ethylene oligomerization reactions were conducted in a *Büchi miniclave* reactor with a 200 mL steel vessel. The reactor was equipped with a cooling and heating jacket, supplied by a thermostat controlled by a thermocouple dipping into the polymerization mixture. The ethylene uptake of the reactor was monitored via Bronkhorst mass-flow meters. Flow charts of the reactors used are provided in Chapter 3.4.5 Additional Spectra and Data (p. 70).

The reactor was evacuated and refilled with argon repeatedly and toluene was added via cannula transfer. After heating to the desired temperature under stirring with 1,000 rpm, a catalyst solution in toluene was added and the reactor was pressurized to the desired pressure. Oligomerization was conducted at constant pressure for the given time. After the desired reaction time, the reactor was vented, the polymer was precipitated in methanol and dried under vacuum.

Cyclic Voltammetry

All electrochemical experiments were performed in a custom-built (Winter research group) cylindrical vacuum-tight one-compartment cell. A spiral-shaped Pt wire and an Ag wire as the counter and reference electrodes, respectively, are sealed into glass capillaries that are introduced via Quickfit screws at opposite sides of the cell. A platinum electrode is introduced as the working electrode through the top port via a Teflon screw cap with a suitable fitting. Prior to the experiment, it was polished with 1 µm and then 0.25 µm diamond paste (Buehler-Wirtz). The cell may be attached to a conventional Schlenk line via a side arm equipped with a Teflon screw valve and allows for experiments to be performed under an atmosphere of argon with approximately 5 mL of analyte solution. NBu_4^+ PF_6^- (0.25 mM) was used as the supporting electrolyte. Referencing was performed with addition of equimolar amounts of decamethylferrocene (Cp*2Fe) or ferrocene (Cp_2Fe), respectively, as an internal standard to the

analyte solution after all data of interest had been acquired. Representative sets of scans were repeated with the added standard. Final referencing was performed against the ferrocene/ferrocenium ($Cp_2Fe^{o/+}$) couple with $E_{1/2}(Cp^*_2Fe^{o/+}) = -550$ mV vs. $Cp_2Fe^{o/+}$. Electrochemical data were acquired with a computer-controlled BAS potentiostat.

Computational Details

All the DFT geometry optimizations were performed at the GGA BP86[156-158] level with the Gaussian09 package.[159] The electronic configuration of the systems was described with the 6-31G basis set for H, C, N, F, and O while for I and Ni the quasi-relativistic LANL2DZ ECP effective core potential was adopted.[160] All geometries were characterized as minimum or transition state through frequency calculations. The reported free energies were built through single point energy calculations on the BP86/6-31G geometries using the M06 functional and the triple-ζ TZVP[161-163] basis set on main group atoms. Solvent effects were included with the PCM model using Toluene as the solvent.[164,165] To this M06/TZVP electronic energy in solvent, thermal corrections were included from the gas-phase frequency calculations at the BP86/6-31G.

6.4.2 Synthesis and Characterization of 2,6-Diubstituted Anilines

3-methyl-5-(trifluoromethyl)phenylboronic acid pinacol ester

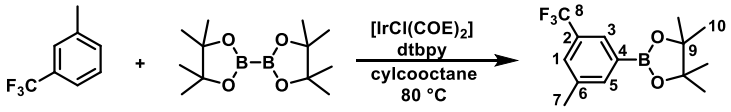

A mixture of 3-(trifluoromethyl)toluene (5 g, 31.2 mmol, 2.2 eq) and bis(pinacolato)diboron (2.6 g, 14.2 mmol, 1.0 eq) was dissolved in 3 mL of cyclooctane. After addition of $[IrCl(COE)_2]$ (95 mg, 213 µmol, 1.5 mol%) and dtbpy (57 mg, 213 µmol, 1.5 mol%) in 2 mL of cyclooctane the reaction was heated to 80 °C and stirred for 3 days. After removing all volatiles under vacuum the product was obtained as a red oil (5.4 g, 13.6 mmol, 96 %).

^{1}H-NMR (400 MHz, $CDCl_3$): δ (ppm) = 7.86 (s, 1H, *H-3*), 7.79 (s, 1H, *H-5*), 7.51 (s, 1H, *H-1*), 2.41 (s, 3H, *H-7*), 1.36 (s, 12H, *H-10*).

^{13}C-NMR (101 MHz, $CDCl_3$): δ (ppm) = 138.8 (m, C-5), 138.1 (C-6), 130.2 (q, $^2J_{CF}$=31.6 Hz, C-2), 128.6 (q, $^3J_{CF}$=3.9 Hz, C-3), 128.5 (q, $^3J_{CF}$=3.7 Hz, C-1), 124.5 (q, $^1J_{CF}$=272.5 Hz, C-8), 84.4 (C-9), 25.0 (C-10), 21.2 (C-7). *Note: C-4 adjacent to the boron was not detected in the ^{13}C NMR spectrum.*

Thiophenyl-2-boronic acid pinacol ester

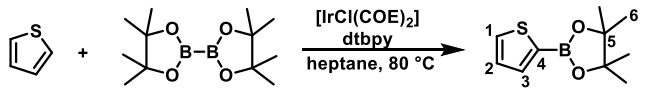

The thiopheneboronic acid pinacol ester was prepared according to a reported procedure.[152] To a mixture of bis(pinacolato)diboron (5.1 g, 20 mmol, 1.0 eq), [IrCl(COE)$_2$] (135 mg, 0.3 mmol, 1.5 mol%), and dtbpy (81 mg, 0.3 mmol, 1.5 mol%) was added 16.8 g of thiophene (200 mmol, 10.0 eq) and 60 mL of heptane. The brown suspension was heated to 80 °C for 3 days. After removing all volatiles under vacuum, the resulting brown solid was recrystallized from pentane at -30 °C to yield the product as a white solid (4.8 g, 22.8 mmol, 57 %).

^{1}H-NMR (400 MHz, $CDCl_3$): δ (ppm) = 7.66 (dd, $^3J_{HH}$=3.5 Hz, $^4J_{HH}$=0.9, 1H, *H-1*), 7.64 (dd, $^3J_{HH}$=4.7 Hz, $^4J_{HH}$=0.9 Hz, 1H, *H-3*), 7.20 (dd, $^3J_{HH}$=3.5 Hz, $^3J_{HH}$=4.7 Hz, 1), 1.35 (s, 12H, *H-6*).

^{13}C-NMR (101 MHz, $CDCl_3$): δ (ppm) = 137.3 (C-1), 132.5 (C-3), 128.3 (C2-), 84.2 (C-5), 24.9 (C-6). *Note: C-4 adjacent to the boron was not detected in the ^{13}C NMR spectrum.*

2,6-Lutidine-4-boronic acid pinacol ester

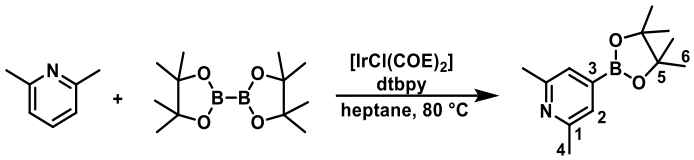

The lutidineboronic acid pinacol ester was prepared according to a literature procedure.[152] To a mixture of bis(pinacolato)diboron (2.5 g, 10 mmol, 1.0 eq), [IrCl(COE)$_2$] (67 mg, 150 µmol, 1.5 mol%), and dtbpy (40 mg, 150 µmol, 1.5 mol%) was added 10.7 g of 2,6-lutidine (100 mmol, 10.0 eq) and 60 mL of heptane. The brown suspension was heated to 80 °C for 3 days. After removing all volatiles under vacuum, the resulting brown solid was sublimated at 50 °C to yield the product as a white solid (4.1 g, 17.6 mmol, 88 %).

^{1}H-NMR (400 MHz, $CDCl_3$): δ (ppm) = 7.24 (s, 2H, *H-2*), 2.46 (s, 6H, *H-4*), 1.28 (s, 12H, *H-6*).

^{13}C-NMR (101 MHz, $CDCl_3$): δ (ppm) = 157.2 (C-1), 125.3 (C-2), 84.5 (C-5), 25.0 (C-6), 24.4 (C-4). *Note: C-3 adjacent to the boron was not detected in the ^{13}C NMR spectrum.*

3,5-dimethyl-3',5'-bis(trifluoromethyl)terphenyl amine ($^{Me/CF3}$1-NH_2)

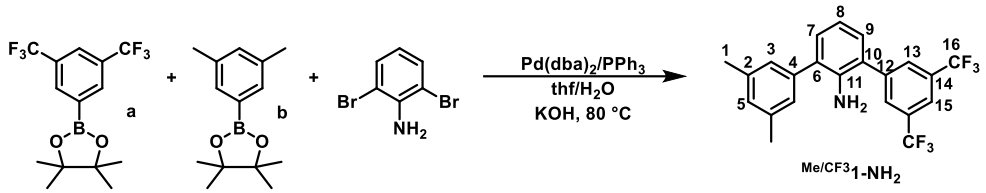

To a suspension of 2,6-dibromoaniline (1.25 g, 5.0 mmol, 1.0 eq), **a** (1.70 g, 5.0 mmol, 1.0 eq), **b** (1.16 mg, 5.0 mmol, 1.0 eq) and KOH (1.4 g, 25 mmol, 5 eq) in 10 mL of water and 5 mL of THF, a solution of $Pd(dba)_2$ (29 mg, 50 µmol, 1 mol %) and PPh_3 (32 mg, 120 µmol, 2.4 mol%) in 5 mL of THF was added and the orange solution was heated to 80 °C for 20 hours. After cooling to room temperature the reaction was stirred for one hour under air. After addition of 25 mL of THF, the organic phase was then extracted three times with 20 mL of 5 M KOH solution. The combined organic layers were dried over $MgSO_4$. After removal of the solvent the product was purified via column chromatography on silica using pentane/toluene (3:1) as the eluent (R_f=0.4). $^{Me/CF3}$**1-NH_2** was obtained as a white solid (758 mg, 1.9 mmol, 38 %).

^{1}H-NMR (600 MHz, $CDCl_3$): δ (ppm) = 8.02 (s, 2H, *H-13*), 7.78 (s, 1H, *H-15*), 7.18 (dd, $^3J_{HH}$=7.5 Hz, $^4J_{HH}$=1.7 Hz, 1H, *H-9*), 7.09 (s, 2H, *H-3*), 7.08 (dd, $^3J_{HH}$=7.5 Hz, $^4J_{HH}$=1.7 Hz, 1H, *H-7*), 7.03 (s, 1H, *H-5*), 6.92 (t, $^3J_{HH}$=7.5 Hz, 1H, *H-8*), 3.48 (br, 2H, *NH_2*), 2.38 (s, 6H, *H-1*).

^{13}C-NMR (151 MHz, $CDCl_3$): δ (ppm) = 142.3 (C-4), 140.7 (C-11), 139.1 (C-12), 138.8 (C-2), 132.3 (q, $^2J_{CF}$=33.3 Hz, C-14), 131.1 (C-9), 129.8 (m, C-13), 129.6 (C-7), 129.4 (C-5), 129.2 (C-6), 127.1 (C-3), 124.7 (C-10), 123.6 (q, $^1J_{CF}$=273.1 Hz, C-16), 121.2 (m, C-15), 118.8 (C-8), 21.5 (C-1).

^{19}F-NMR (376 MHz, $CDCl_3$): δ (ppm) = -62.81 (s).

Elemental Analysis (%) for $C_{22}H_{17}F_6N$: Found (Calculated): C 64.55 (65.02); H 4.19 (4.80); N 3.42 (3.49).

3,3'-dimethyl-5,5'-bis(trifluoromethyl)terphenyl amine ($^{(MeCF3)}$1-NH_2)

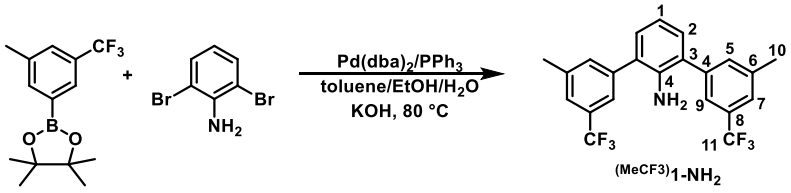

To a suspension of 2,6-dibromoaniline (960 mg, 3.8 mmol, 1.0 eq), boronic acid ester (2.5 g, 8.8 mmol, 2.3 eq), and KOH (1.1 g, 19 mmol, 5 eq) in 12 mL of toluene, 3 mL of water and 3 mL of EtOH, a solution of $Pd(dba)_2$ (22 mg, 38 µmol, 1 mol %) and PPh_3 (24 mg, 91 µmol, 2.4 mol%) in 2 mL of EtOH was added and the orange solution was heated to 95 °C for 3 days. After cooling to room temperature the reaction was stirred for one hour under air. The organic phase was then extracted three times with 20 mL of 5 M KOH solution. The combined organic layers were dried

over $MgSO_4$. After removal of the solvent the product was purified via recrystallization from pentane. $^{(MeCF_3)}$**1-NH$_2$** was obtained as a yellow solid (1.2 g, 3.0 mmol, 79 %).

^{1}H-NMR (400 MHz, $CDCl_3$): δ (ppm) = 7.57 (s, 2H, *H-9*), 7.51 (s, 2H, *H-5*), 7.44 (s, 2H, *H-7*), 7.12 (d, $^3J_{HH}$=7.6 Hz, 2H, *H-2*), 6.90 (t, $^3J_{HH}$=7.6 Hz, 1H, *H-1*), 3.75 (s, 2H, *NH$_2$*), 2.48 (s, 6H, *H-10*).
^{13}C-NMR (101 MHz, $CDCl_3$): δ (ppm) = 140.7 (C-4), 140.4 (C-6), 139.7 (C-4), 133.5 (C-5), 131.4 (q, $^2J_{CF}$=32.1 Hz, C-8), 130.3 (C-2), 126.9 (C-3), 125.0 (q, $^3J_{CF}$=3.2 Hz, C-7), 124.4 (q, $^1J_{CF}$=272.5 Hz, C-11), 123.4 (q, $^3J_{CF}$=3.9 Hz, C-9), 118.6 (C-1), 21.5 (C-10).
^{19}F-NMR (376 MHz, $CDCl_3$): δ (ppm) = -62.53.

2,6-diferrocenylaniline (^{Fc}5-NH$_2$)

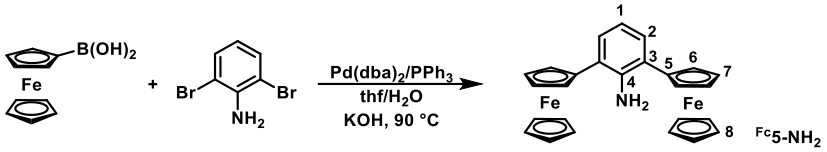

To a suspension of 2,6-dibromoaniline (1.15 g, 4.6 mmol, 1.0 eq), ferrocene boronic acid (2.5 g, 9.6 mmol, 2.1 eq), and KOH (1.3 g, 23 mmol, 5 eq) in 10 mL of water and 5 mL of THF, a solution of $Pd(dba)_2$ (27 mg, 46 µmol, 1 mol %) and PPh_3 (29 mg, 110 µmol, 2.4 mol%) in 5 mL of THF was added and the orange solution was heated to 90 °C for 2 days. After cooling to room temperature the reaction was stirred for one hour under air. THF was removed under vacuum and the resulting black aqueous phase was extracted with ether three times. The combined organic layers were then extracted three times with 20 mL of 5 M KOH solution and then dried over $MgSO_4$. After removal of the solvent the product was purified via column chromatography on silica using pentane/Et_2O (5 %) as the eluent (R_f=0.7). ^{Fc}**5-NH$_2$** was obtained as an orange solid (207 mg, 450 µmol, 10 %).

^{1}H-NMR (400 MHz, $CDCl_3$): δ (ppm) = 7.31 (d, $^3J_{HH}$=7.6 Hz, 2H, *H-2*), 6.71 (t, $^3J_{HH}$=7.6 Hz, 1H, *H-1*), 5.28 (s, 2H, *NH$_2$*), 4.62 (vt, $^3J_{HH}$=1.9 Hz, 4H, *H-6*), 4.37 (vt, $^3J_{HH}$=1.9 Hz, 4H, *H-7*), 4.21 (s, 10H, *H-8*).
^{13}C-NMR (101 MHz, $CDCl_3$): δ (ppm) = 142.5 (C-4), 129.1 (C-2), 122.3 (C-3), 117.5 (C-1), 86.2 (C-5), 69.3 (C-8), 68.6 (C-6), 68.3 (C-7).

2,6-difuranylaniline (^{Fur}5-NH$_2$)

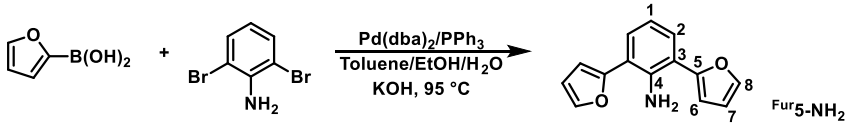

To a suspension of 2,6-dibromoaniline (2.4 g, 9.7 mmol, 1.0 eq), 2-furanylboronic acid (2.5 g, 22.4 mmol, 2.3 eq), and KOH (2.7 g, 49 mmol, 5 eq) in 35 mL of toluene, 6 mL of water and 6 mL of EtOH, a solution of $Pd(dba)_2$ (56 mg, 97 µmol, 1 mol %) and PPh_3 (61 mg, 232 µmol, 2.4 mol%)

in 2 mL of EtOH was added and the orange solution was heated to 95 °C for 3 days. After cooling to room temperature the reaction was stirred for one hour under air. The organic phase was then extracted three times with 20 mL of 5 M KOH solution. The combined organic layers were dried over $MgSO_4$. After removal of the solvent the product was purified via column chromatography on silica using pentane/ethyl acetate (10:1) as the eluent (R_f=0.6). **^{Fur}5-NH$_2$** was obtained as a yellow solid (437 mg, 1.7 mmol, 18 %).

^{1}H-NMR (400 MHz, $CDCl_3$): δ (ppm) = 7.53 (dd, $^3J_{HH}$=1.9 Hz, $^4J_{HH}$=0.7 Hz, 2H, *H-8*), 7.45 (d, $^3J_{HH}$=7.7 Hz, 2H, *H-2*), 6.84 (t, $^3J_{HH}$=7.7 Hz, 1H, *H-1*), 6.64 (dd, $^3J_{HH}$=3.4 Hz, $^4J_{HH}$=0.7 Hz, 2H, *H-6*), 6.54 (dd, $^3J_{HH}$=3.4 Hz, $^3J_{HH}$=1.9 Hz, 2H, *H-7*), 5.06 (s, 2H, *NH*$_2$).

^{13}C-NMR (101 MHz, $CDCl_3$): δ (ppm) = 153.2 (C-5), 141.7 (C-8), 140.8 (C-4), 128.1 (C-2), 118.0 (C-1), 117.5 (C-3), 111.5 (C-7), 107.4 (C-6).

2,6-dithiophenylaniline (^{Thio}5-NH$_2$)

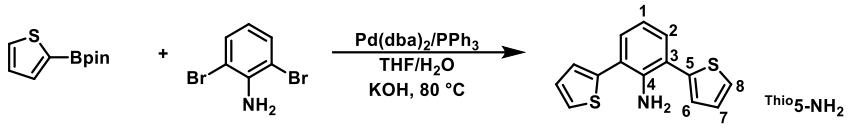

To a suspension of 2,6-dibromoaniline (1.25 g, 5.0 mmol, 1.0 eq), 2-thiopheneboronic acid (2.1 g, 10 mmol, 2.0 eq), and KOH (1.4 g, 25 mmol, 5 eq) in 10 mL of water and 5 mL of THF, a solution of $Pd(dba)_2$ (14 mg, 25 µmol, 0.5 mol %) and PPh_3 (18 mg, 70 µmol, 1.4 mol%) in 5 mL of THF was added and the orange solution was heated to 80 °C for 5 days. After cooling to room temperature the reaction was stirred for one hour under air. THF was removed under vacuum and the resulting black aqueous phase was extracted with ether three times. The combined organic layers were then extracted three times with 20 mL of 5 M KOH solution and then dried over $MgSO_4$. After removal of the solvent the product was purified via column chromatography on silica using pentane/ethyl acetate (10:1) as the eluent (R_f=0.8). **^{Thio}5-NH$_2$** was obtained as a white solid (120 mg, 500 µmol, 10 %).

^{1}H-NMR (400 MHz, $CDCl_3$): δ (ppm) = 7.37 (dd, $^3J_{HH}$=5.2 Hz, $^4J_{HH}$=1.1 Hz, 2H, *H-8*), 7.26 (d, $^3J_{HH}$=7.6 Hz, 2H, *H-2*), 7.24 (dd, $^3J_{HH}$=3.5 Hz, $^4J_{HH}$=1.1 Hz, 2H, *H-6*), 7.14 (dd, $^3J_{HH}$=3.5 Hz, $^3J_{HH}$=5.2 Hz, 2H, *H-7*), 6.81 (dd, $^3J_{HH}$=7.6 Hz, 1H, *H-1*), 4.38 (s, 2H, *NH*$_2$).

^{13}C-NMR (101 MHz, $CDCl_3$): δ (ppm) = 142.4 (C-4), 141.1 (C-5), 131.2 (C-2), 127.7 (C-7), 126.4 (C-6), 125.7 (C-8), 120.5 (C-3), 118.0 (C-1).

2,6-dilutidinylaniline (^{Lut}5-NH$_2$)

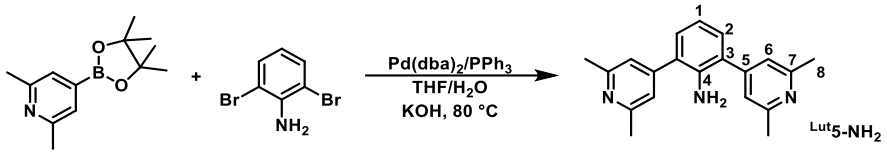

To a suspension of 2,6-dibromoaniline (1.3 g, 5.0 mmol, 1.0 eq), 2,6-lutidine-4-boronic acid (2.3 g, 10 mmol, 2.0 eq), and KOH (1.4 g, 25 mmol, 5 eq) in 20 mL of water and 10 mL of THF, a solution of $Pd(dba)_2$ (56 mg, 100 µmol, 2 mol %) and PPh_3 (73 mg, 280 µmol, 5.6 mol%) in 10 mL of THF was added and the orange solution was heated to 80 °C for 3 days. After cooling to room temperature the reaction was stirred for one hour under air. THF was removed under vacuum and the resulting black aqueous phase was extracted with ether three times. The combined organic layers were then extracted three times with 20 mL of 5 M KOH solution and then dried over $MgSO_4$. After removal of the solvent the product was purified via recrystallization from THF at -30 °C. **^{Lut}5-NH$_2$** was obtained as an off-white solid (1.2 g, 4 mmol, 79 %).

^{1}H-NMR (400 MHz, $CDCl_3$): δ (ppm) = 7.10 (m, 6H, *H-2/6*), 6.89 (t, $^3J_{HH}$=7.6 Hz, 1H, *H-1*), 2.58 (s, 12H, *H-8*).

^{13}C-NMR (101 MHz, $CDCl_3$): δ (ppm) = 158.7 (C-7), 148.2 (C-5), 140.3 (C-4), 130.2 (C-2), 125.9 (C-3), 120.7 (C-6), 118.7 (C-1), 24.7 (C-8).

6.4.3 Synthesis and Characterization of Salicylaldimines

[2,6-di(naphthalene-1-yl)-phenyl]-4,6-diiodosalicylaldimine (^{Naph}5-N^OH)

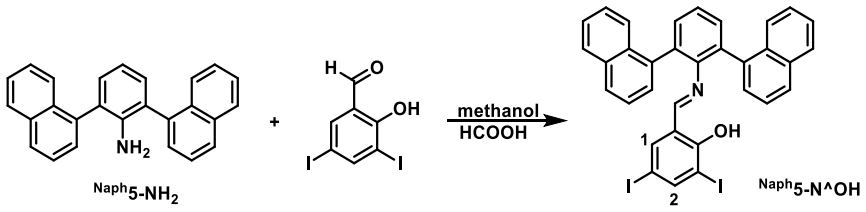

Under air, 345 mg of the 2,6-dinaphthalenylaniline (1 mmol, 1.0 eq) and 449 mg of 3,5-diiodosalicylaldehyde (1.2 mmol, 1.2 eq) were suspended in 7 mL of methanol and three drops of formic acid were added. The suspension was heated to 65 °C for 1 h whereby a yellow precipitate formed. After stirring at room temperature over night the yellow solid was centrifuged off and washed with 3 mL of methanol three times. After drying under vacuum, **^{Naph}5-N^OH** was obtained as a yellow solid (673 mg, 960 µmol, 96 %).

^{1}H-NMR (400 MHz, $CDCl_3$): δ (ppm) = 7.89 – 7.79 (m, 4H), 7.76 – 7.71 (m, 1H), 7.70 (dd, $^3J_{HH}$=2.08 Hz, $^3J_{HH}$=4.81 Hz, 1H, *H-2*), 7.68 – 7.63 (m, 1H), 7.56 – 7.41 (m, 12H), 6.58 (dd, $^3J_{HH}$=2.08 Hz, $^3J_{HH}$=5.04 Hz, 1H, *H-1*).

N-[2-(3,5-dimethyl-3',5'-bis(trifluoromethyl)terphenyl]-4,6-diiodosalicyl-aldimine ($^{Me/CF3}$1-N^OH)

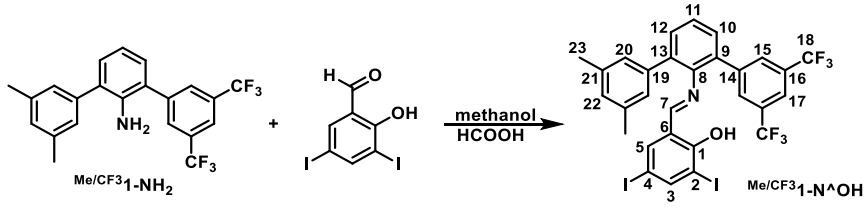

Under air, $^{Me/CF3}$**1-NH$_2$** (1.0 g, 2.34 mmol, 1.0 eq), 3,5-diiodosalicylaldehyde (875 mg, 2.34 mmol, 1.0 eq) and 3 drops of formic acid were suspended in 12 mL of methanol and heated to 65 °C for 60 minutes while all starting materials dissolved. The reaction mixture was stirred at room temperature overnight. After cooling to 0 °C, the orange product was centrifuged off and washed with small portions of cold methanol. The yellow solid was washed one time with pentane and dried under vacuum. $^{Me/CF3}$**1-N^OH** was obtained as a yellow solid (1.5 g, 1.9 mmol, 82 %).

^{1}H-NMR (400 MHz, $CDCl_3$): δ (ppm) 13.41 (s, 1H, *OH*), 8.00 (d, $^4J_{HH}$=2.0 Hz, 1H, *H-3*), 7.84 (s, 2H, *H-15*), 7.82 (s, 1H, *H-17*), 7.77 (s, 1H, *H-7*), 7.50 (m, 1H, *H-10*), 7.41 (m, 2H, *H-11/12*), 7.10 (d, $^4J_{HH}$=2.0 Hz, 1H, *H-5*), 6.95 (s, 2H, *H-20*), 6.92 (s, 1H, *H-22*), 2.28 (s, 6H, *H-23*).

^{13}C-NMR (101 MHz, $CDCl_3$): δ (ppm) = 167.0 (C-7), 159.9 (C-1), 149.7 (C-3), 144.1 (C-8), 141.4 (C-19), 140.3 (C-5), 138.4 (C-21), 138.3 (C-9), 135.4 (C-13), 132.4 (C-14), 132.1 (C-10), 131.8 (q, $^2J_{CF}$=33.6 Hz, C-16), 130.0 (m, C-15), 129.7 (C-12), 129.3 (C-22), 127.5 (C-20), 126.9 (C-11), 123.3 (q, $^1J_{CF}$=273.7 Hz, C-18), 121.3 (m, C-17), 119.8 (C-6), 86.9 (C-2), 80.0 (C-4), 21.4 (C-23).

^{19}F-NMR (376 MHz, $CDCl_3$): δ (ppm) = -62.62.

N-[2-(3,3'-dimethyl-5,5'-bis(trifluoromethyl)terphenyl]-4,6-diiodosalicyl-aldimine ($^{(MeCF3)}$1-N^OH)

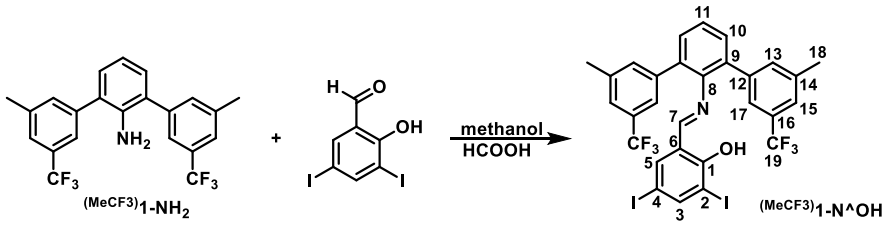

Under air, $^{(MeCF3)}$**1-NH$_2$** (0.6 g, 1.46 mmol, 1.0 eq), 3,5-diiodosalicylaldehyde (548 mg, 1.46 mmol, 1.0 eq) and 3 drops of formic acid were suspended in 8 mL of methanol and heated to 65 °C for 60 minutes while all starting materials dissolved. The reaction mixture was stirred at room temperature for 2 days. After cooling to 0 °C, the orange product was centrifuged off

and washed with small portions of cold methanol. After drying under vacuum, $^{(MeCF_3)}$**1-N^OH** was obtained as a yellow solid (841 mg, 1.1 mmol, 75 %).

^{1}H-NMR (400 MHz, $CDCl_3$): δ (ppm) = 13.45 (s, 1H, *OH*), 8.00 (d, $^4J_{HH}$=2.0 Hz, 1H, *H-3*), 7.73 (s, 1H, *H-7*), 7.43 (m, 5H, *H-17/10/11*), 7.37 (s, 2H, *H-13*), 7.36 (s, 2H, *H-15*), 7.10 (d, $^4J_{HH}$=2.0 Hz, 1H, *H-5*), 2.39 (s, 6H, *H-18*).

^{13}C-NMR (101 MHz, $CDCl_3$): δ (ppm) = 166.7 (C-7), 159.8 (C-1), 149.6 (C-3), 144.2 (C-8), 140.3 (C-5), 139.6 (C-12), 139.3 (C-14), 133.9 (C-9), 133.8 (C13-), 131.1 (q, $^2J_{CF}$=32.0 Hz, C-16), 130.8 (C-10), 126.9 (C-11), 124.9 (q, $^3J_{CF}$=3.8 Hz, C-15), 124.2 ($^1J_{CF}$=273.0 Hz, C-19), 123.8 (q, $^3J_{CF}$=3.7 Hz, C-17), 119.8 (C-6), 86.9 (C-2), 80.0 (C-4), 21.5 (C-18).

^{19}F-NMR (376 MHz, $CDCl_3$): δ (ppm) = -62.71.

N-[2,6-diferrocenylphenyl]-4,6-diiodosalicylaldimine (^{Fc}5-N^OH)

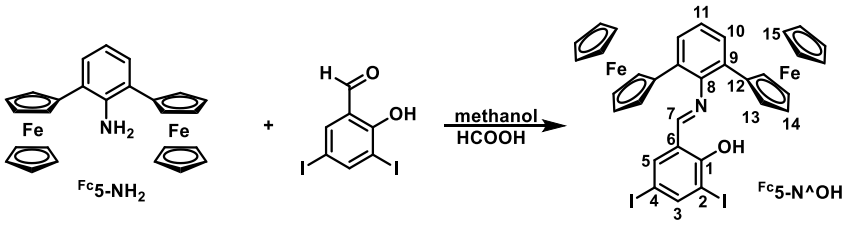

Under air, the 2,6-diferrocenylaniline (200 mg, 383 µmol, 1.0 eq), 3,5-diiodosalicylaldehyde (216 mg, 575 µmol, 1.5 eq) and 3 drops of formic acid were suspended in 7 mL of methanol and heated to 65 °C for 60 minutes while all starting materials dissolved. The reaction mixture was stirred at room temperature for overnight. After cooling to 0 °C, the orange product was centrifuged off and washed with small portions of cold methanol. After drying under vacuum, ^{Fc}**5-N^OH** was obtained as a yellow solid (166 mg, 203 µmol, 53 %).

^{1}H-NMR (400 MHz, $CDCl_3$): δ (ppm) = 14.22 (s, 1H, *OH*), 8.06 (d, $^4J_{HH}$=2.0 Hz, 1H, *H-3*), 7.70 (d, $^3J_{HH}$=7.8 Hz, 2H, *H-10*), 7.67 (s, 1H, *H-7*), 7.23 (m, 2H, *H-5/11*), 4.34 (vt, $^3J_{HH}$=1.8 Hz, 4H, *H-13*), 4.21 (vt, $^3J_{HH}$=1.8 Hz, 4H, *H-14*), 4.10 (s, 10H, *H-15*).

^{13}C-NMR (101 MHz, $CDCl_3$): δ (ppm) = 166.0 (C-7), 160.4 (C-1), 149.3 (C-3), 145.0 (C-8), 140.4 (C-5), 131.0 (C-9), 129.2 (C-10), 125.4 (C-11), 120.3 (C-6), 87.4 (C-2), 84.4 (C-12), 79.9 (C-4), 70.3 (C-13), 69.8 (C-15), 68.7 (C-14).

N-[2,6-difuranylphenyl]-4,6-diiodosalicylaldimine (^{Fur}5-N^OH)

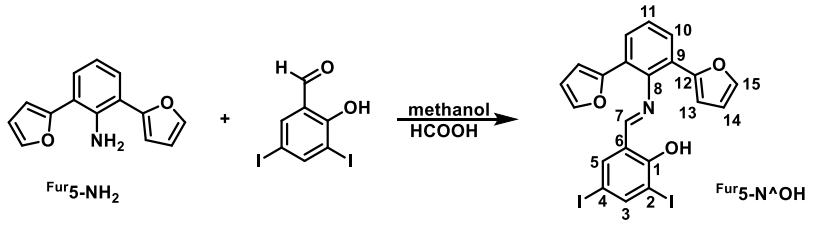

Under air, the 2,6-difuranylaniline (430 mg, 1.7 mmol, 1.0 eq), 3,5-diiodosalicylaldehyde (636 mg, 1.7 mmol, 1.0 eq) and 3 drops of formic acid were suspended in 8 mL of methanol and heated to 65 °C for 60 minutes while all starting materials dissolved. The reaction mixture was stirred at room temperature for 1 h. After cooling to 0 °C, the orange product was centrifuged off and washed with small portions of cold methanol. After drying under vacuum, **^{Fur}5-N^OH** was obtained as a yellow solid (879 mg, 1.5 mmol, 89 %).

^{1}H-NMR (400 MHz, $CDCl_3$): δ (ppm) = 13.96 (s, 1H, *OH*), 8.16 (d, $^4J_{HH}$=2.0 Hz, 1H, *H-3*), 8.11 (s, 1H, *H-7*), 7.76 (d, $^3J_{HH}$=7.9 Hz, 2H, *H-10*), 7.48 (d, $^4J_{HH}$=2.0 Hz, 1H, *H-5*), 7.43 (m, 2H, *H-15*), 7.34 (t, $^3J_{HH}$=7.9 Hz, 1H, *H-11*), 6.38 (dd, $^3J_{HH}$=1.8 Hz, $^4J_{HH}$=3.4 Hz, 2H, *H-13*), 6.34 (d, $^3J_{HH}$=3.4 Hz, 2H, *H-14*).
^{13}C-NMR (101 MHz, $CDCl_3$): δ (ppm) = 167.2 (C-7), 160.2 (C-1), 150.6 (C-12), 150.0 (C-3), 142.3 (C-15), 142.2 (C-8), 140.9 (C-5), 126.7 (C-10), 126.2 (C-11), 123.4 (C-9), 120.3 (C-6), 112.0 (C-13), 110.1 (C-14), 87.5 (C-2), 80.5 (C-4).

N-[2,6-di(thiophenyl)phenyl]-4,6-diiodosalicylaldimine (^{Thio}5-N^OH)

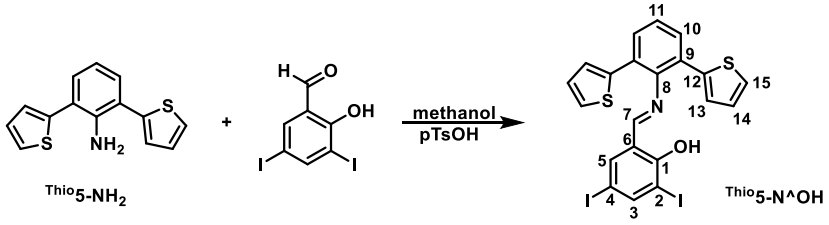

Under air, the 2,6-dithiophenylaniline (120 mg, 500 µmol, 1.0 eq), 3,5-diiodosalicylaldehyde (374 mg, 1.0 mmol, 2.0 eq) and a catalytic amount of *p*TsOH were suspended in 10 mL of methanol and heated to 65 °C for 60 minutes while all starting materials dissolved. The reaction mixture was stirred at room temperature for 1 h. After cooling to 0 °C, the orange product was centrifuged off and washed with small portions of cold methanol and pentane. After drying under vacuum, **^{Thio}5-N^OH** was obtained as a yellow solid (297 mg, 485 µmol, 97 %).

^{1}H-NMR (400 MHz, $CDCl_3$): δ (ppm) = 13.62 (s, 1H, *OH*), 8.12 (d, $^4J_{HH}$=2.0 Hz, 1H, *H-3*), 8.07 (s, 1H, *H-7*), 7.60 (d. $^3J_{HH}$=7.8 Hz, 2H, *H-10*), 7.39 (d, $^4J_{HH}$=2.0 Hz), 7.32 (m, 3H, *H-11/15*), 7.14 (dd, $^3J_{HH}$=3.6 Hz, $^4J_{HH}$=1.1 Hz, 2H, *H-13*), 7.02(d, $^3J_{HH}$=3.6 Hz, $^3J_{HH}$=5.1 Hz, 2H, *H-14*).

^{13}C-NMR (101 MHz, $CDCl_3$): δ (ppm) = 168.6 (C-7), 160.6 (C-1), 150.3 (C-3), 144.7 (C-8), 141.4 (C-5), 140.6 (C-12), 130.6 (C-10), 127.8 (C-9), 127.8 (C-13/C-14), 127.2 (C-15), 126.6 (C-11), 120.9 (C-6), 87.4 (C-2), 80.4 (C-4).

N-[2,6-di(2,6-lutidinyl)phenyl]-4,6-diiodosalicylaldimine (^{Lut}5-N^OH)

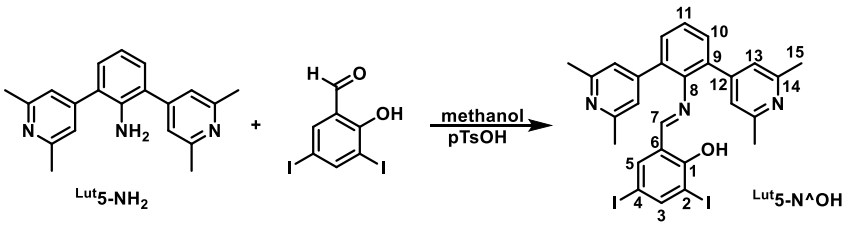

Under air, the 2,6-dilutidinylaniline (500 mg, 1.65 mmol, 1.0 eq), 3,5-diiodosalicylaldehyde (1.23 g, 3.3 mmol, 2.0 eq) and a catalytic amount of *p*TsOH were suspended in 6 mL of methanol and heated to 65 °C for 60 minutes while all starting materials dissolved. The reaction mixture was stirred at room temperature for 2 h. After cooling to 0 °C, the orange product was centrifuged off and washed with small portions of cold methanol and pentane. After drying under vacuum, **^{Lut}5-N^OH** was obtained as a yellow solid (424 mg, 643 µmol, 39 %).

^{1}H-NMR (400 MHz, $CDCl_3$): δ (ppm) = 13.54 (s, 1H, *OH*), 7.72 (d, $^{4}J_{HH}$=2.3 Hz, 1H, *H-3*), 7.13 (d, $^{3}J_{HH}$=6.8 Hz, 2H, *H-10*), 7.06 (m, 1H, *H-11*), 6.79 (s, 4H, *H-13*), 6.61 (d, $^{4}J_{HH}$=2.3 Hz, 1H, *H-5*), 2.44 (s, 12H, *H-16*).
^{13}C-NMR (101 MHz, $CDCl_3$): δ (ppm) = 166.8 (C-7), 160.2 (C-1), 158.7 (C-14), 145.0 (C-3), 147.1 (C-12), 144.6 (C-8), 140.7 (C-5), 133.6 (C-9), 130.8 (C-10), 126.7 (C-11), 120.8 (C-13), 119.9 (C-6), 87.5 (C-2), 80.5 (C-4), 24.6 (C-16).

6.4.4 Synthesis and Characterization of Complexes

{*N*-[2,6-bis(naphthalene-1-yl)phenyl]-4,6-diiodosalicylaldiminato-κ^2-*N,O*}methylpyridine-nickel(II) (^{Naph}5-pyr)

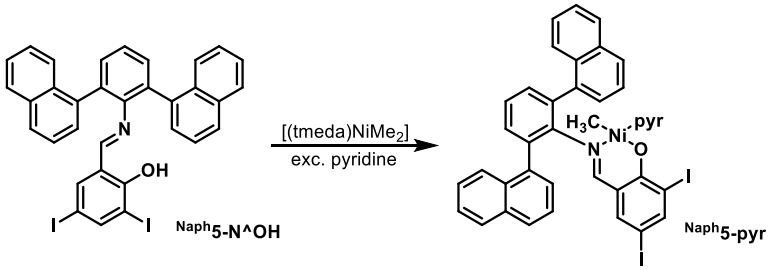

In a 25 mL Schlenk tube 351 mg (500 µmol, 1.0 eq) of **^{Naph}5-N^OH** and 107 mg (525 µmol, 1.05 eq) of [(tmeda)$NiMe_2$] were cooled to -45 °C and dispersed in 5 mL of toluene and 100 µL (1.25 mmol, 2.5 eq). The mixture was allowed to slowly warm to 0 °C over 45 min while the color changed to dark red. After removing all volatiles under vacuum, the red-orange solid was

redissolved in benzene and filtered over a syringe filter. Sublimation of the benzene under vacuum yielded ^{Naph}**5-pyr** as a red-orange solid (361 mg, 423 µmol, 85 %).

NMR: NMR assignment of ^{Naph}**5-pyr** was not possible due to overlapped signals and the presence of two isomers (probably due to hindered rotation) with resonances for the Ni-Me groups arising at -0.75 and -0.93 ppm, respectively (in CD_2Cl_2) (ratio of 1 : 1.6).

Elemental Analysis (%) for $C_{39}H_{28}I_2N_2NiO$: Found (Calculated): C 54.25 (54.90); H 3.75 (3.31); N 3.87 (3.28).

{*N*-[2-(3,5-dimethyl-3',5'-bis(trifluoromethyl)terphenyl]-4,6-diiodosalicyl-aldiminato-κ^2-*N,O*}-methylpyridinenickel(II) ($^{Me/CF3}$1-pyr)

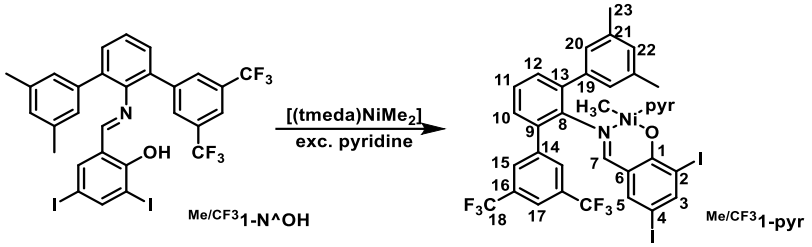

In a 25 mL Schlenk tube 383 mg (500 µmol, 1.0 eq) of $^{Me/CF3}$**1-N^OH** and 107 mg (525 µmol, 1.05 eq) of [(tmeda)$NiMe_2$] were cooled to -45 °C and dispersed in 5 mL of toluene and 100 µL (1.25 mmol, 2.5 eq). The mixture was allowed to slowly warm to 0 °C over 45 min while the color changed to dark red. After removing all volatiles under vacuum, the red-orange solid was redissolved in benzene and filtered over a syringe filter. Sublimation of the benzene under vacuum yielded $^{Me/CF3}$**1-pyr** as a red-orange solid (417 mg, 455 µmol, 91 %).

^{1}H-NMR (400 MHz, CD_2Cl_2): δ (ppm) = 8.37 (d, $^3J_{HH}$=5.2 Hz, 2H, *o-H pyr*), 8.21 (s, 2H, *H-15*), 7.98 (s, 1H, *H-17*), 7.87 (d, $^4J_{HH}$=2.3 Hz, 1H, *H-3*), 7.64 (t, $^3J_{HH}$=7.7 Hz, 1H, *p-H pyr*), 7.49 (s, 1H, *H-7*), 7.46 (m, 1H, *H-11*), 7.40 (m, 2H, *H-10/12*), 7.26 (s, 2H, *H-20*), 7.14 (vt, $^3J_{HH}$=6.9 Hz, 2H, *m-H pyr*), 7.10 (s, 1H, *H-22*), 7.06 (d, $^4J_{HH}$=2.3 Hz, 1H, *H-5*), 2.40 (s, 6H, *H-23*), -1.02 (s, 3H, *Ni-CH$_3$*).

^{13}C-NMR (101 MHz, CD_2Cl_2): δ (ppm) = 167.6 (C-7), 163.7 (C-1), 152.0 (*o*-C pyr), 150.1 (C-8), 149.5 (C-3), 142.6 (C-19), 142.0 (C-5), 139.2 (C-9), 138.5 (C-21), 136.9 (C-13), 133.2 (C-14), 132.0 (C-11), 131.9 (q, $^2J_{CF}$=33.1 Hz, C-16), 131.2 (m, C-15), 129.9 (C-10), 129.6 (C-22), 128.6 (C-20), 127.1 (C-12), 124.1 (q, $^1J_{CF}$=272.6 Hz, C-18), 123.9 (*m*-C pyr), 121.6 (m, C-17), 120.7 (C-6), 96.9 (C-2), 72.1 (C-4), 21.8 (C-23), -7.5 (Ni-CH_3).

^{19}F-NMR (376 MHz, $CDCl_3$): δ (ppm) = -62.53.

Elemental Analysis (%) for $C_{35}H_{26}F_6I_2N_2NiO$: Found (Calculated): C 45.95 (45.84); H 3.51 (2.86); N 3.92 (3.05).

{*N*-[2-(3,3'-dimethyl-5',5'-bis(trifluoromethyl)terphenyl]-4,6-diiodosalicylaldiminato-κ^2-*N,O*}-methylpyridinenickel(II) ($^{(MeCF3)}$1-pyr)

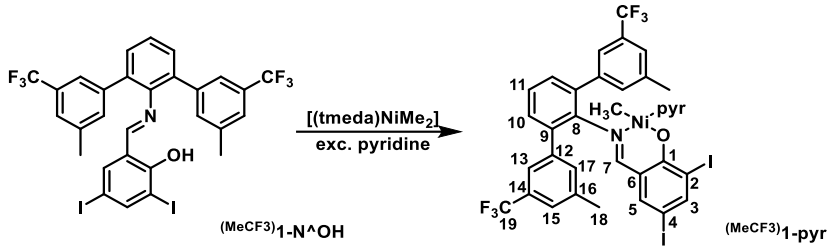

In a 25 mL Schlenk tube 383 mg (500 µmol, 1.0 eq) of $^{(MeCF_3)}$**1-N^OH** and 107 mg (525 µmol, 1.05 eq) of [(tmeda)$NiMe_2$] were cooled to -45 °C and dispersed in 5 mL of toluene and 100 µL (1.25 mmol, 2.5 eq). The mixture was allowed to slowly warm to 0 °C over 45 min while the color changed to dark red. After removing all volatiles under vacuum, the red-orange solid was redissolved in benzene and filtered over a syringe filter. Sublimation of the benzene under vacuum yielded $^{(MeCF_3)}$**1-pyr** as a red-orange solid (389 mg, 424 µmol, 85 %).

^{1}H-NMR (400 MHz, CD_2Cl_2): δ (ppm) = 8.36 (d, $^3J_{HH}$=5.2 Hz, 2H, *o-H pyr*), 7.87 (m, 3H, *H-3/13*), 7.63 (t, $^3J_{HH}$=7.7 Hz, 1H, *p-H pyr*), 7.59 (s, 2H, *H-17*), 7.53 (s, 2H, *H-15*), 7.47 (s, 1H, *H-7*), 7.42 (m, 3H, *H-10/11*), 7.13 (vt, $^3J_{HH}$=7.0 Hz, 2H, *m-H pyr*), 7.05 (d, $^4J_{HH}$=2.3 Hz, 1H, *H-5*), 2.45 (s, 6H, *H-18*), -1.03 (s, 3H, *Ni-CH_3*).
^{13}C-NMR (101 MHz, CD_2Cl_2): δ (ppm) = 167.6 (C-7), 163.6 (C-1), 152.0 (*o*-C pyr), 150.1 (C-8), 149.5 (C-3), 142.1 (C-5), 140.6 (C-12), 139.7 (C-16), 137.2 (*p*-C pyr), 135.2 (m, C-17), 135.0 (C-9), 131.0 (q, $^2J_{CF}$=31.8 Hz, C-14), 130.9 (C-10), 127.1 (C-11), 125.2 (q, $^3J_{CF}$=3.8 Hz, C-15), 125.0 (q, $^1J_{CF}$=272.0 Hz, C-19), 124.7 (q, $^3J_{CF}$=3.9 Hz, C-13), 123.9 (*m*-C pyr), 120.8 (C-6), 96.8 (C-2), 72.1 (C-4), 21.8 (C-18), -7.7 (Ni-CH_3).
^{19}F-NMR (376 MHz, $CDCl_3$): δ (ppm) = -62.73.
Elemental Analysis (%) for $C_{35}H_{26}F_6I_2N_2NiO$: Found (Calculated): C 45.69 (45.84); H 3.54 (2.86); N 3.47 (3.05).

{*N*-[2,6-bis(ferrocenyl)phenyl]-4,6-diiodosalicylaldiminato-κ^2-*N,O*}-methylpyridine-nickel(II) (^{Fc}5-pyr)

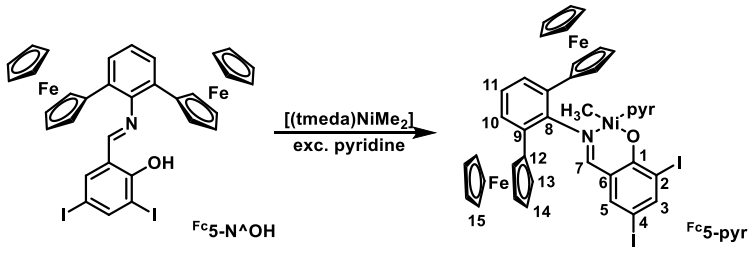

In a 25 mL Schlenk tube 44 mg (50 µmol, 1.0 eq) of ^{Fc}**5-N^OH** and 10 mg (50 µmol, 1.0 eq) of [(tmeda)$NiMe_2$] were dissolved in 2 mL of benzene and 100 µL (1.25 mmol, 25 eq). The dark red solution was stirred at room temperature for 1 hour. After sublimation of benzene under

vacuum, the orange solid was washed with small portions of pentane. **^{Fc}5-pyr** was obtained as red-orange solid (34 mg, 35 µmol, 70 %).

^{1}H-NMR (400 MHz, CD_2Cl_2): δ (ppm) = 8.66 (d, $^3J_{HH}$=5.3 Hz, 2H, *o-H pyr*), 7.93 (d, $^4J_{HH}$=2.3 Hz, 1H, *H-3*), 7.69 (d, $^3J_{HH}$=7.7 Hz, 2H, *H-10*), 7.66 (t, $^3J_{HH}$=7.6 Hz, 1H, *p-H pyr*), 7.29 (s, 1H, *H-7*), 7.20 (m, 3H, *H-11/m-H pyr*), 7.09 (d, $^4J_{HH}$=2.3 Hz, 1H, *H-5*), 5.45, 4.67, 4.46, and 4.42 (m, 4x2H, *H-13/14*), 4.10 (s, 10H, *H-15*), -1.02 (s, 3H, *Ni-CH_3*).

^{13}C-NMR (101 MHz, CD_2Cl_2): δ (ppm) = 166.4 (C-7), 163.9 (C-1), 152.5 (*o*-C pyr), 149.6 (C-8), 149.1 (C-3), 142.3 (C-5), 137.1 (*p*-C pyr), 132.9 (C-9), 128.8 (C-10), 125.7 (C-11), 124.0 (*m*-C pyr), 121.4 (C-6), 97.1 (C-2), 84.5 (C-12), 72.0 (C-4), 71.9 , 71.7 , 69.3, and 69.1 (C-13/14), 70.3 (C-15), -8.2 (Ni-CH_3).

Elemental Analysis (%) for $C_{39}H_{32}Fe_2I_2N_2NiO$: Found (Calculated): C 48.39 (48.24); H 3.96 (3.34); N 3.28 (4.22).

{*N*-[2,6-bis(furanyl)phenyl]-4,6-diiodosalicylaldiminato-κ^2-*N,O*}-methylpyridinenickel(II) (^{Fur}5-pyr)

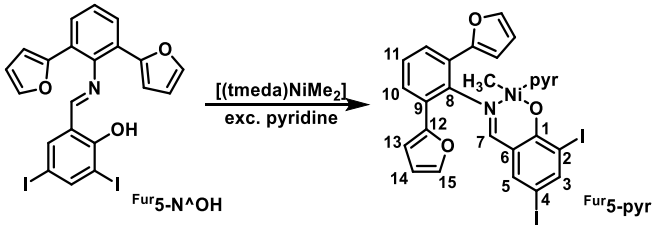

In a 25 mL Schlenk tube 291 mg (500 µmol, 1.0 eq) of **^{Fur}5-N^OH** and 107 mg (525 µmol, 1.05 eq) of [(tmeda)$NiMe_2$] were cooled to -45 °C and dispersed in 5 mL of toluene and 100 µL (1.25 mmol, 2.5 eq). The mixture was allowed to slowly warm to 0 °C over 45 min while the color changed to dark red. After removing all volatiles under vacuum, the red-orange solid was redissolved in benzene and filtered over a syringe filter. Sublimation of the benzene under vacuum yielded **^{Fur}5-pyr** as a red-orange solid (349 mg, 476 µmol, 95 %).

Crystals suitable for single x-ray diffraction analysis were obtained by slow evaporation of solvent from a benzene solution of complex **^{Fur}5-pyr** (20 mg in 0.5 mL of benzene).

^{1}H-NMR (400 MHz, CD_2Cl_2): δ (ppm) = 8.78 (d, $^3J_{HH}$=6.1 Hz, 2H, *o-H pyr*), 8.01 (d, $^4J_{HH}$=2.2 Hz, 1H, *H-3*), 7.86 (d, $^3J_{HH}$=7.9 Hz, 2H, *H-10*), 7.77 (d, $^3J_{HH}$=3.5 Hz, 2H, *H-15*), 7.70 (tt, $^3J_{HH}$=7.8 Hz, $^4J_{HH}$=1.6 Hz, 1H, *p-H pyr*), 7.61 (d, $^3J_{HH}$=1.7 Hz, 2H, *H-13*), 7.56 (s, 1H, *H-7*), 7.35 (t, $^3J_{HH}$=7.9 Hz, 1H, *H-11*), 7.25 (d, $^4J_{HH}$=2.2 Hz, 1H, *H-5*), 7.23 (vt, $^3J_{HH}$=7.0 Hz, 2H, *m-H pyr*), 6.66 (dd, $^3J_{HH}$=3.5 Hz, $^3J_{HH}$=1.7 Hz, 2H, *H-14*), -1.17 (s, 3H, *Ni-CH_3*).

^{13}C-NMR (101 MHz, CD_2Cl_2): δ (ppm) = 167.4 (C-7), 164.4 (C-1), 152.7 (*o*-C pyr), 151.0 (C-12), 149.8 (C-3), 145.7 (C-8), 142.7 (C-5), 142.7 (C-13), 137.4 (*p*-C pyr), 126.7 (C-11), 125.8 (C-9), 125.7 (C-10), 124.2 (*m*-C pyr), 121.8 (C-6), 112.7 (C-14), 112.5 (C-15), 97.3 (C-2), 72.6 (C-4), -8.5 (Ni-CH_3).

Elemental Analysis (%) for $C_{27}H_{20}I_2N_2NiO_3$: Found (Calculated): C 44.25 (42.25); H 3.07 (2.75); N 4.12 (3.82).

{*N*-[2,6-bis(thiophenyl)phenyl]-4,6-diiodosalicylaldiminato-κ^2-*N,O*}-methylpyridine-nickel(II) (^{Thio}**5-pyr**)

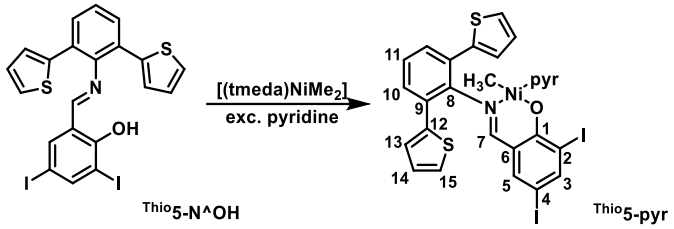

In a 25 mL Schlenk tube 123 mg (200 µmol, 1.0 eq) of ^{Thio}**5-N^OH** and 43 mg (210 µmol, 1.05 eq) of [(tmeda)$NiMe_2$] were cooled to -45 °C and dispersed in 2 mL of toluene and 40 µL (1.25 mmol, 2.5 eq). The mixture was allowed to slowly warm to 0 °C over 45 min while the color changed to dark red. After removing all volatiles under vacuum, the red-orange solid was redissolved in benzene and filtered over a syringe filter. Sublimation of the benzene under vacuum yielded ^{Thio}**5-pyr** as a red-orange solid (145 mg, 189 µmol, 95 %).

^{1}H-NMR (400 MHz, C_6D_6): δ (ppm) 8.57 (d, $^3J_{HH}$=4.9 Hz, 2H, *o-H pyr*), 8.06 (d, $^4J_{HH}$=2.2 Hz, 1H, *H-3*), 7.63 (d, $^3J_{HH}$=3.6 Hz, 2H, *H-15*), 7.49 (d, $^3J_{HH}$=7.8 Hz, 2H, *H-10*), 7.07 (s, 1H, *H-7*), 6.95 (t, $^3J_{HH}$=7.8 Hz, 1H, *H-11*), 6.90 (d, $^3J_{HH}$=5.1 Hz, 2H, *H-13*), 6.85 (d, $^4J_{HH}$=2.2 Hz, 1H, *H-5*), 6.81 (dd, $^3J_{HH}$=5.1 Hz, $^3J_{HH}$=3.6 Hz, 2H, *H-14*), 6.65 (t, $^3J_{HH}$=7.3, 1H, *p-H pyr*), 6.32 (vt, $^3J_{HH}$=6.4, 2H, *m-H pyr*), -0.57 (s, 3H, *Ni-CH_3*).
^{13}C-NMR (101 MHz, C_6D_6): δ (ppm) = 168.2 (C-7), 164.3 (C-1), 152.3 (*o*-C pyr), 149.7 (C-3), 148.2 (C-8), 142.6 (C-5), 140.8 (C-12), 136.0 (*p*-C pyr), 129.8 (C-9), 129.0 (C-10), 128.0 (C-15), 127.3 (C-14), 127.1 (C-13), 126.4 (C-11), 123.1 (*m*-C pyr), 121.5 (C-6), 97.9 (C-2), 72.7 (C-4), -7.8 (Ni-CH_3).
Elemental Analysis (%) for $C_{27}H_{20}I_2N_2NiOS_2$: Found (Calculated): C 43.18 (42.39); H 3.10 (2.63); N 3.92 (3.66); S 10.12 (8.38).

{*N*-[2,6-bis(lutidinyl)phenyl]-4,6-diiodosalicylaldiminato-κ^2-*N,O*}-methyl-pyridinenickel(II) (^{Lut}**5-pyr**)

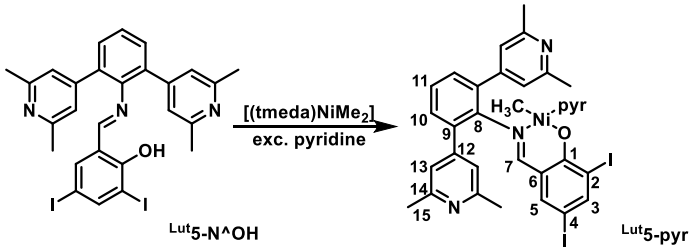

In a 25 mL Schlenk tube 164 mg (250 µmol, 1.0 eq) of ^{Lut}**5-N^OH** and 54 mg (263 µmol, 1.05 eq) of [(tmeda)$NiMe_2$] were cooled to -45 °C and dispersed in 2 mL of toluene and 500 µL (625 µmol, 25 eq). The mixture was allowed to slowly warm to 0 °C over 45 min while the color changed to dark red. After removing all volatiles under vacuum, the red-orange solid was

redissolved in 5 mL of benzene and filtered over a syringe filter. Sublimation of the benzene under vacuum yielded ^{Lut}**5-pyr** as a red-orange solid (180 mg, 223 µmol, 89 %).

NMR Spectroscopy: *The presence of multiple signals for the Ni-Me group in the ^{1}H NMR spectra and broadened signals indicates the presence of several species which was attributed to the formation of multinuclear species via intermolecular coordination of the lutidine moieties to the nickel.*

Elemental Analysis (%) for $C_{27}H_{20}I_2N_2NiOS_2$: Found (Calculated): C 47.02 (48.87); H 3.90 (3.73); N 6.46 (6.91).

6.4.5 Additional Spectra and Data

Differential Scanning Calorimetry

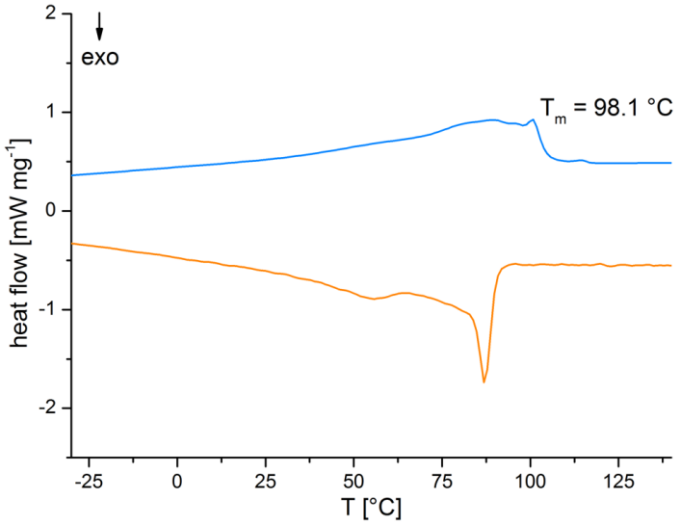

Figure 6.12: DSC trace of polymer obtained with $^{Me/CF_3}$**1-pyr** at 20 bar and 40 °C (entry 5, **Table 6.4**).

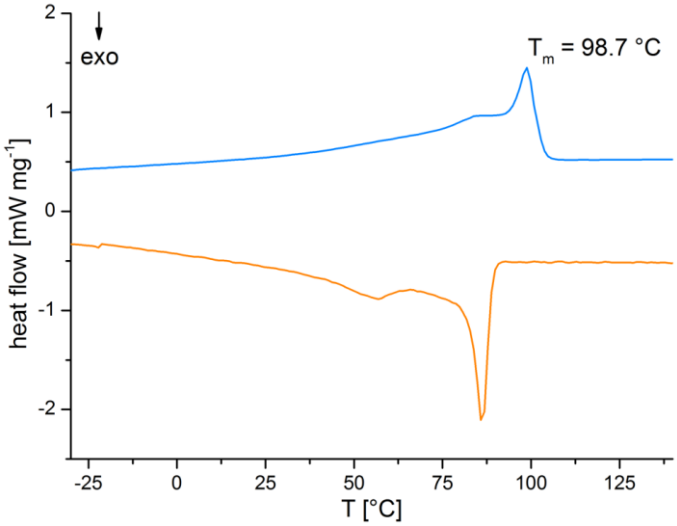

Figure 6.13: DSC trace of polymer obtained with $^{(MeCF_3)}$**1-pyr** at 20 bar and 40 °C (entry 6, **Table 6.4**).

Cyclic Voltammetry

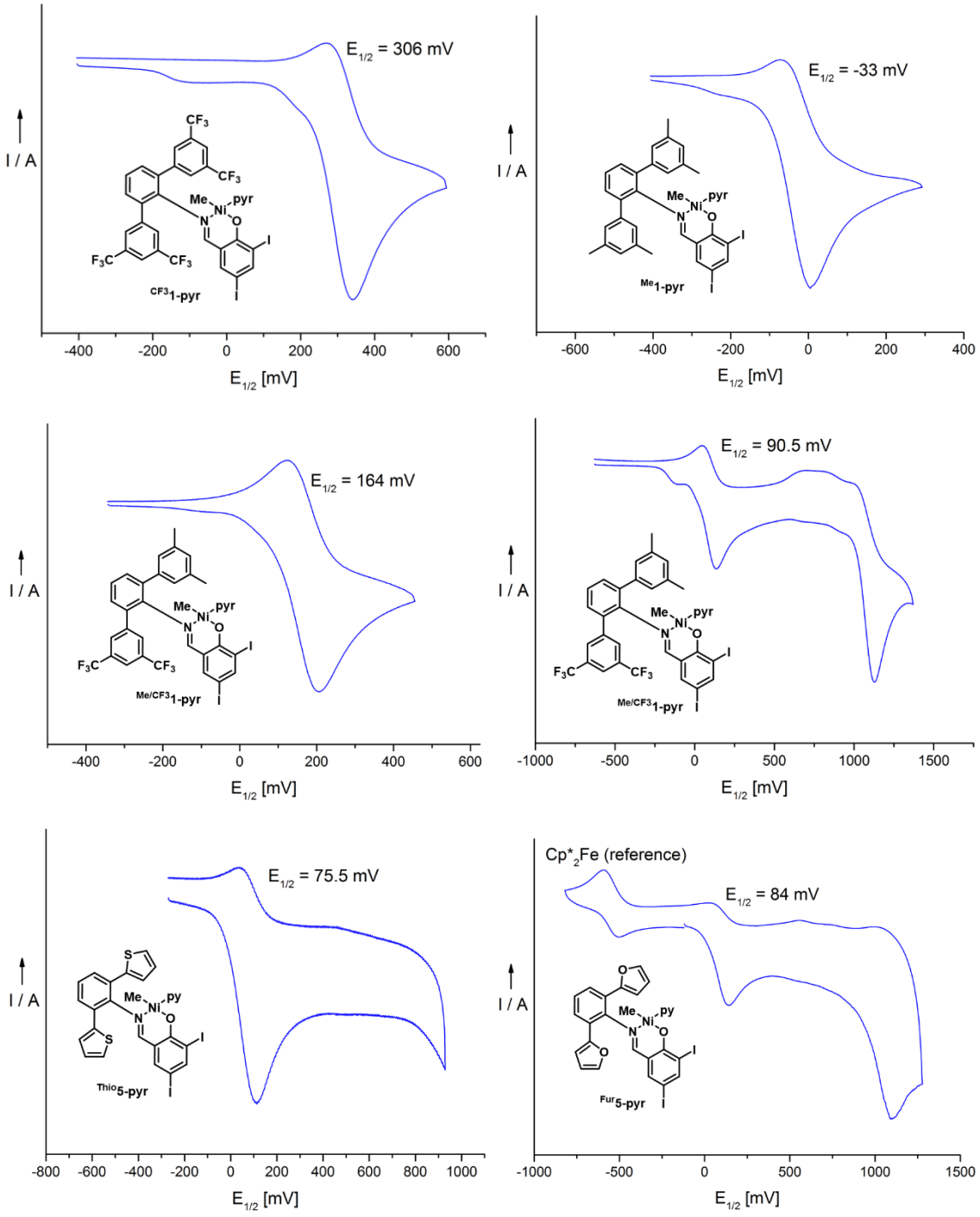

Figure 6.14: Cyclic voltammograms of selected Ni(II) salicylaldiminato complexes.

7 Conclusive Summary

Beyond the well-known applications of polyethylenes like HDPE or LDPE as thermoplastic materials, lower molecular weight ethylene oligomers can serve numerous functions. Concerning their synthesis, the Ziegler Alfol process is an illustrative and practically important example. Chain-growth on aluminum yields longer chain aluminum alkyls. Subsequent oxidation and hydrolysis affords linear long-chain terminal alcohols, stoichiometric in aluminum. Chain growth on metallocenes with simultaneous chain transfer reactions is employed for the production of linear polyethylene waxes. These are also functionalized by oxidation under severe conditions, to yield linear oligoethylenes with an undefined number of a mixture of different functional groups (primarily carboxylic acids) per chain. Precisely chain-end functionalized linear oligoethylenes are accessible by 'chain shuttling' processes. Like in the Ziegler Alfol process, functionalization occurs in a second step from main group metal or zinc alkyls in a stoichiometric fashion. Chain growth occurs catalytically on a smaller amount of transition metal catalyst. All these reported procedures afford linear wax-like oligoethylenes. Highly branched oligoethylenes would also be of interest as functional additives, for example in lubricants or surface modifiers. Considering possible approaches for their synthesis, the known capability of late transition metal catalysts to produce highly branched high molecular weight polyethylenes appears attractive. Cationic Pd(II) and Ni(II) α-diimine catalysts allow for the synthesis of highly branched, high molecular weight entirely amorphous rubbery material due to extensive chain walking during polymerization. For these complexes, bulky substituents on the diimine ligand are responsible for both the high molecular weights and high degrees of branching. Shielding of the apical positions of the square planar metal center at the same time increases the rate of chain propagation and suppresses chain termination reactions. At the same time β-hydride elimination is still very pronounced (without a subsequent chain transfer reaction) and results in extensive chain walking. In consequence, the Pd(II) complexes lacking bulky substituents afford low molecular weight moderately branched oligomers with very low activities and the Ni(II) analogues only afford linear α-olefins. Thus, for this type of catalyst the synthesis of highly branched material is usually limited to high molecular weights. For the

generation of branched oligoethylenes neutral Ni(II) κ^2-(*N,O*)-salicylaldiminato catalysts, especially *N*-terphenyl substituted representatives, are promising candidates (**Scheme 7.1**). In these complexes, substituents on the peripheral aromatic rings have a remarkable effect on the catalytic properties, despite their remoteness from the active center. Depending on the substituents' electronic nature, a broad range of different material properties are accessible. Electron withdrawing groups afford high molecular weight, linear polyethylene while more electron donating substituents favor branch formation and chain transfer and thus yield low molecular weight, highly branched oligomers. In general, there are very few examples of the synthesis of ethylene oligomers (< 5,000 g mol^{-1}) with high degrees of branching, and such materials have been little characterized and studied. Functionalized, much less precisely monofunctionalized materials have not yet been reported.

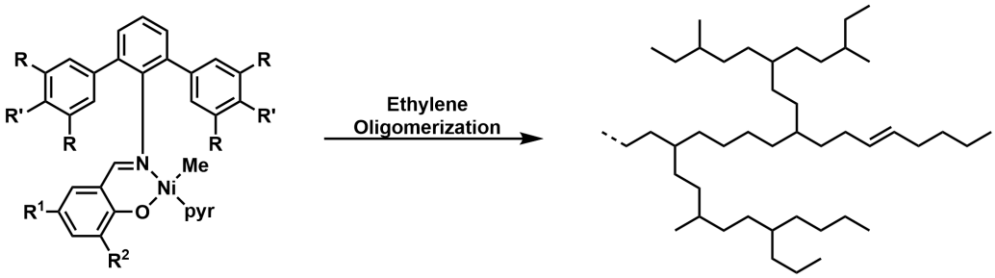

Scheme 7.1: Branching ethylene oligomerization with *N*-terphenyl Ni(II) salicylaldiminato complexes.

In this thesis, highly branched oligomers were synthesized and investigated systematically for the first time. A special interest was dedicated to a more detailed insight in the microscopic chain architecture of such branched oligoethylenes obtained by Ni(II) salicylaldiminato catalysts. With 33 new κ^2-(*N,O*)-salicylaldiminato nickel complexes synthesized, a wide variety of oligomers with different material properties were synthesized and investigated. This allowed for a detailed understanding of the dependence of polymer molecular weights, degrees of branching, and the microstructure on the catalyst design. Additionally, fine tuning of theses material properties was probed with temperature and ethylene pressure dependent oligomerization studies. Versatile and more importantly selective functionalization of these oligomers for the first time allowed for the synthesis of monofunctional oligoethylenes with a hyperbranched microstructure, giving access to a completely new class of functional oligomers.

In Chapter 3, a detailed oligomerization study at different temperatures and ethylene pressures was carried out with the known complex ^{Me}**1-pyr**. The catalyst is highly active under all reaction conditions studied with turnover numbers of up to 50,000 mol [C_2H_4] mol^{-1} [Ni]. Molecular weights and degrees of branching were found to be dependent on both the ethylene concentration as well as on the reaction temperature. At high temperatures and low ethylene

pressures, lower molecular weight oligomers with fewer branches are obtained (**Figure 7.1**, left). This is attributed to an increased tendency for β-hydride elimination under these conditions resulting in more chain transfer and chain walking. Thus, adjusting the oligomerization conditions, temperature in particular, allows for an easy and straightforward fine-tuning of the resulting oligomer branching structure and molecular weight.

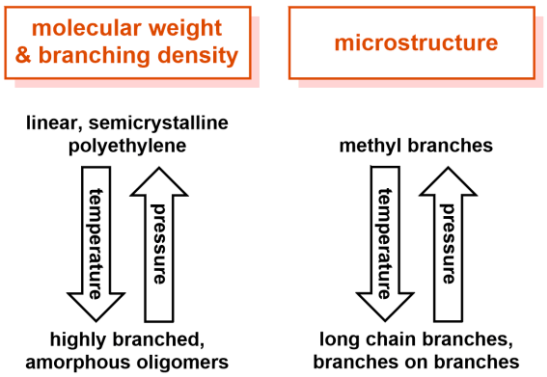

Figure 7.1: Temperature and pressure dependence of polymer molecular weight, degree of branching, and microstructure.

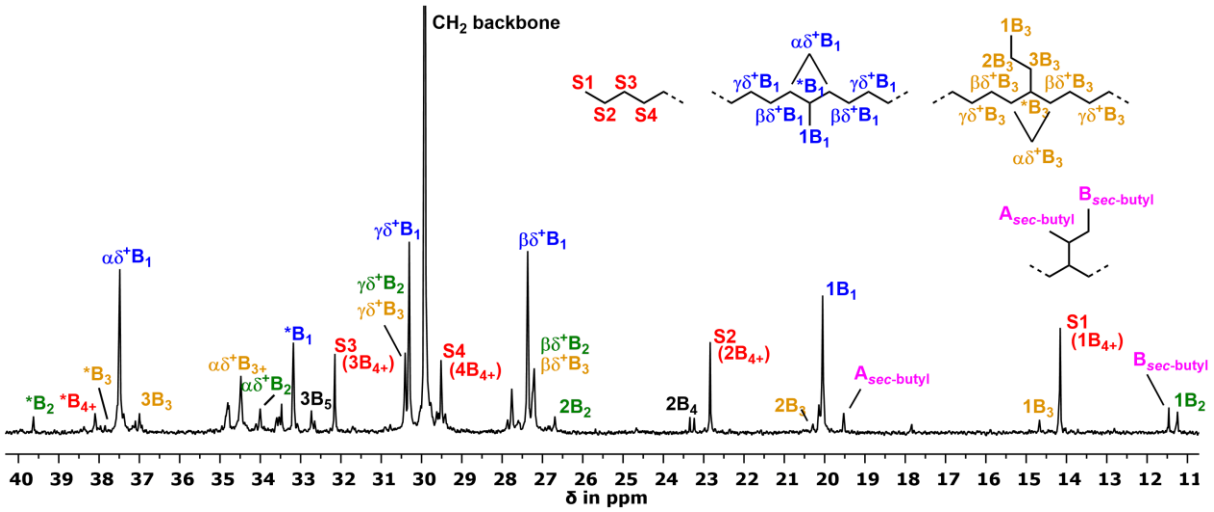

Figure 7.2: Representative ^{13}C NMR spectrum of a hyperbranched ethylene oligomer.

A detailed investigation of the microscopic chain architecture with ^{13}C NMR spectroscopy revealed the unique branching pattern of the oligomers formed (**Figure 7.2**). While the oligoethylenes mainly comprise methyl branches, they also contain significant amounts of ethyl, propyl, and longer chain alkyl branches (C_{4+}). Remarkably, all oligomers afforded by ^{Me}**1-pyr** even feature a hyperbranched microstructure as indicated by the presence of *sec*-butyl groups representing the smallest and only spectroscopically detectable branch on branch motif. Such highly branched products are unprecedented in this low molecular weight regime. Additionally, the oligomer microstructure is also dependent on the reaction conditions. At higher

temperatures and lower ethylene pressures, the amount of methyl branches decreases in favor of longer chain branches (**Figure 7.1**, right).

The effect of sterically more hindered remote alkyl substituents on the catalyst and its potential utility for fine tuning of oligomer microstructures was probed by oligomerizations with the ethyl and *iso*-propyl substituted complexes ^{Et}**1-pyr** and ^{iPr}**1-pyr** as catalyst precursors. Higher molecular weights and lower degrees of branching are obtained on going from methyl to ethyl and *iso*-propyl substituents (**Table 7.1**). Both catalysts are highly active with turnover frequencies easily exceeding 150,000 mol [C_2H_4] mol^{-1} [Ni] h^{-1} using ideal reaction conditions. Also, both are capable of producing hyperbranched oligomer structures, but they produce oligomers with distinctively higher percentages of methyl branches (>80%) and minor amounts of longer chain branches. *sec*-Butyl branches can only be obtained at high reaction temperatures using these two catalysts.

Table 7.1: Comparison of oligomers obtained with ^{Me}**1-pyr**, ^{Et}**1-pyr**, and ^{iPr}**1-pyr**.

entry	catalyst	M_n (NMR) [g mol^{-1}][a]	branches /1,000 C[b]	methyl[b] [%]	ethyl [b] [%]	propyl[b] [%]	C_{4+}[b] [%]	*sec*-butyl[b] [%]
1	^{Me}**1-pyr**	1,000	81	69	7	4	12	8
2	^{Et}**1-pyr**	1,500	73	82	8	3	2	4
3	^{iPr}**1-pyr**	3,300	57	90	6	1	1	2

reaction conditions: 20 bar of ethylene at 60 °C. [a] calculated from ^{1}H NMR spectra. [b] calculated from ^{13}C NMR spectra

Figure 7.3: Comparison of a moderately branched polyethylene (**left**, 6,300 g mol^{-1}, 50 branches / 1,000 C) and a highly branched ethylene oligomer (**right**, 1,700 g mol^{-1}, 80 branches / 1,000 C).

Controlling the microstructure (degree of branching and branching structure) and the molecular weight of the products with catalyst design and by adjusting the reaction condition, a wide range of different materials from semicrystalline polyethylene to completely amorphous oligoethylenes become accessible (**Figure 7.3**). Overall, the findings of this thesis show that molecular weights correlate with the overall branch density as well as the average branch length.

As a result, higher molecular weight oligomers always come with lower branch densities and almost exclusively comprise methyl branches. Beneficially, desirable features such as high degrees of branching and hyperbranched structures as well as low oligomer molecular weight (ca. 1,000 g mol^{-1}) go along with one another.

From β-hydride elimination as the underlying step for chain transfer during the catalytic oligomerization, every oligomer chain comprises a single unsaturated end group. Selective functionalization of theses double bonds for the first time gave access to monofunctional highly branched oligoethylenes (Chapter 4). Selective introduction of one primary carboxylic acid ester functional group per highly branched oligoethylene molecule was achieved by isomerizing ethoxycarbonylation and alternatively by cross metathesis with ethyl acrylate followed by hydrogenation (**Scheme 7.2**).

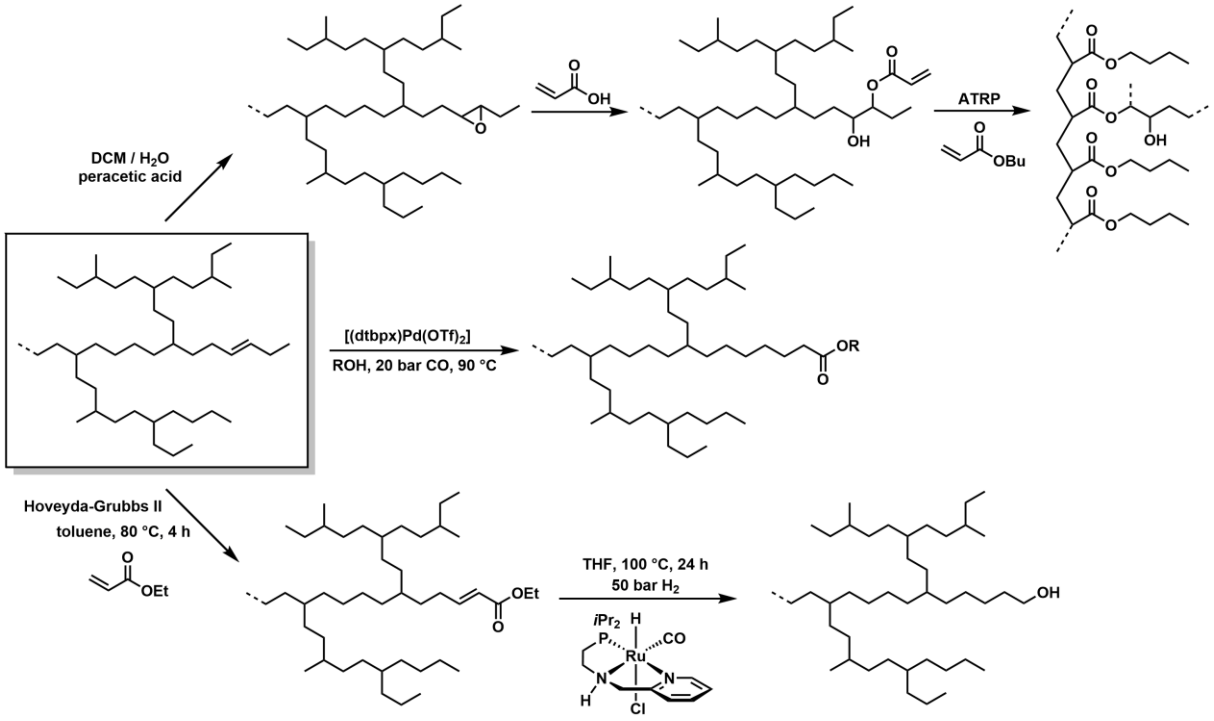

Scheme 7.2: Synthesis of monofunctional hyperbranched oligoethylenes.

The latter approach results in complete functionalization and no essential loss of branched oligomer material and molecular weight, as the reacting double bonds are close to a chain end. Reduction yielded an alcohol-functionalized oligomer. Introduction of one reactive epoxide group per branched oligomer occurs completely and selectively under mild conditions. All reaction steps involved in the monofunctionalization are efficient and readily scalable. The ring opening of epoxide oligomers with acrylic acid and derivatives gives access to acrylate functionalized macromonomers. A controlled radical copolymerization (ATRP) with *n*-butyl acrylate allowed for the synthesis of poly(*n*-butyl acrylate-*graft*-hyperbranched oligoethylene)

copolymers. The copolymerization is easily controllable with respect to macromonomer incorporation by adjusting the macromonomer to *n*-butyl acrylate ratio and copolymers with up to 10 mol% (44 wt%) macromonomer content are accessible. The highly branched oligomers as well as their functionalized derivatives were prepared on a scale well over 100 g.

Complexes with a strongly simplified ligand structure in Chapter 5 allow for a significantly more cost efficient catalyst synthesis for the production of highly branched ethylene oligomers. A series of *N*-2,6-dibromophenyl salicylaldiminato nickel complexes were synthesized starting from inexpensive anilines and aldehydes (**Scheme 7.3**).

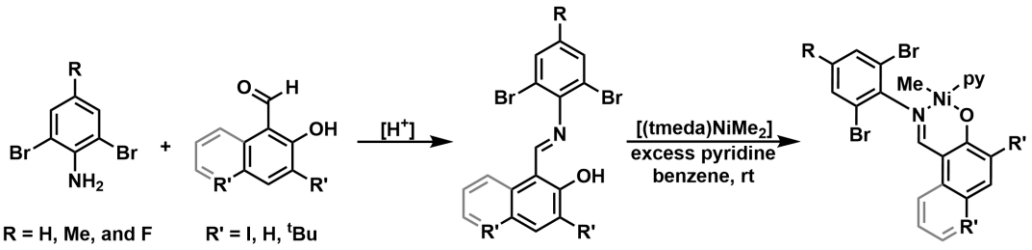

Scheme 7.3: Synthesis of simplified salicylaldiminato Ni(II) complexes from inexpensive and commercially available anilines and aldehydes.

Microstructure analysis of the oligomers afforded by these catalysts revealed their hyperbranched chain architecture. Remarkably, in terms of molecular weight and degree of branching as well as the distribution of different branch lengths, the simplified catalysts are capable of producing similar products compared to the *N*-terphenyl based complexes. Especially $^{\text{Sal-Me}}$**4-pyr** and $^{\text{Naph-Me}}$**4-pyr** are promising candidates and afford low molecular weight oligomers with degrees of branching as high as 91 and 86 branches per 1,000 carbon atoms, respectively. The lower activity observed for all simplified catalyst (TOF < 20,000 mol $[C_2H_4]$ mol^{-1} [Ni] h^{-1}) is well compensated for by their significantly less time consuming and costly synthesis procedure. However, the synthesis of highly branched oligoethylenes with very high activity appears to be limited to the more sophisticated complexes with an *N*-terphenyl motif.

In Chapter 6, the remarkable effect of the remote substituents in these terphenyl amine based complexes was investigated in detail. As a potential explanation, a weak π-interaction of the aryl groups with the nickel center was proposed. However, studies with symmetrical and asymmetrical complexes combining electron donating and withdrawing properties – containing methyl as well as CF_3 substituents – are ambiguous and do not directly indicate or contradict such an interaction. The concept was further studied with the introduction of heteroarenes like furan and thiophene as potentially coordinating motifs. Remarkably, both complexes $^{\text{Fur}}$**5-pyr** and $^{\text{Thio}}$**5-pyr** show an unexpected but desirable catalytic behavior. Both yield oligomers with an unprecedentedly high amount of branches (up to 127 per 1,000 C). Even so – despite their

evidently high propensity for β-hydride elimination and chain walking – they mainly produce methyl branches and only few longer chain branches and branch on branch motifs.

To shed more light on the origin of the remote substituent effect with experimental results, the electronic properties of selected nickel salicylaldiminato complexes were investigated. Cyclic voltammetry measurements allow for an indirect investigation of the electronic situation at the nickel center (**Figure 7.4**).

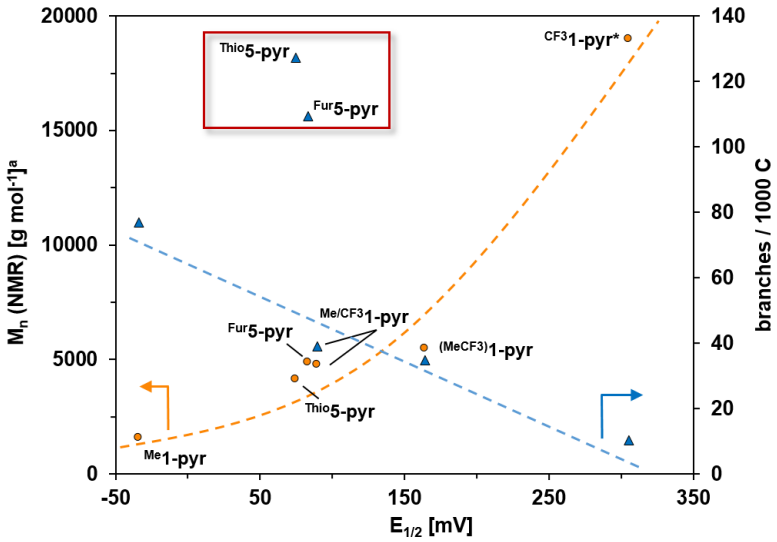

Figure 7.4: Correlation of the catalysts half-wave potentials vs. polymer molecular weight and degree of branching. [a] molecular weight of polymers synthesized at 40 °C and 20 bar of ethylene; * polymer obtained at 40 °C and 40 bar of ethylene according to ref. 53. Dashed lines are merely a guide to the eye.

Given the correlation between the electronic nature of the remote substituents and the polymer microstructure and molecular weights, for the terphenyl amine based catalysts, the half-wave potential was found to also correlate with the degree of branching and molecular weight of the products afforded. Complexes with electron donating substituents yielding highly branched oligomers are oxidized more easily (reflected by a lower redox potential) compared to their analogues bearing electron withdrawing groups. Generally, high half-wave potentials of a complex go along with low molecular weight products with high degrees of branching. Thus, for these complexes the oligomer microstructure obtained can be explained by the electronic properties of the nickel center. The two complexes **^{Fur}5-pyr** and **^{Thio}5-pyr** with potential coordinating motifs in the ligand backbone do follow this correlation but not quantitatively. Though they exhibit similar half-wave potentials compared to **$^{(MeCF_3)}$1-pyr**, they produce three times more branches for the same molecular weight polymers.

Density functional theory calculations carried out for the two systems **^{Me}1-pyr** and **^{CF_3}1-pyr** by Lucia Caporaso and Laura Falivene give a complete insight in all important steps of the catalytic cycle of ethylene oligomerization for **^{CF_3}1-pyr** and **^{Me}1-pyr**. The calculations are in very

good agreement with experimental results and can explain the different products obtained with respect to molecular weight and degree of branching using ^{Me}**1-pyr** and ^{CF3}**1-pyr**. Remarkably, they support the idea of a π-interaction of the aryl groups of the ligand with the nickel center proposed in this thesis. The calculations show that for ^{Me}**1-pyr** such an intermediate is able to significantly reduce the energy barrier that has to be overcome to access chain transfer and chain walking pathways (**Scheme 7.4**). In agreement with experimental results for ^{Me}**1-pyr**, similar overall energy barriers were calculated for linear chain growth and branch formation. For ^{CF3}**1-pyr**, the proposed π-interaction was found to be much weaker due to the lower electron density of the aryl rings and does not give such easy access to chain termination and branch formation pathways. Overall, the lowest barrier is therefore calculated for linear chain growth which nicely explains the formation of higher molecular weight products with less branches obtained with this catalyst compared to its methyl substituted analogue.

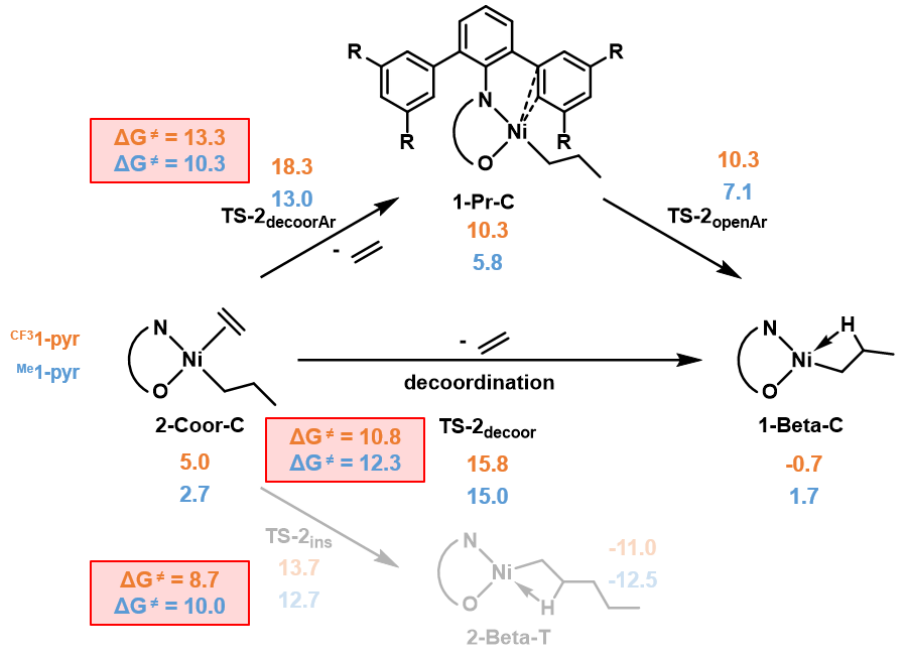

Scheme 7.4: Two potential pathways for the decoordination of ethylene to form **1-Beta-C** as the key reaction step to give access to chain transfer and branch formation. Gibbs free energies (G in kcal mol^{-1}) of all intermediates for ^{Me}**1 pyr** (blue) and ^{CF3}**1-pyr** (orange).

8 Crystallographic Appendix

X-Ray diffraction analyses were performed at 100 K on a STOE IPDS-II diffractometer equipped with a graphite-monochromated radiation source (λ = 0.71073 Å) and an image plate detection system. The crystals were mounted on a fine glass fiber with silicon grease. The selection, integration and averaging procedure of the measured reflex intensities, the determination of the unit cell dimensions and a least-squares fit of the 2θ values as well as data reduction, LP-correction and space group determination were performed using the X-Area software package delivered with the diffractometer.[166] A semi-empirical absorption correction was performed. The structures were solved by the Patterson or Direct method (SHELXS-97),[167] completed with difference Fourier syntheses, and refined with full-matrix least-square using SHELXL-97,[168] minimizing $\omega(F_o^2-F_c^2)^2$. Weighted R factor (wR_2) and the goodness of fit GooF are based on F^2. All non-hydrogen atoms were refined with anisotropic displacement parameters. All hydrogen atoms were treated in a riding model. Graphical output (Ortep plots) were created using ORTEP-3 V2.02 for Windows XP.[169]

Table 8.1: Crystallographic data of complex ^{Me}**1-pyr**.

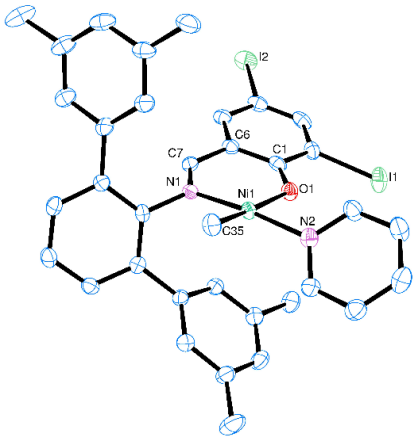

CCDC Number	**955722**	
Empirical formoula	$C_{35}H_{32}I_2N_2NiO$	
Formula weight	809.14	
Temperature	100(2) K	
Wavelength	0.71073 Å	
Crystal system	Monoclinic	
Space group	P21/c	
Unit cell dimensions	a = 11.1038(5) Å	α = 90°
	b = 16.6839(9) Å	β = 107.125(4)°
	c = 18.0283(9) Å	γ = 90°
Volume	3191.8(3) Å^3	
Z	4	
Density (calculated)	1.684 g cm^{-3}	
Absorption coefficient	2.572 mm^{-1}	
F(000)	1592	
Crystal size	0.35 x 0.24 x 0.15 mm^3	
θ range for data collection	1.70 – 28.02°	
Index ranges	-14 ≤ h ≤ 14, -21 ≤ k ≤ 22, -23 ≤ l ≤ 23	
Reflections collected	35684	
Independent Reflections	7658 [*R*(int) = 0.0504]	
Completeness to θ = 26.35°	99.1 %	
Absorption correction	Integration	
Max. and min. transmission	0.7930 and 0.5313	
Refinement method	Full-matrix least-squares on F^2	
Data / restraints / parameters	7658 / 0 / 375	
Goodness-of-fit on *F*^{2}	1.049	
Final *R* indices [*I* > 2 sigma(*I*)]	*R1* = 0.0346, *wR2* = 0.0755	
R indices (all data)	*R1* = 0.0538, *wR2* = 0.0804	
Largest diff. peak and hole	-1.437 and 0.852 e.Å^{-3}	

Table 8.2: Crystallographic data of complex **[($^{Naph\text{-}Me}$N^O)$_2$Ni]**.

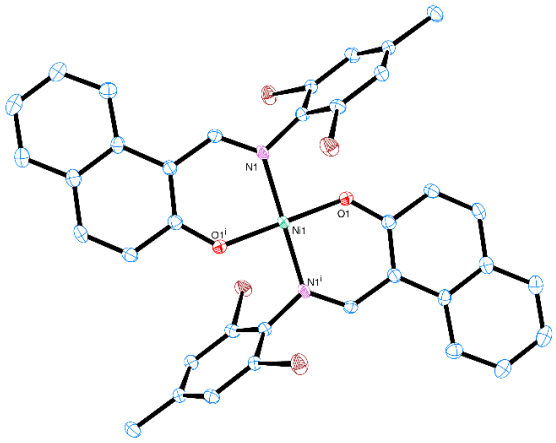

Identification code	**[($^{Naph\text{-}Me}$N^O)$_2$Ni]**	
Empirical formoula	$C_{40}H_{36}Br_4N_2NiO_4S_2$	
Formula weight	1051.18	
Temperature	100(2) K	
Wavelength	0.71073 Å	
Crystal system	triclinic	
Space group	P-1	
Unit cell dimensions	a = 8.3374(7) Å	α = 87.406(7)°.
	b = 10.6467(9) Å	β = 83.733(7)°
	c = 11.6699(9) Å	γ = 69.915(6)°
Volume	967.04(14) Å^3	
Z	1	
Density (calculated)	1.805 g/cm^3	
Absorption coefficient	4.786 mm-1	
F(000)	522	
Crystal size	0.1 x 0.4 x 0.5 mm^3	
θ range for data collection	1.76 to 27.97°	
Index ranges	-10 ≤ h ≤ 10, -13 ≤ k ≤ 14, -15 ≤ l ≤ 15	
Reflections collected	15913	
Independent Reflections	4627 [*R*(int) = 0.1008]	
Completeness to θ = 26.35°	99.3 %	
Absorption correction	Numerical	
Max. and min. transmission	0.7092 and 0.2970	
Refinement method	Full-matrix least-squares on F^2	
Data / restraints / parameters	4627 / 0 / 244	
Goodness-of-fit on *F*^{2}	0.959	
Final *R* indices [*I* > 2 sigma(*I*)]	*R1* = 0.0385, *wR2* = 0.0929	
R indices (all data)	*R1* = 0.0520, *wR2* = 0.0975	
Largest diff. peak and hole	-1.514 and 0.901 e.Å^{-3}	
Remarks	One dmso molecule was omitted for clarity	

References

[1] Baier, M. C.; Zuideveld, M. A.; Mecking, S. *Angew. Chem., Int. Ed.* **2014**, *53*, 9722-9744.

[2] Mülhaupt, R. *Macromol. Chem. Phys.* **2003**, *204*, 289-327.

[3] Whiteley, K. S.; Heggs, T. G.; Koch, H.; Mawer, R. L.; Immel, W.: Polyolefins. In *Ullmann's Encyclopedia of Industrial Chemistry*; Wiley-VCH Verlag GmbH & Co. KGaA: 2000.

[4] Ziegler, K.; Holzkamp, E.; Breil, H.; Martin, H. *Angew. Chem.* **1955**, *67*, 541-547.

[5] Natta, G.; Pino, P.; Corradini, P.; Danusso, F.; Mantica, E.; Mazzanti, G.; Moraglio, G. *J. Am. Chem. Soc.* **1955**, *77*, 1708-1710.

[6] *Ziegler Catalysts; Recent Scientific Innovations and Technological Improvements*; Fink, G.; Mülhaupt, R.; Brintzinger, H.-H., Eds.; Springer: Berlin, 1995.

[7] Hogan, J. P.; Banks, R. L. (Phillips Petroleum) US2825721, 1956

[8] Guan, Z.; Carnahan, E. M. *Metal catalysts in olefin polymerization*; Springer-Verlag: Berlin, 2009.

[9] Ittel, S. D.; Johnson, L. K.; Brookhart, M. *Chem. Rev.* **2000**, *100*, 1169-1204.

[10] Mecking, S. *Angew. Chem., Int. Ed.* **2001**, *40*, 534-540.

[11] Keim, W.; Kowaldt, F. H.; Goddard, R.; Krüger, C. *Angew. Chem., Int. Ed.* **1978**, *17*, 466-467.

[12] Keim, W. *Chemie Ingenieur Technik* **1984**, *56*, 850-853.

[13] Keim, W. *Angew. Chem., Int. Ed.* **2013**, *52*, 12492-12496.

[14] Johnson, L. K.; Killian, C. M.; Brookhart, M. *J. Am. Chem. Soc.* **1995**, *117*, 6414-6415.

[15] Gates, D. P.; Svejda, S. A.; Oñate, E.; Killian, C. M.; Johnson, L. K.; White, P. S.; Brookhart, M. *Macromolecules* **2000**, *33*, 2320-2334.

[16] Killian, C. M.; Johnson, L. K.; Brookhart, M. *Organometallics* **1997**, *16*, 2005-2007.

[17] McCord, E. F.; McLain, S. J.; Nelson, L. T. J.; Ittel, S. D.; Tempel, D.; Killian, C. M.; Johnson, L. K.; Brookhart, M. *Macromolecules* **2007**, *40*, 410-420.

[18] Mecking, S.; Johnson, L. K.; Wang, L.; Brookhart, M. *J. Am. Chem. Soc.* **1998**, *120*, 888-899.

[19] Johnson, L. K.; Mecking, S.; Brookhart, M. *J. Am. Chem. Soc.* **1996**, *118*, 267-268.

[20] Drent, E.; van Dijk, R.; van Ginkel, R.; van Oort, B.; Pugh, R. I. *Chem. Commun.* **2002**, 744-745.

[21] Nakamura, A.; Anselment, T. M. J.; Claverie, J.; Goodall, B.; Jordan, R. F.; Mecking, S.; Rieger, B.; Sen, A.; van Leeuwen, P. W. N. M.; Nozaki, K. *Acc. Chem. Res.* **2013**, *46*, 1438-1449.

[22] Svejda, S. A.; Johnson, L. K.; Brookhart, M. *J. Am. Chem. Soc.* **1999**, *121*, 10634-10635.

[23] Deng, L.; Woo, T. K.; Cavallo, L.; Margl, P. M.; Ziegler, T. *J. Am. Chem. Soc.* **1997**, *119*, 6177-6186.

[24] Froese, R. D. J.; Musaev, D. G.; Morokuma, K. *J. Am. Chem. Soc.* **1998**, *120*, 1581-1587.

[25] Möhring, V. M.; Fink, G. *Angew. Chem., Int. Ed.* **1985**, *24*, 1001-1003.

[26] Woo, T. K.; Margl, P. M.; Blöchl, P. E.; Ziegler, T. *J. Phys. Chem. B* **1997**, *101*, 7877-7880.

[27] Michalak, A.; Ziegler, T. *Organometallics* **1999**, *18*, 3998-4004.

[28] Musaev, D. G.; Froese, R. D. J.; Morokuma, K. *Organometallics* **1998**, *17*, 1850-1860.

[29] Svejda, S. A.; Brookhart, M. *Organometallics* **1999**, *18*, 65-74.

[30] Schmid, M.; Eberhardt, R.; Klinga, M.; Leskelä, M.; Rieger, B. *Organometallics* **2001**, *20*, 2321-2330.

[31] Meinhard, D.; Wegner, M.; Kipiani, G.; Hearley, A.; Reuter, P.; Fischer, S.; Marti, O.; Rieger, B. *J. Am. Chem. Soc.* **2007**, *129*, 9182-9191.

[32] Moody, L. S.; Mackenzie, P. B.; Killian, C. M.; Lavoie, G. G.; Ponasik, J. A.; Barrett, A. G. M.; Smith, T. W.; Pearson, J. C. (Eastman Chemical Company) WO 00/50470, 2000

[33] Gautier, P. A.; Lutz, E. F. (Shell) EP0177999, 1986

[34] Behr, A.: Homogeneous Catalysis. In *Ullmann's Encyclopedia of Industrial Chemistry*; Wiley-VCH Verlag GmbH & Co. KGaA: 2000.

[35] O'Donnelli, A. E.; Gum, C. (Shell Oil Company) US4260844, 1981

[36] Vogt, D.: Organic-organic biphasic catalysis. In *Multiphase Homogeneous Catalysis*; Cornils, B., Herrmann, W. A., Horváth, I. T., Leitner, W., Mecking, S., Olivier-Bourbigou, H., Vogt, D., Eds.; Wiley-VCH Verlag GmbH: 2008, p 310-337.

[37] Klabunde, U. (DuPont) US4698403, 1987

[38] Klabunde, U.; Itten, S. D. *J. Mol. Catal.* **1987**, *41*, 123-134.

[39] Klabunde, U.; Mülhaupt, R.; Herskovitz, T.; Janowicz, A. H.; Calabrese, J.; Ittel, S. D. *J. Polym. Sci., Part A: Polym. Chem.* **1987**, *25*, 1989-2003.

[40] Starzewski, K. A. O.; Witte, J. *Angew. Chem., Int. Ed.* **1985**, *24*, 599-601.

[41] Johnson, L. K.; Bennett, A. M. A.; Ittel, S. D.; Wang, L.; Hauptman, E.; Simpson, R. D.; Feldman, J.; Coughlin, E. B. (DuPont) WO 98/30609, 1998

[42] Wang, C.; Friedrich, S.; Younkin, T. R.; Li, R. T.; Grubbs, R. H.; Bansleben, D. A.; Day, M. W. *Organometallics* **1998**, *17*, 3149-3151.

[43] Younkin, T. R.; Connor, E. F.; Henderson, J. I.; Friedrich, S. K.; Grubbs, R. H.; Bansleben, D. A. *Science* **2000**, *287*, 460-462.

[44] Chan, M. S. W.; Deng, L.; Ziegler, T. *Organometallics* **2000**, *19*, 2741-2750.

[45] Zeller, A.; Strassner, T. *J. Organomet. Chem.* **2006**, *691*, 4379-4385.

[46] Bauers, F. M.; Mecking, S. *Macromolecules* **2001**, *34*, 1165-1171.

[47] Zuideveld, M. A.; Wehrmann, P.; Röhr, C.; Mecking, S. *Angew. Chem., Int. Ed.* **2004**, *43*, 869-873.

[48] Wehrmann, P.; Zuideveld, M.; Thomann, R.; Mecking, S. *Macromolecules* **2006**, *39*, 5995-6002.

[49] Wehrmann, P.; Mecking, S. *Macromolecules* **2006**, *39*, 5963-5964.

[50] Göttker-Schnetmann, I.; Wehrmann, P.; Röhr, C.; Mecking, S. *Organometallics* **2007**, *26*, 2348-2362.

[51] Bastero, A.; Göttker-Schnetmann, I.; Röhr, C.; Mecking, S. *Adv. Synth. Catal.* **2007**, *349*, 2307-2316.

[52] Osichow, A.; Göttker-Schnetmann, I.; Mecking, S. *Organometallics* **2013**, *32*, 5239-5242.

[53] Zuideveld, M. A.; Wehrmann, P.; Röhr, C.; Mecking, S. *Angew. Chem.* **2004**, *116*, 887-891.

[54] Jenkins, J. C.; Brookhart, M. *J. Am. Chem. Soc.* **2004**, *126*, 5827-5842.

[55] Berkefeld, A.; Mecking, S. *J. Am. Chem. Soc.* **2009**, *131*, 1565-1574.

[56] Berkefeld, A.; Drexler, M.; Möller, H. M.; Mecking, S. *J. Am. Chem. Soc.* **2009**, *131*, 12613-12622.

[57] Berkefeld, A. PhD Thesis, University of Konstanz, 2009.

[58] Connor, E. F.; Younkin, T. R.; Henderson, J. I.; Waltman, A. W.; Grubbs, R. H. *Chem. Commun.* **2003**, 2272-2273.

[59] Chen, Z.; Mesgar, M.; White, P. S.; Daugulis, O.; Brookhart, M. *ACS Catalysis* **2015**, *5*, 631-636.

[60] Ziegler, K. *Angew. Chem.* **1952**, *64*, 323-329.

[61] Washecheck Paul, H.: Manufacture of Higher Straight-Chain Alcohols by the Ethylene Chain Growth Process. In *Monohydric Alcohols*; AMERICAN CHEMICAL SOCIETY: 1981; Vol. 159, p 87-100.

[62] Behr, A.: Ziegler Processes. In *Ullmann's Encyclopedia of Industrial Chemistry*; Wiley-VCH Verlag GmbH & Co. KGaA: 2000.

[63] Britovsek, G. J. P.; Cohen, S. A.; Gibson, V. C.; Maddox, P. J.; van Meurs, M. *Angew. Chem., Int. Ed.* **2002**, *41*, 489-491.

[64] van Meurs, M.; Britovsek, G. J. P.; Gibson, V. C.; Cohen, S. A. *J. Am. Chem. Soc.* **2005**, *127*, 9913-9923.

[65] Gibson, V. C. *Science* **2006**, *312*, 703-704.

[66] Arriola, D. J.; Carnahan, E. M.; Hustad, P. D.; Kuhlman, R. L.; Wenzel, T. T. *Science* **2006**, *312*, 714-719.

[67] Amin, S. B.; Marks, T. J. *Angew. Chem., Int. Ed.* **2008**, *47*, 2006-2025.

[68] Mazzolini, J.; Espinosa, E.; D'Agosto, F.; Boisson, C. *Polym. Chem.* **2010**, *1*, 793-800.

[69] Pelletier, J.-F.; Mortreux, A.; Olonde, X.; Bujadoux, K. *Angew. Chem., Int. Ed.* **1996**, *35*, 1854-1856.

[70] Bogaert, S.; Chenal, T.; Mortreux, A.; Carpentier, J.-F. *J. Mol. Catal. A: Chem.* **2002**, *190*, 207-214.

[71] Daugulis, O.; Brookhart, M. *Organometallics* **2002**, *21*, 5926-5934.

[72] Desjardins, S. Y.; Way, A. A.; Murray, M. C.; Adirim, D.; Baird, M. C. *Organometallics* **1998**, *17*, 2382-2384.

[73] Bessel, M.; Mecking, S.; Wiedemann, T.; Frank, A.; Omeis, J.; Tchernook, A.; Göttker-Schnetmann, I. (Byk Chemie GmbH) EP2891511 (A1), 2015

[74] Wolfmeier, U.; Schmidt, H.; Heinrichs, F.-L.; Michalczyk, G.; Payer, W.; Dietsche, W.; Boehlke, K.; Hohner, G.; Wildgruber, J.: Waxes. In *Ullmann's Encyclopedia of Industrial Chemistry*; Wiley-VCH Verlag GmbH & Co. KGaA: 2000.

[75] Rose, J. M.; Cherian, A. E.; Coates, G. W. *J. Am. Chem. Soc.* **2006**, *128*, 4186-4187.

[76] Cotts, P. M.; Guan, Z.; McCord, E.; McLain, S. *Macromolecules* **2000**, *33*, 6945-6952.

[77] Guan, Z.; Cotts, P. M.; McCord, E. F.; McLain, S. J. *Science* **1999**, *283*, 2059-2062.

[78] Xiang, P.; Ye, Z.; Subramanian, R. *Polymer* **2011**, *52*, 5027-5039.

[79] Pietsch, J.; Braunstein, P.; Chauvin, Y. *New Journal of Chemistry* **1998**, *22*, 467-472.

[80] Song, D.-P.; Wang, Y.-X.; Mu, H.-L.; Li, B.-X.; Li, Y.-S. *Organometallics* **2011**, *30*, 925-934.

[81] Osichow, A.; Rabe, C.; Vogtt, K.; Narayanan, T.; Harnau, L.; Drechsler, M.; Ballauff, M.; Mecking, S. *J. Am. Chem. Soc.* **2013**, *135*, 11645-11650.

[82] Weberski, M. P.; Chen, C.; Delferro, M.; Zuccaccia, C.; Macchioni, A.; Marks, T. J. *Organometallics* **2012**, *31*, 3773-3789.

[83] Soshnikov, I. E.; Semikolenova, N. V.; Zakharov, V. A.; Möller, H. M.; Ölscher, F.; Osichow, A.; Göttker-Schnettmann, I.; Mecking, S.; Talsi, E. P.; Bryliakov, K. P. *Chem. Eur. J.* **2013**, *19*, 11409-11417.

[84] Diemer, V.; Chaumeil, H.; Defoin, A.; Fort, A.; Boeglin, A.; Carré, C. *Europ. J. Org. Chem.* **2006**, *2006*, 2727-2738.

[85] Wiedemann, T.; Voit, G.; Tchernook, A.; Roesle, P.; Göttker-Schnetmann, I.; Mecking, S. *J. Am. Chem. Soc.* **2014**, *136*, 2078-2085.

[86] Izunobi, J. U.; Higginbotham, C. L. *J. Chem. Educ.* **2011**, *88*, 1098-1104.

[87] Longo, P.; Oliva, L.; Grassi, A.; Pellecchia, C. *Die Makromolekulare Chemie* **1989**, *190*, 2357-2361.

[88] Randall, J. C. *J. Macromol. Sci., Polym. Rev.* **1989**, *29*, 201-317.

[89] Galland, G. B.; de Souza, R. F.; Mauler, R. S.; Nunes, F. F. *Macromolecules* **1999**, *32*, 1620-1625.

[90] Soula, R.; Saillard, B.; Spitz, R.; Claverie, J.; Llaurro, M. F.; Monnet, C. *Macromolecules* **2002**, *35*, 1513-1523.

[91] Bastero, A.; Franciò, G.; Leitner, W.; Mecking, S. *Chem. Eur. J.* **2006**, *12*, 6110-6116.

[92] Kim, H. S.; Banwell, M. G.; Willis, A. C. *J. Org. Chem.* **2013**, *78*, 5103-5109.

[93] Popeney, C. S.; Levins, C. M.; Guan, Z. *Organometallics* **2011**, *30*, 2432-2452.

[94] Armarego, W. L. F.; Chai Christina Li Lin *Purification of laboratory chemicals*; 5. ed.; Butterworth-Heinemann: Amsterdam u.a., 2003.

[95] Wunderlich, B.; Czornyj, G. *Macromolecules* **1977**, *10*, 906-913.

[96] Franssen, N. M. G.; Reek, J. N. H.; de Bruin, B. *Chem. Soc. Rev.* **2013**, *42*, 5809-5832.

[97] Hillmyer, M. A.; Laredo, W. R.; Grubbs, R. H. *Macromolecules* **1995**, *28*, 6311-6316.

[98] Walker, R.; Conrad, R. M.; Grubbs, R. H. *Macromolecules* **2009**, *42*, 599-605.

[99] Nakamura, A.; Ito, S.; Nozaki, K. *Chem. Rev.* **2009**, *109*, 5215-5244.

[100] Qiao, J.; Guo, M.; Wang, L.; Liu, D.; Zhang, X.; Yu, L.; Song, W.; Liu, Y. *Polym. Chem.* **2011**, *2*, 1611-1623.

[101] Boaen, N. K.; Hillmyer, M. A. *Chem. Soc. Rev.* **2005**, *34*, 267-275.

[102] Brookhart, M.; DeSimone, J. M.; Grant, B. E.; Tanner, M. J. *Macromolecules* **1995**, *28*, 5378-5380.

[103] Gottfried, A. C.; Brookhart, M. *Macromolecules* **2003**, *36*, 3085-3100.

[104] Chung, T. C.; Rhubright, D. *J. Polym. Sci., Part A: Polym. Chem.* **1993**, *31*, 2759-2763.

[105] Chung, T. C.; Lu, H. L.; Li, C. L. *Macromolecules* **1994**, *27*, 7533-7537.

[106] Matyjaszewski, K.; Saget, J.; Pyun, J.; Schlögl, M.; Rieger, B. *J. Macromol. Sci., Part A* **2002**, *39*, 901-913.

[107] Kang, K. K.; Shiono, T.; Ikeda, T. *Macromolecules* **1997**, *30*, 1231-1233.

[108] Kaneko, H.; Kojoh, S.-i.; Kawahara, N.; Matsuo, S.; Matsugi, T.; Kashiwa, N. *J. Polym. Sci., Part A: Polym. Chem.* **2005**, *43*, 5103-5118.

[109] Pugh, R. I.; Drent, E.; Pringle, P. G. *Chem. Commun.* **2001**, 1476-1477.

[110] Jimenez Rodriguez, C.; Foster, D. F.; Eastham, G. R.; Cole-Hamilton, D. J. *Chem. Commun.* **2004**, 1720-1721.

[111] Stempfle, F.; Quinzler, D.; Heckler, I.; Mecking, S. *Macromolecules* **2011**, *44*, 4159-4166.

[112] Quinzler, D.; Mecking, S. *Angew. Chem., Int. Ed.* **2010**, *49*, 4306-4308.

[113] Stempfle, F.; Ritter, B. S.; Mulhaupt, R.; Mecking, S. *Green Chemistry* **2014**, *16*, 2008-2014.

[114] Jiménez-Rodriguez, C.; Eastham, G. R.; Cole-Hamilton, D. J. *Inorg. Chem. Commun.* **2005**, *8*, 878-881.

[115] Busch, H.; Stempfle, F.; Heß, S.; Grau, E.; Mecking, S. *Green Chemistry* **2014**, *16*, 4541-4545.

[116] Roesle, P.; Dürr, C. J.; Möller, H. M.; Cavallo, L.; Caporaso, L.; Mecking, S. *J. Am. Chem. Soc.* **2012**, *134*, 17696-17703.

[117] Roesle, P.; Caporaso, L.; Schnitte, M.; Goldbach, V.; Cavallo, L.; Mecking, S. *J. Am. Chem. Soc.* **2014**, *136*, 16871-16881.

[118] Chatterjee, A. K.; Choi, T.-L.; Sanders, D. P.; Grubbs, R. H. *J. Am. Chem. Soc.* **2003**, *125*, 11360-11370.

[119] Vougioukalakis, G. C.; Grubbs, R. H. *Chem. Rev.* **2009**, *110*, 1746-1787.

[120] Abbas, M.; Slugovc, C. *Monatsh. Chem.* **2012**, *143*, 669-673.

[121] Mathers, R. T.; Coates, G. W. *Chem. Commun.* **2004**, 422-423.

[122] Oliván, M.; Caulton, K. G. *Inorg. Chem.* **1999**, *38*, 566-570.

[123] Bielawski, C. W.; Louie, J.; Grubbs, R. H. *J. Am. Chem. Soc.* **2000**, *122*, 12872-12873.

[124] Drouin, S. D.; Zamanian, F.; Fogg, D. E. *Organometallics* **2001**, *20*, 5495-5497.

[125] Ortmann, P.; Mecking, S. *Macromolecules* **2013**, *46*, 7213-7218.

[126] Spasyuk, D.; Smith, S.; Gusev, D. G. *Angew. Chem., Int. Ed.* **2012**, *51*, 2772-2775.

[127] Matoishi, K.; Nakai, K.; Nagai, N.; Terao, H.; Fujita, T. *Catal. Today* **2011**, *164*, 2-8.

[128] Hyun, M. Y.; Kim, S. H.; Song, Y. J.; Lee, H. G.; Jo, Y. D.; Kim, J. H.; Hwang, I. H.; Noh, J. Y.; Kang, J.; Kim, C. *J. Org. Chem.* **2012**, *77*, 7307-7312.

[129] LaScala, J.; Wool, R. P. *J. Am. Oil Chem. Soc.* **2002**, *79*, 59-63.

[130] Habib, F.; Bajpai, M. *Chemistry & Chemical Technology* **2011**, *5*, 317-326.

[131] Peng, C.-C.; Abetz, V. *Macromolecules* **2005**, *38*, 5575-5580.

[132] Hawker, C. J.; Mecerreyes, D.; Elce, E.; Dao, J.; Hedrick, J. L.; Barakat, I.; Dubois, P.; Jérôme, R.; Volksen, W. *Macromol. Chem. Phys.* **1997**, *198*, 155-166.

[133] Roos, S. G.; Müller, A. H. E.; Matyjaszewski, K. *Macromolecules* **1999**, *32*, 8331-8335.

[134] Börner, H. G.; Beers, K.; Matyjaszewski, K.; Sheiko, S. S.; Möller, M. *Macromolecules* **2001**, *34*, 4375-4383.

[135] Hong, S. C.; Jia, S.; Teodorescu, M.; Kowalewski, T.; Matyjaszewski, K.; Gottfried, A. C.; Brookhart, M. *J. Polym. Sci., Part A: Polym. Chem.* **2002**, *40*, 2736-2749.

[136] Muehlebach, A.; Rime, F. *J. Polym. Sci., Part A: Polym. Chem.* **2003**, *41*, 3425-3439.

[137] Cai, Y.; Hartenstein, M.; Müller, A. H. E. *Macromolecules* **2004**, *37*, 7484-7490.

[138] Ohno, S.; Matyjaszewski, K. *J. Polym. Sci., Part A: Polym. Chem.* **2006**, *44*, 5454-5467.

[139] Radke, W.; Müller, A. H. E. *Makromol. Chem., Macromol. Symp.* **1992**, *54-55*, 583-594.

[140] Bevington, J. C.; Harris, D. O. *J. Polym. Sci., Part B: Polym. Lett.* **1967**, *5*, 799-802.

[141] Jia, W.; Chen, X.; Guo, R.; Sui-Seng, C.; Amoroso, D.; Lough, A. J.; Abdur-Rashid, K. *Dalton Trans.* **2009**, *0*, 8301-8307.

[142] Jäntti, A.; Wagner, M.; Wagner, M.; Suontamo, R.; Kolehmainen, E.; Rissanen, K. *Eur. J. Inorg. Chem.* **1998**, *1998*, 1555-1562.

[143] Makio, H.; Fujita, T. *Acc. Chem. Res.* **2009**, *42*, 1532-1544.

[144] So, L.-C.; Liu, C.-C.; Chan, M. C. W.; Lo, J. C. Y.; Sze, K.-H.; Zhu, N. *Chem. Eur. J.* **2012**, *18*, 565-573.

[145] Möller, H. M.; Baier, M. C.; Mecking, S.; Talsi, E. P.; Bryliakov, K. P. *Chem. Eur. J.* **2012**, *18*, 848-856.

[146] Bryliakov, K. P.; Talsi, E. P.; Möller, H. M.; Baier, M. C.; Mecking, S. *Organometallics* **2010**, *29*, 4428-4430.

[147] Stephenson, C. J.; McInnis, J. P.; Chen, C.; Weberski, M. P.; Motta, A.; Delferro, M.; Marks, T. J. *ACS Catalysis* **2014**, 999-1003.

[148] Mecking, S.; Keim, W. *Organometallics* **1996**, *15*, 2650-2656.

[149] Jeffrey, J. C.; Rauchfuss, T. B. *Inorg. Chem.* **1979**, *18*, 2658-2666.

[150] Bader, A.; Lindner, E. *Coord. Chem. Rev.* **1991**, *108*, 27-110.

[151] Slone, C. S.; Weinberger, D. A.; Mirkin, C. A.: The Transition Metal Coordination Chemistry of Hemilabile Ligands. In *Progress in Inorganic Chemistry*; John Wiley & Sons, Inc.: 2007, p 233-350.

[152] Takagi, J.; Sato, K.; Hartwig, J. F.; Ishiyama, T.; Miyaura, N. *Tetrahedron Lett.* **2002**, *43*, 5649-5651.

[153] Ishiyama, T.; Takagi, J.; Ishida, K.; Miyaura, N.; Anastasi, N. R.; Hartwig, J. F. *J. Am. Chem. Soc.* **2001**, *124*, 390-391.

[154] Boller, T. M.; Murphy, J. M.; Hapke, M.; Ishiyama, T.; Miyaura, N.; Hartwig, J. F. *J. Am. Chem. Soc.* **2005**, *127*, 14263-14278.

[155] Tzschucke, C. C.; Murphy, J. M.; Hartwig, J. F. *Org. Lett.* **2007**, *9*, 761-764.

[156] Perdew, J. P. *Phys. Rev. B* **1986**, *33*, 8822-8824.

[157] Perdew, J. P. *Phys. Rev. B* **1986**, *34*, 7406-7406.

[158] Becke, A. D. *Phys. Rev. A* **1988**, *38*, 3098-3100.

[159] M. J. Frisch et al. Gaussian 09 Revision A.1, Gaussian, Inc., Wallingford, CT, 2009.

[160] Weigend, F.; Ahlrichs, R. *Phys. Chem. Chem. Phys.* **2005**, *7*, 3297-3305.

[161] Häussermann, U.; Dolg, M.; Stoll, H.; Preuss, H.; Schwerdtfeger, P.; Pitzer, R. M. *Mol. Phys.* **1993**, *78*, 1211-1224.

[162] Küchle, W.; Dolg, M.; Stoll, H.; Preuss, H. *J. Chem. Phys.* **1994**, *100*, 7535-7542.

[163] Leininger, T.; Nicklass, A.; Stoll, H.; Dolg, M.; Schwerdtfeger, P. *J. Chem. Phys.* **1996**, *105*, 1052-1059.

[164] Tomasi, J.; Persico, M. *Chem. Rev.* **1994**, *94*, 2027-2094.

[165] Barone, V.; Cossi, M. *J. Phys. Chem. A* **1998**, *102*, 1995-2001.

[166] X-RED version 1.31 Stoe Data Reduction Program, Darmstadt, Germany, 2005.

[167] Sheldrick, G. M. SHELXS-97 Program for Crystal Structure Analysis, University of Göttingen, Germany, 1997.

[168] Sheldrick, G. M. SHELXL-97 Program for Crystal Structure Refinement, University of Göttingen, Germany, 1997.

[169] Faruggia, L. J. ORTEP-3 V2.02 for Windows XP, University of Glasgow, Scotland, 2008.